Gene expression profiles and biomarker identification for KMT5A identifies novel potential therapeutic targets in prostate cancer

A Thesis submitted in part requirement for the degree of Doctor of Philosophy

Zainab Adnan Hatem Alebady

Solid Tumour Target Discovery Group

Northern Institute of Cancer Research

Newcastle University

October 2016

Abstract

Prostate cancer (PC), is initially androgen dependent due to the androgenic nature of the organ. Hence, initial therapy comprises androgen depletion via chemical castration in conjunction with an anti-androgen therapeutic. However, patients relapse and the tumours aggressively re-grow in a castrate resistant (CRPC) manner.

In CRPC, androgen receptor (AR) signaling remains functional via numerous mechanisms hence the AR remains a viable therapeutic target. However, treatment with current AR targeting therapeutics also results in relapse indicating the potential of targeting AR signaling indirectly by targeting AR co-factors. Recently, KMT5A, a lysine methyltransferase, has been identified as an AR co-activator exclusively in models of CRPC. A number of KMT5A inhibitors have been identified recent years, which would enhance the possibility of targeting KMT5A in PC.

This thesis aims to determine the signature of genes that are regulated directly by KMT5A or by combined activities of AR and KMT5A in PC cell lines and to further identify biomarkers for KMT5A activity. These aims were approached using Illumina Human HT-12 arrays to detect KMT5A gene expression profiles in an *in vitro* cell line model of androgen independent PC (LNCaP-AI cells). Microarray data analysis revealed a number of androgen-regulated genes to be modulated by KMT5A concurrently, and other genes that were found to be regulated by KMT5A activity, and a further cohort of genes that were found to be regulated solely by KMT5A.

CDC20 was selected for further study from the identified KMT5A regulated genes as a possible biomarker for KMT5A activity in aggressive PC. KMT5A was found to regulate CDC20 mRNA and protein expression. The enzymatic activity of KMT5A was demonstrated to affect CDC20 expression through the enrichment of the H4K20me1 mark at the CDC20 promoter in androgen-sensitive (LNCaP) and androgen-independent (LNCaP-AI) cells. The regulation of CDC20 by KMT5A expression, therefore identifies CDC20 as putative biomarker for KMT5A activity. KMT5A was also shown to influence CDC20 expression via p53. Knockdown of KMT5A inhibited the mono-methylation of p53 at K382 to enhance p53 activity, demonstrated by increased p21 expression which negatively regulated CDC20

expression. These findings were confirmed using commercially available KMT5A inhibitors Ryuvidine and UNC0379.

In summary, KMT5A inhibition in PC cells using small molecule inhibitors may provide benefit to patients that have relapsed on AR- targeting therapeutics and as such requires further investigation as a potential therapeutic target. CDC20 was identified as a putative biomarker for KMT5A activity which may prove useful to detect effective KMT5A inhibition in these studies.

Acknowledgements

First of all, I would like to thank my supervisors, Prof. Craig N. Robson and Dr. Kelly Coffey, for their continuous help, guidance and support over the last three years. I am very grateful for the opportunity they have given me to become one of their laboratory members. My thanks also extend to all members of the Solid Tumour Discovery Laboratory, both present and past members for their assistance, advice and support, especially Dr. Scott Walker, Dr. Luke Gaughan, Mahsa Azizyan, Claudia –Ryan Mendel, Laura Wilson, Dr. Kasturi Rao, Dr. Stuart Williamson, Dr. Anastasia Hepburn, Dr. Mark Wade and James Grey.

I would also like to give special thanks to my country Iraq and my sponsor The Higher Committee for Education Development in Iraq, for awarding me this scholarship to study for my PhD in the UK.

My deep gratitude for my parents Mr. Adnan Hatem Alebady and Mrs. Nawal Abdulraheem Fayyad for their unlimited love, help, support and prayers, you have always been the light at the end of the tunnel for me, and your love is my biggest achievement ever.

My love and thanks to my sisters and brothers for being in my life and for their unconditional love.

At the beginning and the end my greatest appreciations for my lovely husband Mr. Massar Alsamraae and my exquisite son Sohaib for their patience, love and support throughout my PhD journey, without you it would not have been possible.

Finally, thanks to all members of staff at the Northern Institute for Cancer Research for creating such an amazing welcoming atmosphere within the institute and for their continuous help.

List of abbreviations

AdoMet	S-adenosylmethionine
ADT	Androgen deprivation therapy
AF	Activation function
APC	Anaphase promoting complex
APS	Ammonium persulphate
AR	Androgen receptor
ARE	Androgen response element
ATP	Adenosine-5'-triphosphate
Aurora A	Aurora Kinase A
BM	Basal medium
BPH	Benign prostate hyperplasia
BSA	Bovine serum albumin
PC	Prostate cancer
CAFs	Cancer-associated fibroblast
CBP	CREB binding protein
Cdk	Cyclin dependent kinase
cDNA	Complementary DNA
ChIP	Chromatin immunoprecipitation
CRPC	Castration resistant prostate cancer

CTD	C terminal domain
DAB	3,3'-Diaminobenzidine
DBD	DNA binding domain
DCC	Dextran coated charcoal
DDR	DNA damage repair
DEPC	Diethylpyrocarbonate
DHT	5 α-dihydrotestosterone
DMSO	Dimethyl sulfoxide
DNA	Deoxyribonucleic acid
dNTP	Deoxyribonucleoside triphosphate
DSBs	Double strand breaks
EDTA	Ethylenediaminetetraacetic acid
EGF	Epidermal growth factor
EMT	Epithelial-mesenchymal transition
FCS	Foetal calf serum
FM	Full medium
FOXM1	Forkhead box protein M1
GADD	Growth arrest and DNA-damage-inducible
G-phase	Gap phase
GR	Glucocorticoid receptor
H	Histone
HAT	Histone acetyltransferase

HBD	Histone binding domain
HDAC	Histone deacetylase
HGPIN	High grade prostatic intraepithelial neoplasia
HMT	Histone methyl transferase
HPRT-1	Hypoxanthine phosphoribosyl transferase 1
HSPs	Heat shock proteins
HTS	High throughput screening
IGF	Insulin-like growth factor
IHC	Immunohistochemistry
IP	Immunoprecipitation
ITC	Isothermal titration calorimetry
JMJD	Jumonji domain containing
K	Lysine
kDa	Kilo Dalton
KGF	Keratinocyte growth factor
KLK2	Kallikrein-related peptidase 2
KMT	Lysine methyltransferase
L3MBTL1	Lethal 3 malignant brain tumour 1
LBD	Ligand binding domain
LEF-1	Lymphoid enhancer-binding factor 1
LH-RH	Luteinizing hormone –releasing hormone
MAPK	Mitogen activated protein kinase

Me	Methyl group
miRNA	microRNA
MMLV	Murine moloney leukaemia virus
M-phase	Mitosis phase
mRNA	Messenger RNA
N	NH2
NHEJ	Non- homologues end joining
NR3C4	Nuclear receptor subfamily 3, group C, member 4
N/S	Non silencing
NTD	N terminal domain
Oligo	Oligonucleotide
p53	Protein 53
PBS	Phosphate buffered saline
PCNA	Proliferating cell nuclear antigen
PGS	Protein G sepharose
PHD	Plant homeo domain
PI	Propidium iodide
PIN	Prostatic intraepithelial neoplasia
PIP	PCNA interacting peptide
PLK1	Polo like kinase-1
PMSF	Phenyl methane sulfonyl fluoride
PSA	Prostate specific antigen

QRT-PCR	Quantitative real time polymerase chain reaction
RNA	Ribonucleic acid
RTK	Receptor tyrosine kinase
S	Serine
SDM	Steroid depleted medium
SDS-PAGE	Sodium dodecyl sulphate polyacrylamide gel electrophoresis
SETD8	SET domain containing (lysine methyltransferase) 8
shRNA	Short hairpin RNA
siRNA	Small interfering RNA
Skp-2	S phase associated kinase protein 2
SPA	Scintillation proximity imaging assay
S-phase	Synthesis phase
SPR	Surface plasmon resonance
SRC	Steroid receptor coactivator
TBS	Tris buffered saline
TCF-4	Transcription factor-4
TEMED	Tetramethyl ethylene diamine
TMPRSS2	Transmembrane protease serine 2
TNM	Tumour, Node and Metastasis
TTBS	TBS Tween20
Ub	Ubiquitination
VEGF	Vascular endothelial growth factor

| Wnt | Wingless |
| WT | Wild type |

Table of contents

List of Figures

List of tables

1

Chapter 1 . Introduction

1.1. The prostate

1.1.1. *Function of the prostate*

In the adult male, the prostate gland is a pyramid-shaped organ weighing 30-40 g. About the size of a walnut, it lies below the urinary bladder and is located in front of the rectum in the pelvis. The base contacts the bladder and the apex contacts the urethra. The prostate is responsible for secreting a milky, alkaline fluid containing secretory proteins that help to nurture and protect the sperm as well as maintaining its viability and motility (Abate-Shen and Shen, 2000; McNeal, 2006a).

1.1.2. *Zonal anatomy of the prostate*

The prostate gland contains three major glandular regions which differ histologically and biologically: the peripheral zone, the central zone, and the transition zone (Figure 1.1)(McNeal, 2006b; Shah, 2012)

•**Transition zone:** forms about 5-10 % of the prostate volume, and surrounds the urethra between bladder neck and colliculus. A detectable increase in this zone volume occurs in benign prostatic hyperplasia (BPH) accompanied by lower urinary tract symptoms (LUTS) (McNeal, 2006a).

•**Central zone:** forms about 25 % of the prostate volume. The central zone forms a funnel (sagittal section) or ring-like (horizontal) zone that contains the ejaculatory ducts. This zone is relatively resistant to carcinoma and other disease (McNeal, 2006a).

•**Peripheral zone**: forms about 70 % of the prostate volume. The anterior fibromuscular stroma forms about 5 % of the prostate volume, and is located anterior to the urethra and extends into the transition zone (McNeal, 2006a).

There are also several important non glandular regions concentrated in the anteromedial portion of the gland. Each glandular zone has specific architectural and stromal features. In all zones, both ducts and acini are lined by secretory epithelium. In each zone, there is a layer of basal cells beneath the secretory lining, as well as interspersed endocrine-paracrine cells (Benninghoff, 1988).
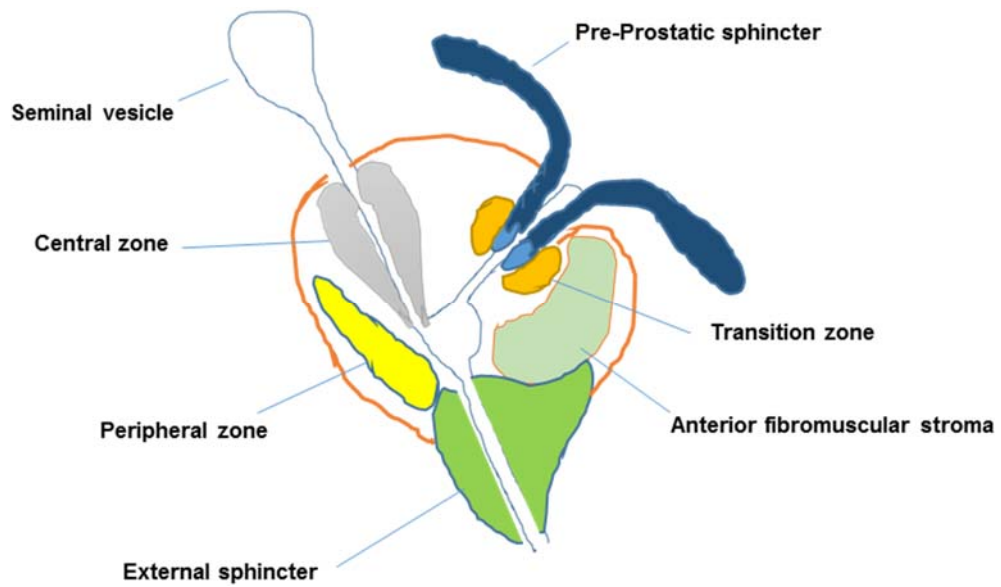
Figure 1-1 Zonal anatomy of the prostate gland. Schematic illustrating the anatomy of the human prostate, adapted from (McLaughlin et al., 2005).

1.1.3. *Histology of the prostate*

The prostate epithelium comprises the prostatic ducts with four cell types, including basal, secretory luminal, neuroendocrine and stem cells. The stromal part of the prostate consists of smooth muscle, vascular endothelial cells, nerve cells, fibroblasts, inflammatory cells, soluble factors and insoluble matrix (Josson *et al.*, 2010). The secretory luminal cells are androgen-dependent cells which are responsible for the secretion of the secretory proteins into the luminal duct. The basal cells are located between the luminal cells and the basement membrane, and although they are regarded as androgen-independent, they are thought to be the site of the putative prostate stem cells.

Following androgen deprivation therapy, stem cells are suggested to play a role in androgen independent prostate cancer (PC) growth and development (Richardson *et al.*, 2004). In the case of androgen dependent PC models, studies showed that androgen depletion will reduce the putative stem cells proportion in the tumour cells population, and with the progression of the disease into the androgen independent stage, the ratio of androgen- independent stem cells will be highly increased, and that androgen replacement prior to the progression of the disease might enhance the susceptibility of hormonal manipulation of the androgen dependent tumour (Hussain *et al.*, 2013).

Neuroendocrine cells are the third most common cell type of prostatic epithelium. Neuroendocrine cells have been regarded as part of the diffuse APUD (Amine Precursor Uptake and Decarboxylation) system, elements of which display epithelial, endocrine as well as neuronal characteristics with nerve-like dendritic processes. It also considered as androgen independent cells (Szczyrba *et al.*, 2016)(Figure 1.2).

Prostate specific antigen *(*PSA*)* screening test is used for detection of PC. *KLK3* is an androgen regulated gene encoding a serine protease that is a major prostate secreted protein that maintains fluidity in the seminal fluid. Serum PSA levels can be used as a tumour marker for PC. The age-specific cut-off PSA measurements recommended by the Prostate Cancer Risk Management Programme are as follows: aged 50−59 years ≥ 3.0 ng/ml; aged 60−69 years ≥ 4.0 ng/ml and aged 70 years and older ≥ 5.0 ng/ml, according to the referral guidelines for suspected cancer issued by NHS in 2005. However, a widespread controversy about PSA screening test has been developed (Hamdy *et al.*, 2016). Two large-scale randomized screening trials, the Prostate, Lung, Colorectal and Ovary (PLCO) cancer trial in the USA and the European Randomized Screening for Prostate Cancer (ERSPC) trial in Europe were done to assess whether screening reduces prostate cancer mortality. The age of the participants at enrolment varies by country between 50–74 years. A PSA test is the

principal screening method at all centres, and several centres also use digital rectal examination and/or transrectal ultrasound as additional screening tests. The results showed that organized screening reduces PC mortality but is associated with over diagnosis. Opportunistic PSA testing had little if any effect on PC mortality and resulted in more over diagnosis, with almost twice the number of men needed to be diagnosed to save one man from dying from PC compared to men offered an organized biennial screening program (Godtman *et al.*, 2015).
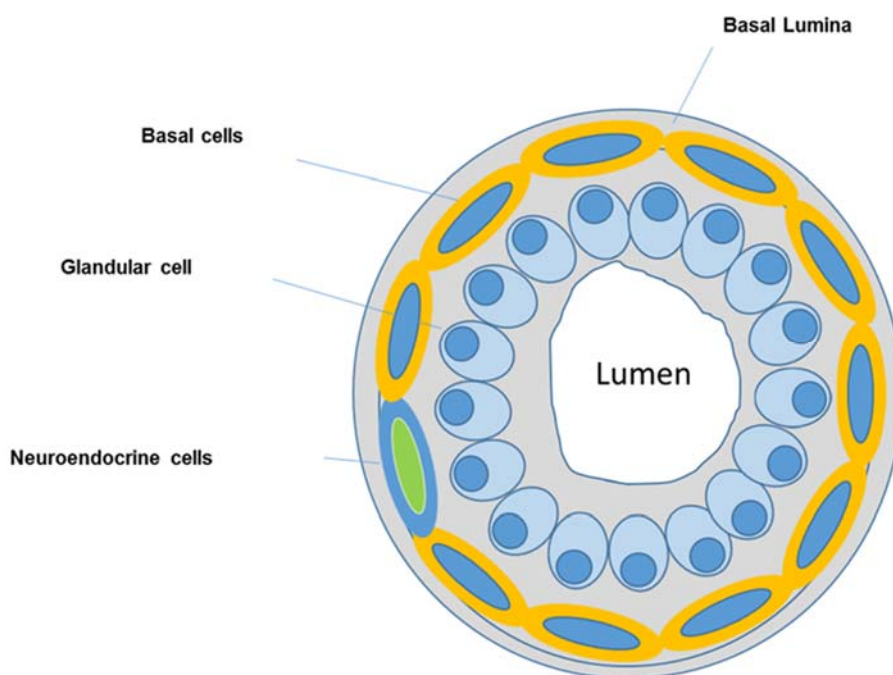
Figure 1-2 Schematic overview of cells in the prostate epithelium.

1.2. Androgen receptor

1.2.1. *Structure of androgen receptor*

The effect of androgen is mediated through the androgen receptor (AR) and plays a crucial role in controlling the embryonic development and adult function of the prostate, as well as growth of PC. AR is a transcription factor that regulates gene expression in response to its ligand in target cells. It is a member of the nuclear receptors superfamily of transcription factors (Shah, 2012; El-Amm, 2013; Gelman, 2002) and categorized as NR3C4 (nuclear receptor subfamily 3, group C, member 4) (Fang *et al*, 2003; Lu *et al.*, 2006). The AR gene is composed of eight exons that encode four functional domains (Shah, 2012; El-Amm, 2013):

- The NH2-terminal transactivation domain (NTD).

- The central DNA-binding domain (DBD)

- Hinge region.

- COOH-terminal ligand-binding domain (LBD).

The eight exons in AR encode a protein of ~919 amino acids (Koochekpour, 2010). The AF-1 and AF-2 transactivation domains are located in the NTD and the LBD respectively and are required for optimal transactivation (Figure 1.3) (Shafi *et al.*, 2013).

AR is expressed as two isoforms: the first is the predominant isoform B (110 kDa) and the second is the less dominant isoform A (~80 kDa). Additional novel AR splice variants have been described in androgen-insensitive PC cell lines designated as AR1, AR2, AR3, AR4, and A5A, AR6 (Hu *et al.*, 2009; Koochekpour, 2010) and androgen receptor splice variant 7 messenger RNA (AR-V7) which was identified in circulating tumour cells from patients receiving enzalutamide or abiraterone. Although multiple androgen-receptor variants have been discovered, AR-V7 is the only known androgen-receptor variant encoding a functional protein product that is detectable in clinical specimens (Antonarakis *et al.*, 2014). The amino acid length of the AR protein varies between individuals due to difference in the numbers of polyglutamine (for most men 19–25) and polyglycine repeats. The polyglutamine length has been inversely associated with AR transcriptional activity. Both repeats are encoded within exon 1 in the amino terminal domain. Higher levels of transcriptional activity in multiple cell types are a result of shorter glutamine repeats (Beisel *et al.*, 2002) (Figure 1.3).
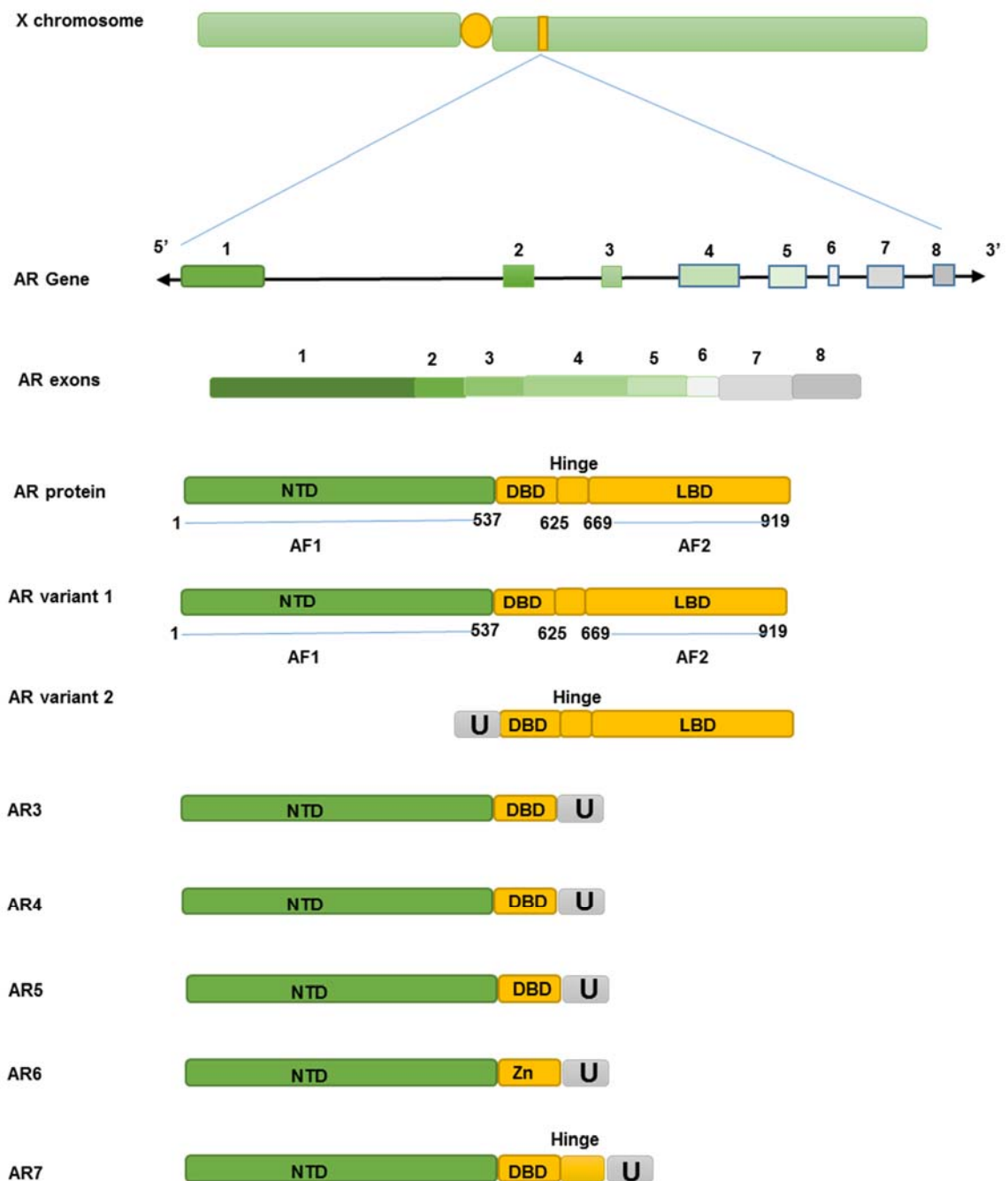
Figure 1-3 Schematic representation of the androgen receptor gene and protein, with indications of its specific domains and splice variants.U: unique N- or C-terminal sequence. Adapted from (Guo and Qiu, 2011; Lonergan and Tindall, 2011).

1.2.2. *Mechanism of action*

The majority of testosterone entering the cell is converted by membrane-bound enzyme 5α-reductase to 5α-dihydrotestosterone (DHT) in the cytoplasm. DHT is a more potent form of androgen that has a higher binding affinity for the AR (Feldman and Feldman, 2001). AR becomes detached from heat shock proteins (HSP) that were bound to prevent unnecessary activation of AR and to stabilise the receptor. AR then undergoes a conformational changes, dimer formation and nuclear translocation for subsequent DNA interaction.

There are different regions of the AR that are involved in dimerization. These include, DBD – mediated dimerization which facilitates AR binding to DNA elements known as androgen responsive elements (AREs) in target gene promoter and regulates transcription (Feldman and Feldman, 2001; Li and Al-Azzawi, 2009). AR (LBD and DBD) domains in addition to AR protein-protein interaction play an important role in the androgen regulated gene expression. AR protein-protein interaction is mediated by DBD interaction in AR homodimers, a process which usually follows an interaction between AR coactivator grooves in the LBD with the FQNLF motif in the N-terminal domain (N/C interaction) occurring in the cytoplasm, prior to DBD interaction, an initial step for nuclear N/C interaction (van Royen *et al.*, 2012).

In the nucleus, the AR dimer binds to AREs in the target genes and initiates the recruitment of a number of cofactors that are necessary for regulation of gene expression. AR transcriptional activity is controlled by the co-regulators which impact on AR binding capacity and ligand selectivity (Li and Al-Azzawi, 2009). The function of AR can be regulated by these co-regulators either by inhibiting (co-repressors) such as Calreticulin, Cyclin D1, HBO1, or promoting (co-activator) transcriptional activity such as ARA24, STUB1, NCOR2, ART-27, TF11F, Zimp, CBP, AES, TFIIH, STAT3, BRCA1, DAXX, BRCA2, SRC1, GSN, Rb, PIAS1, p300, ARIP4, ARIP3/PIASXa, ARA55/HIC-5, TRAP220, ARA70/NCOA4, TIP60, TIF2/GRIP1/SRC2, ARA54, AIB3/ASC-2, CYCLIN D1, ARA160/TMF1, NCOR1, AIB1/SRC3/ NCOA3. These co- regulators have a role in DNA modification at the promoter of target genes either directly by modification of histones or indirectly through the recruitment of chromatin-modifying complexes which also play a role in the recruitment of the basal transcriptional machinery (Heemers and Tindall, 2007; Li and Al-Azzawi, 2009) (Figure 1.4).
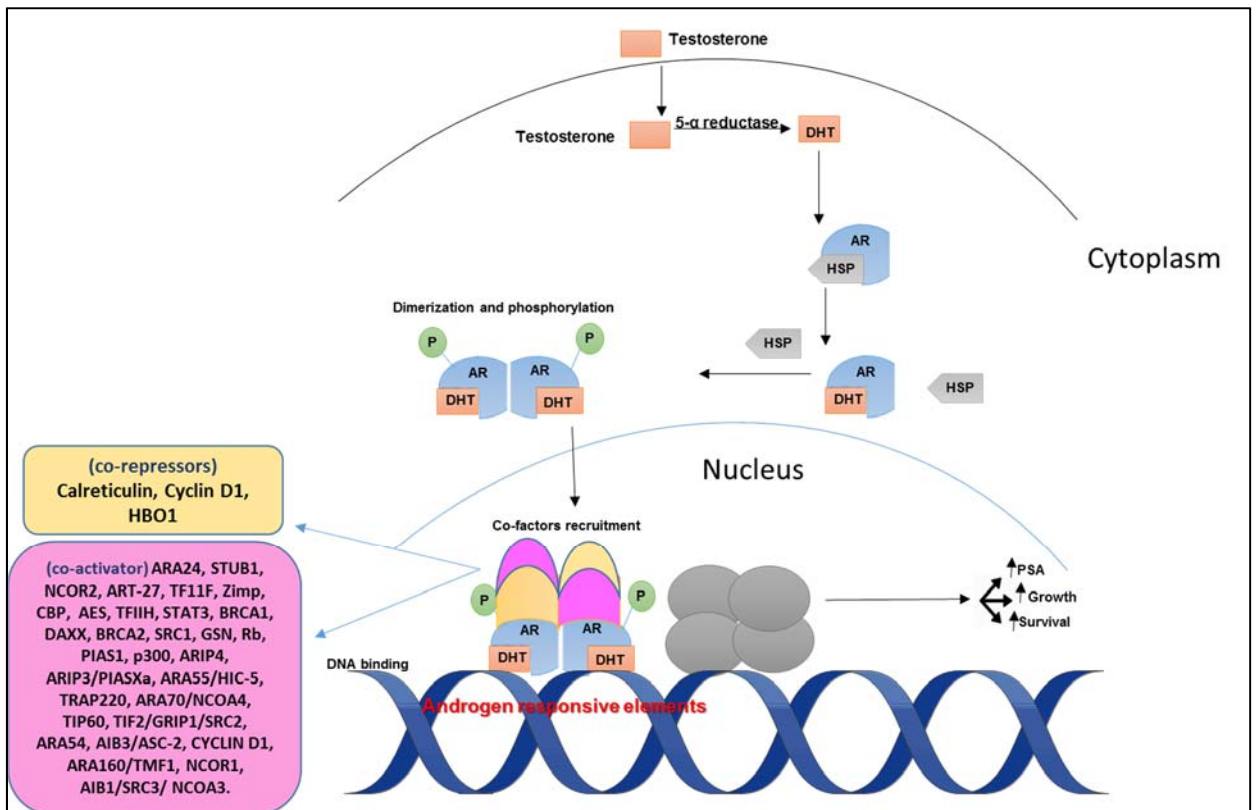
Figure 1-4 Mechanism of androgen receptor action. Testosterone is converted to DHT by 5-alpha reductase in the membrane of the cell. DHT then binds to the AR, HSPs dissociate, and conformational changes take place to allow homo-dimerization, phosphorylation and translocation into the nucleus where AR binds to sequences in the DNA, termed androgen response elements to activate transcription. Adapted from (Li and Al-Azzawi, 2009).

1.3. Prostate Diseases

1.3.1. *Benign prostatic hyperplasia (BPH)*

BPH is a pathological condition of the prostate that is caused by changes in the epithelial and stromal cells of the prostate, due to the effect of DHT on the aging prostate. BPH commonly arises in the transition zone and occurs in about 70 % of men over 70 years old. Increased pressure produced by increased stromal tissue content, which can reach up to 60 % of the prostate size, results in obstruction of the urinary flow and is considered as the major symptom of the disease (Foster, 2000). To prevent the disease progression, 5α-reductase inhibitors such as finasteride are often used to reduce the conversion of testosterone to DHT and thus the proliferative potential of the transition zone. In addition to this, selective α1-adrenergic inhibitors such as alfuzosin are used to relax the smooth muscle, thereby reducing the constriction of the urethra (Bechis *et al.*, 2014) (Figure 1.5.A).

1.3.2. *Prostatic Intraepithelial Neoplasia (PIN)*

Malignant transformation of cells is a gradual process which starts within benign cells which evolves into a malignant form. PIN is a pre-malignant condition of the prostate cells that has been defined as "neoplastic growth of epithelial cells within pre-existing benign prostatic acini or ducts." (Kim and Yang,2002). It is considered as the intermediate stage between benign epithelium and invasive carcinoma (Ayala and Ro, 2007). PIN can be identified histologically by the changes in the ductal structure as it becomes darker and thicker than the normal surrounding ducts with some intra-luminal growth abnormalities which can also be detected (Ayala and Ro, 2007).Three grades of PIN have been identified based on the histological changes that take place starting from low grade PIN to high grade PIN (HGPIN) (McNeal and Bostwick, 1986). As with PC, the severity and incidence of HGPIN is increased with age and they are both more likely to develop within the peripheral zone of the prostate (Ayala and Ro, 2007) (Figure 1.5.B).

1.3.3. *Prostate Cancer*

Adenocarcinomas comprise the majority (more than 95 %) of PC. Transitional cell carcinomas account for approximately 4.5 %, with the remainder being rare neuro-endocrine carcinomas or sarcomas (Kumar and Anderson, 2002; Swallow *et al.*, 2012). Prostate adenocarcinoma cells are characterised by enlarged, hyperchromatic nuclei with projecting nucleoli and profuse cytoplasm. In PC, the basal cell layer is frequently absent, while it is present in the normal glands and in BPH glands.

About 10% of PCs occur within the central zone, 20 % originate in the transition zone and 70% are found in the peripheral zone. High-grade PIN is associated with invasive PC in 80 % of cases, whereas low-grade has this association in only 20% of cases (Kumar and Anderson, 2002; Swallow *et al.*, 2012). PC can be classified histologically into 5 grades: Grade 1(only individual discrete well-formed glands), Grade 2 (predominantly well-formed glands with lesser component of poorly formed/fused/cribriform glands), Grade 3 (predominantly poorly formed/ fused/cribriform glands with lesser component of well-formed glands), Grade 4 (Only poorly formed/fused/cribriform glands or- predominantly well-formed glands and lesser component lacking glands - predominantly lacking glands and lesser component of well-formed glands), and Grade5 (lack of gland formation (or with necrosis) with or without poorly formed/fused/cribriform glands)(Epstein *et al.*, 2016) (Figure 1.5.C).

A

B

C
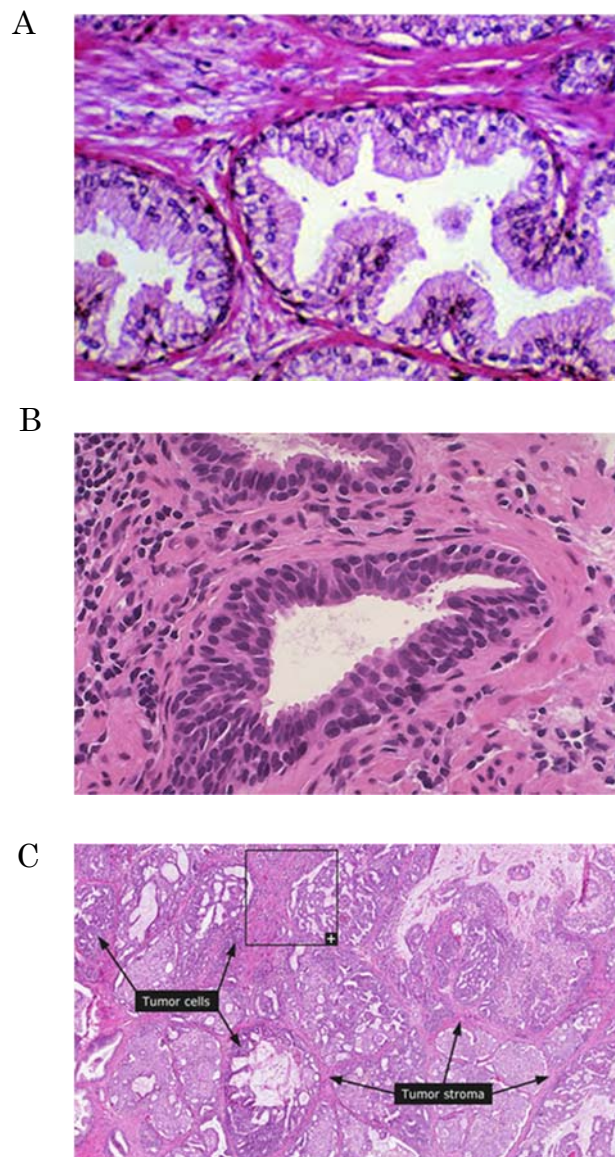
Figure1-5 Prostate diseases. (A)Benign prostatic hyperplasia (www.sciencephoto.com) (B)Prostatic Intraepithelial Neoplasia (library.med.utah.edu)(C) Prostate Cancer (www.proteinatlas.org).

1.3.4. *Castration resistant prostate cancer*

Although chemical or surgical castration, which can reduce serum testosterone levels to <50 ng/dl, has remained the most effective treatment for this disease for more than 60 years, recent studies indicate that PCs may generate intra-tumour androgenic steroids or become hypersensitive to low steroid levels through AR gene mutations or amplification of the AR gene supporting continued tumour growth. AR-regulated genes contribute in several cellular processes that participate in PC initiation and progression. For patients with advanced PC, blocking AR signalling through specific inhibitors such as bicalutamide (Casodex) and enzalutamide or by androgen deprivation with abiraterone has been utilized as standard treatments (Attard *et al.*, 2009; Cheng *et al.*, 2015).

In most patients the treatment is initially effective, but the diseases will develop into a lethal form that is known as castration resistant PC (CRPC). CRPC is characterized as showing an increase in serum PSA levels before the onset of additional symptoms (Andersen *et al.*, 2010).

The molecular mechanisms of castration resistance have been investigated recently and indicate that AR signalling continues in CRPC and plays an essential role in the progression of the disease (Sung and Cheung., 2013) The role of AR in CRPC is supported by research showing that the same genes which are elevated by androgens in androgen-dependent PC xenografts are also found increased in CRPC. This suggests that the AR in CRPC can be activated in the absence of testicular androgens and lead to recommencement of tumour growth (Sung and Cheung., 2013).

A recent study refers to the role of the glucocorticoid receptor (GR) in activation of a subset of target genes that is similar to those target genes of AR and maintenance of the resistant phenotype. AR mediated a negative feedback on GR, which was inhibited by the effect of anti-androgens and leads to up- regulation of GR. The study referred to the effect of using dexamethasone (GR agonist) in conferring enzalutamide resistance, while using GR antagonist to re-establish the sensitivity to enzalutamide. These findings may explain the continued expression of AR target genes which play a role in CRPC by GR activation acting as an AR mimic (Arora *et al.*, 2013).

Previously, MYB (a proto-oncogene protein, a member of the MYB (myeloblastosis) family of transcription factors) was found to interact with androgen-receptor (AR) in prostate cancer cells, and facilitates the nuclear localization of AR in a ligand-independent manner. It

additionally been suggest to play critical role in the CR progression of PC. Overexpression of MYB in mice models was found to significantly increased the tumour growth, while castration of the same mice models with overexpression of MYB have a slight effect of tumour growth (Srivastava *et al.*, 2016).

Additionally, a high-throughput genetic screen was performed to identify kinases that enable tumour formation by androgen-dependent prostate epithelial cells under androgen-deprived conditions. A mitotic-related serine/threonine kinase, NEK6, was identified as a mediator of androgen-independent tumour growth. Silencing NEK6 in CRPC cells was enough to restore the sensitivity to castration in a mouse xenograft model system. NEK6 was found to be overexpressed in a subset of human prostate cancers, and that NEK6 signalling was established as a central mechanism mediating castration-resistant prostate cancer(Choudhury *et al.*, 2016).

1.3.5. *Risk factors of prostate cancer*

There are many risk factors that could help to explain the high prevalence of PC. These factors are summarized as follow:

1. Family history (Agalliu *et al.*, 2013).

2. Diet (Kristal *et al.*, 2010).

3. Genetic and environmental factors (Virlogeux *et al.*, 2015).

4. Chemicals (Koutros *et al.*, 2013).

 5. Social status (Henry and O'Mahony, 1999).

1.3.6. *Treatment of prostate cancer*

There are a number of options for treatment of early stage PC: surgery, hormone therapy, radiotherapy, observation also known as active surveillance or watchful waiting (Postma, 2006), also chemotherapy (Figure 1.6.).

1. Radical prostatectomy: for elderly men with stable health conditions or young patients with more than 10 years life expectancy, surgical removal of the prostate gland is usually the most preferable treatment method (Henry and O'Mahony, 1999).Radical prostatectomy was

also suggested to reduce mortality among men with localized prostate cancer (Bill-Axelson *et al.*, 2014)

2. Hormone therapy: hormone therapy has been suggested as an adjuvant in combination with radiotherapy as it helps to increase survival rate of patients (Polkinghorn *et al.*, 2013).Depleting androgens involves the use of chemicals that interfere with the hypothalamic-pituitary-gonadal axis that controls prostate growth. The anterior pituitary gland is responsible for synthesis and releasing of luteinising hormone (LH) controlled by the hypothalamic luteinising hormone releasing hormone (LHRH) secreted in a pulsatile fashion. In the testis, the release of the testosterone by the Leydig cells is stimulated by the pituitary LH   (Feldman and Feldman, 2001). In the prostate, as previously mentioned, testosterone is reduced to DHT by the effect 5α- reductase. DHT then binds to the AR to induce transcription of androgen regulated genes to induce growth, proliferation and differentiation of PC cell. Therefore, LHRH agonists are used as one of PC possible therapies. However, the continuous administration of an LHRH agonist, which generally has substitutions of amino acids for glycine at six positions, increasing its affinity for the receptor and stability of binding makes LH release refractory to hypothalamic regulation. There is an initial rise in LH and testosterone levels, whilst LHRHR levels fall due to being continuously occupied; LH and testosterone levels begin to decline within three to four weeks. To prevent the initial flare in testosterone, either oestrogen or an anti-androgen pre-treatment can be used. LHRH agonists are considered as the standard of care in hormonal therapy because these agents have the potential of reversibility and enable the use of intermittent androgen-deprivation therapy (ADT), avoid the physical and psychological discomfort associated with orchiectomy, have a lower risk of cardiotoxicity than observed with diethylstilbestrol, andresult in equivalent oncologic efficacy) have been shown to lead to a survival benefit in men with CRPC (Henry and O'Mahony, 1999; Schweizer and Antonarakis, 2014).

Another aspect of hormone therapy of PC is by using of anti-androgens such as FlutamideTM and BicalutamideTM which competitively bind to the AR and prevent the activation of the receptor (Di Lorenzo et al., 2005), thereby inhibiting the effect of androgens.

Additional example of hormonal therapy of PC is Abiraterone acetate, which is a small molecular inhibitor that has been shown to have anti-tumour effects in CRPC. Castration is known to block gonadal testosterone generation. However, it has been suggested that androgens from non-gonadal sources drive the AR in CRPC. Abiraterone targets CYP17, a microsomal enzyme that has a key role in the synthesis of androgen by catalysing two

independent steroid reactions (Attard et al., 2008). Abiraterone has been shown to have significant anti-tumour activity in CRPC (Payton, 2012).

3. Radiation therapy: Radiotherapy is recommended if the tumour extends beyond the capsule or has invaded the seminal vesicle. It can be delivered in two forms:

* External beam irradiation: such as three-dimensional conformal radiation therapy which is suitable for fit elderly and young adult patients with more than 10 years life expectancy, it offers equivalent overall survival prospects to radical surgery (Henry and O'Mahony, 1999).

* Brachytherapy: implanting radioactive seeds into the prostate gland under CT scan or ultrasound guidance, these seeds remain *in situ* and give a permanent intense local dose of radiation (Henry and O'Mahony, 1999). It allows for delivery of high doses of radiation to the prostate with relatively minimal dose to surrounding normal tissues (Kumar *et al.*, 2016)

4. Active surveillance: usually suitable for older men, patients with advanced incurable disease and also patients with important co-morbidities. Presently, participants treated with active surveillance are selected based on specific criteria including localized disease, low *KLK3* level, and Gleason score of 6 or lower (Postma, 2006).

5. Chemotherapy: Cytotoxic chemotherapy is rising as an effective treatment method for men with PC. In 2004, two important Phase III studies showed for the first time that chemotherapy provided a survival benefits in patients with CRPC. Both studies utilised docetaxel-based regimens; docetaxel plus prednisone became the standard first line therapy of CRPC. As a result of these studies, many researchers have tested this agent both in combination with other established agents and with novel chemotherapeutic and targeted therapies (Petrylak, 2005). Furthermore, cabazitaxel has demonstrated its efficacy in patients pre-treated with docetaxel (Schweizer and Antonarakis, 2014). Another example is using mitoxantrone with a corticosteroid for patients with symptomatic hormone-refractory PC (SHRPC) which gives significant palliation with minimal toxicity. Estramustine can also be used combined with a variety of microtubular inhibitors (Gilligan and Kantoff, 2002).
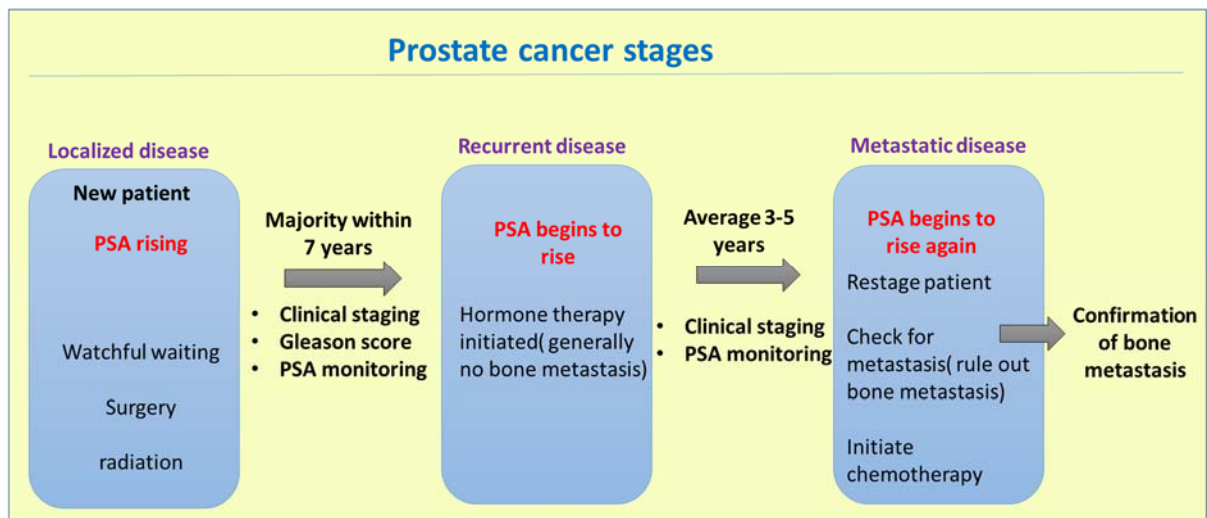
Figure 1-6 Treatment of prostate cancer with stages. Adapted from (www.medscape.org).

1.4. Mechanisms of androgen independence in PC

Various mechanisms can account for how PC can grow independently of androgens, these include:

1. Intra-tumour androgens: through *in situ* metabolism and synthesis of androgens to overcome the low levels of circulating androgen by increasing the activity of the 5-α reductase enzyme which is responsible for converting testosterone to DHT (Feldman and Feldman, 2001).

2. AR amplification and hypersensitivity pathway: AR gene amplification is thought to be one of the methods by which cells become hypersensitive to androgen. Androgen independent cells in CRPC have been found to be activated by about four times less DHT than androgen dependent cells due to increased AR expression and stability (Gregory *et al.*, 2001). Patients with AR amplification have been found to have a greater survival rate than those with non-AR amplified tumours, as they are found to better respond to second line total androgen blockade therapy (Palmberg *et al.*, 2000).

3. Promiscuous pathway: This could result from mutations in the AR LBD, that enable it bind to alternative ligands such as the AR antagonists flutamide and bicalutamide, or to progesterone to alternatively activate the AR. Gene amplification and point mutations have been frequently detected in PC and are associated with increased AR transcriptional activity and also correlate with tumour aggressiveness (Robinson *et al.*, 2015; Munkley *et al.*, 2016). Reducing its expression in PC cell lines decreases AR-dependent proliferation and inhibits the ability of AR either to activate or to repress target genes (Feldman and Feldman, 2001; Agoulnik *et al.*, 2006; Mitsiades, 2013).

4. Qualitative changes in the coregulatory components of the AR complex: AR coactivators and corepressors that modulate the transcriptional response can be dysregulated in cancer. For example, all three steroid receptor coactivators (SRC) of the p160 family (SRC-1, SRC-2, and SRC-3) have been reported to be overexpressed in PC. SRC3 located on human chromosome 20q21 is more frequently amplified while amplification of either SRC1 or SRC2 is rare in cancer (Xu *et al.*, 2009).

5. Activation of the AR complex by other signalling pathways (outlaw pathway): here AR can be activated independently of its ligand. In the absence of androgens, many factors have

been found to activate AR such as insulin, fibroblast and epidermal growth factors (IGF, KGF and EGF). In addition, receptor tyrosine kinases (RTKs) are also found to be correlated with the phosphorylation of AR by either the AKT (protein kinase B) or the mitogen-activated protein kinase (MAPK) pathways, producing a ligand-independent activated AR (Feldman and Feldman, 2001; Mitsiades, 2013) (Figure 1.7).
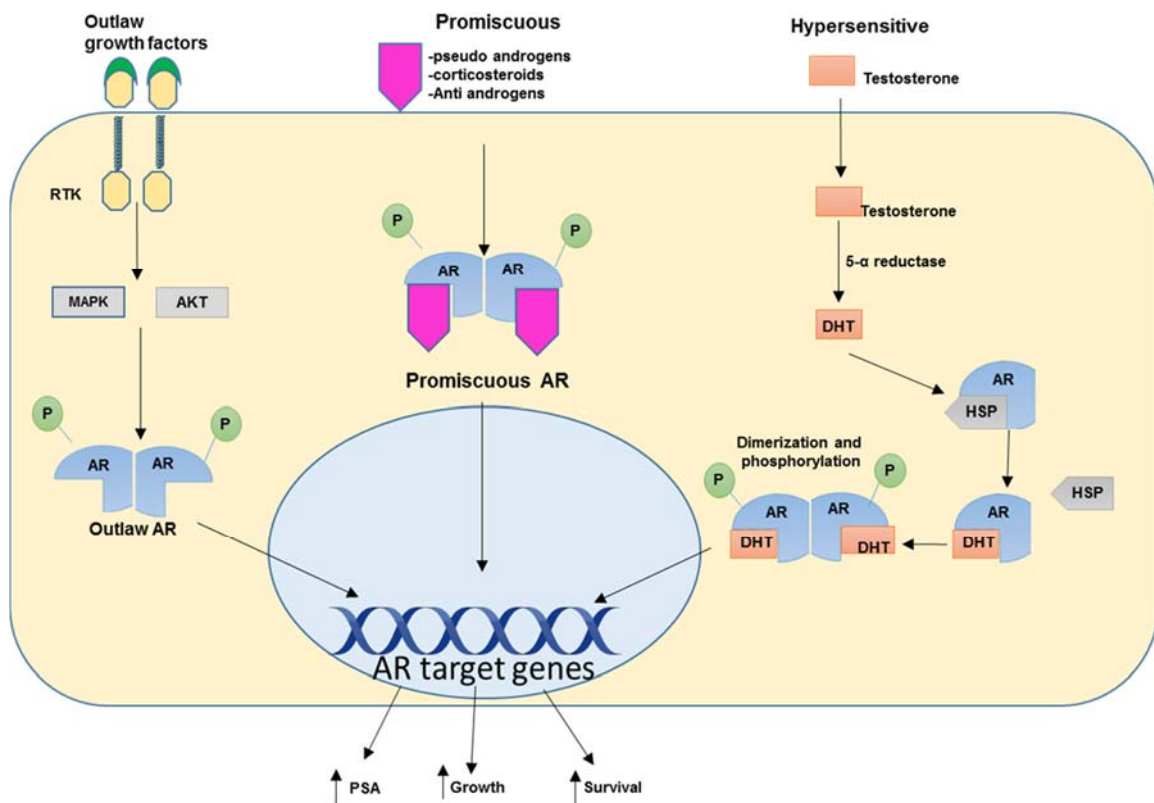
Figure 1-7 Mechanisms of androgen independence in PC. The hypersensitive pathway (AR gene amplification). The promiscuous pathway, the specificity of the AR is extended so that it can be activated by non-androgenic molecules. The outlaw pathway, receptor tyrosine kinases (RTKs) are activated, and the AR is phosphorylated by either the AKT (protein kinase B) or the mitogen-activated protein kinase (MAPK) pathway producing a ligand-independent AR. Adapted from Feldman and Feldman (2001).

1.5. Post-translational modification of the AR

The AR is regulated by a number of PTMs including: phosphorylation, acetylation, methylation, sumoylation and ubiquitination. These modifications impact the AR through various mechanisms such as, modulating AR stability, localisation, structure or the AR interacting partners (Gioeli and Paschal, 2012) (Figure 1.8).
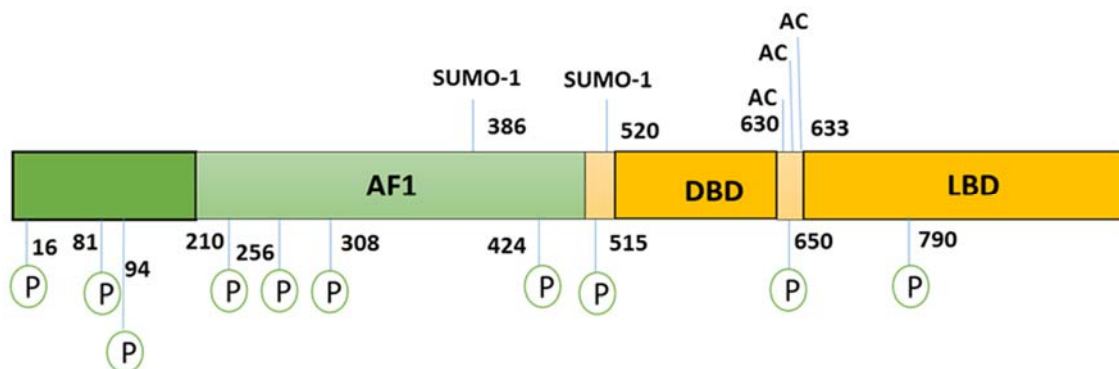
Figure 1-8 Androgen receptor post translational modifications sites. Adapted from: https://commons.wikimedia.org

- **Phosphorylation**

Phosphorylation of the AR plays an important role in regulating AR activity through increasing or decreasing protein interaction with AR domains (Gioeli and Paschal, 2012). The AR can be phosphorylated on serine, threonine and tyrosine residues by a number of kinases. For example, Cdk1, Cdk5 and Cdk9 mediate the phosphorylation of the AR on serine 81 (S81) which is known to be essential in regulating the activity and localisation of the AR. Considering both pARser81 and pARser213 in combination may serve as a prognostic biomarker for CRPC and potential novel therapeutic targets (McAllister *et al.*, 2016). Furthermore, AR phosphorylation at S256 and S308 are increased during AR nuclear localisation, whilst it is mainly phosphorylated at S94 when the AR is located in the cytoplasm. In addition to enhancing ligand-dependent activation, phosphorylation can enhance ligand independent activation of the AR which is mediated by the EGF family of receptor tyrosine kinases (Ferraldeschi *et al.*, 2015). Moreover, phosphorylation can also cause upregulated AR activation by increasing AR-co-activator activity or by modifying AR itself, mediated by Aurora Kinase A (Aurora A) and Cdk1(Gioeli and Paschal, 2012). De-

phosphorylation of the AR can be mediated by either altering the accessibility of the phosphosites or by the effect of Protein phosphatase 1 and 2A (PP1a, PP2A) which has been suggested to cause a site specific AR de-phosphorylation (Gioeli and Paschal, 2012).

- **Acetylation**

AR acetylation is also an important regulator of AR activity, a process that is mediated by p300 and p300/CREB binding protein (CBP)-associated factor at lysine residues K630, K632 and K633 within the KLKK motif. Furthermore, it has been suggested that AR acetylation is a key regulator of PC cell apoptosis and growth (Fu *et al.*, 2003). The AR undergoes de-acetylation by SIRT1 and the histone deactylases, HDAC1(Gioeli and Paschal, 2012).

- **Sumoylation**

Sumoylation is the covalent attachment of a small ubiquitin-like modifier (SUMO) through an iso-peptide linkage on lysine residues. This process is catalysed by three enzymes, E1, E2 and E3. AR sumoylation results in alteration in AR transcriptional regulation, nucleo-cytoplasmic localisation, DNA replication and repair, cell cycle, and apoptosis. Two sumoylation sites, K386 and K520, have been identified which reside in the AR NTD (Van der Steen *et al.*, 2013). Sumoylation of AR at its NTD weakens the interaction with LBD, a process necessary for transcriptional activation of AR (Coffey and Robson, 2012). AR sumoylation is mainly enhanced in the presence of androgen which would be explained by increasing the nuclear localisation of AR where the sumoylation enzymes are mostly present especially E1 and E2 (Coffey and Robson, 2012; Van der Steen *et al.*, 2013). The role of AR variants SUMOylation in CRPC are currently being investigated (Kounatidou and Gaughan, 2016)

- **Ubiquitination**

Ubiquitination is the process of covalently attaching a highly conserved small protein, ubiquitin (Ub) to the substrate protein. An isopeptide bond links the C-terminal glycine residue of Ub to a lysine residue in the target protein which could lead to substrate inactivation through proteasomal-mediated degradation. For example, AR ubiquitination by CHIP, SPOP and MDM2 marks the AR for proteolysis by the proteasome. In addition to protein stability, ubiquitination also regulates the activity of its substrate protein (Coffey and Robson, 2012; Van der Steen *et al.*, 2013). It is suggested that AR- Ub on androgen-responsive genes promoters may prepare the promoter for the subsequent transcription process (Coffey and Robson, 2012).

It has previously been suggested that resveratrol, a polyphenol with antioxidant properties, has anti-cancerous effects in PCa by inducing apoptosis and inhibiting cell proliferation, and might indeed regulate ARV7 protein levels via the ubiquitin degradation pathway in CRPC (Cavero, 2016).

Methylation

The most recently described PTM of the AR is the methylation process. It has been found that the AR can be regulated indirectly through histone methylations and de-methylation, a process that can regulate AR transcription (Coffey and Robson, 2012). Two lysine residues, K630 and K632 which are located in the AR hinge region are subject to methylation which overlap with the acetylation sites (Van der Steen *et al.*, 2013). SET9 has been described as one methyltransferase that catalyses AR methylation to facilitate N/C terminal domains interaction enabling the AR to interact with AREs in response to androgens. Moreover, SET9 regulates the chromatin structure at AR regulated genes to modulate AR transcriptional activity (Gaughan *et al.*, 2011; Ko *et al.*, 2011). Knockdown of SET9 results in reduced AR binding to its target gene promoter *KLK3* (Van der Steen *et al.*, 2013). Demethylation of the AR is mediated by the demethylase family members (KDM4A, KDM4B, KDM4C and KDM4D) which are considered as AR co-activators as demethylation of AR facilitates its acetylation at the same lysine residues (Van der Steen *et al.*, 2013). In addition, a histone lysine methyl transferase (HMT), KMT5A, was identified as a putative AR regulatory protein by siRNA library screening. (Coffey et al, un-published data).

1.6. KMT5A (SET8, Pre-SET7)
1.6.1. *KMT5A structure and isoforms*
SETD8, which is the gene that encodes the KMT5A protein, is located on chromosome 12q24.31. KMT5A is a member of the SET domain methyltransferase family that uses the cofactor S-adenosylmethionine (AdoMet) to catalyse the methylation of selected lysine residues in proteins. The SET methyltransferases were first discovered in *Drosophila* and took their name from the suppressor of variegation genes, **S**u (var)3-9, **E**nhancer of zeste and **T**rithorax (Couture *et al.*, 2005).

In particular, KMT5A is responsible for catalysing the majority of mono-methylation on histone H4 at lysine 20 (K20). Its specific function as a mono-methyltransferase is due to an evolutionarily conserved tyrosine residue in the enzymatic site of the SET domain, which hydrogen bonds with mono-methylated lysine residues, thereby inhibiting addition of further

methyl groups (guowei, 2002). Being a methyltransferase, KMT5A specificity to only mono-methylate H4K20 was explained by crystallographic studies, which referred to KMT5A recognition channel as being too narrow to accommodate tri-methylated species (Beck, 2012).

KMT5A protein consist of 393 amino acids (www.uniprot.org) comprising the following distinct functional domains (guowei, 2002):

- **The histone binding domain (HBD)**: located between residues 51-194 (Couture *et al.*, 2005; Yin *et al.*, 2008a).
- **The enzymatically active SET domain:** this conserved domain located between residues 195-393 (Couture *et al.*, 2005; Yin *et al.*, 2008a). The SET domain contains what is known as the inserted SET or iSET region in its structure. Both the sequence and the structure of iSET have a key role in determining the substrate specificity of the methyltransferase (Couture *et al.*, 2005).
- **Two PCNA integrated peptides (PIP) domains**: which target KMT5A for degradation during the S phase of the cell cycle. The PIP 1 box is located between residues 51-58, and the PIP 2 box is located between residues 178-185. When these regions are deleted KMT5A protein level is stabilised during S phase (Beck, 2012) (Figure 1.9).

KMT5A protein resolves as a doublet on standard SDS-PAGE. PCR in the human osteosarcoma derived cell line U2OS, revealed that there are two isoforms of KMT5A, produced by alternative splicing. In addition to the known isoform within *SETD8* exon 2, a second isoform for human KMT5A exist. The two isoforms are referred to as KMT5Aa and KMT5Ab (Abbas *et al.*, 2010b). The larger isoform is migrate as 42 kDa protein, and the second isoform is around 3 kDa smaller as it lacks the first 41 amino acids in the KMT5A N-terminus (http://www.uniprot.org/uniprot/Q9NQR1).
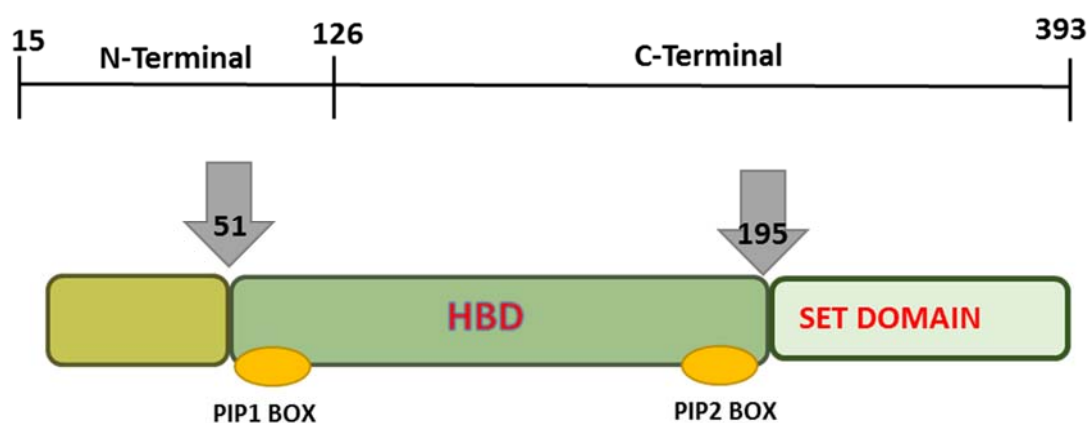
Figure 1-9 KMT5A protein structure. KMT5A consists of 393 amino acids and has two distinct functional domains; the histone binding domain (HBD) (residue 51-194) and the SET domain or enzymatic domain (residues 195-393). There are two PIP boxes in its structure located in the HBD. PIP 1 box located between residues 51-58, while PIP 2 box located between 178-185 amino acid residues, through which KMT5A is targeted for degradation.

1.6.2. *Post-translational modifications and regulation of KMT5A expression level*

The level of KMT5A fluctuates during the individual phases of the cell cycle. This regulation is seen at the protein level whereby protein destruction and stabilisation play key roles. Specifically, KMT5A is significantly increased during late S phase and the G2/M transition as the enzyme is specifically localized to mitotic chromosomes, then the levels of KMT5A decline during the transition to G1 (Rice *et al.*, 2002).

During M phase (specifically from prophase to metaphase), KMT5A becomes phosphorylated (Georgi *et al.*, 2002). The predominant site of KMT5A phosphorylation during mitosis is at serine 29 (S29). The cdk1/cyclin B complex recognizes a short conserved region containing a Cdk phosphorylation consensus sequence, to induce the S29 phosphorylation of KMT5A specifically in the transition from prophase to anaphase (Brustel *et al.*, 2011). Importantly, this phosphorylation event has two functional consequences. Firstly, phosphorylation of KMT5A results in its removal from mitotic chromosomes and relocation to the extrachromosomal space, subsequent to global accumulation of H4K20me1 in G2 phase. Secondly, phosphorylation of KMT5A stabilizes KMT5A levels by directly inhibiting its ubiquitination and degradation by the APC^{cdh1} E3 ubiquitin ligase (Wu *et al.*, 2010).

During early anaphase, it was found that KMT5A is dephosphorylated by the Cdc14 phosphatase resulting in anaphase promoting complex (APC^{cdh1})-mediated ubiquitination and degradation of KMT5A consistent with the observed decrease in KMT5A levels at G1 phase (Wu *et al.*, 2010).

It was previously reported that endogenous KMT5A levels during G1phase are sustained, although greatly reduced compared to G2/M until cells begin to transition through S phase (Wu and Rice, 2011). Prior to S phase at the G1/S transition, KMT5A is ubiquitinated by the SCF^{Skp2} ubiquitin ligase resulting in the degradation of KMT5A. SCF^{Skp2} remains active during DNA replication suggesting that it may also participate in KMT5A degradation during S phase (Yin *et al.*, 2008a).

KMT5A was recently reported to be recruited to DNA replication foci via interaction with the proliferating cell nuclear antigen (PCNA) and importantly, this recruitment was shown to be required for proper DNA replication (Wu and Rice, 2011). Interestingly, the KMT5A protein is virtually undetectable during S phase despite relatively high levels of KMT5A transcription indicating that KMT5A must be rapidly degraded following its recruitment to replication foci. Several reports demonstrate that the CRL4^{cdt2} ubiquitin ligase complex is specifically

responsible for the degradation of chromatin-bound KMT5A during S phase (Wu *et al.*, 2010).

Fluctuations in the level of H4K20me1 during the cell cycle, which peaks during mitosis appears to be consistent with the expression and localization of KMT5A. The resulting Lys-20 methylation can be preserved beyond a single round of cell division, suggesting that KMT5A imprints an epigenetic inscription in transcriptional silencing (Couture *et al.*, 2005) (Figure 1.10).
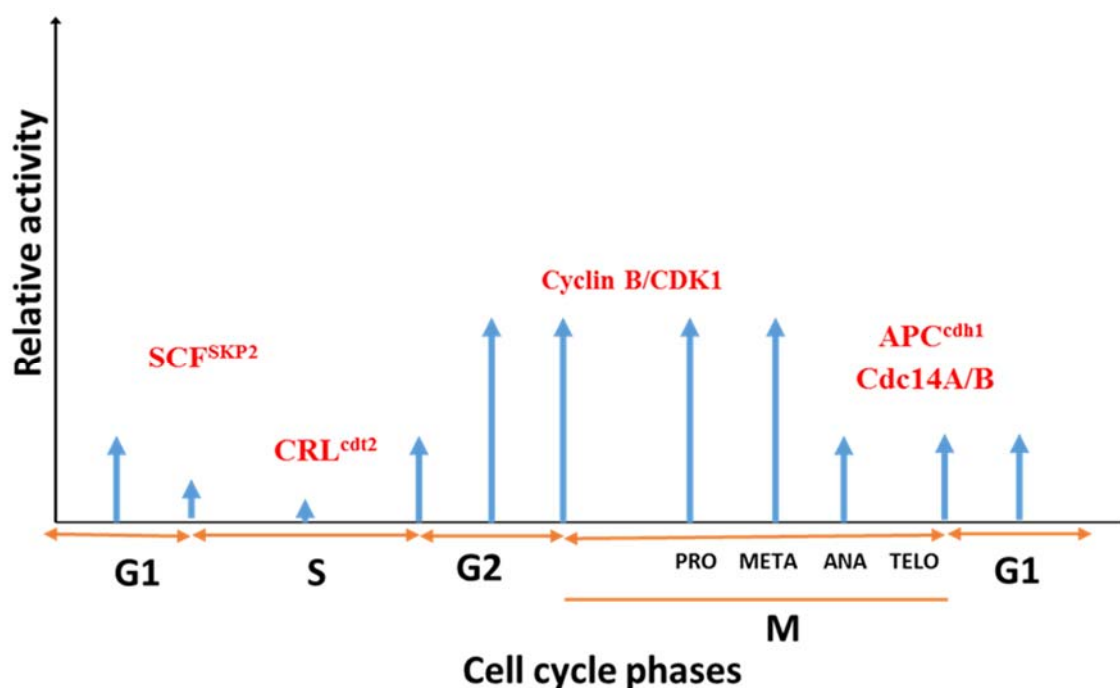
Figure 1-10 KMT5A levels of activity during cell cycle. KMT5A degraded by the SCFskp2 ubiquitin ligase to allow the entrance into S phase, which results in removal of KMT5A from chromatin. KMT5A degradation is mainly mediated by the CRLcdt2 ubiquitin ligase during S-phase to prevent DNA re-replication and defective chromatin condensation. Cyclin B/CDK1 then catalyse the increase in KMT5A expression for mitotic entry mainly at the transition between S and G2 phase. APCcdh1 catalyse KMT5A degradation to mediate a proper transition from metaphase to anaphase.

1.6.3. *Functions of KMT5A*

1.6.3.1. *Methylation of H4K20*

The specific mono-methylation of lysine 20 of histone H4 (H4K20) has been found in a large number of species, which would indicate that this methylation is an evolutionarily conserved process. This process plays an essential role in cell cycle dependent transcriptional silencing and mitotic regulation in metazoans (Couture *et al.*, 2005). The mono-, di- and tri-methylation of H4K20 is mainly catalysed by histone methyltransferases that belong to the SET domain family of proteins. However, Dot1 can also catalyse this activity although it is not a SET domain family member (Balakrishnan and Milavetz, 2010).

The main SET domain containing H4K20 methyltransferases are KMT5A (responsible for generating H4K20me1), Suv4-20 (Suv4-20h1/KMT5B), (responsible for generating H4K20me2) and Suv4-20h2/KMT5C (responsible for generating H4K20me3) (Fang *et al.*, 2002; Pannetier *et al.*, 2008).

In vivo studies suggest that the loss of KMT5A reduces the creation of H4K20me1 as well as subsequent methylated states, i.e. H4K20me2 and H4K20me3. This suggests that in order for enzymatic activity to be accomplished, the KMT5B and KMT5C methyltransferases require a template in the form of H4K20me1 for catalysing di- and tri-methylation (Balakrishnan and Milavetz, 2010).

Histone H4 inserts in the substrate-binding cleft of KMT5A as an extended parallel β strand, while, residues located N-terminal to Lys-20 in H4 are involved in an extensive array of salt bridge, hydrogen bond, and van der Waals interactions with KMT5A while the residues C-terminal to Lys-20 residues bind through mainly hydrophobic interactions. Mutational analysis of both histone H4 and the substrate-binding cleft indicated that interactions with residues in the N and C termini of the H4 peptide are important to produce the substrate specificity (Couture *et al.*, 2005).

KMT5A, independent of its methyltransferase activity, has also been suggested to play a part in creating a trans-tail histone code by recruiting a H3K4 methyltransferase to mark distinct regions of silent chromatin within the mammalian epigenome (Sims *et al.*, 2006). The histone methyltransferase KMT5A specifically mono-methylates H4K20 to maintain silent chromatin and effect chromatin compaction as a prerequisite for mitotic chromosome separation (Lee and Zhou, 2010), also the studies on KMT5A showed that it has a role in transcriptional silencing in metazoans (Couture *et al.*, 2005). In addition, Ash1, which is a multi-catalytic

histone methyltransferase, can methylate K20 in H4 and lysine residues 4 and 9 in H3. Transcriptional activation by Ash1 relates to methylation of these three lysine residues at Ash1 target gene promoters (Beisel *et al.*, 2002). Hence, there is still a debate in the field of chromatin biology about the preferential localization of this histone modification, despite the evidence of the distribution of these proteins throughout chromatin (Balakrishnan and Milavetz, 2010).

Lysine methylation can be reversed in humans by two demethylase families, firstly the Jumonji C and secondly the lysine-specific demethylase families. Deregulated expression observed for several histone demethylases in cancer and the regulatory role of histone demethylases in controlling the function of steroid receptors, including both the oestrogen receptor and AR, suggest a significant role in development and progression of tumours such as prostate and breast (Stratmann and Haendler, 2012).

1.6.3.2. *Methylations of non-histone proteins*

KMT5A catalytic activity is not restricted to histone proteins, as like many other methyltransferases, KMT5A can methylate non-histone proteins including:

p53

The tumour suppressor p53 is a key transcription factor induced in response to DNA damage and recognized as a binding partner for L3MBTL1 and as a methylation substrate of KMT5A. p53 is methylated on lysine 382 by KMT5A which is shown to inhibit the transcription of a number of target genes, including the CDK inhibitor, p21. In normal cell cycle conditions, this methylation is essential to inhibit the transcription of p21 and allow the cell cycle to progress (Jørgensen *et al.*, 2013). The inhibitory consequence of p53 methylation at K382 by KMT5A on p53 transcriptional activity can be explained by this specific methylation site being located within the binding site of L3MBTL1 (West *et al.*, 2010). p53 K382me1 has been found to be attenuated at the promoter of some cell cycle arrest and apoptosis genes, while it is enriched at the promoter of GADD45 (p53 dependent DNA repair genes), which may indicate a shift in the transcriptional program of p53 K382me1 toward DNA repair in tumour cells (Shi *et al.*, 2007).

Numb

Numb initially known as the determinant of cell fate in *Drosophila*, has four main isoforms (p65, p66, p70, and p71) which all contain a C-terminal proline-rich region (PRR) and an N-terminal phospho-tyrosine binding (PTB) domain. The differences between theses domains

are short sequence that may be present or absent in the PRR and/or PTB regions. KMT5A has been found to methylate Numb in its phospho-tyrosine-binding (PTB) domain, which leads to inhibition of p53-dependent apoptosis, while demethylation of Numb promotes p53-dependent apoptosis (Dhami *et al.*, 2013).

1.6.3.3. *DNA damage and repair*

Following the formation of a DNA double strand break (DSBs), which is one of the cytotoxic types of DNA damage that if improperly repaired may lead to oncogenic chromosomal rearrangement, the DNA damage repair (DDR) pathway is activated to recruit a number of proteins required for efficient DNA repair to take place. Previous studies have reported the role of KMT5A in the mono-methylation of H4K20 across the genome which is required for 53BP1 to bind to the chromatin. Following DNA damage, H4K20me1 has been shown to be associated with the accessibility of DNA damage foci for DNA repair proteins recruitment (Houston *et al.*, 2008). However, the mechanism by which this occur is not clear. Following DSB formation, the first event in DNA damage repair (DDR) is the phosphorylation of γH2AX at serine 139 by ATM, ATR, and DNA-PK. This is followed by MDC1 binding (a direct γH2AX reader) and RNF8 mediated ubiquitination of histones and non-histone proteins at the site of damage. In turn, this results in the recruitment of important repair proteins including BRCA1 and 53BP1. 53BP1 is one of the key factors found at DSBs as it acts as scaffold for other proteins to accumulate for non-homologous end joining (NHEJ) and DNA repair. The localization of 53BP1 to the DSBs is affected by several determinates including the ubiquitin signalling mediated by RNF8/RNF168, as well as H4K20 me1 (Dulev *et al.*, 2014). Notably, depleting KMT5A in embryonic stem cells leads to massive DNA damage and γH2AX foci formation (Oda *et al.*, 2009; Yu *et al.*, 2013).

Furthermore, KMT5A is required for DNA replication fork progression (Jørgensen *et al.*, 2007). KMT5A is recruited to DNA replication foci, via the interaction with PCNA, during S-phase, which is essential for proper DNA replication. KMT5A is also suggested to repress the genes required for DNA replication initiation, which would prevent S phase entry (Jørgensen *et al.*, 2007; Tardat *et al.*, 2007). This might be mediated by Chk1 as suggested by depletion of KMT5A by small interference RNA, which results in accumulation of the cells at S phase of the cell cycle (Oda *et al.*, 2009; Yu *et al.*, 2013).

1.6.3.4. *Epithelial-mesenchymal progression*

TWIST is a helix-loop-helix transcriptional factor that play a vital role in facilitating the epithelial-mesenchymal transition (EMT) but the molecular events leading to this are still not

fully understood (Yang *et al.*, 2012b). KMT5A is substantially associated with TWIST, and together are responsible for promoting EMT and facilitating the invasive potential of breast cancer cells both *in vitro* and *in vivo*. Interestingly, TWIST can also regulate AR expression via binding to E-boxes in the AR promoter region. Furthermore, silencing of TWIST induces cell-cycle arrest at the G1 phase and cellular apoptosis in the AR-expressing LNCaP cell line as well as castration-resistant LNCaP derivatives. Castration mediated oxidative stress causes Twist1 overexpression to promote AR expression which could result in the acquisition of castration resistance (Shiota, 2010).

In addition to the essential role of TWIST in moderating the behaviour of mesenchymal cells, Twist1 is also an oncogene in a number of aggressive tumours including gastric, liver and breast cancers. The oncogenic role of Twist1 to enable the pathological EMT of cells within a primary tumour similar to its function in development, and not by facilitating cell transformation. During EMT, tumour cells acquire properties to aid them to migrate away from the primary tumour, and then enter the blood/ lymphatic systems, and finally, settle into secondary tumour sites (Stratmann and Haendler, 2012).

Studies have shown that TWIST knockdown leads to reduced level of expression of N-cadherin which inhibited the migration rate of the PC cell line, PC-3 cells. In addition to promoting the hallmark changes associated with EMT, such as N-cadherin up-regulation and E-cadherin down-regulation, Twist1 also increases the angiogenic factor, VEGF in prostate and bladder cancers and Twist 1 level correlate with metastasis (Qin *et al.*, 2012).

KMT5A acts as a dual epigenetic modifier on the promoters of the TWIST target genes E-cadherin and N-cadherin through mono-methylation activity on H4K20. KMT5A expression is negatively correlated with E-cadherin and positively correlated with metastasis and the expression of TWIST and N-cadherin in breast cancer samples (Yang *et al.*, 2012b).

Metastatic PC cells have a particular preference to migrate to bone sites. The sensitivity of androgen independent PC cells to anticancer drugs was increased by down-regulation of Twist1. In addition, migration and invasion was suppressed, which may suggest inactivation of Twist1 as a potential strategy to control the growth and metastasis of these cells (Qin *et al.*, 2012).

1.6.3.5. *Chromatin compaction*

During cell proliferation, the accurate copying of the chromosomes usually occurs during S phase followed during meiosis by compaction of the chromatin, a process suggested to be controlled by changing in the activity of KMT5A during cell cycle progression (Brustel *et al.*,

2011). The expression levels of KMT5A are regulated by the E3 ubiquitin ligase CRL4^{Cdt2} which targets KMT5A on the chromatin for destruction, an event that is accompanied by DNA replication. KMT5A binds to the chromatin via PCNA where binding occurs at a specific degron sequence in KMT5A to results in a reduction of H4K20me1. Mutations in this degron result in premature chromatin compaction, H4K20m1 accumulation and G2 arrest (Centore *et al.*, 2010).

The precise mechanism for how KMT5A mono-methylates H4K20 is not fully understood, but possible mechanisms are derived based on nucleosome structural studies. One of the suggested mechanisms is particle contact between histone H2A and K20 on the H4 N-terminal tail to result in H4K20me1 affecting the chromatin structure. Another possibility is that H4-K20me1 mark is a binding site for chromatin condensation-related proteins, such as L3MBTL1 which can trigger local chromatin compaction in association with the mitotic chromosome, by interacting with methylated lysines on two close nucleosomes *in vitro* (Brustel *et al.*, 2011).

1.6.3.6. *Gene transcription*

The mono-methylation activity of KMT5A against H4K20 was always thought of as a transcription suppression process and many articles are supportive of this understanding. Analyzing of H4K20me1 associated genes on chromosome 21 and 22 in human cells showed an enrichment of H4K20me1 on the first half of gene bodies of specific genes. Regardless of basal expression levels of these genes, H4K20me1 was required to transcriptionally repress the expression of these genes (Congdon *et al.*, 2010).

However, another study suggested gene transcription activation by KMT5A mono-methylation activity on H4K20, especially in the canonical Wnt signaling pathway (Li *et al.*, 2011b). Wnt3a specifically stimulates H4K20 monomethylation at the T cell factor (TCF)-binding element through KMT5A. KMT5A is crucial for activation of the Wnt reporter gene and target genes in both mammalian cells and zebrafish. Additionally, KMT5A interacts with lymphoid enhancing factor-1 (LEF1)/TCF4 directly, and this interaction is regulated by Wnt3a. KMT5A was suggested to be a Wnt signaling mediator and is recruited by LEF1/TCF4 to regulate the transcription of Wnt-activated genes, possibly through H4K20 monomethylation at the target gene promoters. It also indicate that H4K20me-1 is a marker for gene transcription activation, at least in canonical Wnt signaling (Li *et al.*, 2011b)

1.6.3.7. *Cell proliferation and cell cycle progression*

Cell proliferation includes a number of events that are precisely regulated to ensure that the genome and its chromatin are replicated successfully in S phase, followed by condensation and segregation of the two sister chromatids in the newly formed daughter cells during mitosis. Any defect during this process may lead to DNA damage and may stimulate genomic instability as an early step of cancer development (Brustel *et al.*, 2011).

In addition to the fact that KMT5A expression levels are regulated during the cell cycle phases by specific factors, KMT5A presence and histone mono- methylation activity also play an essential role in cell cycle progression itself. For example, depleting KMT5A results in growth arrest due to increasing DNA damage and defective cell cycle progression in embryonic stem cells (Oda *et al.*, 2009). Both the presence of KMT5A and its enzymatic activity is important in maintaining cell cycle progression, mitosis, DNA replication, genomic stability and transcription (Beck *et al.*, 2012) (Table 1.1).

Table 1-1 KMT5A function

Repression	Activation
P53	DNA damage repair
E-cadherin	N-cadherin
	Chromatin compaction
	Gene transcription activation by KMT5A mono- methylation activity on H4K20, especially in the canonical Wnt signaling pathway
	RNA polymerase II
	ERα

1.7. KMT5A previous findings in the lab

Recently, a histone lysine methyl transferase (HMT), KMT5A, was identified as a putative AR regulatory protein by siRNA library screening. Upon further investigation it was discovered that KMT5A switches from an AR co-repressor to an AR co-activator upon acquisition of therapeutics resistance in a prostate cancer cell line model. Indeed, in LNCaP-AI cells, a model of androgen independence, it was observed that KMT5A knockdown could inhibit proliferation, AR association with the PSA enhancer and inhibit transcription of AR regulated genes. In LNCaP cells, a model of androgen dependence, KMT5A knockdown resulted in an enhanced level of KLK3 transcription after 48 hours of DHT stimulation. However, proliferation was still inhibited, probably due to the effects of KMT5A depletion on the cell cycle and DNA repair pathways (Coffey et al, un-published data) (Figure 1.11& 12). . Based on these observations KMT5A warrants further investigation as a potential therapeutic target in PC and will be the focus of this thesis (Figure 1.13).
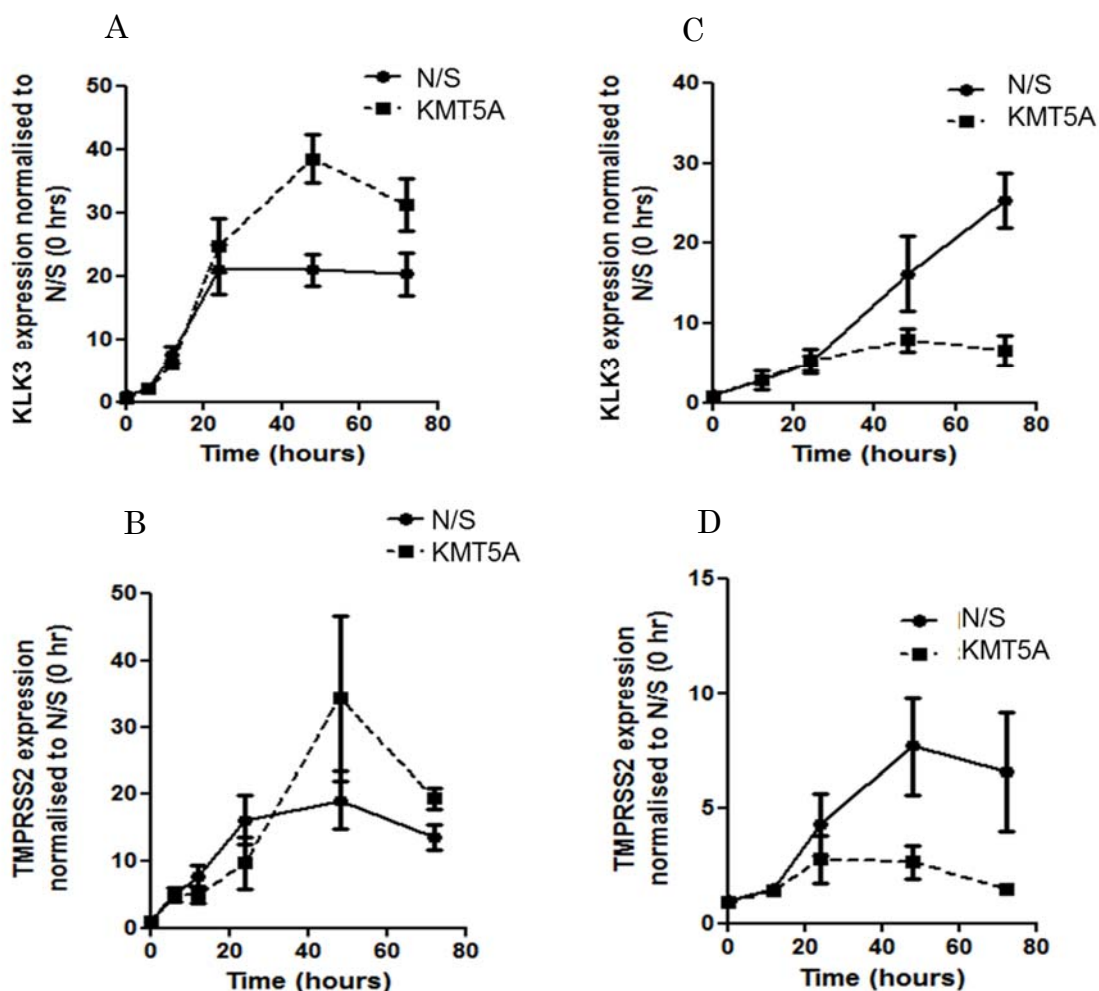
Figure 1-11 Androgen receptor target genes expression in the presence and absence of KMT5A. LNCaP (A, B) and LNCaP-AI (C, D) cells were reverse transfected with siRNA against KMT5A for 72 hours. RNA was collected and *KLK3* and *TMPRSS2* mRNA expression was determined by QRT-Error bar represents the mean ± SD for triplicate independent experiments. p-values were determined by t-test (* p-value <0.05, ** p-value <0.01, *** p-value <0.001 and **** p- value < 0.0001).
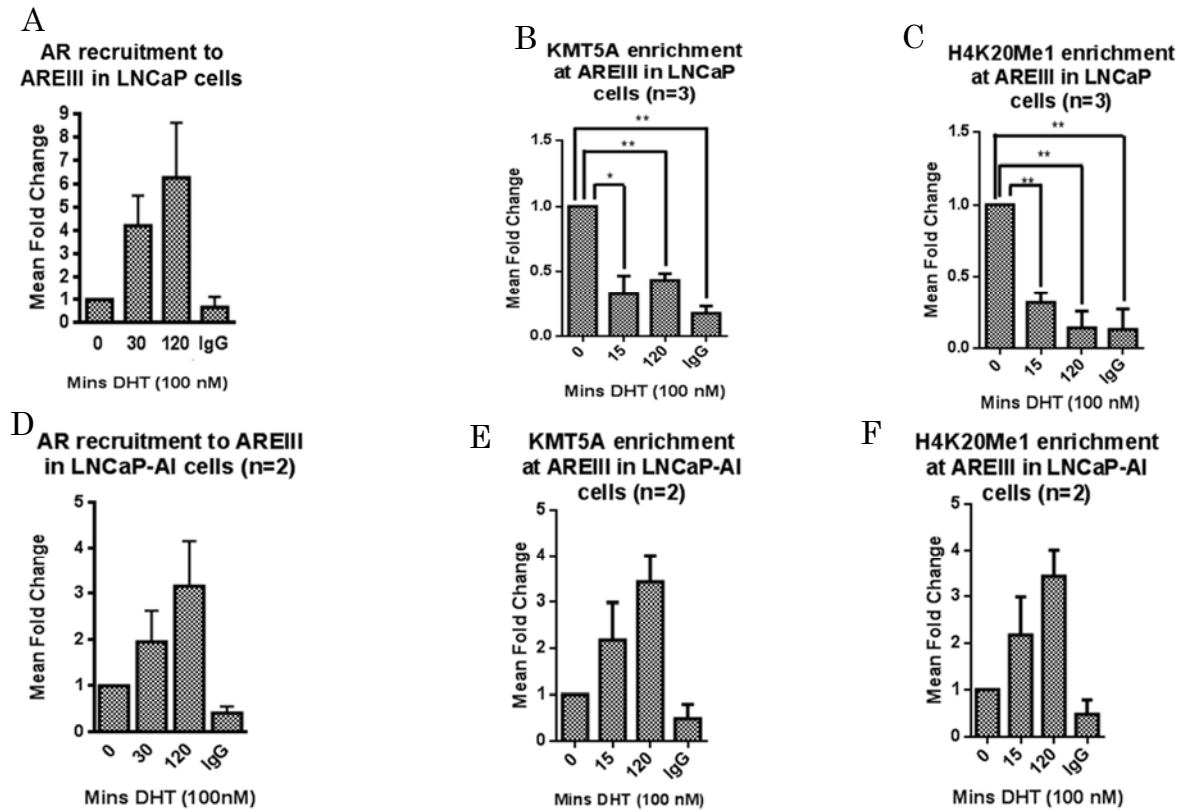
Figure 1-12 Androgen receptor, KMT5A and H4K20me1 enrichment at ARIII promoter. LNCaP (A, B, C) cells and LNCaP-AI (D, E, F) cells were starved in SDM for 72hours followed by DHT (100 nM) stimulation for 0, 15, 30 and 120 minutes. Chromatin immunoprecipitation assay was performed. Rabbit IgG was used as negative control. Results are expressed relative to the values of untreated samples. Error bars represent the mean ± SD for triplicate independent experiments.
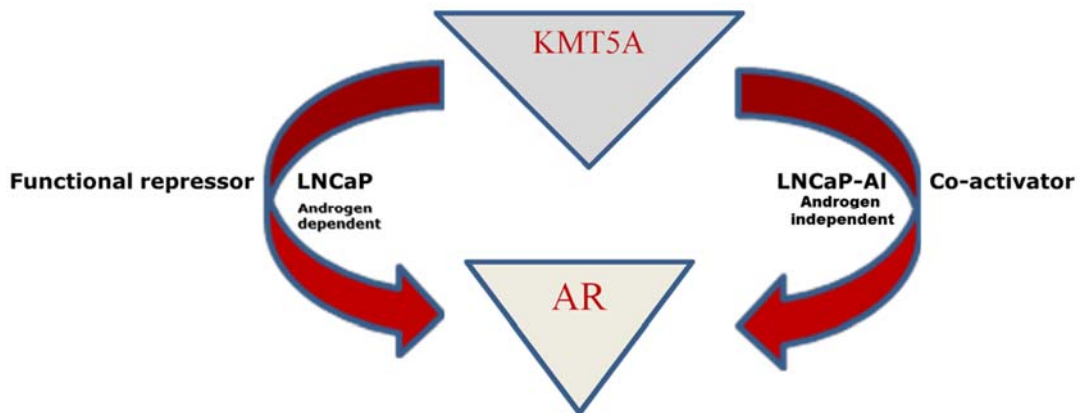
Figure 1-13 KMT5A activity in LNCaP and LNCaP-AI cell lines. KMT5A switches from an AR co-repressor to an AR co-activator upon acquisition of therapeutics resistance in a prostate cancer cell line model

1.8. Project aim

Due to the increasing interest in KMT5A as an important enzyme in itself and also the potentially important role it plays in regulating AR in PC, so this project is put together to:

- Identify KMT5A regulated genes and AR regulated genes that are modulated by KMT5A.
- Further investigate the relationship between KMT5A and AR.
- Validate selected target genes as selectively regulated by KMT5A and/ or AR.
- Investigate the possibility of using KMT5A target genes as biomarkers to determine the activity of KMT5A in aggressive PC, due to the fact that the activity rather than the presence is what required to be determined for KMT5A.
- Investigating the potential of targeting KMT5A therapeutically.

Chapter 2 . General Materials and Methods

2.1. Materials and Reagents

Chemicals that are regularly used in the lab were either analytical or molecular biology grade, unless otherwise stated. These chemicals were purchased from Merck Biosciences (Nottingham, UK), VWR International (Leicestershire, UK) and Sigma-Aldrich (Dorset, UK). Oligonucleotide primers were designed by National Centre for Biotechnology Information NCBI (http://www.ncbi.nlm.nih.gov/) and purchased from Sigma-Aldrich (Dorset, UK), and diluted with sterile distilled water to 1 µg/µl as a final stock concentration. Plastic-ware used in tissue culture was purchased from Corning (Surrey, UK) and Becton Dickinson (BD, Oxford, UK).

2.2. General Methodology

2.2.1. *Mammalian Cell Culture*

2.2.1.1. *Cell lines*

All cell lines used in this study were purchased from the American Type Culture Collection (Manassas, VA, USA). The androgen sensitive LNCaP cell line (Lymph Node Carcinoma of the Prostate) is considered as a model of androgen dependent PC which was derived from a 50 years old patient in 1977 from a left supraclavicular lymph node prostate carcinoma metastasis (Horoszewicz *et al*., 1980). LNCaP-AI, an LNCaP sub-clone, was used as a model of androgen independent PC. This was generated by the Solid Tumour Target Discovery (STTD) group at Newcastle University by continuous culturing of LNCaP cells in RPMI 1640 media supplemented with 10% foetal calf serum (FCS) that had been stripped of steroids by treatment with dextran-coated charcoal (SDM) (Rigas *et al*., 2007). All cell lines used in the project was authenticated by cell morphology and RNAseq as they have identified the known mutations in the parental cell line –T877A in the AR. AR gene was also fully sequenced in all the derivatives of the AR which confirmed their origin.

2.2.1.2. *Cell Passaging*

LNCaP cells were maintained in full medium (FM) (RPMI 1640 medium containing HEPES buffer (25 mM)), 10% foetal calf serum (FCS) and L-Glutamine (20 mM) at 37 °C in a humidified atmosphere of 5% CO_2.

LNCaP-AI cells were grown in steroid depleted medium (SDM) (RPMI 1640 10 % charcoal treated FCS at 37 °C in a humidified atmosphere of 5% CO_2. (Thermo Scientific HyClone, Logan, USA). Sub- confluent cells were passaged every 3-5 days. Medium was aspirated under sterile conditions and then the cells were washed with sterile phosphate buffered saline

(PBS). Cells were then trypsinised (1 x trypsin/ EDTA) for 3-5 minutes at 37 °C followed by neutralisation by adding the appropriate medium (FM, SDM) according to the cell line. Cells were then transferred to a new flask and incubated at 37 °C in a humidified atmosphere of 5% CO_2.

2.2.1.3. *Cryopreservation of cell lines*

Multiple stocks of all cell lines were cryopreserved for storage. After passaging the cells as mentioned above, cells were pelleted by centrifugation at 400 x g for 5 min followed by aspiration of all the supernatant and re-suspending the pellet with 1 ml of freezing medium (80 % FM, 10 % FCS, 10 % dimethyl sulfoxide (DMSO)) at 2-5 x 10^6 cells/ml. Cells were frozen at 80°C in cryovials. To re-culture the cells from cryopreservation, cells were defrosted at 37 °C and gently transferred into 10 ml of FM, followed by centrifuging at 400 x g for 5 minutes to create a cell pellet. The supernatant was then aspirated to remove any remaining DMSO and the pellet re-suspended in 10 ml of the respective medium, transferred to a new flask and incubated at 37 °C.

2.2.1.4. *Sulphorhodamine B (SRB) Assay*

Cellular proliferation and growth inhibition were determined by Sulphorhodamine B (SRB) assay, based on a protocol by Skehan *et al* (Skehan *et al.*, 1990). SRB dye binds cellular proteins, to reflect the number of cells in each well.

Cells were seeded out in 96 well plates and incubated at 37 °C for 7 days. Cells were then fixed with ice cold Trichloroacetic acid (TCA) at a final concentration of 10 % for 1 hour at 4 °C. Wells were then washed 4-5 times with tap water to remove any residual TCA and growth media. Plates were dried at 37 °C. Cells were then stained with 100 µl of 0.4 % SRB (a 1 % solution of SRB in 1 % acetic acid was prepared and then diluted to 0.4 % using 1 % acetic acid) and stored at room temperature for 30 minutes. Following this staining period, cells were then washed 5 times with 1 % acetic acid ensuring that all unbound dye is removed and left to air dry prior to the solubilisation of the dye in 10 mM Tris (pH 10.5) for 30 minutes with agitation. The absorbance was detected using a plate reader (Bio-Rad Model 680 Microplate Reader(Hercules, CA) at 570 nm (Skehan *et al.*, 1990).

2.2.1.5. *Cell growth*

Cell growth was assessed by cell counting using Incucyte Zoom live cell imager (Essen Bioscience). The IncuCyte® live-cell imaging and analysis system permits real-time, automated cell proliferation assays within tissue culture incubator. Cell proliferation was

observed by analysing the percentage of confluency of cells over time. As cells proliferate, the confluence increases. For this assay, cells were grown in 96 well plates (3000 cell/well for LNCaP cells and 3500 cell/well for LNCaP-AI cells) with 6 replicate well/plate and incubated in the Incucyte for 168 hours with 6 hours interval scan. Data were presented as the average fold difference in confluence relative to the control from three independent experiments.

2.2.2. *Gene Expression Analysis*

2.2.2.1. *RNA isolation*

All techniques were carried out under RNase free conditions using filter tips (Axygen) and Diethylpyrocarbonate (DEPC) treated water for all the required solutions.

Trizol® reagent (Invitrogen) a monophasic solution of phenol and guanidine isothiocyanate, which maintains RNA integrity whilst lysing cells, was used to isolate RNA from cells. Adherent cells were washed with 1x PBS then Trizol® (500 µl) was added and incubated at room temperature for 5 minutes following the manufacture protocol. Chloroform (200 µl) was added followed by centrifugation at 12000 x g for 15 minutes to separate the aqueous phase which exclusively contained the RNA. The aqueous phase was collected and Isopropanol (500 µl) was added to precipitate the RNA, during a 10 minutes incubation at room temperature. The precipitated RNA was then pelleted by centrifugation at 12000 x g for 15 minutes at 4 °C. Following a washing step with 500 µl of 75 % ethanol, and centrifugation at 7500 x g for 5 minutes, the RNA pellet was re-suspended in an appropriate volume of DEPC treated water. The concentration and purity of RNA was measured using a NanoDrop® ND-1000 UV-Vis Spectrophotometer (Labtech, East Sussex, UK. The concentration of the sample was calculated by the program using Beers law, and the integrity of the sample was assessed by the 260/280 ratio (the ratio of absorbance at 260 nm and 280 nm). Optimal 260/280 ratio for RNA is 2.0.

2.2.2.2. *Reverse Transcription*

Murine Moloney Leukaemia virus (MMLV) reverse transcriptase system (Promega, Madison, USA) was used for cDNA preparation. Complementary DNA (cDNA) was prepared by diluting 1 µg of RNA in the required volume of DEPC water to a final volume of 12.7 µl. RNA was incubated at 65 °C for 5 minutes to denature the secondary structure of RNA. A master mix of MMLV was prepared, containing 4 µl of 5 x reverse transcriptase (RT) MMLV Buffer, 2 µl of 4 mM dNTPs (dGTP, dATP, dCTP and dTTP) (Bioline, London, UK), 1 µl of 5 µM oligo (dT)[16] and 0.3 µl of MMLV reverse transcriptase enzyme. MMLV master mix

was added to each sample to make up a final volume of 20 µl and mixed well by vortex. Samples were incubated at 37 °C for 1 hour, followed by incubation at 100 °C for 5 minutes then transferred immediately to ice to inactivate the MMLV-RT enzymes. The cDNA was then stored at -20 °C until required.

2.2.2.3. *Quantitative Real Time Polymerase Chain Reaction (QRT-PCR)*

Following reverse transcription, standard cDNA, known to express the transcript of interest, was used to quantify relative amounts of cDNA produced in the PCR reactions. A fluorescent reporter (SyBr Green) was used to detect the amount of DNA template in the samples. SyBr Green intercalates with the DNA by binding to the minor groove of the double helix. Upon binding, SyBr Green fluorescence is enhanced significantly, which make it easier to be detected by real time PCR thermocycling. A 5 µl reaction master mix was prepared (2 µl of diluted cDNA, 2.5 µl of Platinum® SYBR® Green qPCR SuperMix-UDG plus ROX (Invitrogen, New York, USA), 0.2 µl forward and 0.2 µl reverse primer and 0.1 µl sterile distilled water), and loaded into a 384 well plate.

For the standard curve, sample cDNAs were diluted in sterile H_2O prior to use. A serial dilution of a sample known to express the gene of interest and included 7 dilution data points: 1, 1/5, 1/10, 1/50, 1/100, 1/500 and 1/1000. The same sterile H_2O used for cDNA dilution was loaded first on the plate as non-template control, followed by master mix loading, standard curve dilutions and finally the tested samples. Samples were run in triplicate on each plate. The plate was then sealed with a clear plastic cover and ran under the following PCR conditions: denaturation step 40 cycles of 95 °C for 15 seconds followed by annealing step with 60 °C for 1 minute then dissociation step which consisted of 95 °C for 15 seconds, 60 °C for 15 seconds and 95 °C for 15 seconds. Hypoxanthine phosphoribosyltransferase 1 (HPRT1) was used as a housekeeping gene to normalise expression levels. The absolute quantification method was used on an ABI 7900 sequence detection system (Applied Biosystems, UK) according to the manufacturers' instructions. A single peak in the resultant dissociation curve indicates the production of single product. Results were analysed using SDS 2.2 software (Applied Biosystems, Warrington), comparing expression with an endogenous control (Target/Control = normalised target value) (Normalised target value /calibrator normalised target value = relative expression).

2.2.3. *Protein Expression Analysis*

2.2.3.1. *Sodium dodecyl sulphate-polyacrylamide gel electrophoresis (SDS-PAGE)*

Cells were lysed in SDS sample buffer (0.125 M Tris-HCl, pH 6.8; 2 % SDS, 10 % glycerol, 10% β-mercaptoethanol, 0.005 % bromophenol blue) which was added directly to cells in the culture plate after washing with PBS to remove all traces of growth media. Cell lysates were then incubated at 100 °C for 10 minutes to denature proteins prior to electrophoresis.

Polyacrylamide gels were prepared by pouring a 12 % resolving gel (0.375 M Tris-HCl, pH 8.8, 0.1 % SDS, 12 % acrylamide:bisacrylamide mix, 1 % ammonium persulfate (APS) and 0.1 % N,N,N′,N′-Tetramethylethylenediamine (TEMED)) under a 6 % stacking gel (0.125 M Tris-HCL, pH 6.8, 0.1 % SDS, 6% acrylamide:bisacrylamide mix, 1 % APS and 0.1 % TEMED). Protein lysates (10-15 μl) were loaded alongside the Spectra™ Multicolor Broad Range Protein Ladder (Thermo Fisher Scientific) as a molecular weight reference. Samples were then resolved in reservoir buffer (25 mM Tris-HCl, 190 mM glycine, 0.1 % SDS) at 200 V for 45-60 minutes.

2.2.3.2. *Western blotting*

Following SDS-PAGE electrophoresis, protein were then transferred onto a Hybond C membrane (GE Healthcare, Wisconsin, USA) by electrophoresis in transfer buffer (25 mM Tris-HCl, pH 8.3; 0.15 M glycine, 10 % methanol) for 1 hour at 100 volts or overnight at 30 volts. Membranes were blocked in 5 % non-fat powdered Marvel™ milk in Tris- buffered saline (TBS-20 mM Tris-HCl, 500 mM NaCl) to block nonspecific antibody binding for an hour, followed by washing with 0.001 % Tween TBS (TTBS) for 10 minutes. The membrane was probed with the appropriate primary antibody overnight at 4 °C then washed with TTBS twice for 5 minutes then probed with the horseradish peroxidase HRP-conjugated secondary antibody at room temperature for 1 hour (Table 2.1). The antibodies were diluted according to optimized conditions in 1 % (w/v) Marvel™ diluent, α tubulin was used as a loading control. ECL reagents (1:1 from reagent 1 and 2) was then spread over the membrane and incubated for 1 minute (GE Healthcare), before being exposed to X-ray film (Fuji Film) for an appropriate length of time, before being developed using an automated MediPhot 937 developer.

Table 2-1 Western blot secondary antibodies.

Antibody	*Species*	*Catalogue number*
HRP-conjugated ***Rabbit anti-mouse***	Mouse polyclonal	DakoCytomation (P0260)
HRP- conjugated ***Swine anti-Rabbit***	Rabbit polyclonal	DakoCytomation (P0217)
HRP-conjugated ***Light chain Mouse*** ***Anti-rabbit***	Mouse polyclonal	Abcam (ab99697)

2.2.4. *Flow Cytometry*

Flow cytometry can be used to measures multiple features of individual cells that are flowing in single file in a stream of fluid through an illumination and light detection system. Light scattering at different angles can distinguish differences in size and internal complexity, whereas light emitted from fluorescently labelled antibodies can identify a wide array of cell surface and cytoplasmic antigens (Brown and Wittwer, 2000).

2.2.4.1. *Cell harvesting for Fluorescence-activated cell sorting (FACS) analysis*

Cells were harvested for DNA staining. Firstly, media from the wells was collected in a FACS tube (BD biosciences). Cells were then washed with 500 μl PBS (which was also retained for analysis) then detached from the well with 500 μl 1 x trypsin/EDTA. Trypsin was neutralised by adding the cells to the collected PBS and media. Cells were then pelleted by centrifugation at 2000 x rpm for 5 minutes and resuspended in 100 μl citrate buffer (0.25M

sucrose, 40 mM sodium citrate, pH 7.6). Cell permeabilization was achieved by using 0.74 % TritonX-100, cells were stained with 2.5 mg/ml propidium Iodide, and 100 µg/ml RNase. FACScan (BD Biosciences, California, USA) was used to analyse the samples which measures 10,000 events per sample.

2.2.4.2. *Data analysis*

Cyflogic software was used for data acquisition and analysis. Cells were gated on Forward Scatter versus Side Scatter to exclude cell debris and FL2-Width versus FL2-Area dot-blot was used to doublet discriminate to ensure only single cells were examined for cell cycle analysis.

2.2.5. *Immunoprecipitation*

In order to examine protein-protein interactions, immunoprecipation was used. Cells were washed with 1 ml PBS and scraped from the plate using cell scrapper, then pelleted by centrifugation at 400 x g for 5 minutes and lysed by adding 1 ml of lysis buffer (50 mM Tris pH 7.5, 150 mM NaCl, 1 mM phenylmethanesulfonylfluoride (PMSF), 1 mM dithiothreitol (DTT), 1 x complete protease inhibitor cocktail tablet per 10 ml, 1 % NP-40 alternative, 0.2 mM Na_3VO_4). The lysate was then transferred into Eppendorf tubes and incubated for 2 hours at 4 °C with rotation to enhance cell lysis. Meanwhile, the appropriate volume of Protein G Sepharose (PGS) (GE Healthcare, UK) was prepared by washing it 3 times with 1 ml of the lysis buffer prepared above, followed by a centrifugation at 14,000 x g for 3 minutes.

Debris was removed from the cell lysate by centrifugation at 14,000 x g for 3min and the supernatant transferred to a new tube. An input sample (100 µl) was taken from each lysate, mixed with 50 µl SDS sample buffer and stored at -20 °C until required for Western analysis. PGS (30 µl) was added to the supernatant and incubated at 4 °C for 2 hours with rotary agitation to preclear the samples. From the pre-cleared supernatant, half (450 µl) was taken for the IP reaction to which the appropriate primary antibody was added (2 µg), the remaining 450 µl was used as a negative control to which 2 µg of rabbit IgG antibody was added. Furthermore, 2 µg of the appropriate primary antibody was added to 450 µl of lysis buffer as an antibody only control. Following the overnight incubation period, 20 µl PGS was added to immunoprecipitate the protein-antibody complexes, and incubated at 4 °C for 1 hour with rotation to allow the target antigen to bind to the immobilized antibody. PGS beads were collected by centrifugation at 14,000 x g for 3minutes and the supernatant was discarded. Beads were then washed using 1 ml IP wash buffer A (PBS, 0.2 % Triton, 350 mM NaCl)

followed by two washes with 1 ml IP wash buffer B (PBS, 0.2 % TritonX-100). Beads were then resuspended in SDS sample buffer (40-80 µl). Samples were analysed by SDS-PAGE and Western analysis as described previously.

2.2.6. *Chromatin Immunoprecipitation (ChIP)*

Cells were seeded in 150 mm dishes to 50 % confluence, followed by 72 hours starvation in SDM. This starvation period is essential to diminish AR activity and to remove the AR from target gene promoters. Cells were then treated with dihydrotestosterone (DHT) according to the specific experiment (see specific materials and methods in each results chapter). Formaldehyde (1 % final concentration) was added to the medium for 10 minutes at room temperature in order to achieve protein-DNA crosslinks. Excess formaldehyde was neutralised by the addition of 125 mM glycine for 5 minutes at room temperature. Cells were then washed twice in warmed PBS to remove traces of medium and formaldehyde then scraped into ice cold PBS and transferred into pre-chilled tubes. Cell pellets were then generated by centrifugation for 10 minutes at 900 x g. Following the removal of the supernatant, cell pellets were then re-suspended in 400 µl lysis buffer (1 % SDS, 10 mM EDTA, 50 mM Tris-HCl pH 8.1, 1 mM PMSF, 40 µg/ml RNase (Sigma) and 1 x complete protease inhibitor cocktail tablet per 10 ml (Roche, Basel, Switzerland)) and incubated on ice for 10 minutes. Lysed cells were sonicated using a bioruptor coupled to a water cooler (Diagenode Inc. USA) for 3 pulses of 5 minutes '30 seconds ON and 30 seconds OFF' to shear the DNA. DNA-protein solutions were then centrifuged to remove cell debris and the chromatin was measured using NanoDrop® ND-1000 UV-Vis Spectrophotometer.

Chromatin was diluted by 10 fold using dilution buffer (20 mM Tris-HCl (pH 8.1), 150 mM NaCl, 1 % Triton-X 100, 2 mM EDTA, 1 mM PMSF, 1 x complete protease inhibitor cocktail tablet per 10 ml) in order to enable antibody-protein binding by reducing the concentration of the SDS. From the diluted chromatin, 100 µl was stored as an input sample at -20 °C.

In order to prevent any non-specific binding, the remaining chromatin solution was pre-cleared with 40 µl salmon sperm DNA/protein A agarose (Millipore, Massachusetts, USA) for 30 minutes at 4 °C, on a rotating wheel, to remove potentially reactive components from the diluted chromatin. Samples were then centrifuged at 2,500 x g for 5 minutes, and then pre-cleared chromatin solution supernatant was transferred to a fresh tube. ChIP grade antibodies were added to the pre-cleared chromatin (2-4 µg per 100 µg of chromatin) overnight at 4 °C on a rotating wheel to immunoprecipitate protein-chromatin complexes.

Following the incubation, antibody-protein complexes were precipitated by adding 50 µl of salmon sperm DNA/protein A agarose for 1 hour at 4 °C. Beads were then collected by centrifugation and washed with 1 ml of Buffer I [(0.1 % SDS, 1 % Triton-X 100, 2 mM EDTA, 20 mM Tris-HCl (pH 8.1) and 150 mM NaCl), followed by Buffer II (0.1 % SDS, 1 % Triton-X-100, 2 mM EDTA, 20 mM Tris-HCl (pH 8.1) and 500 mM NaCl), and then Buffer III, (0.25 M LiCl, 1 % NP40, 1 % sodium deoxycholate, 1 mM EDTA and 10 mM Tris-HCl (pH 8.1))], for 5 minutes at room temperature. Finally the beads were washed twice with TE Buffer pH 8.1 (10 mM Tris-HCl (pH 8.1) and 1 mM EDTA). Protein-DNA complexes were eluted at room temperature in 250 µl of elution buffer (1 % SDS and 1 mM NaHCO$_3$) for 20 minutes on a rotating wheel, and repeated, combining eluates.

All samples (including inputs) were incubated with NaCl (200 mM) overnight at 65 °C to reverse protein-DNA complex crosslinks. To digest the protein in the samples, proteinase K solution (40 µg/ml proteinase K (Qiagen), 10 mM EDTA and 40 mM Tris-HCl pH 6.5) was added to the samples for 2 hours at 45 °C. DNA was recovered using GenElute Mammalian Genomic DNA miniprep kit (Sigma) following the manufacturer's protocol and stored at -20 °C until analysis by QRT-PCR using primers designed against the promoters of interest.

2.2.7. *Cytoplasmic and Nuclear extraction*

Nuclear-Cytoplasmic extracts for Western blot analysis were generated using the Thermo Scientific™ NE-PER™ Nuclear and Cytoplasmic Extraction Kit (Thermo Fisher Scientific). Cells were pelleted by centrifugation at 400 g for 5 minutes and then re-suspended in 200 µl CER1 by vortexing vigorously for 15 seconds and then incubated on ice for 10 minutes. Ice cold CERII (11 µl) was added to the tube, and vortexed for 5 seconds then incubated on ice for 1 min followed by another mixing by vortex for 5 seconds. Samples were then centrifuged at 16000 g for 10 minutes at 4 °C to separate the cytoplasmic fraction according to the manufacture instructions. The supernatant (cytoplasmic extract) was transferred into a new pre-chilled tube and stored in -80°C until required. The insoluble pellet fraction was re-suspended with 100 µl of NER mixed by vortex for 15 seconds and placed on ice for 40 minutes. Samples were vortexed for 5 sec every 10 min. Samples was centrifuged at 16000 g for 4 °C for 10 minutes, and the supernatant (nuclear extract) then transferred into fresh pre-chilled tube and stored at -80 °C until used or re-suspended in SDS sample buffer and boiled at 100 °C for 10 minutes before being subjected to SDS-PAGE.

2.2.8. *General statistical analysis*

Statistical analysis was performed for the obtained data. To overcome the inter experimental variation fold changes of individual, experimental repeats were compared rather than raw data, and for the intra experimental variation, 3 independent experiments were minimally done for each data set. Student's t-test was used for data analysis. Student's t-test indicates whether two sets of data are statistically different. This test deals with the problems associated with interference based on small samples by the generation of p-value. When non-randomly selected two samples are compared, a paired test should be performed. For examples, compare two similar samples with and without treatment. P-value <0.05 is significant.

For microarray data, Samples were processed by oxford gene technologies (OGT) for microarray analysis using a direct hybridization Illumina HT12 v4 BeadChip Array. Functional clustering and annotation of genes featuring on lists presented in chapter 7 were performed using the online tool: Database for Annotation, Visualisation and Integrated Discovery (DAVID), v6.7. The DAVID software was used to analyse large gene lists and perform comprehensive clustering to outline genes with a similar function or biological theme. KEGG pathway analysis on steroid biosynthesis was included in the DAVID output.

Chapter 3 . Determining KMT5A regulated gene expression profiles in a cell line model representative of androgen-independent prostate cancer

3.1. Introduction

Histone methylation plays an important role in regulating chromatin compaction, and gene transcription. Histone methyltransferase enzymes catalyse the methylation process on the N-terminal tail of histone proteins in the nucleosome, and several of these enzymes are also implicated in the methylation of non-histone proteins (Ma *et al.*, 2014c). Loss of KMT5A reduces the level of mono-methylation at H4K20 and also impacts on the di and tri-methylation states as indicated by *in vivo* studies. This suggests that a methylated template in the form of mono-methylated H4K20 is required for the formation of subsequent di- and tri-methylation which is mediated by KMT5B and KMT5C, respectively (Balakrishnan and Milavetz, 2010). KMT5A has also been suggested to participate in creating a trans-tail histone code in cooperation with H3K9 methyltransferases to mark distinct regions in the silent chromatin of the mammalian epigenome (Sims *et al.*, 2006).

KMT5A (SET8, Pre-SET7), was first identified in 2002 (guowei, 2002) and is the sole histone lysine methyltransferase responsible for catalysing the mono-methylation of histone H4 on lysine 20, to regulate the global levels of H4K20me1. Deposition of H4K20me1 sustains chromatin silencing and compaction as a requirement for mitotic chromosome separation (Couture *et al.*, 2005; Lee and Zhou, 2010; Beck, 2012). KMT5A plays a role in numerous cellular processes including cell cycle progression (Abbas *et al.*, 2010b), DNA replication (Sims *et al.*, 2006) and DNA damage repair. In particular, recent evidence demonstrates the role of KMT5A during DNA damage repair (DDR) at double- strand breaks (DSBs), particularly in the non-homologous end joining (NHEJ) pathway, where it is required for the accumulation of 53BP1 at DNA break sites (Dulev *et al.*, 2014). It is also considered as an essential developmental gene, as deletion of KMT5A leads to early lethality of mice and Drosophila embryos (Lee and Zhou, 2010). Furthermore, KMT5A is over-expressed in a number of cancers and its expression positively correlates with metastatic potential (Yang *et al.*, 2012a).

In CRPC, androgen receptor (AR) signalling remains functional via numerous mechanisms hence the AR remains a viable therapeutic target (Sung and Cheung., 2013). The AR participates in controlling the expression of genes involved in the development and transformation of the prostate thorough association with a number of co-regulatory proteins that regulate the activation status of target genes following post-translational modification of the AR (Coffey and Robson, 2012). One such modification is lysine methylation of the AR (Gaughan *et al.*, 2011; Shang *et al.*, 2012). In order to regulate gene transcription, steroid receptors recruit a number of cofactors to form multi-protein complexes that assist in

modifying chromatin structure to enhance DNA accessibility for the transcriptional machinery. Methylation and demethylation are examples of these modifications that are mediated by a number of enzymes, which add or remove histone marks and consequently play an essential role in the regulation of gene expression (Stratmann and Haendler, 2012).

Recently, a study performed in our laboratory investigated the relationship between KMT5A and AR highlighting that KMT5A changes from an AR functional co-repressor in androgen-dependent LNCaP cells to become an AR co-activator in LNCaP-AI cell line that have acquired androgen-independent growth. Furthermore, depletion of KMT5A in the LNCaP-AI cell line, representative of androgen-independent PC, inhibits AR binding to the PSA enhancer. The study also indicated that there was a difference between LNCaP and LNCaP-AI cells in relation to the presence and activity of KMT5A at androgen regulated promoters. In LNCaP cells, KMT5A is present on AR regulated promoters in the absence of androgen but dissociates from promoters following DHT stimulation. However, in the LNCaP-AI cell line, KMT5A was found to be enriched on androgen responsive promoters in response to androgen stimulation (Coffey *et al.*, unpublished data).

The genes that are regulated directly by KMT5A and the interplay between KMT5A and AR to modulate transcriptional output of downstream targets requires further investigation in both androgen-sensitive and castrate-resistant models of prostate cancer.

The aims of this chapter are:

1. To identify genes that are regulated by KMT5A.
2. To determine genes that are regulated by both the AR and KMT5A, and genes that are regulated by KMT5A independently of the AR.
3. To validate selected target genes as selectively regulated by KMT5A and/ or AR.

3.2. Specific Materials and Methods

3.2.1. Cell lines

LNCaP and LNCaP-AI cells were used in this study as detailed in Chapter 2.1.1.

3.2.2. Antibodies

A number of primary antibodies were used to detect protein expression by Western blotting (Table 3.1).

Table 3-1 Antibodies used for Western blotting.

Antibody	Species	Catalogue number
KMT5A	Rabbit	Cell Signalling (2996)
PSA	Mouse	BioGenex MU014-UCE
a-Tubulin	Mouse	Sigma

3.2.3. Primers

To detect the expression of individual genes at the mRNA level, specific primer sets were used (Table 3.2).

Table 3-2 Primers used for QRT-PCR.

Genes	Forward Primer (5'-3')	Reverse Primer (5'-3')
KMT5A	GATCCCAGGCGGTGACAGAG	CCCGGTAAATACGTTCTCCCC
HPRT1	TTGCTTTCCTTGGTCAGGCA	AGCTTGCGACCTTGACCATCT
KLK3	TCGGCACAGCCTGTTTCAT	TGGCTGACCTGAAATACCTGG
CDC20	TCGCATCTGGAATGTGTGCT	CCGGGATGTGTGACCTTTGA
HIST1H2BD	TAACTTTGCCAAGGGAGAGACA	AGCAAACCAGGATGAGT
YIPF1	GTGGACACCTACCAGGTCTT	ACGTCTTCTCTCCCAGATGGA
CDC42EP3	CGGCGGCCGGTTTGT	TTTGCGAAGATCTGAGCCCT
KIF22	GCCCCTACAGCTAATTCAGGA	GAAAAGGCGGAGTGAGGAGAC
RAB4A	GCCGAGAAACCTACAATGCG	GGTCCAGCTCACCTGATTCG

3.2.4. Small interference RNAs

In order to achieve KMT5A depletion, specific siRNAs were used (Table 3.3).

Table 3-3 Small interference RNAs for KMT5A knockdown in the microarray study.

siRNA	Sense sequence	Anti-sense sequence
Non-silencing (NS) (1022076) (Qiagen	UUCUCCGAACGUGUCACGU	ACGUGACACGUUCGGAGAA
KMT5A#1	CCAUGAAGUCCGAGGAACA	UGUUCCUCGGACUUCAUGG
KMT5A#2	GATGCAACTAGAGAGACA	UGUCUCUCUGUUGCUC

3.2.5. Agilent Bioanalyzer 2100

Total RNA was extracted from LNCaP-AI cells using Trizol® reagent (Invitrogen) with DNase treatment as detailed in Chapter 2.2.1. The integrity and purity of total RNA were assessed using Agilent Bioanalyzer 2100.

3.2.6. Illumina Human HT-12 arrays

The Human HT-12 v4.0 The HumanHT-12 v4 Expression BeadChip content provides genome-wide transcriptional coverage of well-characterized genes, gene candidates, and splice variants, delivering high-throughput processing of 12 samples per BeadChip without the need for expensive, specialized automation. The BeadChip is designed to support flexible usage across a wide-spectrum of experiments. Each array on the HumanHT-12 v4 Expression BeadChip targets more than 47,000 probes.The arrays report probe intensity levels which represents the level of expression of a gene against which a particular probe is targeted. Array processing, normalization, and quality control checks were performed using the R package 'Lumi'. Probe intensity values were converted to VSD (variance-stabilized data) using variance stabilizing transformation. The robust spline normalization (RSN) was used as the array normalization method. Outlier samples, poor quality probes (detection threshold <

0.01), and probes that were not detected at all were removed prior to downstream analysis. The remaining probes (21,111) normalized intensities, VSD were used in the differential expression analysis. Differential expression analysis was performed using the R package 'Limma', and p values were adjusted to control the false discovery rate (FDR) using the Benjamini–Hochberg method.

3.3. Results

3.3.1. Identification of an KMT5A regulated gene expression profile

3.3.1.1. Optimisation of DHT dose

The microarray experiment in this study was designed to detect the expression profile of KMT5A regulated genes and also those genes that are regulated by the AR, as well as genes modulated by KMT5A alone. In order to do so, a DHT titration experiment was initially performed in LNCaP and LNCaP-AI cell lines over a time period of 24 hours to select the dose of DHT to be used for subsequent experiments. Both LNCaP and LNCaP-AI cells were grown in SDM for 72 hours prior to DHT treatment in order to diminish AR activity and to deplete the AR from target gene promoters. For the androgen treatment, a 10 fold serial dilution series of DHT was used ranging from 10 nM to 10^{-5} nM. Following 24 hours DHT treatment, RNA was isolated and the expression of the AR regulated gene, *KLK3,* was assessed by QRT-PCR (Figure 3.1.A-B).

From the above experiment, 10 nM DHT was observed to cause a statistically significant ($p \leq 0.05$) increase in *KLK3* expression ~30 fold in the LNCaP cell line and ~75 fold in the LNCaP-AI cell line. Consequently, 10 nM DHT was selected as the dose to be used for stimulation of AR activity in both cell lines for the subsequent experiments as shown in Figure 3.1. Secondly, DHT time course experiments (0, 16, 24, 48, 72 hours) were performed in both cell lines using 10 nM DHT treatment to determine the optimal duration of AR stimulation in both cell lines. *KLK3* expression was determined by QRT-PCR in response to the experimental conditions (Figure 3.1.C-D).

The data showed a rapid and significant increase in *KLK3* expression in LNCaP cells ($p \leq 0.05$) that peaked at ~400 fold after 24 hours followed by a gradual reduction over the remaining time points of the experiment as the AR ubiquination started and affecting the enrichmen of AR at its target gene promoters such as *KLK3*, which was agreed with previously mentioned data about *KLK3* expresssion in LNCaP cells in response to AR stimulation (Figure 3.1.C) (Coffey et al, unpublished data). (Figure 3.1.C). In LNCaP-AI cells there was a gradual but

significant (p≤0.05) increase in *KLK3* expression that peaked at 72 hours, with a ~2000 fold increase (Figure 3.1.D). From this experiment, 24 hours of DHT stimulation at a dose of 10 nM was selected for the subsequent gene profiling experiments in both the LNCaP and LNCaP-AI cell lines, to detect genes that are primarily regulated by the AR and also modulated by KMT5A depletion in both PC cell lines.
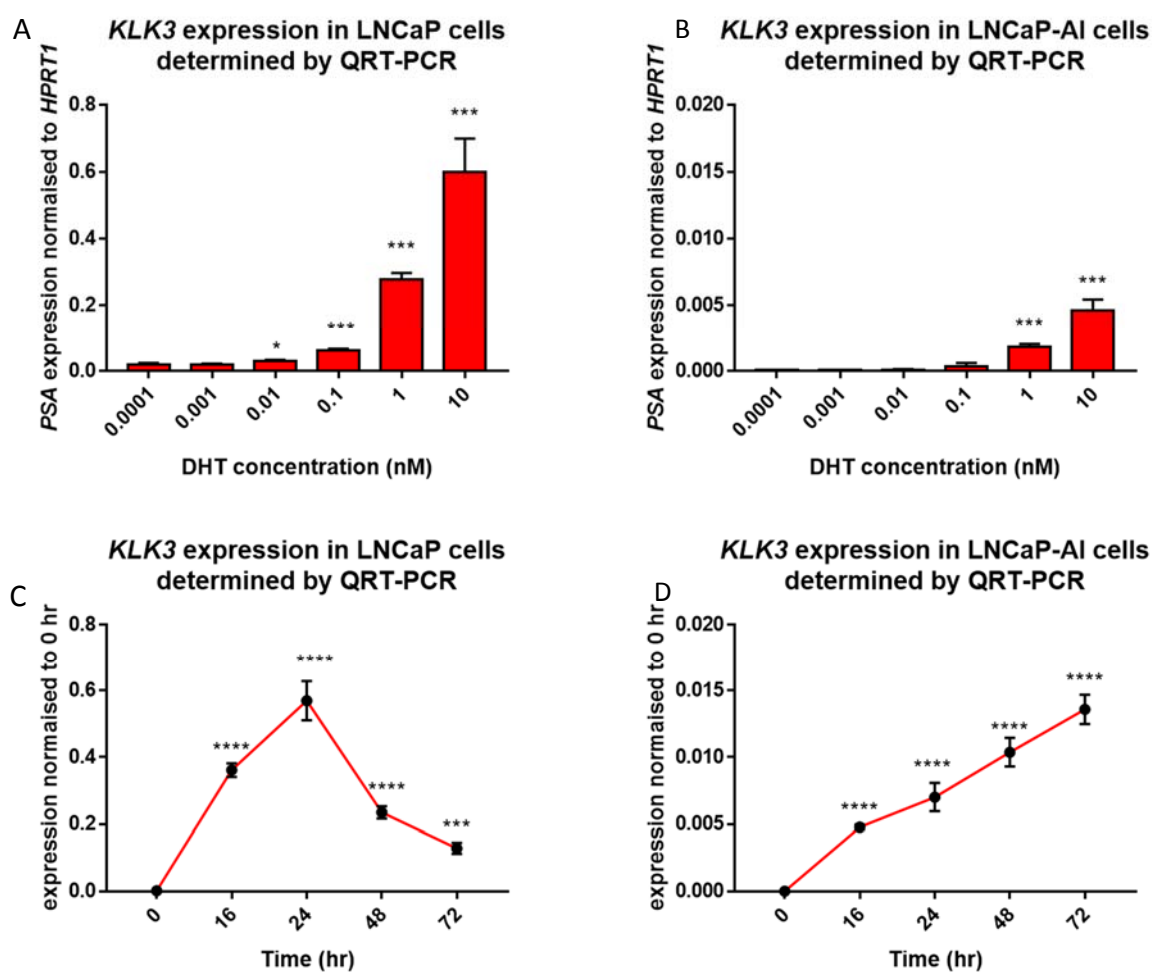
Figure 3-1 *KLK3* expression levels in response to DHT treatment in LNCaP and LNCaP-AI cells. (A) (B) Cellular response to increasing doses of DHT. Cells were grown in SDM for 72 hours prior to DHT treatment. A 10 fold serial dilution of DHT ranging from 10 nM to 10^{-5} nM was added for 24 hours and expression of KLK3 determined by QRT-PCR. (C) (D) Cells were grown in SDM for 72 hours followed by 10 nM DHT treatment for different periods (0, 16, 24, 48, 72 hours). RNA was collected and KLK3 expression levels were detected by QRT-PCR. Error bars represent the mean ± SD for triplicate independent experiments. p-values were determined by t-test (* p-value <0.05, ** p-value 0.01, *** p-value <0.001 and **** p- value < 0.0001).

3.3.1.2. Depletion of KMT5A in PC cells

In order to determine the genes that are regulated by KMT5A depletion and those genes which are under AR regulation but are also modulated by KMT5A depletion, KMT5A knockdown was performed by reverse transfection in SDM for 72 hours using 2 independent KMT5A siRNA sequences, to further confirm the data obtained, (Table 3.3) followed by 10 nM DHT stimulation for 24 hour. Non-Silencing (N/S) siRNA was used as a negative control. RNA was isolated and *KMT5A* knockdown and *KLK3* expression were assessed by QRT-PCR using primers detailed in Table 3.2. The data was normalised to the N/S control. The data showed a significant reduction of ~ 60-80 % in *KMT5A* expression (p≤ 0.05) in KMT5A depleted samples compared to the N/S samples in both DHT treated and untreated arms (Figure 3.2.A). *KK3* expression was significantly increased in the N/S control in the DHT treated arm by ~4 fold compared to N/S control. There was also a significant increase in *KLK3* expression most notably with KMT5A siRNA#1 by a further ~2 fold following DHT treatment compared to N/S control (p≤ 0.05) (Figure 3.2.B). KMT5A knockdown and *KLK3* induction was also confirmed at the protein level by Western blotting in LNCaP cells (Figure 3.2.C).

The same experimental conditions were applied in LNCaP-AI cells. The data showed a statistically significant reduction of ~80 % in *KMT5A* expression (p≤0.05) for the KMT5A depleted samples by both siRNAs compared to the N/S control (Figure 3.3.A). *KLK3* expression was significantly increased in response to DHT stimulation ~15 fold in N/S control which was further enhanced by KMT5A depletion and was most evident for siRNA#1 showing a further ~3 fold increase in response to DHT treatment compared to N/S control (p≤ 0.05) (Figure 3.3.B). The knockdown was also confirmed at the protein level by Western blotting in LNCaP-AI cells (Figure 3.3.C) using the same experimental conditions as shown in Figure 3.2.C.

PSA protein expression was also examined by Western blotting. Due to the very low levels of PSA expression in the LNCaP-AI cell line, the sensitivity of the Western blotting was insufficient to detect the PSA protein.

A

KMT5A expression in LNCaP cells determined by QRT-PCR

B

KLK3 expression in LNCaP cells determined by QRT-PCR

C

KMT5A knockdown confirmation in LNCaP cells
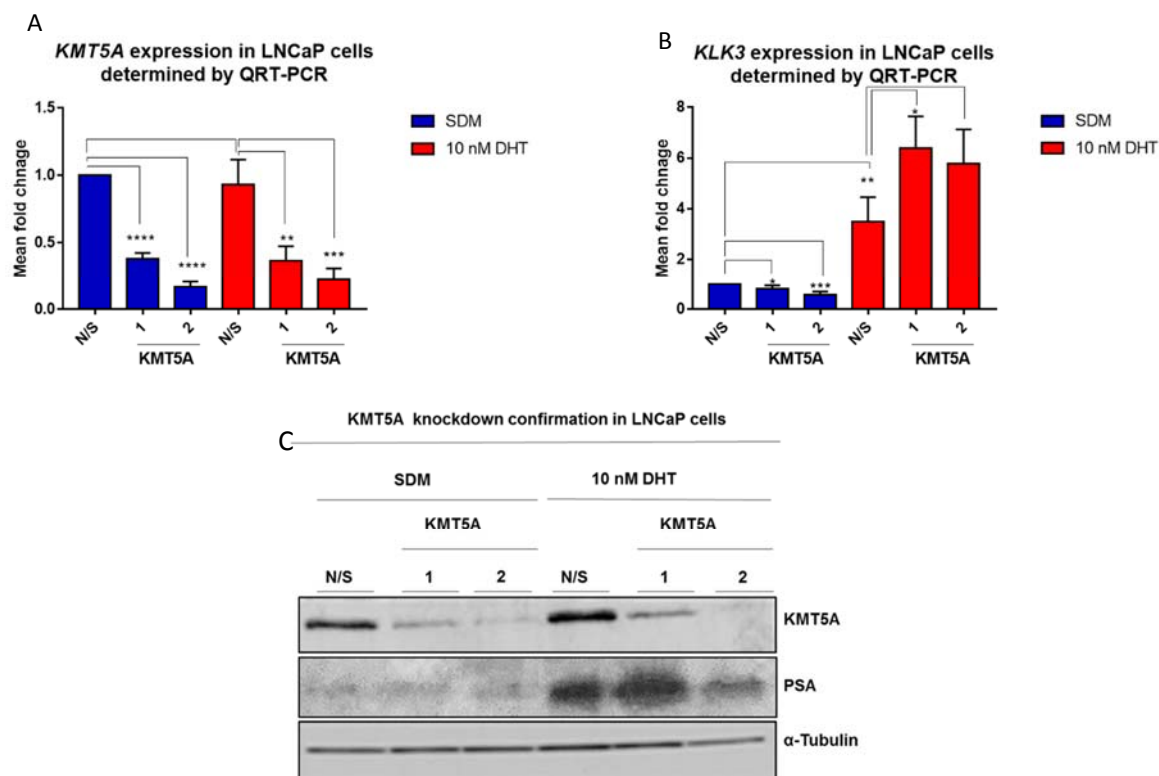
Figure 3-2 KMT5A knockdown confirmation in LNCaP cells and the effect on PSA expression. LNCaP cells were reverse transfected with Non- silencing siRNA or the two selected KMT5A siRNAs for 72 hours in SDM followed by either stimulation with 10 nM DHT or vehicle control for 24 hours. RNA and protein was collected and depletion of KMT5A was confirmed. (A) KMT5A mRNA expression and (B) KLK3 mRNA expression were compared to respective expression for the N/S 0 hour time point (C) KMT5A and PSA protein expression in LNCaP cells were determined.   Error bars represent the mean ± SD for triplicate independent experiments. p-values were determined by t-test (* p-value <0.05, ** p-value <0.01m, *** p-value <0.001 and **** p- value < 0.0001).
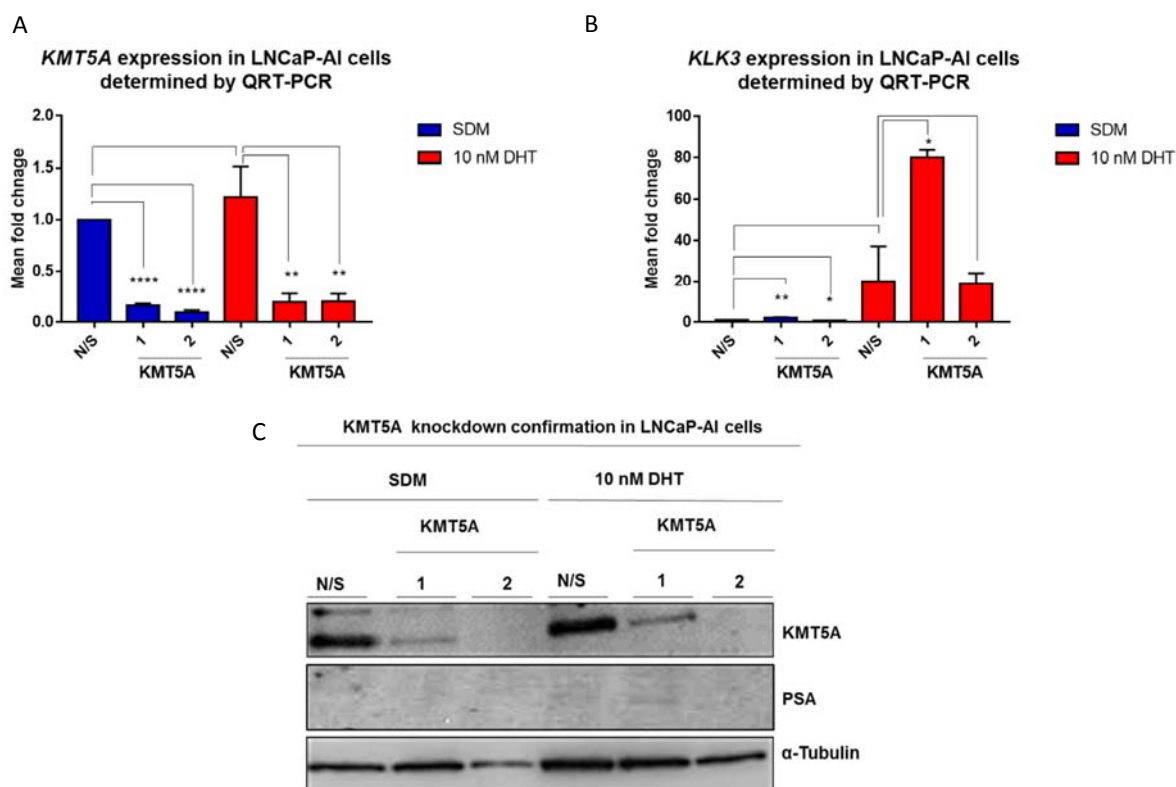
Figure 3-3 KMT5A knockdown confirmation in LNCaP-AI cells and the effect on PSA expression. LNCaP–AI cells were reverse transfected with N/S siRNA or the two selected KMT5A siRNAs for 72 hours in SDM followed by either stimulation with 10 nM DHT or vehicle control for 24 hours. RNA and protein was collected and knockdown of KMT5A was confirmed. (A) KMT5A mRNA expression and (B) KLK3 mRNA expression were compared to respective expression for the N/S 0 hour time point (C) KMT5A and PSA protein expression in LNCaP-AI cells. Error bars represent the mean ± SD for triplicate independent experiments. p-values were determined by t-test (* p-value <0.05, ** p-value <0.01, *** p-value <0.001 and **** p- value < 0.0001).

3.3.1.3. Confirmation of KMT5A target gene regulation

In addition to the functions of KMT5A that have been already mentioned, KMT5A plays an important role in tumour metastasis and progression thorough its effect on the expression of TWIST target genes (Yang *et al.*, 2012a). KMT5A acts as a dual epigenetic modifier on the promoters of E-cadherin and N-cadherin genes thorough its histone mono-methylation activity, thereby regulating their expression and in turn promoting the epithelial-mesenchymal transition (EMT). KMT5A is known to positively regulate the expression of mesenchymal markers while negatively regulating epithelial markers (Yang *et al.*, 2012b). In this study E-cadherin was selected as a representative of epithelial markers and vimentin as a representative of mesenchymal markers (Kalluri and Weinberg, 2009).

To further validate the specificity of KMT5A knockdown (Figure 3.2.A and Figure 3.3.A) for KMT5A regulated genes, known KMT5A regulated genes were investigated. The expression levels of *CDH1* and *VIM* were determined as positive controls for KMT5A knockdown in the LNCaP and LNCaP-AI cells. As expected, knockdown of KMT5A resulted in an increase in *CDH1* expression of ~1.5-2 fold in both DHT treated and untreated arms compared to the N/S control in the LNCaP cells (Figure 3.4.A). In the LNCaP-AI cells an ~2 fold increase in the expression of *CDH1* with KMT5A depletion in the presence of DHT was observed, whereas no significant changes in *CDH1* expression was observed in the absence of DHT following KMT5A depletion (Figure 3.4.B). For *VIM*, both cell lines showed a statistically significant reduction in *VIM* expression following KMT5A depletion in the DHT treated arm, where an ~2-3 fold decrease was observed (Figure 3.4.C). In addition, in the untreated arm of the LNCaP-AI cells, there was an ~2 fold decrease in *VIM* expression compared to N/S control (Figure 3.4.D). The overall data indicated that a successful knockdown of KMT5A was achieved by the two selected siRNAs with some evidence of an effects on the EMT.
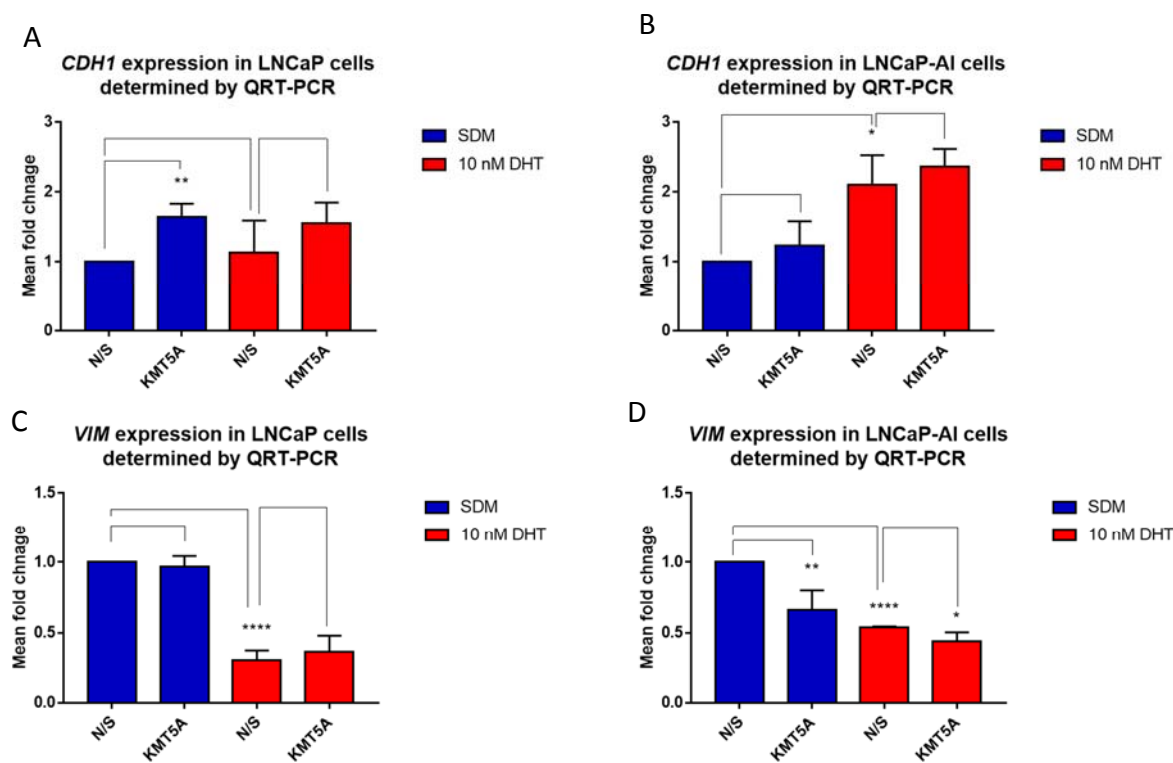
Figure 3-4 KMT5A positively regulates the expression of epithelial-mesenchymal transition markers in LNCaP and LNCaP-AI cells. Cells were reverse transfected with N/S siRNA or the selected KMT5A#1 siRNA for 72 hours followed by either stimulation with 10 nM DHT or vehicle control for 24 hours. RNA was collected and the expression levels of CDH1 and VIM were measured by QRT-PCR. CDH1 expression was measured in (A) LNCaP and (B) LNCaP-AI cells. VIM expression was measured in (C) LNCaP and (D) LNCaP-AI cells. Error bars represent the mean ± SD for triplicate independent experiments. p-values were determined by t-test (* p-value <0.05,** p-value <0.01 and *** p-value <0.001).

3.3.1.4. Microarray experiment in LNCaP-AI cells

Based on the data obtained from Figure 3.1, the microarray experimental conditions were selected and KMT5A knockdown was confirmed in LNCaP and LNCaP-AI cells. The LNCaP-AI cell line samples validated in Figure 3.3 were sent for microarray analysis using Illumina Human HT-12 arrays. However, subsequent validation of the data obtained was more extensive and was performed in both LNCaP and LNCaP-AI cells. In total 24 samples were analysed by microarray (4 biological repeats performed for each of the six conditions) as shown in Table 3.4. Additional validation of *KMT5A* knockdown and *KLK3* expression was confirmed by microarray data. The data showed a statistically significant ~80 % reduction in KMT5A expression using KMT5A siRNA#1 and # 2 compared to the N/S control (p≤0.05) in both the DHT treated and untreated arms, which was consistent with the data from Figure 3.3. For *KLK3* expression, treatment with DHT enhanced the expression of *KLK3* ~4 fold compared to DHT untreated arm. However, there was no significant change in the KMT5A depleted samples following DHT treatment compared to the N/S control (Figure 3.5).

Table 3-1 Microarray experimental conditions

LNCaP-AI cells	
-DHT	**+ 10nM DHT**
N/S	N/S
siKMT5A#1	siKMT5A#1
siKMT5A #2	siKMT5A #2
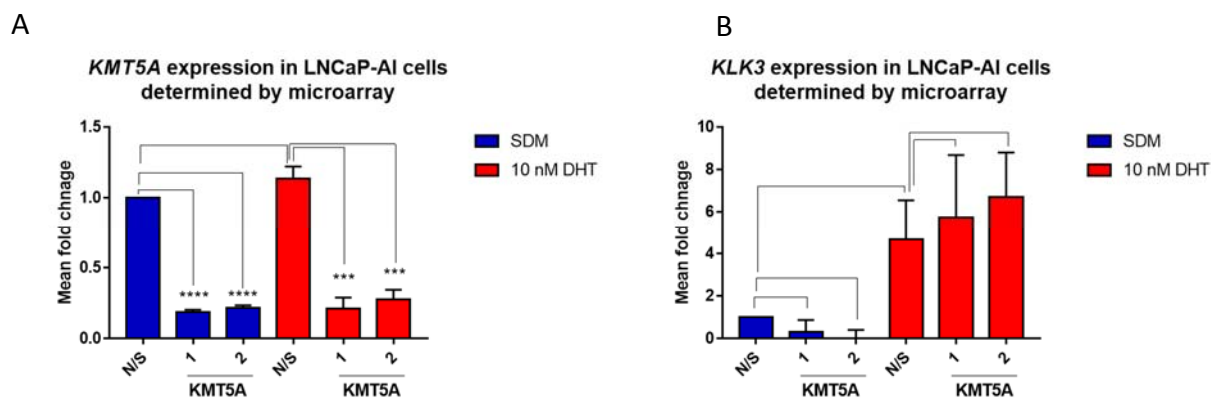
Figure 3-5 Confirmation of KMT5A knockdown and the effect on PSA expression in LNCaP-AI cells determined by microarray. LNCaP-AI cells were reverse transfected with N/S siRNA or the two selected KMT5A siRNAs for 72 hours in SDM followed by either stimulation with 10 nM DHT or vehicle control for 24 hours. RNA was collected and knockdown of KMT5A was confirmed by microarray. (A) KMT5A mRNA expression (B) KLK3 mRNA expression compared to respective expression for the N/S 0 hour time point. Error bars represent the mean ± SD for triplicate independent experiments. p-values were determined by t-test (* p-value <0.05, ** p-value <0.01, *** p-value <0.001 and **** p- value < 0.0001).

3.3.2. Microarray data analysis

Differential expression analysis was performed as outlined in Chapter 2. High quality data was obtained overall. Initial data showed 4 of 6 samples belong to the first set of samples grouped together but there was two outlier (detection threshold < 0.01). The outlier samples were therefore excluded, leaving n=3 for the affected groups. Microarray data analysis revealed that subsequent to KMT5A knockdown, 51 genes were regulated by KMT5A, 199 genes were regulated by KMT5A only in the presence of an active AR and 29 of the genes were common between these two groups.

3.3.2.1. Validation of the selected genes

A number of genes were selected from the microarray data based on the significance of their expression ($p \leq 0.05$) and whether they were significantly up or down regulated ($p \leq 0.05$) by the effect of a particular experimental condition. Microarray data analysis revealed a number of androgen- regulated genes (199 genes) that were also modulated by KMT5A such as *CDC42EP3, YIPF1* and *KIF22*, while some genes were regulated by KMT5A independently of the AR (51 genes) such as *CDC20, HIST1H2BD* and *RAB4A*.Further investigation of other genes included in the microarray data might be done in future experiments.

CDC42EP3 (up-regulated by DHT stimulation)

CDC42EP3 (CDC42 Effector Protein 3) encodes a member of the guanosine triphosphate (GTP) metabolising proteins, and plays a role in actin cytoskeleton reorganisation during changes to cell shape. In solid tumours, cells known as cancer-associated fibroblasts (CAFs) have an important role in tumour invasion and angiogenesis, a function supported by CDC42EP3 in these cells. Depletion of CDC42EP3 in CAFs reduces the fibroblast stimulation by tumour cells, which suggest the likely importance of CDC42EP3 targeting in tumours (Calvo *et al.*, 2015). The mRNA expression level of *CDC42EP3* showed a statistically significant increase in *CDC42EP3* expression in the N/S control following DHT stimulation by ~10 fold in LNCaP-AI cell line in the microarray experiment. However, KMT5A depletion in the DHT treated arm results in a significant reduction in *CDC42EP3* expression by ~4 fold with KMT5A siRNA#1 and ~3 fold with KMT5A siRNA #2 (Figure 3.6.A). The data was further validated using QRT-PCR in the same LNCaP-AI cells that were sent for microarray where similar trends were apparent and an increase in expression in the N/S control by ~2 fold was seen following DHT treatment. However, this effect was diminished by KMT5A depletion as reduction in *CDC42EP3* expression in response to

KMT5A depletion in the DHT treated arm was observed of ~2 fold for siRNA #1 and siRNA#2 (Figure 3.6.B). Both KMT5A siRNAs did reduce the levels of CDC42EP3 mRNA in the presence of androgen (Figure 3.6.B). The experiments were further extended to evaluate changes in *CDC42EP3* mRNA expression in the LNCaP cells line following KMT5A depletion. A statistically significant increase in CDC42EP3 expression in the N/S control following DHT treatment was seen of ~3 fold (p≤0.05). However, this effect was reduced by ~2 fold in the DHT treated arm most notably with siRNA#2, while no significant changes was noticed with siRNA #1 compared to the N/S control (Figure 3.6.C). The data therefore confirmed *CDC42EP3* as an androgen-regulated gene, and that the androgen-induced expression of *CDC42EP3* was diminished following siRNA-mediated depletion of KMT5A (Figure 3.6.B-C).
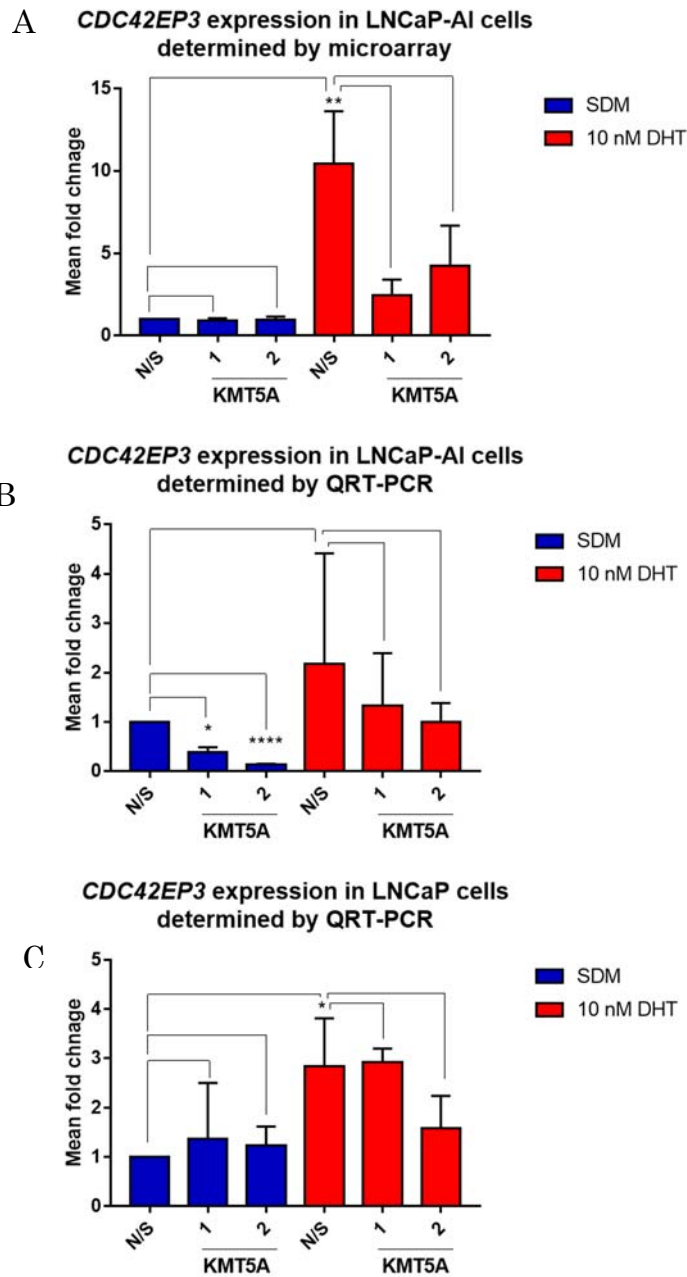
Figure 3-6 KMT5A plays a role in the expression of the androgen regulated gene, CDC42EP3. LNCaP and LNCaP-AI cells were reverse transfected with N/S siRNA or the two selected KMT5A siRNAs for 72 hours followed by either stimulation with 10 nM DHT or vehicle control for 24 hours. RNA was collected and CDC42EP3 mRNA expression was determined by microarray in (A) LNCaP–AI cells, and by QRT-PCR in (B) LNCaP-AI cells and (C) LNCaP cells. Error bars represent the mean ± SD for triplicate independent experiments. p-values were determined by t-test (* p-value <0.05, ** p-value <0.01, *** p-value <0.001 and **** p- value < 0.0001).

YIPF1 (up-regulated by DHT stimulation)

The expression of *YIPF1*, a member of Yipf1 domain family, was validated on microarray samples in LNCaP-AI cells as being an AR-regulated gene. However, this relationship has not been reported previously. The microarray experiment data showed ~2 fold increase in the mRNA expression level of *YIPF1* in the N/S control in the LNCaP-AI cell line in the DHT treated arm compared to N/S untreated control (Figure 3.7.A). Depletion of KMT5A by either siRNAs attenuated the DHT-induced increase in *YIPF1* to similar levels as for the untreated arm. This was further validated by QRT-PCR in the LNCaP-AI, where *YIPF1* expression was increased by ~1.5 fold following DHT treatment in the N/S control, whereas depletion of KMT5A reduced the DHT-induced increase in *YIPF1* expression with both siRNA which was consistent with data from the microarray experiment (Figure 3.7.B). The validation was extended to include the LNCaP cell line. In this case, no detectable changes in *YIPF1* expression was observed in response to DHT treatment, suggesting *YIPF1* is not truely an androgen responsive gene (Figure 3.7.C). Additionally, knockdown of KMT5A with either siRNA failed to alter the expression of *YIPF1*. The findings for LNCaP and LNCaP-AI cells were contradictory and therefore not conclusive in supporting *YIPF1* as an androgen-regulated gene (Figure 3.7.B-C).
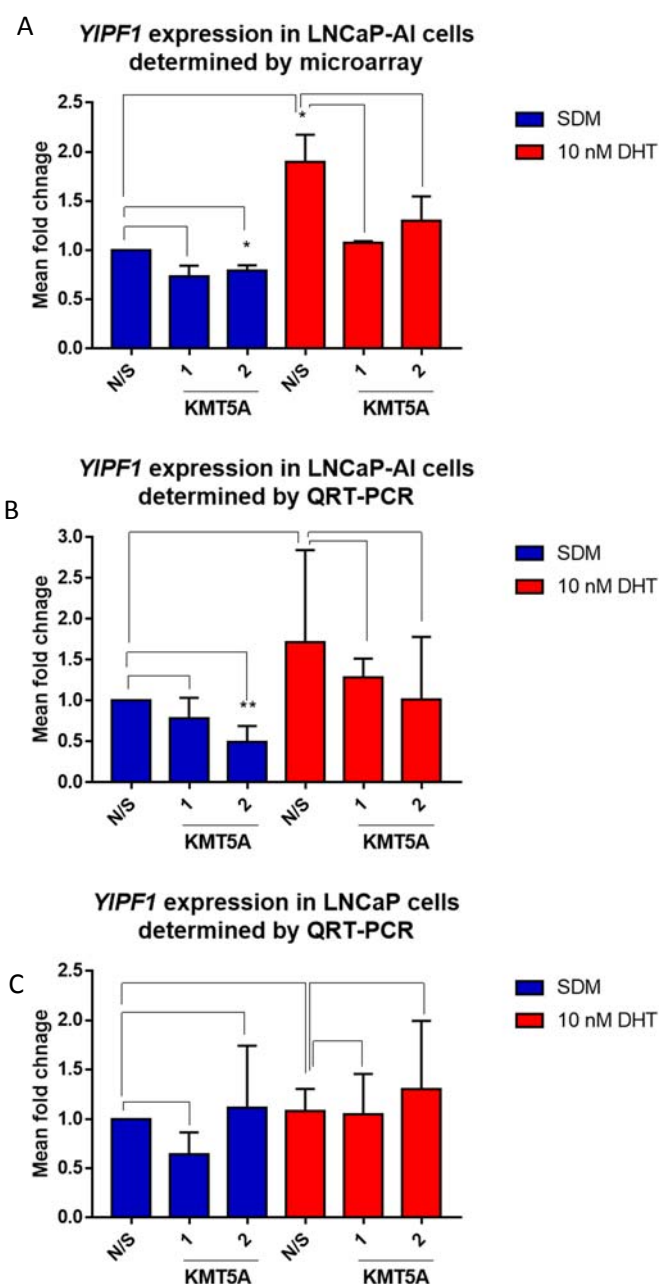
Figure 3-7 KMT5A plays a role in the expression of YIPF1. LNCaP and LNCaP-AI cells were reverse transfected with N/S siRNA or the two selected KMT5A siRNAs for 72 hours followed by either stimulation with 10 nM DHT or vehicle control for 24 hours. RNA was collected and YIPF1 mRNA expression was determined by microarray in (A) LNCaP–AI cells, and by QRT-PCR in (B) LNCaP-AI cells and (C) LNCaP cells. Error bars represent the mean ± SD for triplicate independent experiments. p-values were determined by t-test (* p-value <0.05, ** p-value <0.01, *** p-value <0.001 and **** p- value < 0.0001).

KIF22 (up-regulated by DHT stimulation)

KIF22, kinesin family member 22, is one of the microtubule-dependent molecular motors, which plays a role in the transport of organelles and chromosome movement during cell division. Furthermore, *KIF22* is implicated in cellular proliferation and its depletion results in G2/M phase arrest in tumour cells (Yu *et al.*, 2014). According to the microarray data, depletion of KMT5A reduced the level of *KIF22* in the absence or presence of DHT. DHT treatment enhanced KIF22 expression significantly in the N/S control by ~2 fold (p≤0.05). KMT5A depletion in the DHT treated arm resulted in a significant reduction in *KIF22* expression. The most notable statistically significant effect was observed with siRNA#1 in the absence of DHT, where KIF22 expression was reduced by ~2 fold compared to N/S control (Figure 3.8.A). This data was further validated by QRT-PCR in the LNCaP-AI cell line. A small increase in *KIF22* expression in the N/S control of ~2 fold following DHT treatment was observed. In keeping with the microarray finding, both KMT5A siRNAs reduced the mRNA level of *KIF22* in the absence or presence of DHT (Figure 3.8.B). *KIF22* expression was reduced significantly by ~2 fold with siRNA# 1 and by ~5 fold with siRNA #2 compared to the N/S control in the absence of DHT treatment (p≤0.05). For the DHT treated arm, this effect was reduced significantly by both KMT5A siRNAs by ~2 fold (p≤0.05). The validation was extended to include the LNCaP cell line. In this case the androgenic induction of *KIF22* was confirmed as significant and KMT5A depletion was also found to reduce the level of *KIF22* in the absence and presence of DHT. The most notable effect was observed with siRNA#1 in the absence of DHT where a 2 fold reduction in expression was apparent (p≤0.05) (Figure 3.8.C). Overall, the data suggested *KIF22* is an androgen-regulated gene in both LNCaP and LNCaP-AI cells and that the androgen-induced expression of *KIF22* was reduced following KMT5A depletion using siRNAs (Figure 3.8.B-C).
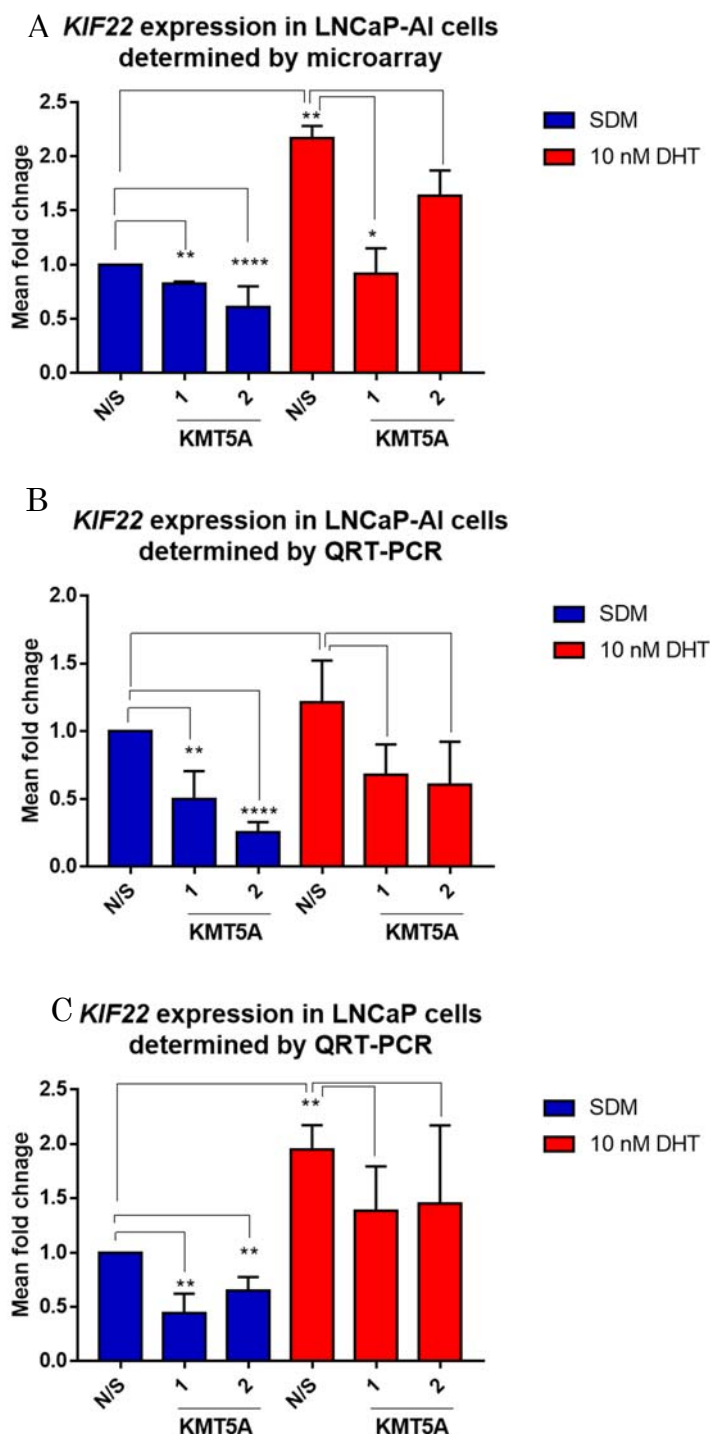
Figure 3-8 KMT5A plays a role in the expression of the androgen regulated gene, KIF22. LNCaP and LNCaP-AI cells were reverse transfected with N/S siRNA or the two selected KMT5A siRNAs for 72 hours followed by either stimulation with 10 nM DHT or vehicle control for 24 hours. RNA was collected and KIF22 mRNA expression was determined by microarray in (A) LNCaP–AI cells, and by QRT-PCR in (B) LNCaP-AI cells and (C) LNCaP cells. Error bars represent the mean ± SD for triplicate independent experiments. p-values were determined by t-test (* p-value <0.05, ** p-value <0.01, *** p-value <0.001 and **** p- value < 0.0001).

HIST1H2BD (up- regulated by reduced KMT5A expression)

Histones play a central role in transcriptional regulation, DNA repair, DNA replication and chromosome stability. Androgen treatment was found to have little or no effect on *HIST1H2BD* expression (Figure 3.9.A) in the microarray experiment conducted with LNCaP-AI cell line. The data revealed a statistically significant increase in mRNA expression level of *HIST1H2BD* (p≤0.05) following either KMT5A siRNA#1 or siRNA#2 treatment resulting in an ~3 and ~4 fold induction of *HIST1H2BD* expression in the absence and presence of DHT, respectively, compared to the N/S control (Figure 3.9.A). The data was further validated by QRT-PCR in the LNCaP-AI cells and also showed a statistically significant increase in *HIST1H2BD* expression (p≤0.05) following KMT5A mRNA depletion (Figure 3.9.B). However, the fold-increase in *HIST1H2BD* expression following KMT5A depletion was much greater than that observed for the microarray experiment with an approximately 20 fold increase in expression in the absence of DHT with both siRNAs and an ~22 fold and ~11 fold with siRNA#2 increase in *HIST1H2BD* expression for siRNA#1 and siRNA#2, respectively in the presence of DHT compared to N/S control (p≤0.05) (Figure 3.9.B). In the LNCaP cells, the validation also showed a statistically significant increase of ~6 fold in *HIST1H2BD* expression with siRNA#1 and ~5 fold with siRNA#2 in the absence of DHT. These results were mirrored following DHT treatment where an ~5 fold and ~4 fold induction in *HIST1H2BD* expression was observed with KMT5A siRNA#1 and siRNA#2 treatment, respectively, relative to the N/S control (p≤0.05) (Figure 3.9.C). The data strongly indicated that *HIST1H2BD* is an KMT5A regulated gene in both cell lines and that the androgen stimulation following KMT5A depletion using siRNAs had no effect on its expression (Figure 3.9.B-C).
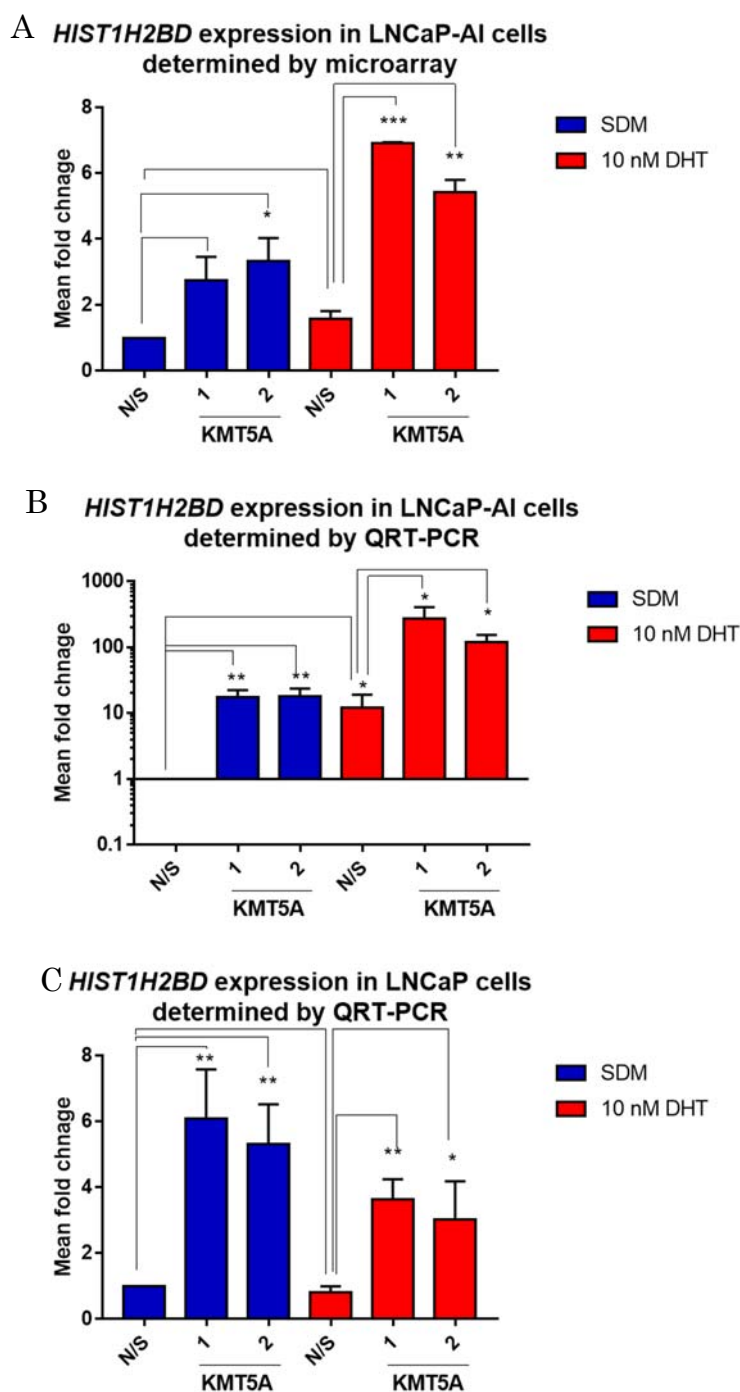
Figure 3-9 KMT5A regulates the expression of HIST1H2BD. LNCaP and LNCaP-AI cells were reverse transfected with N/S siRNA or the two selected KMT5A siRNAs for 72 hours followed by either stimulation with 10 nM DHT or vehicle control for 24 hours. RNA was collected and HIST1H2BD mRNA expression was determined by microarray in (A) LNCaP-AI cells and by QRT-PCR in (B) LNCaP–AI cells and (C) LNCaP cells. Error bars represent the mean ± SD for triplicate independent experiments. p-values were determined by t-test (* p-value <0.05 and ** p-value <0.01).

RAB4A (down-regulated following KMT5A depletion)

The RAB4A gene is a member of the largest group in the Ras superfamily of small GTPases, which regulate membrane trafficking. The encoded protein is associated with early endosomes and is involved in their sorting and recycling. The RAB4A protein also plays a role in regulating the recycling of receptors from endosomes to the plasma membrane (Kachhap *et al.*, 2007; Pirngruber *et al.*, 2009).

The mRNA expression level of *RAB4A* showed a statistically significant reduction by ~2 fold following KMT5A depletion in the microarray experiment for the LNCaP-AI cells in the DHT untreated arm ($p \leq 0.05$) (Figure 3.11.A). A similar reduction in *RAB4A* mRNA expression was found when DHT was included in the experiment (Figure 3.10.A) particularly with siRNA#1. The data was further confirmed by QRT-PCR in the LNCaP-AI cells, where a ~2 fold reduction in *RAB4A* expression was found with both KMT5A siRNA#1 and #2 in the untreated and DHT treated arms compared to N/S control ($p \leq 0.05$)(Figure 3.10.B). In this experiment, DHT caused an ~3 fold increase in *RAB4A* mRNA expression for the N/S control arm, suggesting *RAB4A* as an androgen-regulated gene in the LNCaP-AI cell line.

However, upon examining *RAB4A* expression in the LNCaP cell line using QRT-PCR, no significant changes in *RAB4A* expression were observed in response to either DHT stimulation and/or KMT5A mRNA depletion (Figure 3.10.C). The data only suggested *RAB4A* as a KMT5A regulated gene in the LNCaP-AI cells (Figure 3.10.B-C). Furthermore, *RAB4A* appears to be under androgen regulation in LNCaP-AI cells but not in the LNCaP parental cell line.
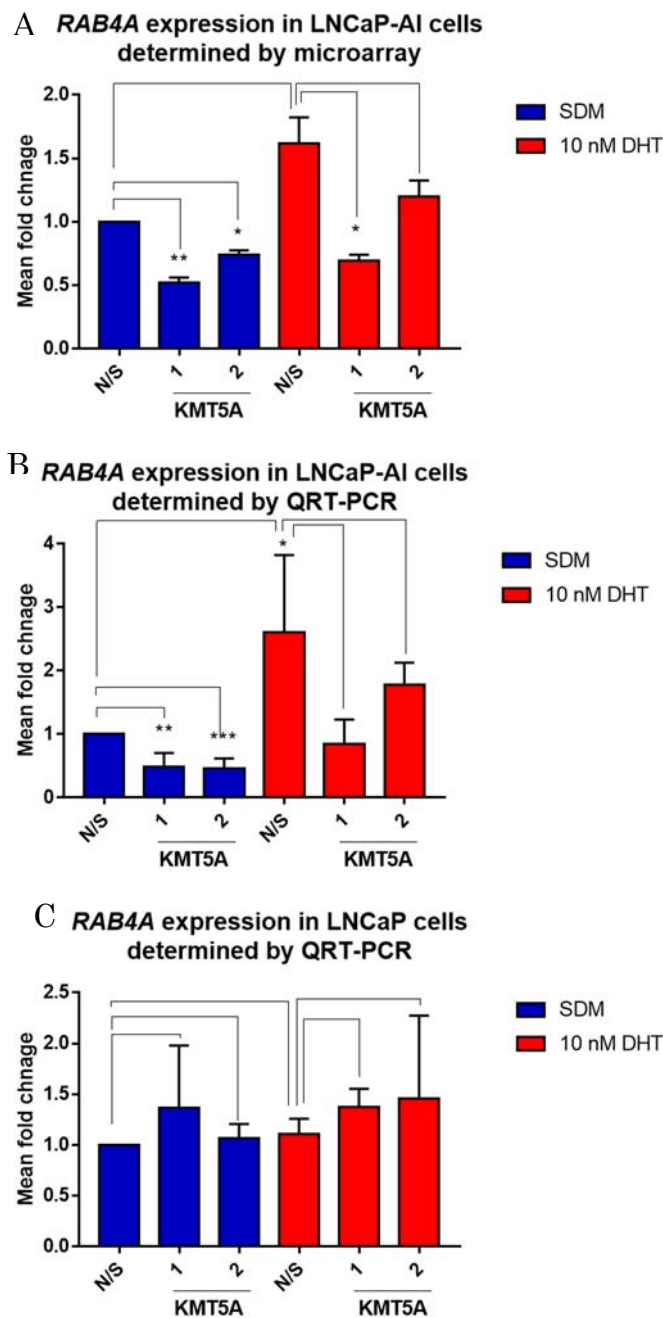
Figure 3-10 KMT5A regulates the mRNA expression of RAB4A. LNCaP and LNCaP-AI cells were reverse transfected with N/S siRNA or the two selected KMT5A siRNAs for 72 hours followed by either stimulation with 10 nM DHT or vehicle control for 24 hours. RNA was collected and RAB4A mRNA expression was determined by microarray in (A) LNCaP-AI cells, and by QRT-PCR in (B) LNCaP-AI and (C) LNCaP cells. Error bars represent the mean ± SD for triplicate independent experiments. p-values were determined by t-test (* p-value <0.05, ** p-value <0.01, *** p-value <0.001 and **** p- value < 0.0001).

CDC20 **(down-regulated by reduced KMT5A expression)**

CDC20 (cell division cycle homolog 20) plays an important role in cell cycle progression as an important subunit of the anaphase promoting complex APC (Izawa and Pines, 2015). The microarray experiment indicated that *CDC20* was affected by KMT5A but was not regulated by DHT treatment. However, *CDC20* has previously been reported as an AR-dependent gene which is up-regulated in response to AR stimulation in an androgen-independent cell line derivative of LNCaP, termed LNCaP-Abl cells (Wang *et al.*, 2009). The microarray revealed a statistically significant reduction of ~2 fold in the mRNA expression level of *CDC20* in the LNCaP-AI cell line upon KMT5A knockdown with both siRNAs targeting in the DHT untreated arm (p≤ 0.01) (Figure 3.11.A). Furthermore a similar result was observed for the DHT treatment arm for both KMT5A siRNAs. This was further confirmed by QRT-PCR in LNCaP-AI cells, where a statistically significant reduction in *CDC20* expression was also found with KMT5A siRNA#1 of ~4 fold and siRNA#2 by ~3 fold in the DHT untreated arm compared to N/S control (Figure 3.11.B). The effects of KMT5A depletion on *CDC20* mRNA expression in the DHT treated arm were not as great, but did show a significant 50-60 % reduction in *CDC20* expression (Figure 3.11B). Moreover, in the LNCaP cells, the effects of KMT5A depletion on *CDC20* mRNA expression were comparable to the effects seen in the LNCAP-AI cell line (Figure 3.11.C). In this case, an ~ 3-4 fold reduction in *CDC20* in the absence of DHT was observed following KMT5A knockdown, when compared to the N/S control (Figure 3.11.C). Similarly, when LNCaP cells were stimulated with DHT, the depletion of KMT5A resulted in ~2 fold reduction in *CDC20* mRNA expression compared to the N/S androgen stimulated control (Figure 3.11.C). The data therefore identified *CDC20* as a KMT5A regulated gene in both cell lines and that the androgen stimulation had no effect on *CDC20* expression following KMT5A depletion using siRNAs (Figure 3.11.B-C). A statistically significant reduction (p≤0.05) in *CDC20* expression was apparent for both LNCaP and LNCaP-AI cell lines following KMT5A knockdown.
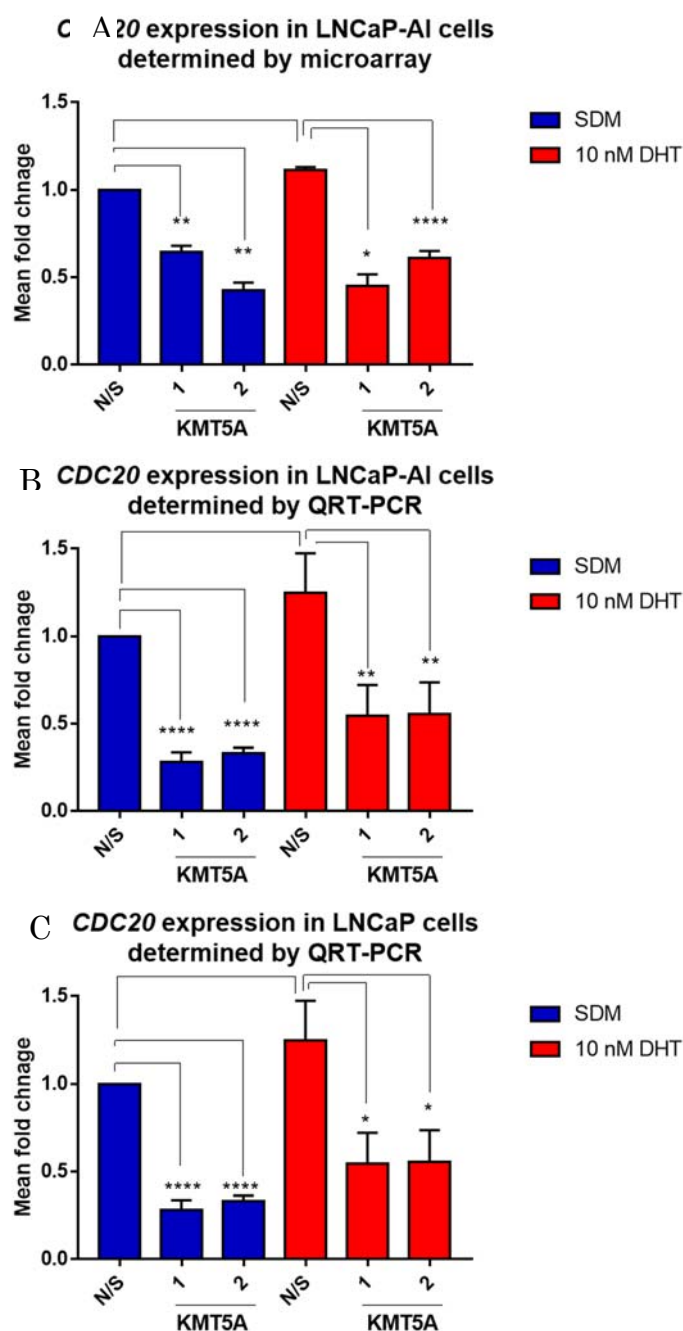
Figure 3-11 KMT5A regulates the expression of CDC20. LNCaP and LNCaP-AI cells were reverse transfected with N/S siRNA or the two selected KMT5A siRNAs for 72 hours followed by either stimulation with 10 nM DHT or vehicle control for 24 hour. RNA was collected and CDC20 mRNA expression was determined by microarray in (A) LNCaP-AI cells, and by QRT-PCR in (B) LNCaP–AI cells and (C) LNCaP cells. Error bar represents the mean ± SD for triplicate independent experiments. p-values were determined by t-test (* p-value <0.05, ** p-value <0.01, *** p-value <0.001 and **** p- value < 0.0001).

3.4. Discussion

Histone modifications are important alterations with critical roles in chromatin regulation and cell cycle progression. The histone methyltransferase KMT5A is the sole enzyme responsible for catalysing mono-methylation of H4 on lysine 20,whilst the di- and tri-methylation of this particular lysine residue are catalysed by KMT5B and KMT5C respectively (Fang *et al.*, 2002).

In PC, the AR remains an important therapeutic target due to the essential role that AR plays in the development and progression of the disease. However, targeting the AR in advanced PC has started to take a different approach in the experimental pre-clinical studies over the last few years, by targeting it indirectly through targeting its co-factors. These include, histone methyltransferases that have been found to methylate some non-histone proteins such as p53, and AR (Gaughan *et al.*, 2011). The AR transcriptional activity has been shown to be influenced thorough the methyl modifications of its lysine residue(s), suggesting it may be valuable to investigate the therapeutic targeting of the AR thorough these methyltransferases. Of these histone methyltransferases, KMT5A was previously found to be a novel co-regulator of the AR (Coffey *et al.*, unpublished data). The ability of KMT5A to regulate AR activity was found to switch from being an AR co-repressor in androgen dependent PC cells to an AR co-activator for androgen independent PC cells (Coffey et al., unpublished data).

In order to understand the function of KMT5A and how its enzymatic activity participates in cellular functions in PC, a microarray study was designed to identify an expression profile of genes that are regulated by KMT5A in an androgen-independent PC cell line model (LNCaP-AI). This was performed by silencing KMT5A expression using two independent siRNA sequences for 72 hours in SDM. Moreover, this was extended to include a subsequent stimulation of the AR activity using 10 nM DHT for 24 hours, in order to be able to distinguish the genes that are primarily regulated by the AR, but also modulated by KMT5A. The comparable experiment was also subsequently conducted in an androgen-dependent PC cell line model (LNCaP), and the samples were used for comparison before initiating the microarray experiment (Figure 3.2 and 3.3).

Prior to microarray analysis a number of optimisation experiments were performed to ensure that the samples generated for analysis were as consistent and robust as possible in order to

ensure that the data generated was of the highest standard. Firstly, the optimum dose of DHT which was applied to the cells to stimulate AR activity was determined.

As a readout of AR activity, *KLK3* expression levels are considered as the most important indicator of PC progression in its early stages, treatment outcome and also disease recurrence (Catalona *et al.*, 2000; Balk and Knudsen, 2008). As such the expression of *KLK3* mRNA was used to determine the response to DHT stimulation in LNCaP and LNCaP-AI cells (Figure 3.1). The expression levels of AR have previously been found to be higher in AR-independent PC compared to AR-dependent PC models, and this is accompanied by higher levels of *KLK3* expression in such cancers (Shi *et al.*, 2004). The titration experiment included serial doses of DHT (5 orders of magnitude) to stimulate AR activity over 24 hours. DHT treatment at 10 nM DHT caused a statistically significant ($p \leq 0.05$) increase in *KLK3* expression with ~30 fold in LNCaP cells and ~75 fold in LNCaP-AI cells. Consequently, 10 nM DHT was selected as the dose to be used for stimulation of AR activity in the subsequent experiments for both LNCaP and LNCaP-AI cells. Furthermore, a DHT time course experiment was then conducted that extended up to 72 hours. The data showed a rapid and statistically significant increase in *KLK3* expression in the LNCaP cells ($p \leq 0.05$) that peaked at 24 hours by ~400 fold followed by a gradual reduction over the remaining time points. In the LNCaP-AI cells there was a gradual but statistically significant ($p \leq 0.05$) increase in *KLK3*expression that began to plateau at 72 hours with an ~2000 fold increase as shown in Figure 3.1. As a result, 24 hours of DHT stimulation at a dose of 10 nM was utilised in the subsequent gene profiling of LNCaP and LNCaP-AI cell lines in order to detect genes that were regulated primarily by the AR in both cell lines. The data was consistent with previously published data revealing that despite the higher levels of the AR protein in the androgen independent PC cells, that the expression levels of *KLK3* are substantially lower in the absence of AR stimulation (Shi *et al.*, 2004).

KMT5A depletion (~80 %) was achieved using selected siRNAs against KMT5A (Figure 3.2, 3.3) in both LNCaP and LNCaP-AI cell lines at both the mRNA and protein levels. In order to confirm KMT5A knockdown prior to the microarray, the expression of a set of genes which are known to be regulated by KMT5A were examined. Such genes included the TWIST target genes *CDH1* and *VIM* which were utilised as a functional readout for KMT5A knockdown. TWIST (also known as TWIST1), is a highly conserved basic helix-loop-helix transcriptional factor, which has a pivotal role in tumour metastasis by promoting epithelial to mesenchymal transition (EMT) (Yang *et al.*, 2012a). Depletion of KMT5A using small interference RNA was shown to result in an increase in the expression of *CDH1* and a reduction in the

expression of *VIM* (Hou *et al.*, 2016) which is consistent with the data shown in Figure 3.4. and the data obtained by the microarray. The ectopic expression of TWIST results in alterations in the expression of some proteins, such as upregulation of mesenchymal markers (e.g., N-cadherin, fibronectin, vimentin, and SM-actin) and downregulation of epithelial protein markers (e.g., E-cadherin, α-catenin, β-catenin, and ɣ-catenin). KMT5A is associated with TWIST and acts through its mono-methylation activity on H4K20 as a dual epigenetic modifier on twist target gene promoters, namely E-cadherin and N-cadherin. KMT5A and TWIST are functionally independent in stimulating EMT (Yang *et al.*, 2012a). This reflect the role that KMT5A plays in tumour progression and metastasis and also as a positive reader of KMT5A knockdown in the PC cell lines that were used in this study.

In order to detect KMT5A regulated gene expression profiles, the Illumina Human HT-12 v4.0 Expression Bead Chip technology was used. Parallel quantification of a large number of transcripts is accessible by this high-throughput technology (Schmid *et al.*, 2010). Analysis of microarray data revealed a number of genes that were regulated directly by KMT5A independently of AR and other genes that were only regulated by KMT5A in the presence of active AR. However, there were a low number of genes (29 in total) that appeared to be AR-regulated but modulated by KMT5A. Following data analysis using differential expression analysis by the R package 'Limma', and p values, a number of genes were selected for further investigation.

CDC42EP3

This gene is one of the CDC42EP family of proteins. In normal cells, alterations to cell shape are stimulated by *CDC42EP3* which induces the assembly of actin filaments. In human male gonads, *CDC42EP3* mRNA was suggested to be transcriptionally regulated by PUMILIO2 binding to a specific nucleotide motif in the *CDC42EP3* 3'UTR (Calvo *et al.*, 2015). In solid tumours, matrix remodelling, invasion of cancerous cells and angiogenesis is facilitated by non-cancerous fibroblast cells known as CAFs. This function is enhanced and supported by *CDC42EP3* in the cancerous cells, and depletion of *CDC42EP3* results in a reduction in angiogenesis and invasion of these cells. *CDC42EP3* plays an important role in coordinating the septin and actin filament in the tumour stroma. In normal fibroblast, depletion of *CDC42EP3* diminishes the fibroblast stimulation by tumour cells (Calvo *et al.*, 2015). The expression of *CDC42EP3* is also documented to be significantly increased in grade III tumours (Gabrovska *et al.*, 2012). The data from the ongoing study identified *CDC42EP3* as an AR regulated gene that can be modulated by KMT5A depletion in PC cells (Figure 3.6). These results might relate to the role that KMT5A plays in regulating cancer invasion and

angiogenesis thorough its cooperative effect with the AR in reducing *CDC42EP3* expression in PC cell lines. Consequently, *CDC42EP3* may reduce the tumour growth promoting ability of the cancer associated fibroblasts. Recently, *CDC42EP3* has been identified in a study using an RNAseq dataset to identify genes that are expressed reciprocally in response to acute androgen stimulation using the synthetic androgen (R1881) in culture, and the expression of these genes in PC patient under androgen deprivation therapy (ADT) (Munkley *et al.*, 2016). *CDC42EP3* expression was significantly increased by ~2 fold in response to 10 nM R1881 treatment for 24 hours. This data is consistent with our data to confirm *CDC42EP3* as an AR regulated gene. However, further investigation is required to understand this relationship in PC.

YIPF1 (**YIP domain family member 1**)

Current literature for *YIPF1* is extremely limited. A small nucleotide polymorphism in the *YIPF1* gene was identified previously as being associated with angiotensin II receptor blocker response in a clinical trial for patients with mild-moderate essential hypertension (Kamide *et al.*, 2013). The data from the microarray herein showed *YIPF1* to be an androgen regulated gene in the LNCaP-AI cell line and that the androgen-induced expression of *YIPF1* was reduced to near basal levels following KMT5A depletion (Figure 3.7). Neither androgen-induction nor KMT5A depletion had any noticeable effect on *YIPF1* expression in the LNCaP cell line. However, *YIPF1* was also included in the study mentioned above (Munkley *et al.*, 2016) as one of the genes that is significantly upregulated by ~2 fold in response to AR stimulation using 10 nM R1881.

KIF22 (**Kinesin family, member 22**)

KIF22 is a microtubule-dependent molecular motor protein that plays an important role in cell mitosis, but also has the ability to bind to DNA (Yu *et al.*, 2014). Depletion of *KIF22* has been shown to result in cell cycle arrest at the G2/M phase which is accompanied by an increase in the activity of CDK1 enzyme and elevated expression of the *KIF22* target gene *CDC25C*. Furthermore, *KIF22* is overexpressed in cancers where it plays a role in promoting cell proliferation (Yu *et al.*, 2014). Consistent with these findings, depletion of *KIF22* results in a delay in mitotic entry accompanied by a reduction in *CDC25C* transcription. (Yu *et al.*, 2014). The microarray data showed significant elevation of *KIF22* mRNA expression when DHT stimulation was applied to LNCaP-AI cells. The QRT-PCR experiment validated the androgen regulation of *KIF22* mRNA for both LNCaP and LNCaP-AI cell lines (Figure 3.8).

Interestingly, the basal expression and androgen-induced expression of *KIF22* was reduced following KMT5A depletion using siRNAs. Therefore, it is speculated that KMT5A might normally play a role in maintaining PC cell proliferation thorough its cooperative effect with the AR in maintaining *KIF22* expression to ensure cells progress through the G2/M phase of the cell cycle. Consistently, *KIF22* expression was recently shown to be significantly increased by ~2 fold in response to 10 nM R1881 treatment for 24 hours (Munkley *et al.*, 2016), confirming *KIF22* as an AR regulated gene. However, further investigation is required to understand this relationship in PC.

HIST1H2BD (**Histone cluster 1, H2BD**)

Histone mRNAs generally lack poly-A tails but contain 3' end, stem loop structures that stabilise the mRNA. However, the replication associated histone genes, *HIST1H2BD* and *HIST1H2AC* can generate alternative transcripts containing poly-adenylated 3' ends. These transcripts change expression during differentiation and tumourigenesis (Kari *et al.*, 2013). CDK9 has a regulatory role in the co-transcriptional replication-dependent 3'-end processing of these histone mRNAs, a process which involves histones H2B mono-ubiquitination and H3 lysine 4 tri-methylation. It was found that depletion of CDK9 led to ~15 fold increase in the read-through of *HIST1H2BD* (Pirngruber *et al.*, 2009). With strong cell cycle links, it was interesting to observe that KMT5A depletion resulted in a statistically significant increase ($p \leq 0.05$) in the expression of *HIST1H2BD* in the presence and absence of DHT in the microarray experiment, which was also confirmed using QRT-PCR in both LNCaP and LNCaP-AI cells (Figure 3.9). KMT5A was previously suggested to repress the genes required for DNA replication initiation, which would prevent S phase entry (Jørgensen *et al.*, 2007; Tardat *et al.*, 2007). *HIST1H2BD* has been shown previously as one of the DNA repair associated genes (Lilach *et al.*, 2013). So the data herein might suggest that depletion of KMT5A in PC cells increases the expression of some DNA damage repair genes, such as *HIST1H2BD* in this case, could in turn increase the possibility of DNA damage repair. However, further investigation would be required.

RAB4A

RAB4A is a member of the RAS oncogene family which is known to regulate membrane trafficking. It is phosphorylated by CDK1 during mitosis which results in its movement from the membrane to the cytoplasm. *RAB4A* has been described as an effector of *NDRG1*, and is an androgen-regulated gene that can localise to the recycling/sorting endosomes. *NDRG1* is

also suggested to play a role in the recycling of E-cadherin, and therefore may play a role in the EMT of PC cells (Kachhap *et al.*, 2007; Pirngruber *et al.*, 2009). Interestingly, depletion of KMT5A was found to result in a reduction of *RAB4A* expression in the microarray data. The trend was also consistent in the QRT-PCR validation data for both the LNCaP-AI and LNCaP cells, although it was not found to be to be significant (Figure 3.10). Based on the relationship between RAB4A and KMT5A found here, as well as preceding information, it may further imply that KMT5A has an important role in regulating the EMT in PC cells. Further investigation of this relationship and its role in EMT is required.

CDC20

CDC20 (Cell cycle division 20 homologue) functions as the substrate recognizing subunit of APC/C complex. During early mitosis, CDC20 is responsible for the role of APC/C in activating mitotic exit at the metaphase-to-anaphase transition. While during late mitosis and G1 phase, Cdh1 can replace CDC20 for this function (Manchado *et al.*, 2010). KMT5A is dephosphorylated during early anaphase by the action of Cdc14 phosphatases which enables KMT5A to undergo ubiquitination and degradation by APC^{Cdh1} causing a reduction in KMT5A levels at the G1 phase of the cell cycle (Wu *et al.*, 2010). This group also suggested that as KMT5A is present in early mitosis in its phosphorylated form, there is a high possibility that the same mechanisms prevents KMT5A degradation by APC^{Cdc20} complex during that phase. Adding to its role as a cell cycle regulator, CDC20 has also been suggested to participate strongly in the development and progression of human cancers, and therefore could be considered as a novel therapeutic target for cancer treatment (Wang *et al.*, 2013). The microarray data showed a statistically significant reduction in CDC20 expression in the presence and absence of DHT in LNCaP-AI cells (p≤0.05), which was further confirmed in the validation data for both LNCaP and LNCaP-AI cells (Figure 3.11). The relationship between KMT5A and CDC20 will be investigated and discussed further in Chapter 4.

The established role of KMT5A in different cellular processes identified by previous studies was also supported by this study. This further strengthens the existing data for the involvement of KMT5A in these cellular processes and identifies specific genes and the possible pathways through which KMT5A is involved in order to accomplish these functions. KMT5A's role in EMT was supported by the significant reduction of *RAB4A* expression following KMT5A depletion (Mendiratta *et al.*, 2009; Calvo *et al.*, 2015). Also, the upregulation of *HIST1H2BD* that followed KMT5A knockdown was also a mechanism to support the effect of KMT5A in the DNA damage repair process through the up-regulation of some DNA damage repair genes. The data also highlights a possible relationship between

KMT5A and AR in regulating the expression of some genes synergistically in PC cell lines. In conclusion, this study has highlighted some of the important and novel functions of KMT5A. Therefore, it further strengthens an argument for therapeutic targeting of KMT5A in PC due to its key involvement in cancer-associated processes, including cell cycle, DNA repair and EMT that promote progression, invasion and metastasis of PC thorough different pathways.

From the genes regulated by KMT5A, CDC20 expression at the protein level in the presence and absence of KMT5A, and the possible mechanism that might role the relationship between KMT5A and CDC20 will be investigated further in Chapter 4.

Chapter 4 . KMT5A indirectly regulates CDC20 expression via p53 methylation

4.1. Introduction

CDC20

 KMT5A was identified in Chapter 3 as a putative novel regulator of CDC20 expression (Figure 3.13). CDC20 is an important cell cycle regulatory protein which associates with APC to target specifically a 9 amino acid D-BOX peptide sequence within proteins for recognition, such as RxxLxxxN for degradation by the ubiquitination pathway during mitosis (Fang *et al.*, 1998). CDC20 consists of 499 amino acids with WD40 repeats at its C-terminus for protein binding which is critical for APC substrate recognition. In addition to CDC20, CDH1 can also function as a substrate recognition subunit for APC. Proteins which do not contain a D-BOX, such as polo-like kinase, are targeted by this complex for destruction during G1. Unlike CDC20, whose expression peaks during mitosis and is reduced during G1 (Figure 4.1), the expression of CDH1 remains persistent during the cell cycle (Fang, 2002). Furthermore, many studies have shown that CDC20 also plays an important role in the growth and development of human cancers and it is also oncogenic in multiple cancers such as ovarian, cervical and gastric cancer (Kidokoro *et al.*, 2008; Smolders and Teodoro, 2011; Wang *et al.*, 2013) (Figure 4.1).

CDC20 is regulated by many factors, including Mad2 and BubR1, which are key components of the Mitotic Checkpoint Complex (MCC). Mad2 and BubR1 bind and inhibit CDC20 activity, which is necessary for the activation of APC (Fang, 2002). Unattached kinetochores recruit and activate Mad2, BubR1 and Bub3 during spindle checkpoint arrest, allowing their association with Cdc20 that has been phosphorylated by Cdc2 and MAPK. Binding of Mad2, BubR1 and Bub3 to Cdc20 prevents Cdc20 from activating the APC (Chung and Chen, 2003). Attached kinetochore does not recruit Mad2 and Cdc20, preventing the generation of new Mad2–BubR1–Bub3–Cdc20 complex. The existing checkpoint complex may be disassembled through dephosphorylation of Cdc20. Inactivation of MAPK by an unknown mechanism may result in initial dephosphorylation of Cdc20 and partial activation of the APC. The APC–Cdc20 then triggers the first phase of cyclin B degradation and inactivation of Cdc2, resulting in further dephosphorylation of Cdc20 and rapid accumulation of active APC–Cdc20 to trigger the anaphase. Mad3/BubR1 inhibits APC/CCdc20 activity by acting as a pseudosubstrate and/or by mediating Cdc20 ubiquitination and degradation(Chung and Chen, 2003; Elowe, 2011). At physiological concentrations, BubR1 and Mad2 reciprocally promote binding of each other to CDC20, to quantitatively inhibit CDC20-APC to prevent premature separation of sister chromatids (Fang, 2002). Thus, the cell cycle is arrested at metaphase

when the checkpoint detects any defects in microtubule–kinetochore attachment or in the tension of the spindles. Only after ensuring proper attachment of the sister chromatids, the MCC complex detaches from CDC20 allowing free CDC20 to activate APC to result in cell cycle progression (Fang, 2002) (Figure 4.2).

Emi1 can also regulate APC^{CDC20} activity by binding to CDC20 as a pseudo-substrate resulting in inhibition of Cyclin B degradation (Reimann *et al.*, 2001) . USP44 (Ubiquitin-specific protease 44) can deubiquitinate CDC20 and prevent the premature APC activation through preventing its inhibitory effect on CDC20-MAD2 complex to regulate mitotic entry (Stegmeier *et al.*, 2007). The RASSIF1, tumour suppressor can also regulate APC^{CDC20} activity during mitosis by preventing degradation of Cyclin A and Cyclin B at the spindle poles, while this activity can be inhibited by Aurora A allowing prometaphase progression of the cell cycle (Song *et al.*, 2004; Song *et al.*, 2009).
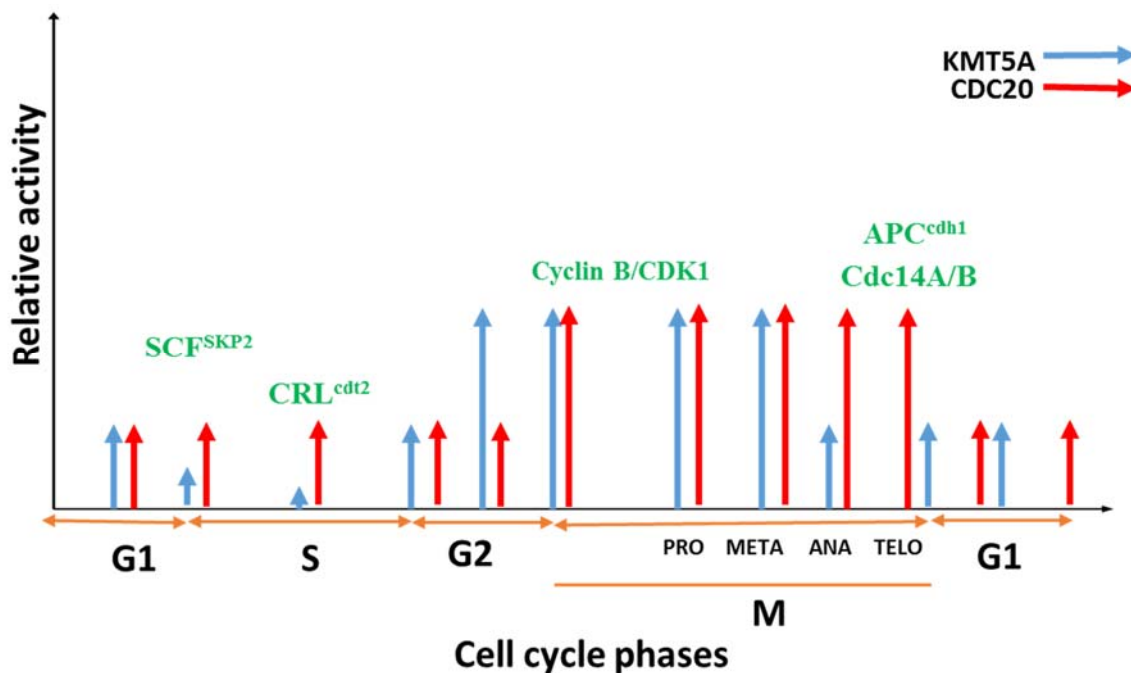
Figure 4-1 CDC20 activity in cell cycle. CDC20 expression peaks during mitosis and is reduced during G1.

Regulation of CDC20 expression

Currently, KMT5A has not been reported to modulate the expression of CDC20 directly and as such in considering CDC20 as a biomarker for KMT5A activity, it is important to determine whether KMT5A can indeed directly affect CDC20 gene expression. As well as Smyd2, Set9 andG9a/Glp, KMT5A is also known to methylate p53. Each of these enzymes can methylate a different lysine on p53; K370, K372, K373 and K382, respectively. It has been found that K382me1 of p53 is reduced in response to DNA damage and that it is the preferred site for binding the chromatin compacting factor, L3MBTL1, to result in decreased transcription. Furthermore, an increase in the enrichment of p53-K382me1 at DNA repair gene promoters and a reduction at promoters of cell cycle arrest and apoptosis genes in tumour cells has been observed, which reflects the changing roles of p53-K382me1 between normal and tumour cells (Huang *et al.*, 2010). KMT5A mediated mono-methylation of p53 at K382 reduces its ability to bind to the p21 promoter thereby reducing p21 expression. p53 is considered as an important negative regulator of CDC20 that can regulate tumour cell growth (Kidokoro *et al.*, 2008).

p53 is a transcriptional regulator of p21, and the p53-p21 pathway has been found to regulate CDC20 expression through CDE–CHR elements (cell cycle dependent element-cell cycle genes homology region). CDE–CHR elements are involved in the regulation of several cell cycle regulators including E2F. p53 inhibits tumour cell growth by indirect regulation of CDC20, which suggests CDC20 may be a potential therapeutic target for a wide range of cancers (Kidokoro *et al.*, 2008). Therefore, due to the impact of p21 on CDC20 expression the effect of KMT5A depletion on CDC20 expression may be occurring via p53.

This chapter is aimed to investigate the possibility of considering CDC20 as a biomarker for KMT5A activity in PC and the possible pathways that govern the relationship between KMT5A and CDC20.
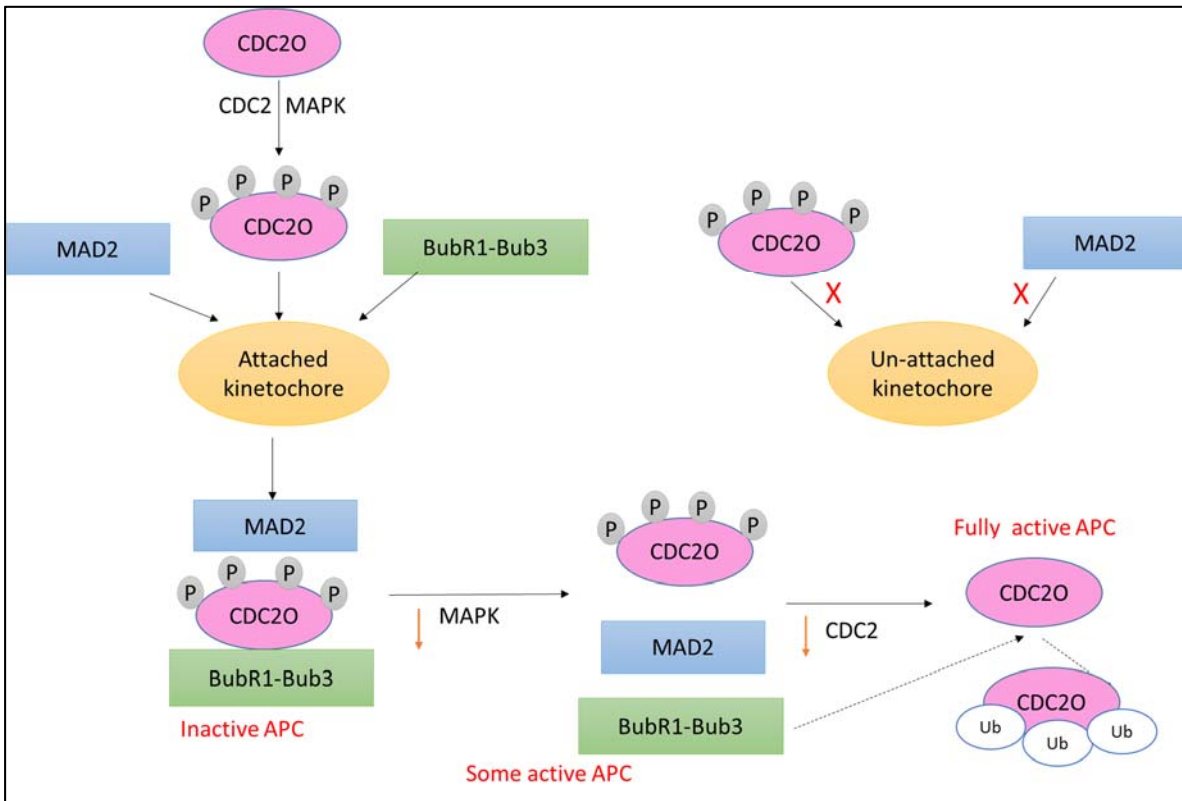
Figure 4-2 Regulation of CDC20. BubR1 and Mad2 reciprocally promote binding of each other to CDC20, to quantitatively inhibit CDC20-APC to prevent premature separation of sister chromatids. After ensuring proper attachment of the sister chromatids, the MCC complex detaches from CDC20 allowing free CDC20 to activate APC to result in cell cycle progression. Adapted from (Chung and Chen, 2003; Elowe, 2011)

4.2. Specific materials and methods

4.2.1. Specific materials

4.2.1.1. Cell lines

LNCaP and LNCaP-AI cells were used in this study as detailed in Chapter 2.1.1.

4.2.1.2. Antibodies

A number of primary antibodies were used to detect protein expression by Western blotting (Table 4.1).

Table 4-1 Western blot antibodies

Antibody	*Species*	*Catalogue number*
KMT5A	Rabbit	Cell Signalling (2996)
CDC20	Mouse	Abcam (Ab190711)
FOXM1	Mouse	Santa Cruz (Sc-502)
PLK1	Mouse	Santa Cruz (Sc-55504)
Cyclin B	Mouse	BD-Pharm(554176)
p53	Mouse	Calbiochem(pAb-421#OP03)
p21	Mouse	Calbiochem(Ab-1#OP64)
Phospho-p53 (Ser15)	Rabbit	Cell Signalling
p53 (acetyl K382)	Rabbit	Abcam (ab75754)
α-Tubulin	Mouse	Sigma

4.2.1.3. *Primer sequences*

To detect the expression of individual genes at the mRNA level, specific primer sets were used (Table 4.2).

Table 4-2 Primers for QRT-PCR.

	Forward Primer (5'-3')	Reverse Primer (5'-3')
KMT5A	GATCCCAGGCGGTGACAGAG	CCCGGTAAATACGTTCTCCCC
HPRT1	TTGCTTTCCTTGGTCAGGCA	AGCTTGCGACCTTGACCATCT
CDC20	TCGCATCTGGAATGTGTGCT	CCGGGATGTGTGACCTTTGA
FOXM1	CAAGCCAGGCTGGAAGAACTC	TGCTGCTTAAACACCTGGTCC
PLK1	CCGCAATTACATGAGCGAGC	TGAGCTTGGTGTGATCCTGG
CCNB	TAAGATTGGAGAGGTTGATGTCGA	CCAGGTGCTGCATAACTGGA
p53	TCAGATAGCGATGGTCTGGC	CGCCCATGCAGGAACTGTTA
CDKN1A	TCACCCTCCAGTGGTGTCTC	TGTTCAGGCGCCATGTCAG
CDC20 promoter	TCTGAGCACATTCATACAATTCACTC	AACACGCCTGGCTTACGCCTCT
AREIII	TGGGACAACTTGCAAACCTG	CCAGAGTAGGTCTGTTTTCAATCCA

4.2.1.4. *siRNAs sequences*

In order to achieve CDC20 and FOXM1 depletion, specific siRNAs were used (Table 4.3).

Table 4-3 Small interference RNA sequences.

siRNA	*Sense sequence*	*Anti-sense sequence*
Non-silencing (NS) (1022076) (Qiagen	UUCUCCGAACGUGUCACGU	ACGUGACACGUUCGGAGAA
CDC20 #1	CGGAAGACCUGCCGUUACA	UGUAACGGCAGGUCUUCCG
CDC20 #2	GGGCCGAACUCCUGGCAAA	UUUGCCAGGAGUUCGGCCC
FOXM1#1	GGACCACUUUCCCUACUUUUU	AAAAAGUAGGGAAAGUGGUCC
FOXM1#2	GUGGCAGAGUCCAACUCUUUU	AAAAGAGUUGGACUCUGCCAC

4.2.2. Specific Methods

4.2.2.1. Chromatin Immunoprecipitation (ChIP)

ChIP technique was used to determine H4K20me1 marker enrichment at the CDC20 promoter in response to DHT mediated AR activation over a time period of 0, 30, 60 and 120 minutes as described in Chapter 2.2.6 with the following specific modifications. LNCaP cells were seeded out in 150 mm dishes in FM. Once cells were 70% confluent, cells were starved in SDM for 72 hours, to diminish AR activity and to ensure AR elimination from target gene promoters. In LNCaP-AI cells, which are routinely grown in SDM, cells were seeded and allowed to adhere for 24 hours prior to stimulation with DHT (100 nM) for 0, 30, 60 and 120 minutes. ChIP grade antibody H4K20me1 were used in order to identify regions of DNA where these proteins are bound.

4.3. Results

4.3.1. *CDC20 protein expression level is reduced significantly with KMT5A knockdown in LNCaP and LNCaP-AI cells*

Data from microarray study showed that KMT5A knockdown by siRNAs results in a significant reduction in CDC20 mRNA expression levels in LNCaP-AI cells of ~2 fold ($p \leq 0.05$). This was further validated by QRT-PCR in both LNCaP and LNCaP-AI cell lines, where an ~3-4 fold and ~2-5 fold, respectively ($p \leq 0.05$) reduction in expression was observed (Figure 3.11). In order to determine whether a reduction at the mRNA levels results in a reduction at the protein level, similar experiments were carried out using Western blotting as an experimental endpoint.

Depletion of KMT5A was achieved in LNCaP and LNCaP-AI cells by reverse transfection in SDM for 72 hours using 2 independent KMT5A siRNA sequences, followed by 10 nM DHT stimulation for 24 hours. Non-silencing (N/S) was used as a negative control. In both cell lines tested, a robust knockdown of KMT5A was observed both in the presence and absence of DHT stimulation. Furthermore, in line with the mRNA data, the levels of KMT5A was unaffected by any DHT stimulation. Similarly to the mRNA data, CDC20 levels were consistently reduced upon KMT5A knockdown in both cell lines irrespective of DHT stimulation, which also had no effect on CDC20 levels in N/S controls (Figure 4.3). The data confirm what was observed at the mRNA level, that CDC20 expression was regulated by KMT5A in PC cells.
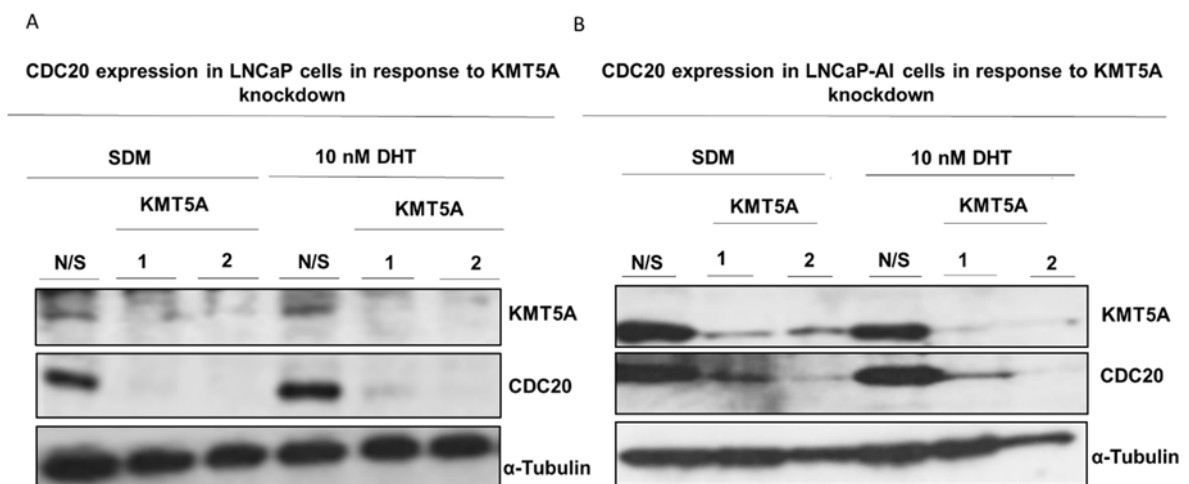
Figure 4-3 KMT5A knockdown reduces CDC20 expression at the protein level. (A) LNCaP and (B) LNCaP-AI cells were reverse transfected with N/S siRNA or the two selected KMT5A siRNAs for 72 hours followed by either stimulation with 10 nM DHT or vehicle control for 24 hours. Protein was collected and knockdown of KMT5A and the effect on CDC20 expression was determined by Western blotting (representative blot).

4.3.2. *KMT5A depletion differentially affects the cell cycle profile in LNCaP and LNCaP-AI cells*

As KMT5A is a cell cycle regulator, the presence of KMT5A and its histone mono-methylation activity play an essential role in cell cycle progression. The cell cycle profile was examined in the presence and absence of KMT5A in LNCaP and LNCaP-AI cell lines. KMT5A knockdown was achieved using the same protocol as in Figure 4.3. Only one siRNA against KMT5A was used for this experiment as both siRNAs gave a significant efficient knockdown for KMT5A. Following the knockdown period, the cells were stained using propidium iodide for 40 minutes, then the cell cycle analysis was conducted by flow cytometry as described in Chapter 2.2.4.

The data was averaged over 3 experiments. No significant changes were detected in cell cycle progression in LNCaP cells when KMT5A expression was depleted with siRNA#1(Figure 4.4.A). However, in LNCaP-AI cells there was a significant reduction ($p \leq 0.05$) in the percentage of cells in G2/M phase of ~50 %, which was accompanied by an increase in the percentage of cells in S phase. However, this was not significant. This data reflects a small disruption in cell cycle distribution in LNCaP-AI cells in response to KMT5A knockdown (Figure 4.4.B).

A Cell cycle progression in LNCaP cells in the presence and absence of KMT5A

B Cell cycle progression in LNCaP-AI cells in the presence and absence of KMT5A
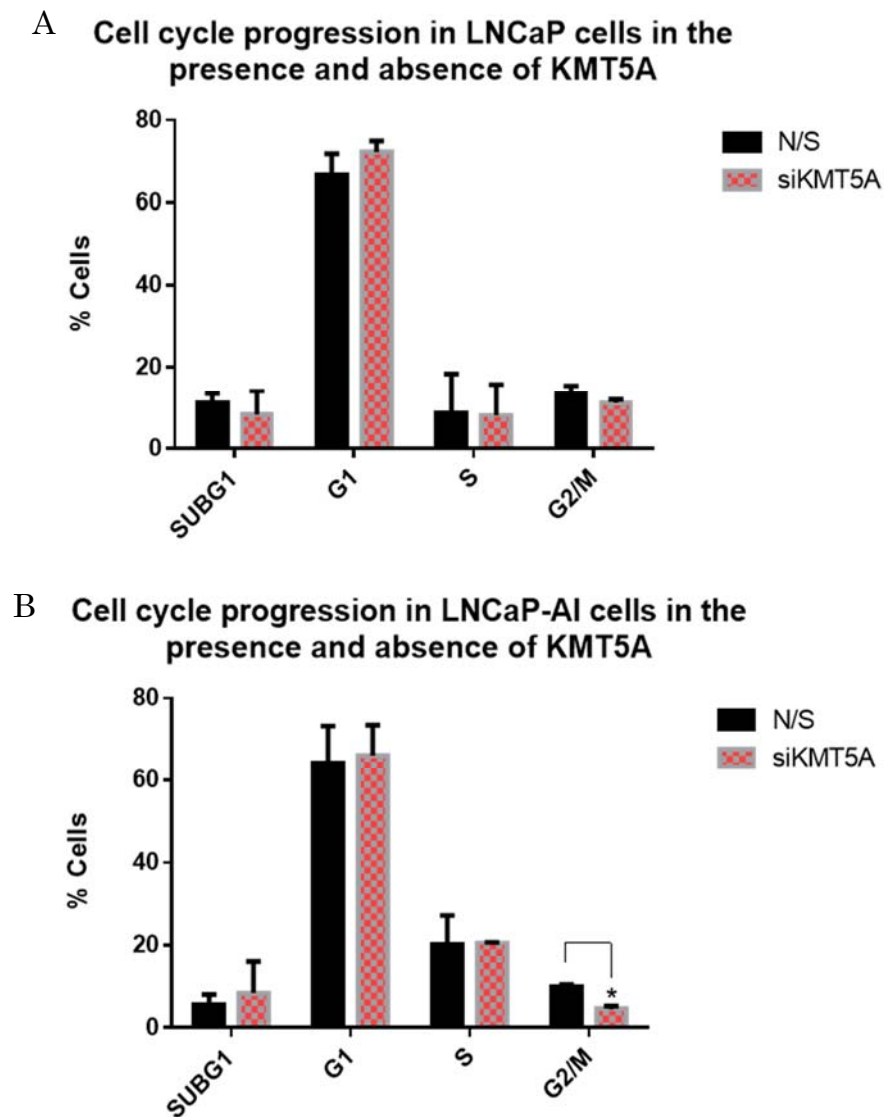
Figure 4-4 Effect of KMT5A depletion on the cell cycle profile in LNCaP and LNCaP-AI cells. (A) LNCaP and (B) LNCaP-AI cells were reverse transfected with N/S siRNA or the selected KMT5A siRNA#1 for 72 hours in 6 well plates. Cell cycle analysis was performed using propidium iodide to stain cellular DNA for 40 minutes. Error bars represent the mean ± SD for triplicate independent experiments. p-values were determined by t-test (* p-value <0.05).

4.3.3. *Reciprocal relationship between CDC20 and KMT5A: CDC20 depletion reduces KMT5A mRNA expression*

Phosphorylated KMT5A during early mitosis is protected from being targeted for ubiquitination by APC^{CDC20}, similar to the other form of this complex, APC^{Cdh1} during the G1 phase of the cell cycle (Wang *et al.*, 2013). Based on this, the relationship between KMT5A and CDC20 was further investigated to test whether depletion of CDC20 would result in an increase in KMT5A protein levels due to decreased turnover by the ubiquitination pathway.

CDC20 knockdown was achieved using two independent siRNA sequences for 72 hours in LNCaP and LNCaP-AI cells. RNA was then collected and it was observed that an ~80 % reduction in CDC20 mRNA level was apparent, when measured by QRT-PCR in LNCaP and LNCaP-AI cells (Figure 4.5.A.i- Bi). Furthermore, KMT5A expression was significantly reduced by ~70-80 % ($p \leq 0.05$) in LNCaP cells and by ~ 60-70 % ($p \leq 0.05$) in LNCaP-AI cells in response to CDC20 depletion (Figure 4.5.Aii- Bii).

In a parallel experiment, protein was collected from LNCaP and LNCaP-AI cells following 72 hours CDC20 knockdown in their respective medium. CDC20 knockdown was confirmed and KMT5A expression was detected at the protein level (Figure 4.5.Aiii-Biii). No robust changes were detected in KMT5A expression in response to CDC20 depletion when loading controls were taken into account. Hence, the changes observed at the mRNA level (Figure 4.5.Aii-Bii) were not reflected at the protein level.
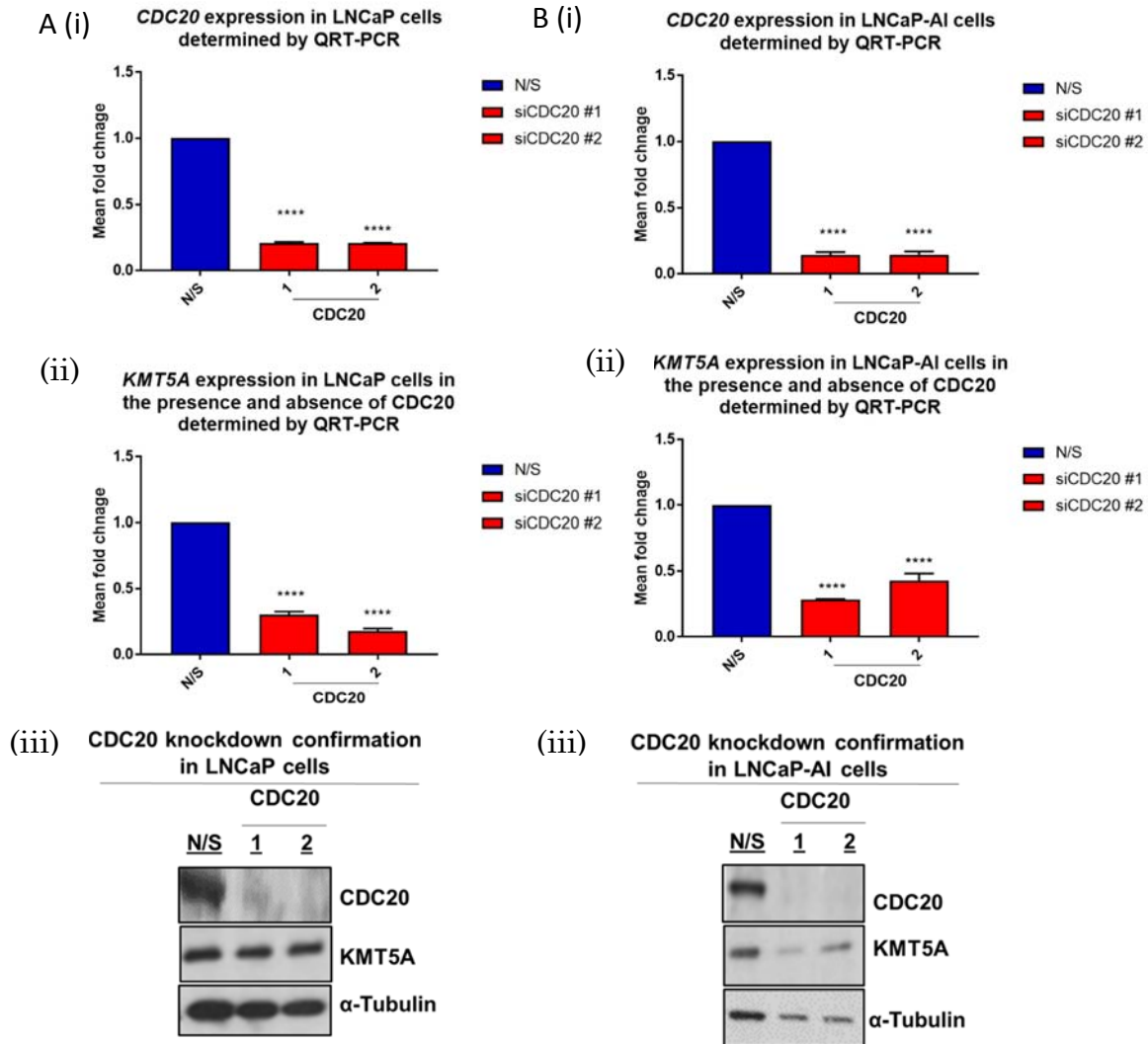
Figure 4-5 Effect of CDC20 depletion on KMT5A mRNA and protein expression in LNCaP and LNCaP-AI cells. (A) LNCaP cells and (B) LNCaP-AI cells were examined for (i) CDC20 mRNA expression (ii) KMT5A mRNA expression and (iii) CDC20 protein expression. Cells were reverse transfected with N/S siRNA or the two selected siRNAs against CDC20 for 72 hours in 6 well plates. RNA and protein were collected and CDC20 knockdown and its effect on KMT5A expression levels was determined by QRT-PCR and Western blotting (representative blots). Error bars represent the mean ± SD for triplicate independent experiments. p-values were determined by t-test (* p-value <0.05, ** p-value <0.01, *** p-value <0.001 and **** p- value < 0.0001).

4.3.4. *The effect of CDC20 depletion on cell cycle profile in LNCaP and LNCaP-AI cells*
As KMT5A depletion showed some disruption in cell cycle progression in LNCaP-AI cells (Figure 4.4) the subsequent effect of a reduction in CDC20 levels, which is also a cell cycle regulator, may be playing a role in this disruption. To test this, the cell cycle profile was examined in the presence and absence of CDC20 in LNCaP and LNCaP-AI cell lines.

CDC20 knockdown was achieved using CDC20 siRNA#1 (Table 4.3) for 72 hours for each cell line in its respective medium. Only one siRNA against CDC20 was used for this experiment as both siRNAs gave a significant efficient knockdown for CDC20. Following the knockdown period, cells were stained using propidium iodide for 40 minutes, then the cell cycle analysis was conducted by flow cytometry as detailed in Chapter 2.2.4.

The data was averaged over 3 experimental repeats. CDC20 depletion was previously reported to prevent the progression of the cell cycle in mitosis. In agreement with this report, in the LNCaP cells there was a statistically significant ~90 % increase ($p \leq 0.05$) in the percentage of cells in G2/M phase compared to the N/S control, suggesting a cell cycle arrest at this phase in response to CDC20 knockdown (Figure 4.6.A). However, in contrast no significant changes were detected in LNCaP-AI cells (Figure 4.6.B).
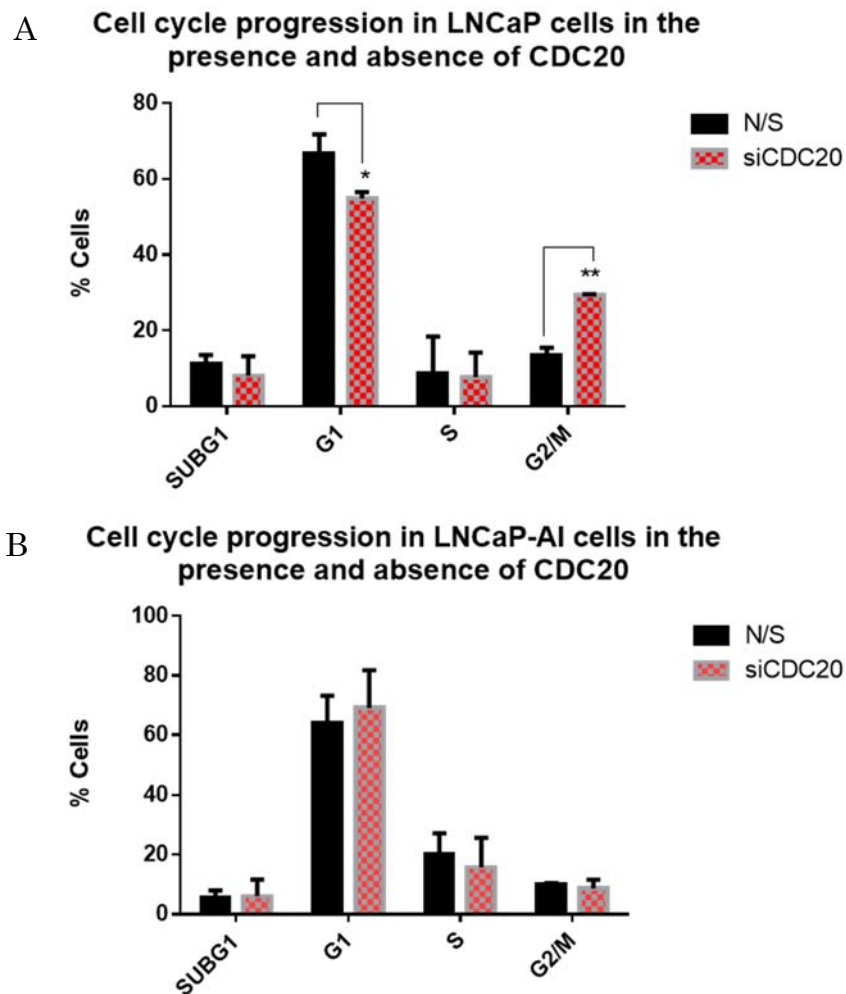
Figure 4-6 Effect of CDC20 depletion on cell cycle profile in LNCaP and LNCaP-AI cells. (A) LNCaP and (B) LNCaP-AI cells were reverse transfected with N/S siRNA or the selected CDCC20 siRNA#1 for 72 hours in 6 well plates. Cell cycle analysis was performed using propidium iodide to stain cellular DNA for 40 minutes. Error bars represent the mean ± SD for triplicate independent experiments. p-values were determined by t-test (* p-value <0.05).

4.3.5. *KMT5A and CDC20 depletion reduce LNCaP and LNCaP-AI cellular proliferation rate*

In order to address the findings from Figure 4.3 and Figure 4.5 which were inconsistent with previously published data regarding cell cycle progression following knockdown of KMT5A or CDC20, an experiment was designed to look at cellular proliferation over a longer time period. In previous experiments, cells were only subjected to 72 hours knockdown prior to the assessment of cell cycle profile. Previously, it has been found that in order for some of these cell cycle enzymes to have a phenotypic effect, cells must undergo a minimum of 2 cell cycles in their absence (Abbas *et al.*, 2010a).

Knockdown of KMT5A or CDC20 was performed in LNCaP and LNCaP-AI cells for 72 hours in their respective medium. Cells were then counted and seeded out in 96 wells plates for a further 96 hours. Cellular proliferation was then determined by SRB assay as described in Chapter 2.2.1.4.

Approximately 50 % reduction in the proliferation was observed following either KMT5A or CDC20 knockdown in LNCaP cells (p≤0.05) (Figure 4.7. A-B), whilst an ~75 % reduction in cellular proliferation was observed in LNCaP-AI cells with both KMT5A and CDC20 knockdown (Figure 4.7.C-D). The data was consistent with previously reported data which showed a rapid reduction in U2OS cell line proliferation in response to KMT5A depletion (Oda *et al.*, 2009), and also with data published regarding CDC20 as one of the genes required for human cancer cell proliferation (Huang *et al.*, 2009).
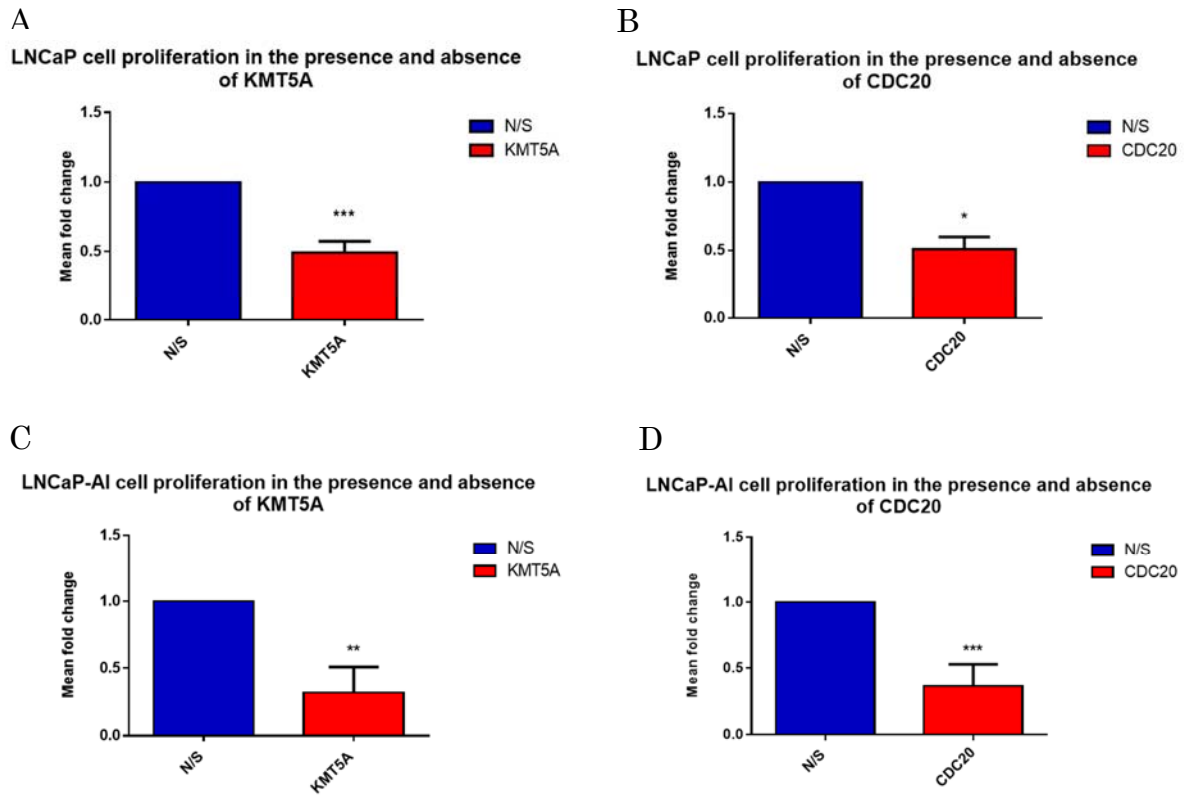
Figure 4-7 Effect of KMT5A and CDC20 depletion on LNCaP and LNCaP-AI cell proliferation. LNCaP cells (A) with KMT5A depletion and (B) CDC20 depletion. LNCaP-AI cells(C) with KMT5A depletion and (D) CDC20 depletion. Cells were reverse transfected with N/S siRNA or the siRNAs against KMT5A and CDC20 for 72 hours in 6 well plates. Cells were then counted and re-seeded in 96 well plates. Cell growth was determined after a period of 4 days using SRB assays. Error bars represent the mean ± SD for triplicate independent experiments. p-values were determined by t-test (* p-value <0.05, ** p-value 0.01 and *** p-value <0.001).

4.3.6. *CDC20 expression in PC cell lines*

CDC20 basal expression was previously reported to be less in LNCaP compared to LNCaP-ABL cells (an androgen independent derivative of LNCaP cells) (Wang *et al.*, 2009). To further expand this observation, CDC20 expression levels were detected in a panel of PC cell lines, which are representative of different stages of the disease.

No robust major changes in CDC20 expression were observed between the different cell lines tested when the loading controls were taken into account A double band was apparent for CDC20 in the DU145 cell line, which may be an indicator of the presence of two isoforms for CDC20 in this cell line, although this has not been investigated further in this study (Figure 4.8.A). CDC20 has previously been reported to have five isoforms in *Arabidopsis thaliana*, where CDC20.1 and CDC20.2 were detailed as the two active and redundant isoforms, which both played a role in the regulation of APC/C activity by binding to the APC10 subunit (Kevei *et al.*, 2011). However, no other isoforms for CDC20 have been reported to date in any other species.

Prior to investigating the relationship between KMTA and CDC20, and in order to clearly understand the localization pattern of KMT5A and CDC20 in PC cells, cellular distribution of both KMT5A and CDC20 was investigated in the LNCaP-AI cell line using methods outlined in Chapter 2.2.7. Fractionation efficiency was confirmed by immunoblot with an α-tubulin antibody that specifically localises its antigen in the cytoplasm, and a PARP antibody that detects its antigen specifically in the nucleus. CDC20 was found to be predominantly localized in the cytoplasm, while KMT5A was detected in both cytoplasmic and nuclear compartment, which is consistent with previously reported data about their cellular localisation in different cancers (Figure 4.8.B). KMTA was previously reported to be localised either in the nucleus or the cytoplasm mainly depending on cell cycle (Yin *et al.*, 2008b) which is consistent with the data in this figure. Whereas for CDC20, it has been reported as being a part of the APC/C complex, its activity toward securin started in the cytoplasm and then on the chromosomes, to stimulate the final and rapid activation of separase on chromosomes before the onset of anaphase (Sivakumar *et al.*, 2014). From the data above, it would be most likely that KMT5A and CDC20 would form any possible

interaction in the cytoplasm as both are localised there at some part of the cell cycle. Further investigation is required to determine the possible interaction.
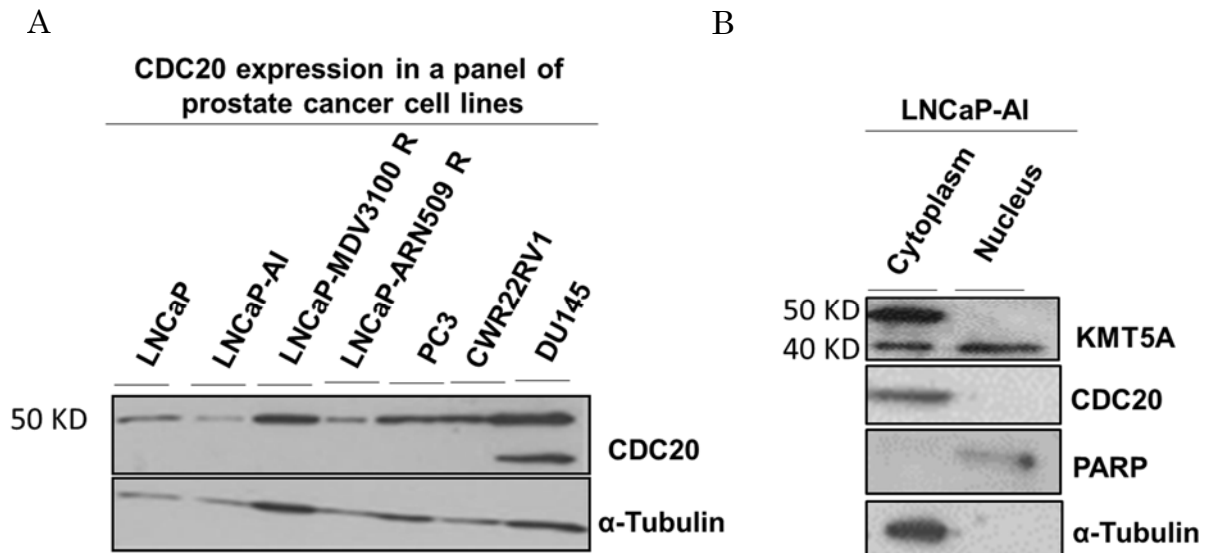
Figure 4-8 CDC20 expression and cellular distribution (A) CDC20 expression in a panel of PC cell lines. Protein lysate were collected from 500000 cells from each cell line and the expression of CDC20 was detected by Western blotting. (B) Cellular localisation of KMT5A and CDC20 in LNCaP-AI cells. LNCaP-AI cells were grown to 70 % confluency in SDM and nuclear cytoplasmic extracts generated using the NE-PER™ Nuclear and Cytoplasmic Extraction Kit were evaluated in Western blot analysis (representative blot).

4.3.7.*KMT5A and CDC20 protein interaction: endogenous and exogenous interaction*
KMT5A has been reported previously to interact with a large number of proteins including PCNA, DDX21 (Qin *et al.*, 2013) and also with p53 where KMT5A binds to K382 to catalyse the methyltransferase function (Scoumanne and Chen, 2008). To investigate if KMT5A can also regulate CDC20 expression via its methylation activity through direct contact, the interaction between KMT5A and CDC20 was investigated.

Firstly, LNCaP and LNCaP-AI cells were grown in their respective medium for 48 hours. Native immunoprecipitation was then performed, as outlined in Chapter 2.2.5. KMT5A was found to be immunoprecipitated from both cell lines as demonstrated by Western blotting and its interaction with CDC20 was confirmed endogenously in both cell lines (Figure 4.9.A).

Secondly, KMT5A-CDC20 interaction was investigated exogenously in 293T cells, when both KMT5A and CDC20 were overexpressed. Cells were grown to 70 % confluency before forward transfection of 1 μg of pFlag-KMT5A WT and / or pHA-CDC20 into 293T cells using Lipofectamine TM LTX (Invitrogen, New York, USA) according to the manufacturer's recommendations. KMT5A was successfully immunoprecipitated from LNCaP and LNCaP-AI cell lines demonstrated by Western blotting, and its interaction with CDC20 was confirmed in both cell lines (Figure 4.9.B). KMT5A interaction was only observed when both constructs were present as a band of 52 kD which represent a full length CDC20 protein. The data indicated that KMT5A and CDC20 do indeed interact which raises the possibility that the two proteins are resident in the same complex.
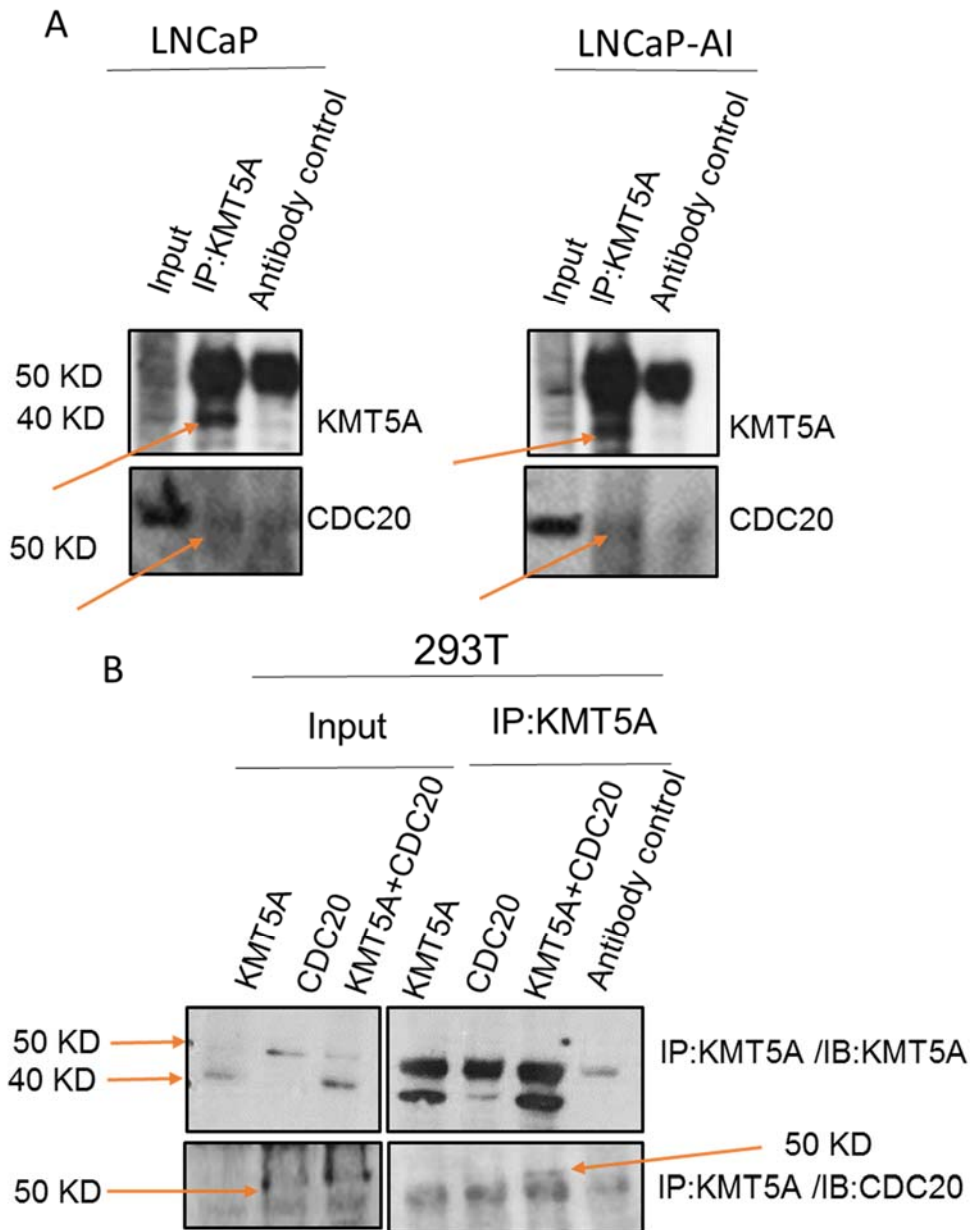
Figure 4-9 KMT5A interacts with CDC20 (A) Endogenous interaction between KMT5A and CDC20 in LNCaP and LNCaP-AI cells. Cells were grown to 70% confluency and a cell pellet was generated by centrifugation and native IP was applied to pull down KMT5A. (B) Exogenous interaction between KMT5A and CDC20 in 293T cells. Cells were grown for 48 hours followed by forward transfection with pFlag-KMT5A WT and / or pHA-CDC20 for 48 hours. Cell lysates were collected, immunoprecipitation performed and subjected to Western blotting using anti-KMT5A to confirm the pull down and anti-CDC20 to confirm the interaction (representative blots).

4.3.8. *H4K20me1 mark is enriched at the CDC20 promoter*

From (Figure 4.7), KMT5A and CDC20 interaction was confirmed. It was next decided to determine whether KMT5A directly controls CDC20 expression through KMT5A enzymatic activity acting via mono-methylation of H4K20 at the CDC20 promoter.

In this experiment, the effect of DHT stimulation on KMT5A activity was also examined to explore whether the differential effect of DHT stimulation on KMT5A expression in LNCaP and LNCaP-AI cells (Coffey *et al*, unpublished data) was due to differences at the promoter level. LNCaP cells were starved in SDM for 72 hours, followed by DHT (100 nM) stimulation for 0, 15, 30 and 120 minutes. The same treatment was also performed in LNCaP-AI cells following 72 hours growth in its respective medium (SDM).

Following DHT treatment, the enrichment of H4K20me1 on the CDC20 promoter was found to vary between the two cell lines tested. In the LNCaP cells, there was a reduction in the level of H4K20me1 at the CDC20 promoter region in response to DHT treatment. However in LNCaP-AI cells, DHT treatment clearly enhanced H4K20me1 which peaked at ~5 fold after 30 minutes stimulation (Figure 4.10). This data is consistent with the data previously obtained in our group (Coffey *et al,* unpublished data), which indicated the difference in KMT5A expression in response to DHT stimulation where KMT5A expression was decreased and increased respectively in LNCaP and LNCaP-AI cells, which would impinge on its mono-methylation activity at the target genes promoters.
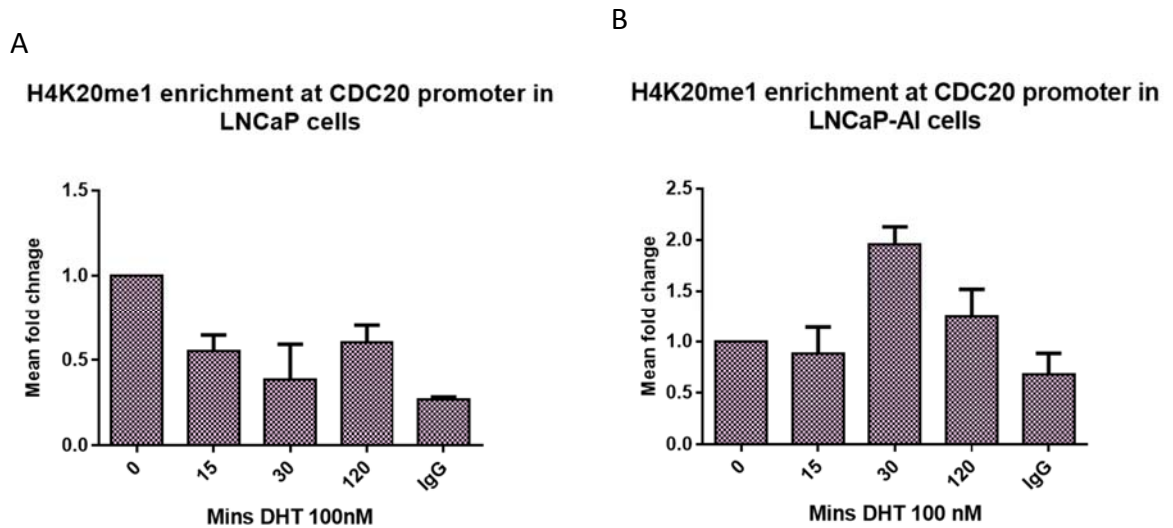
Figure 4-10 Assessment of the H4K20me1 mark at the CDC20 promoter in response to DHT treatment in LNCaP and LNCaP-AI cells. (A) LNCaP cells and (B) LNCaP-AI cells were starved in SDM for 72hours followed by DHT (100 nM) stimulation for 0, 15, 30 and 120 minutes. Chromatin immunoprecipitation assay was performed as previously described. Rabbit IgG was used as negative control under identical conditions and at the same concentration as H4K20me1 antibody. Results are expressed relative to the values of untreated samples. Error bars represent the mean ± SD for triplicate independent experiments.

4.3.9. *KMT5A depletion reduces FOXM1 expression, a potential regulator of CDC20*
KMT5A was confirmed to be able to control CDC20 expression through the mono-
methylation activity in response to DHT stimulation (Figure 4.10). To understand if KMT5A
can affect CDC20 expression indirectly through other pathways that might be affected by
KMT5A depletion, FOXM1 was selected to be investigated as it has been reported as a
transcriptional regulator of CDC20 (Xie *et al.*, 2015). KMT5A depletion resulted in a
significant reduction in FOXM1 expression of ~1.5-2 fold in the absence of DHT most
notably with siRNA#2 ($p \leq 0.05$) in the microarray data (Figure 4.11.A). The data was also
confirmed by QRT-PCR in LNCaP-AI cells as ~2 fold reduction was also observed in the
absence of DHT when compared to the N/S control (Figure 4.11.B). The validation was
extended to include the LNCaP cells were a significant reduction in FOXM1 expression of ~2
fold was observed particularly with siRNA#1 in the DHT untreated arm (Figure 4.11.C).

To further investigate the effect of KMT5A depletion on FOXM1 expression, the protein
expression of FOXM1 was measured in response to KMT5A knockdown in LNCaP and
LNCaP-AI cells. A robust reduction in FOXM1 expression in response to KMT5A depletion
was observed, which was enhanced with DHT treatment in LNCaP cells (Figure 4.11.D) and
also in LNCaP-AI cells (Figure 4.11.E). From the data above, FOXM1 expression in the
LNCaP-AI cells was found to be down-regulated by DHT treatment at the mRNA and protein
level, while in the LNCaP cells a slight up-regulation at both the mRNA and protein level was
observed in response to DHT treatment.

Prior to investigating the effect of KMT5A and FOXM1 on CDC20 expression, the activity of
FOXM1 in response to KMT5A knockdown was also investigated by looking at the
expression level of selected FOXM1 downstream targets (Cyclin B and PLK1). The
microarray data showed a statistically significant reduction in *PLK1* (Figure 4.12.A) and
Cyclin B (Figure 4.12.B) expression of ~3 fold and 2 fold, respectively. Most notable effects
were observed with siRNA#2 in the absence of DHT for *Cyclin B* and also for *PLK1* in the
presence of DHT ($p \leq 0.05$) where a significant ~2-3 fold reduction was observed. Both *Cyclin
B and PLK1* expression levels were correlated with FOXM1 reduction in response to KMT5A
depletion. Interestingly, the same trend was also detected for these FOXM1 substrates in the
initial microarray data set and subsequent Western blotting experiments (Figure 4.11). A
robust reduction in Cyclin B and PLK1 expression at the protein level was detected in LNCaP
and LNCaP-AI cell lines (Figure 4.12. C-D). This data supported the possible effect of
KMT5A depletion on CDC20 via FOXM1 as one of its substrates.
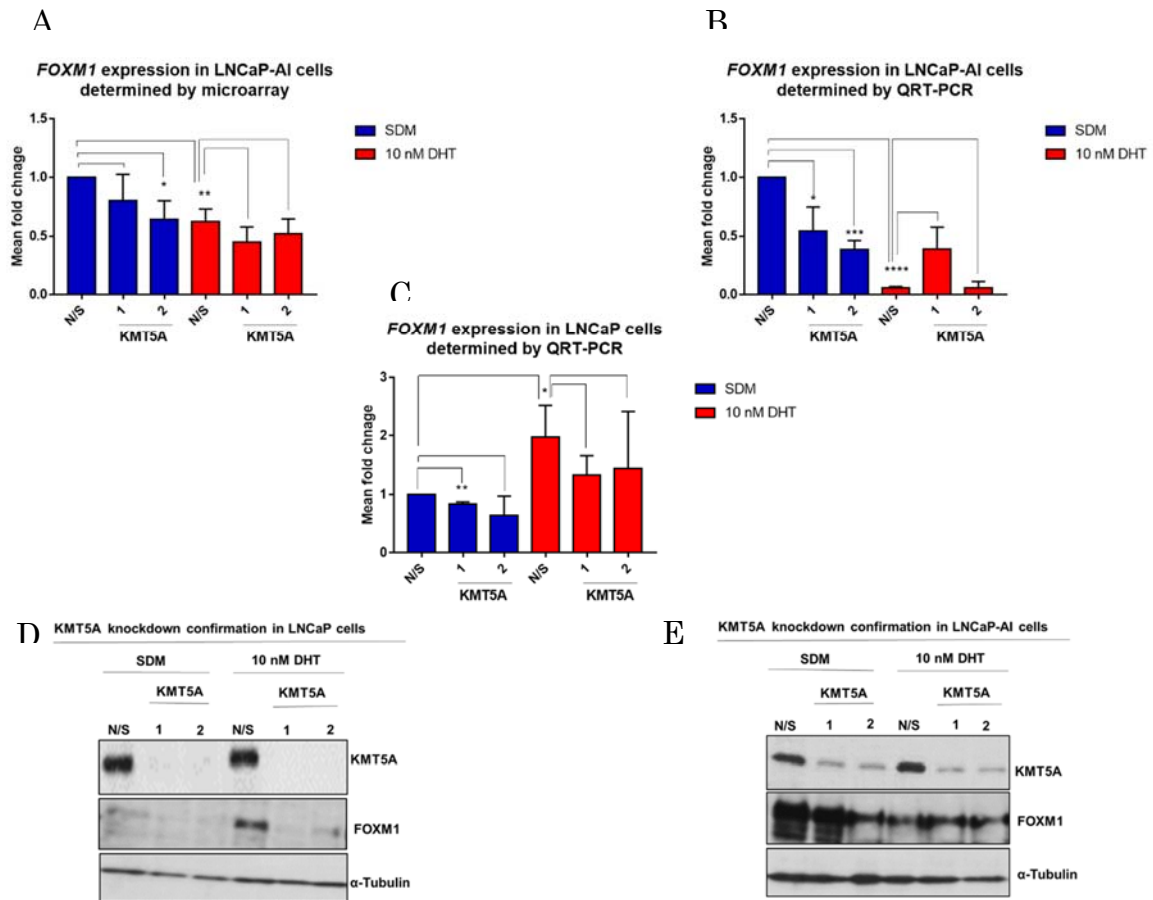
Figure 4-11 Effect of KMT5A knockdown on FOXM1 expression in LNCaP and LNCaP-AI cells. LNCaP-AI (A,B,E) and LNCaP(C,D) cells were reverse transfected with N/S siRNA or the two selected KMT5A siRNAs for 72 hours followed by either stimulation with 10 nM DHT or vehicle control for 24 hours. RNA and protein were collected and KMT5A knockdown and its effect on FOXM1 expression levels were determined by QRT-PCR and Western blotting (representative blots). Error bars represent the mean ± SD for triplicate independent experiments. p-values were determined by t-test (* p-value <0.05, ** p-value <0.01, *** p-value <0.001 and **** p- value < 0.0001).
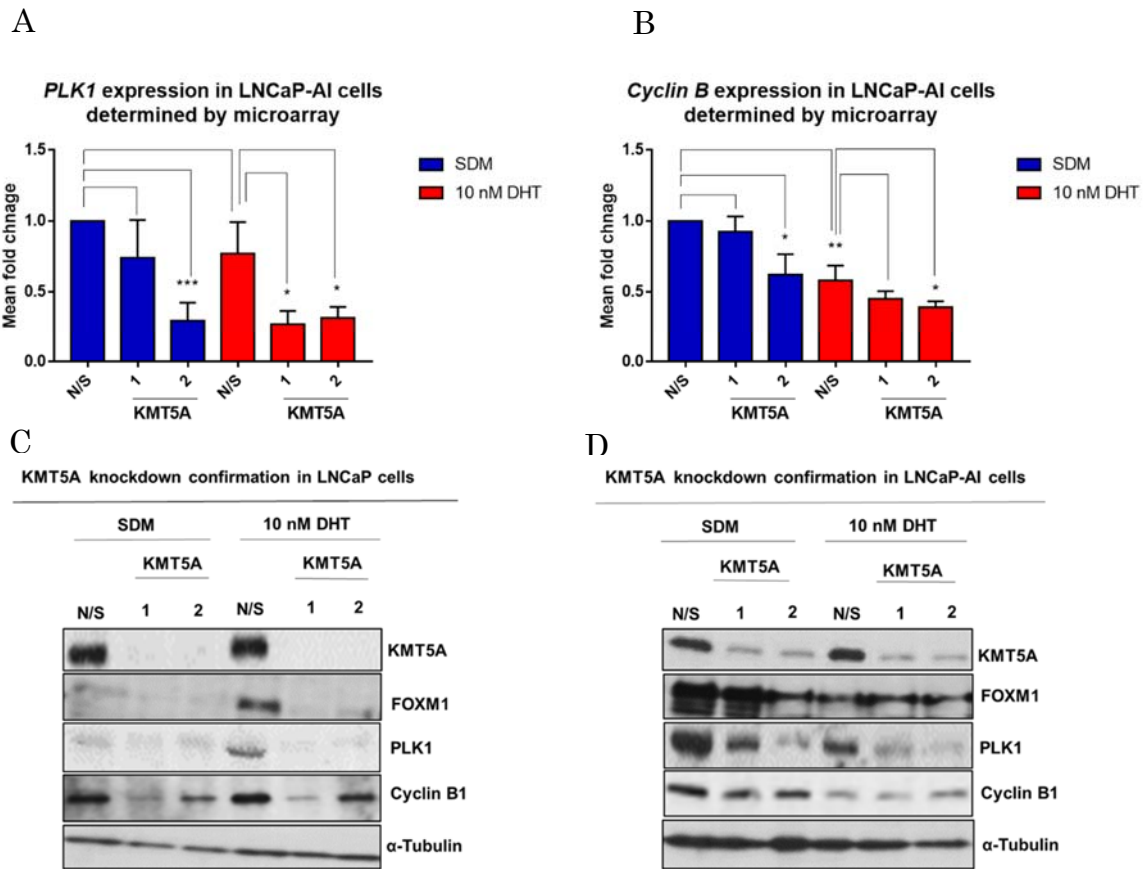
Figure 4-12 KMT5A knockdown reduces FOXM1 and downstream targets in LNCaP and LNCaP-AI cells. LNCaP-AI (A, B, D) and LNCaP(C) cells were reverse transfected with N/S siRNA or the two selected KMT5A siRNAs for 72 hours followed by either stimulation with 10 nM DHT or vehicle control for 24 hours. RNA and protein were collected and KMT5A knockdown and its effect on FOXM1, PLK1 and Cyclin B expression levels was determined by QRT-PCR and Western blotting (representative blots). Error bars represent the mean ± SD for triplicate independent experiments. p-values were determined by t-test (* p-value <0.05, ** p-value <0.01 and *** p-value <0.001)

4.3.10. *The effect of AR stimulation on the regulation of FOXM1 and expression of its downstream substrates*

The differences in FOXM1 expression in response to DHT stimulation between LNCaP and LNCaP-AI cells with KMT5A depletion (Figure 4.11, Figure 4.12) was the driving factor to investigate FOXM1 expression at the protein level in response to DHT treatment over a number of time points. It has been reported previously that FOXM1 indirectly elevated AR dependent transcription and AR protein levels, and that FOXM1 and AR proteins physically interact in PC cells (Liu *et al.*, 2014). Therefore, trying to investigate this reciprocal effect of AR on FOXM1 expression was required.

In order to do so, both LNCaP and LNCaP-AI cells were starved for 72 hours in SDM to down-regulate AR signalling, then stimulated with 10 nM DHT for 0, 8 and 24 hours. Protein was then collected and the expression of FOXM1 and some of its substrates (PLK1, SKP2, c-Myc) were detected by Western blotting. An increase in the expression level of FOXM1 in LNCaP cells was observed in response to DHT treatment. The same trend was also observed for the FOXM1 substrates investigated. In contrast for the LNCaP-AI cells a reduction in FOXM1 and its substrates expression was observed in response to AR stimulation (Figure 4.13). The data suggested that FOXM1 is regulated by AR in PC cells. However, further investigation is required to further understand the underlying mechanism.
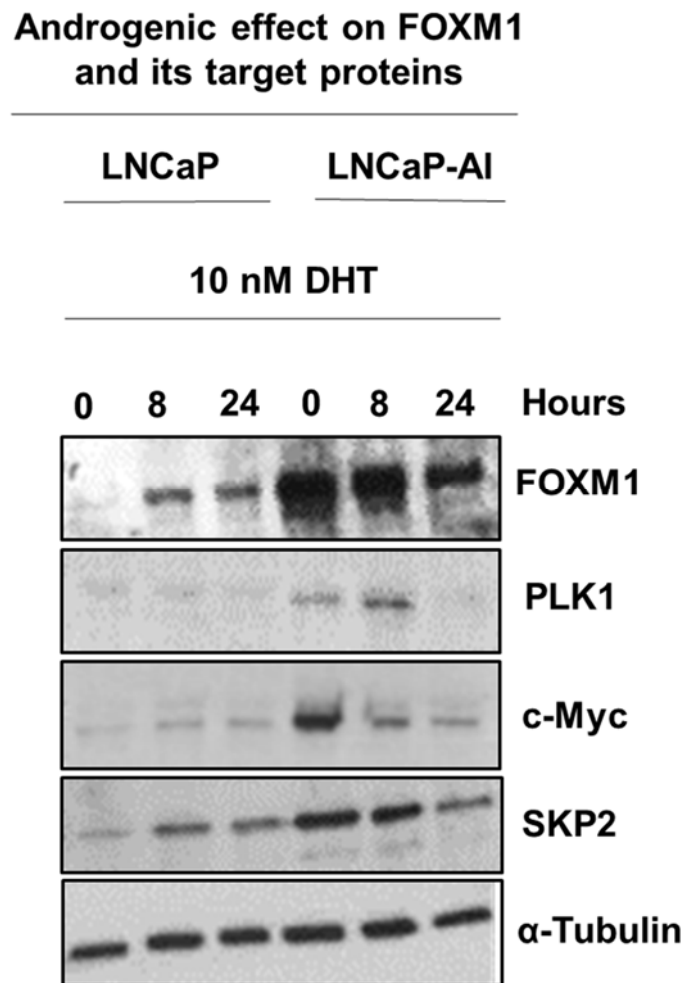
Figure 4-13 Androgenic effect on FOXM1 and its target proteins in LNCaP and LNCaP-AI cell lines. LNCaP and LNCaP-AI cells were grown in SDM for 72 hours followed by treatment with 10 nM DHT for 0, 8 and 24 hours. Protein lysates were collected and FOXM1, PLK1, c-Myc, SKP2 and Alpha-tubulin expression were detected by Western blotting (representative blot).

4.3.11. *The effect of FOXM1 knockdown on CDC20 expression level in LNCaP and LNCaP-AI cells*

As knockdown of KMT5A causes a reduction in FOXM1 expression, which can drive the reduction in CDC20 expression, it is important to directly assess the effect of FOXM1 in these cell lines as a regulator of CDC20. To further investigate CDC20 regulation by FOXM1 in PC cells, FOXM1 itself was depleted using two independent siRNA sequences. The knockdown was performed in LNCaP and LNCaP-AI cell lines each in its own respective medium for 72 hours. RNA and protein was then collected, and the knockdown of FOXM1 was confirmed by QRT-PCR and by Western blotting. Significant knockdown in FOXM1 expression of ~ 70-80 % was achieved at the mRNA level in both cell lines ($p \leq 0.05$) (Figure 4.14.Ai-Bi). However, no significant change in CDC20 mRNA expression was apparent with one of the targeting siRNAs, but there was a very small but significant effect on CDC20 expression with the second siRNA in response to FOXM1 knockdown (Figure 4.14.Aii-Bii) in both LNCaP and LNCaP-AI cell lines. The data was mirrored at the protein level, as a robust reduction in FOXM1 expression at the protein level was seen with no robust changes in CDC20 expression (Figure 4.14.Aiii- Biii). This is a likely indicator that the changes in CDC20 expression in response to KMT5A knockdown are not driven by FOXM1, but probably act through a different pathway independent of FOXM1.
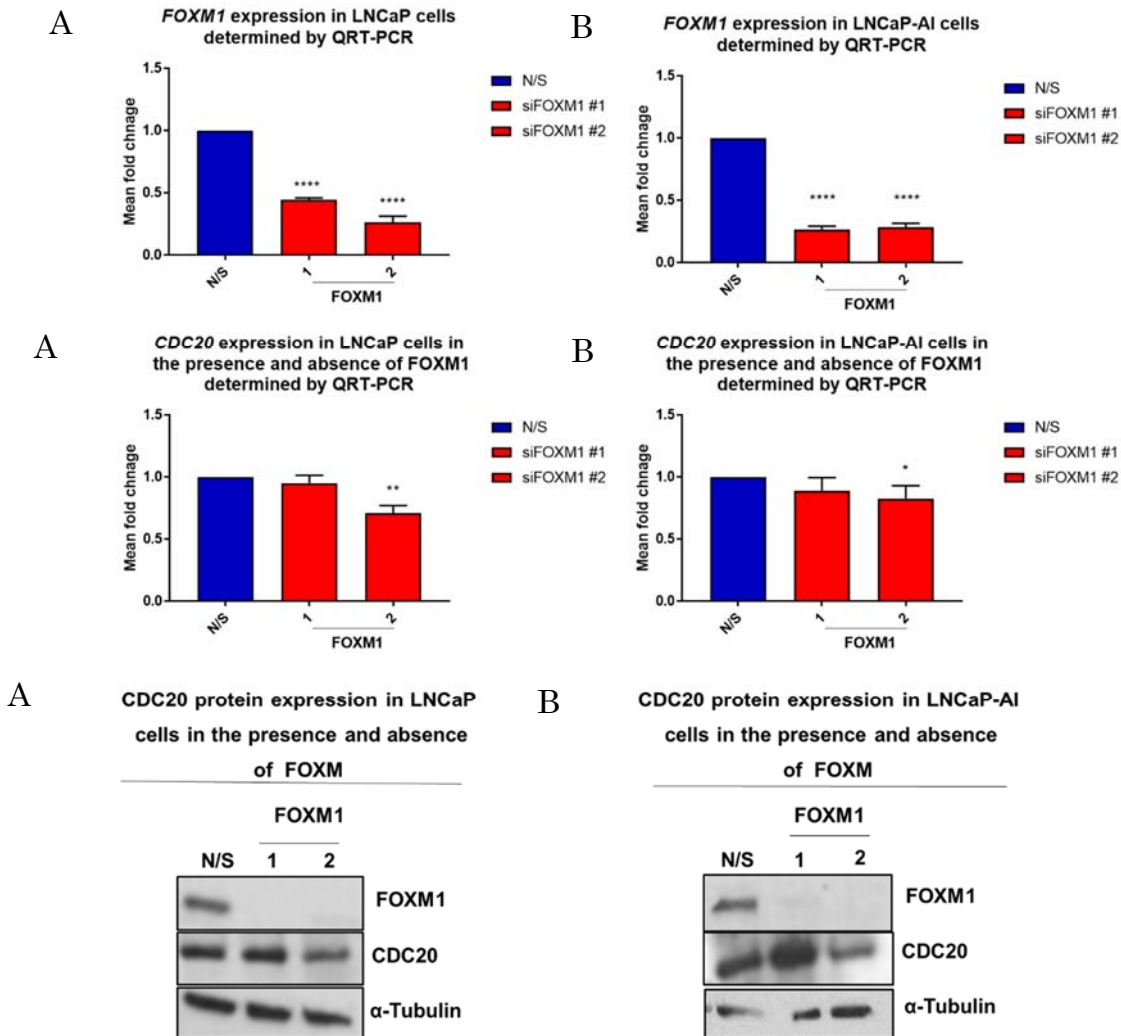
Figure 4-14 FOXM1 depletion does not affect CDC20 expression. (A) LNCaP cells and (B) LNCaP-AI cells (i) FOXM1 depletion and (ii) CDC20 expression, (iii) FOXM1 depletion at protein level. Cells were reverse transfected with N/S siRNA or the two selected siRNAs against FOXM1 for 72 hours in 6 well plates. RNA and protein were collected and FOXM1 knockdown and its effect on CDC20 expression levels was determined by QRT-PCR and Western blotting (representative blots). Error bars represent the mean ± SD for triplicate independent experiments. p-values were determined by t-test (* p-value <0.05, ** p-value <0.01, *** p-value <0.001 and **** p- value < 0.0001).

4.3.12. *p53 regulates CDC20 expression in response to KMT5A mono-methylation at K382: a proposed model*

CDC20 expression is clearly regulated by the expression of KMT5A (Figure 4.3). The transcriptional regulation of CDC20 by FOXM1 in response to KMT5A knockdown was tested revealing that indeed KMT5A can modulate the levels of FOXM1, but, FOXM1 does not play a role in CDC20 expression in the PC cell lines tested.

 Interestingly, CDC20 has been reported to be regulated by p53, to exert its anti-tumour activity, which in turn has been reported to be modulated by KMT5A under certain cellular conditions (Kidokoro *et al.*, 2008). p53 can down-regulate CDC20 expression in response to DNA damage by direct binding to a p53 consensus sequence within the CDC20 promoter in a response element (RE) located 689-bp upstream of the transcription start site (TSS). p53 can also regulate CDC20 expression through a CDE-CHR element, but acting independently of p21 and only under conditions of p53 overexpression and not in response to DNA damage (Banerjee *et al.*, 2009; Nath *et al.*, 2015; Wang *et al.*, 2015).

p53 mono-methylation at K382 by KMT5A can reduce p53 activation by reducing the acetylation of p53 at the same lysine residue. Down-regulation of KMT5A upon DNA damage, can reverse the mono-methylation process on K382 to result in increased p53 stability by converting the mono-methylated p53-K382 into p53-K832me2/3 by histone methyltransferase (Shi *et al.*, 2007; Williams *et al.*, 2014).

As a combination of what has been explained above, a model is suggested to be further investigated in this thesis. This model suggests that in the presence of KMT5A, KMT5A can mono-methylate p53 at K382 resulting in inhibition of its transcriptional activity, therefore diminishing its negative regulation of CDC20 and increasing CDC20 expression. However, when KMT5A is depleted as in silencing of KMT5A by siRNAs, the mono-methylation activity of KMT5A on p53-K382 will be reduced. This results in an increase in p53 activity to transcriptionally down-regulate CDC20 expression, or through binding to CDE-CHR element independently of p21 (Figure 4.15).
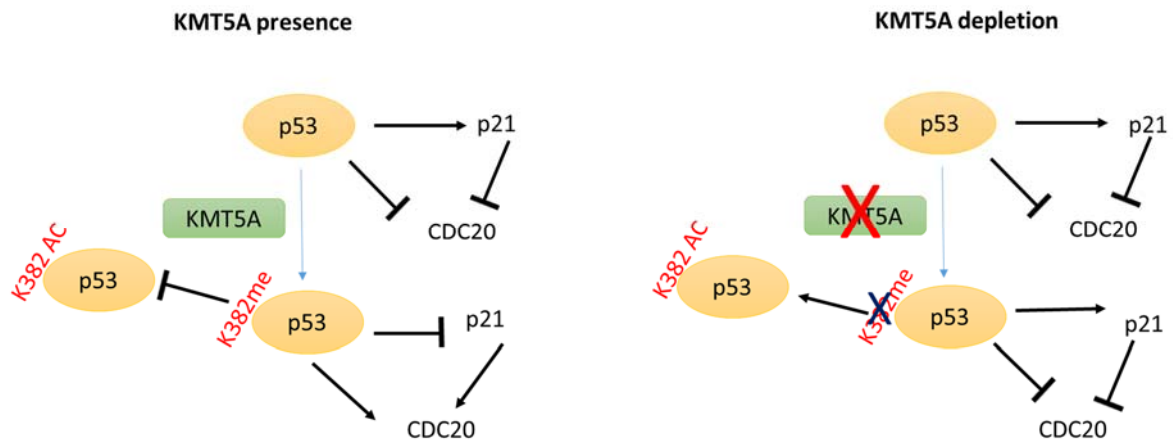
Figure 4-15 p53 regulates CDC20 expression in response to KMT5A mono-methylation at K382: a proposed model. KMT5A can mono-methylate p53 at K382 resulting in inhibition of its transcriptional activity therefore reducing its negative regulation of CDC20. KMT5A depletion enables p53 activity resulting in transcriptional down-regulation of CDC20 expression directly by binding to its promoter or indirectly through binding to CDE-CHR independently of p21 resulting in down-regulation of CDC20 expression.

4.3.13. CDKN1A *expression increases in response to KMT5A knockdown in LNCaP and LNCaP-AI cells*

In order to test the model of how KMT5A can regulate CDC20 through p53, the expression levels of *CDKN1A* were examined in the microarray data. A significant increase in *CDKN1A* expression was observed in the microarray data, particularly with siRNA#2 of ~3 fold in LNCaP-AI cells (p≤0.05) (Figure 4.16.A). A similar trend was seen overall in subsequent validation experiments for both LNCaP cells where an ~2 fold increase in expression with siRNA# 1 and in LNCaP-AI cells where an ~6 fold increase in expression with siRNA# 2 was observed (p≤0.05) (Figure 4.16.B-C).
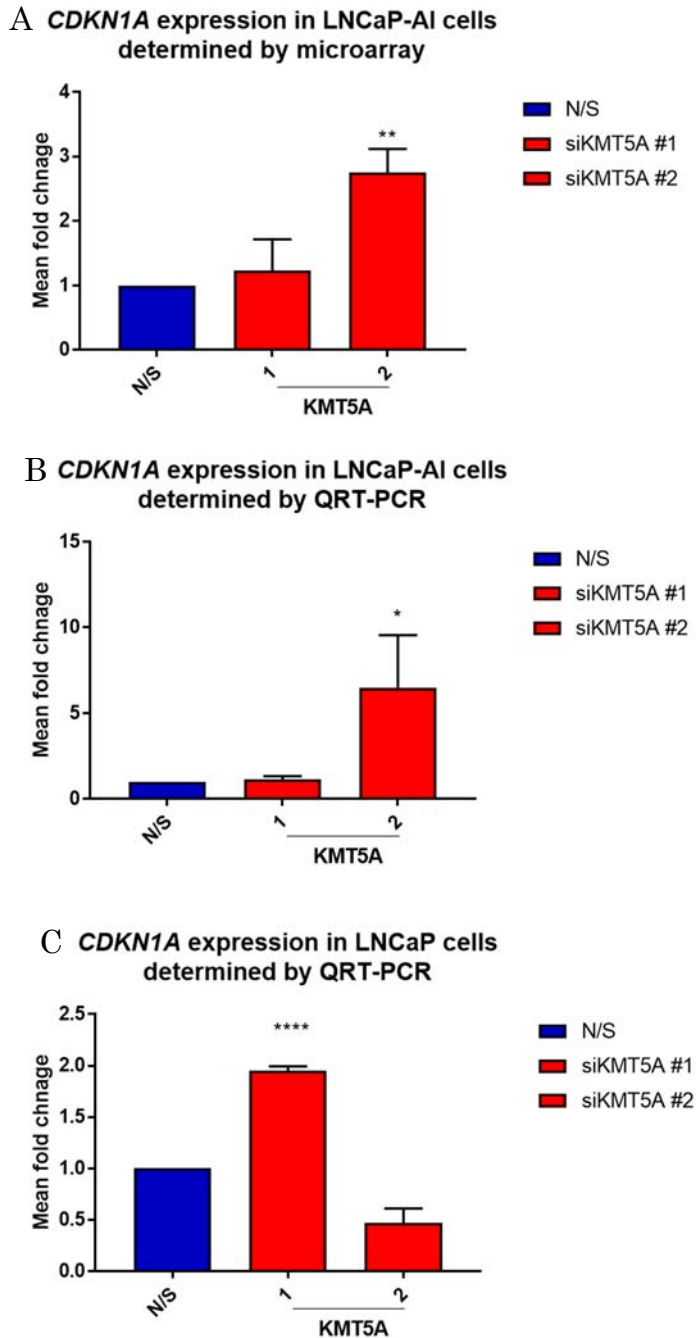
Figure 4-16 KMT5A knockdown increases CDKN1A expression. LNCaP cells (C, F) and LNCaP-AI cells (A, B, D, E) were reverse transfected with N/S siRNA or the two selected KMT5A siRNAs for 72 hours. RNA was collected and knockdown of KMT5A and the effect on CDKN1A expression at mRNA level was determined by QRT-PCR. Error bars represent the mean ± SD for triplicate independent experiments. p-values were determined by t-test (* p-value <0.05, ** p-value <0.01, *** p-value <0.001 and **** p- value < 0.0001).

4.3.14. *The expression of p53 and p21 in response to KMT5A depletion at the protein level*

The expression levels of p53 and p21 were then examined at the protein level using the same experimental conditions as Figure 4.14. KMT5A knockdown was performed using two selected siRNA in both LNCaP and LNCaP-AI cells grown in SDM for 72 hours. Protein was collected and KMT5A knockdown was confirmed by Western blotting. In LNCaP cells, there was a slight increase in p53 expression in response to KMT5A knockdown. However, p21 showed a reproducible increase in expression with one of the siRNA sequences, while a reduced expression was observed with the second siRNA. This was consistent with the mRNA expression (Figure 4.17. A). In LNCaP-AI cells, p53 showed a small reduction in expression and this was associated with a substantial increase in p21 protein in response to KMT5A knockdown supporting the proposed model (Figure 4.17.B).
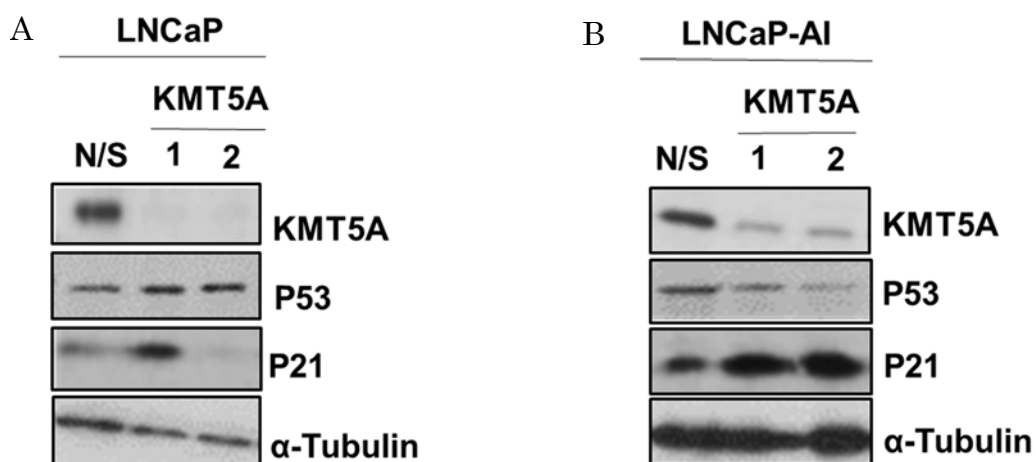
Figure 4-17 KMT5A knockdown increases p21 protein expression. (A) LNCaP and (B) LNCaP-AI cells were reverse transfected with N/S siRNA or the two selected KMT5A siRNAs for 72 hours. Protein was collected and knockdown of KMT5A and the effect on p53 and p21 expression at protein level was determined by Western blotting (representative blot).

4.3.15. *The effect of KMT5A knockdown on MDM2 protein expression level in LNCaP and LNCaP-AI cells*

p53 protein levels are usually very low in the cells, and rapidly increase following DNA damage to promote cell cycle arrest to allow the DNA damage to be repaired. The function and protein levels of p53 are tightly regulated by MDM2, as its binding results in reduced p53 activity and also reduced protein levels through ubiquitin-mediated proteasomal degradation (Kubbutat *et al.*, 1997). To rule out MDM2 involvement in p53 mediated regulation of CDC20, MDM2 expression levels were evaluated in response to KMT5A knockdown under identical experimental conditions as those used in Figure 4.17. A small reduction in MDM2 protein expression was observed in both cell lines. It has not been reported that KMT5A can affect MDM2 expression, which is consistent with these observations (Figure 4.18).
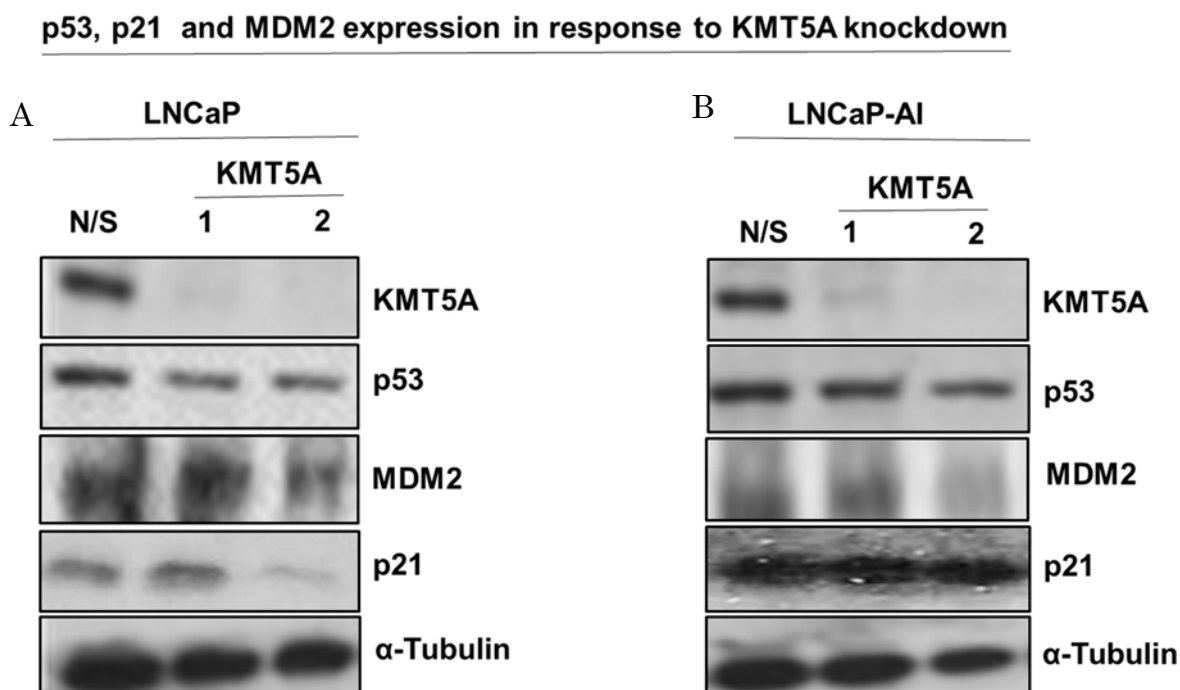
Figure 4-18 KMT5A knockdown has a small effect on MDM2 protein expression. (A) LNCaP and (B) LNCaP-AI cells were reverse transfected with N/S siRNA or the two selected KMT5A siRNAs for 72 hours. Protein was collected and expression of KMT5A and the effect on MDM2, p53, and p21 protein expression was determined by Western blotting (representative blot).

4.3.16. *KMT5A knockdown affects phosphorylation of p53 at Serine 15*

p53 phosphorylation facilitates the binding of the p53 co-activator acetyltransferase KAT3A/B which catalyses p53 acetylation at lysine residues (K373 and K382) to initiate transcription which further stabilizes p53 and promotes p53-DNA interaction (Scoumanne and Chen, 2008). Phosphorylation of p53 at S15/S20 promotes the recruitment of these transcriptional coactivators through reducing the affinity of p53 for its primary negative regulator Hdm2 (Dai and Gu, 2010).

As p53 is mono-methylated by KMT5A at K382, the effect of p53 phosphorylation at S15 was tested in this experiment to examine the effect of KMT5A depletion on levels of phosphorylated p53. KMT5A was depleted in both cell lines for 72 hours in SDM. Protein was then collected and the knockdown was confirmed by Western blotting (Figure 4.19). Depletion of KMT5A in LNCaP-AI cells resulted in an increase in p53 phosphorylation at S15. However, the opposite effect was seen with LNCaP cells as both siRNAs resulted in a reduction in p53 phosphorylation at S15 (Figure 4.19).
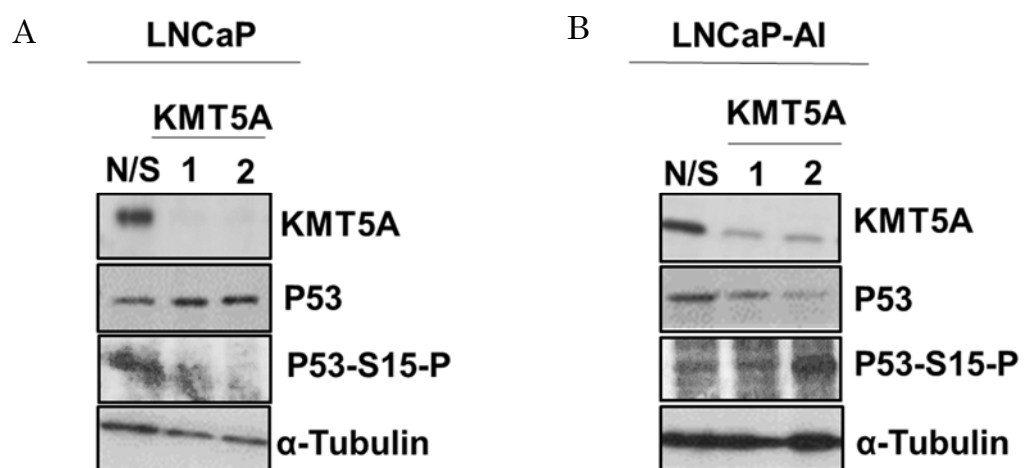
Figure 4-19 Effect of KMT5A knockdown on p53-S15-P expression in LNCaP and LNCaP-AI cells. (A) LNCaP and (B) LNCaP-AI cells were reverse transfected with N/S siRNA or the two selected KMT5A siRNAs for 72 hours. Protein was collected and knockdown of KMT5A and the effect on p53-S15-P expression was determined by Western blotting (representative blot).

4.3.17. *Acetylation of p53 at K382 following KMT5A knockdown*

KMT5A has the ability to mono-methylate p53 at K382 which prevents the acetylation of p53 at the same lysine residue to prevent the activation process of p53 (Scoumanne and Chen, 2008). To test if p53-K382 acetylation is affected by KMT5A depletion, the expression of p53 –K382 acetylation in the presence and absence of KMT5A was investigated in LNCaP and LNCaP-AI cells growing in SDM. The data was inconsistent between the two cell lines. In the LNCaP cells, there was a reduction in p53–K382 acetylation with KMT5A knockdown. In the LNCaP-AI cells there was an increase in acetylation with only one of the siRNAs used in the experiment (Figure 4.20). This data was consistent with the expression levels of p53-S15-P (Figure 4.19), which has been mentioned to be considered as a preceding step to the acetylation of p53 at the same lysine residues K382 used by KMT5A for the methylation of p53. This data part supports the effect of KMT5A in the regulation of p53 in PC cells.
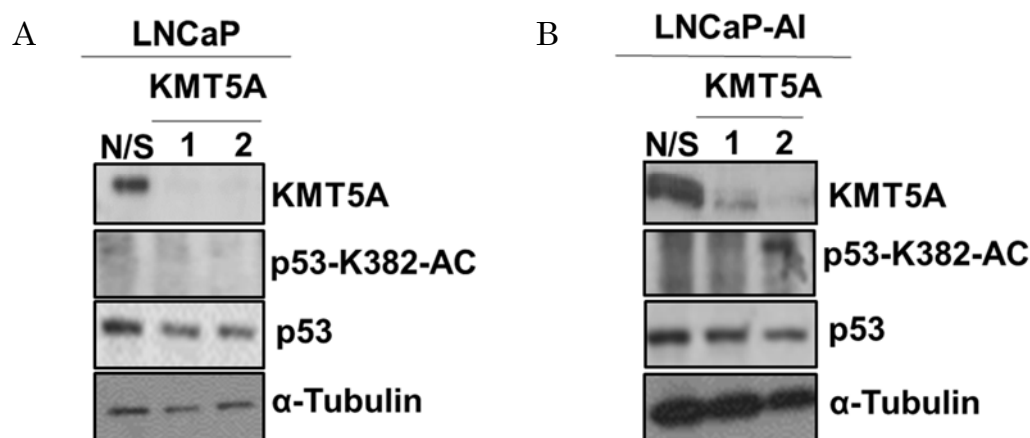
Figure 4-20 Effect of KMT5A knockdown on the expression of p53-K382-AC in LNCaP and LNCaP-AI cells. LNCaP and LNCaP-AI cells were reverse transfected with N/S siRNA or the two selected KMT5A siRNAs for 72 hours. Protein was collected and knockdown of KMT5A and the effect on p53-K382-AC expression was determined by Western blotting (representative blot).

KMT5A knockdown was also performed in LNCaP cells grown in FM for 72 hours, to test if AR has any effect on KMT5A in the proposed model. The data showed a slight reduction in total p53 expression and a substantial reduction in p21 expression, which is consistent with their expression in response to KMT5A knockdown in LNCaP cells grown in SDM. This indicated independent function of KMT5A from AR in the proposed model (Figure 4.21). However, p53-S15-P and p53-K382-AC expression in LNCaP cells in FM were inconsistent. here was an increase in p53-S15-P and p53-K382-AC expression with the siRNA#2, while no changes were seen using siRNA#1, which demonstrated lower efficiency in depleting KMT5A compared to the siRNA#2 (Figure 4.21). The differences observed for the two KMT5A-depleting siRNAs might be due to the residual levels of KMT5A present in the cells, as near 100 % depletion of KMT5A protein was achieved with siRNA #2, whilst siRNA# 1 was estimated to cause 80-90 % KMT5A depletion. It would appear that near total removal of KMT5A is required to induce both phosphorylation at S15 and acetylation at K382 of p53 (Figure 4.21). The absence of KMT5A suggests its methylase activity directed against K382 of p53 is important in regulating alternative post-translational modifications of p53.The generation of a commercial antibody targeted at p53 K382–me1 would greatly aid progress into mechanisms controlling p53 transcriptional activity.

p53-S15-P and p53-K382-AC expression in the presence and absence of KMT5A in LNCaP cells grown in FM
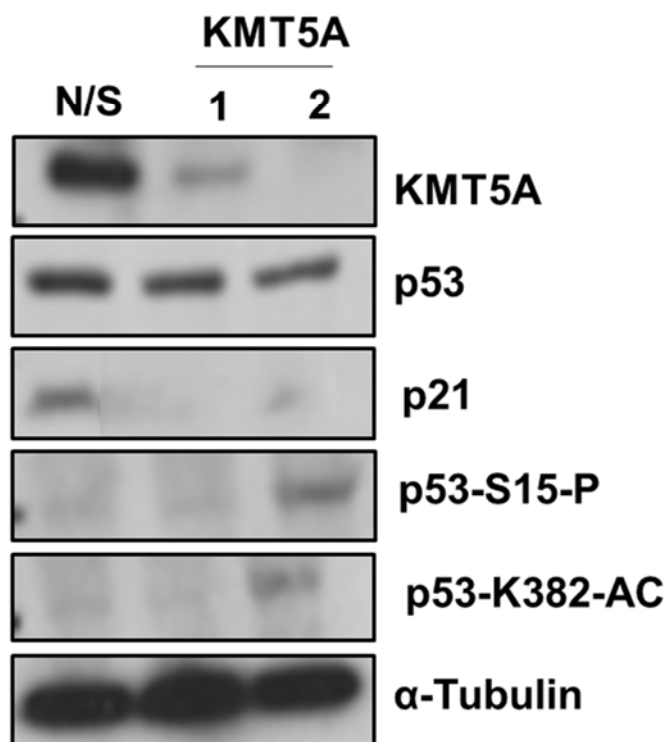
Figure 4-21 Efficient KMT5A knockdown increase p53-S15-P and p53-K382-AC expression in LNCaP cells grown in FM. LNCaP cells were reverse transfected in FM with N/S siRNA or the two selected KMT5A siRNAs for 72 hours. Protein was collected and knockdown of KMT5A and the effect on p53-S15-P and p53-K382-AC expression was determined by Western blotting (representative blot).

4.3.18. *The MDM2-p53 inhibitor, Nutlin3 (MDM2 inhibitor) affects the expression of p53, p21 and CDC20 proteins in LNCaP and LNCaP-AI cells*

To further confirm the role of p53 and p21 in the regulation of CDC20 expression in PC cells, an experiment was designed using Nutlin3, small molecule MDM2 antagonist that interacts with the p53 binding domain of MDM2, preventing negative regulation of p53 by MDM2, therefore allowing the persistence of p53-mediated signalling (Valentine *et al.*, 2011) . Cells were grown in their own respective medium for 24 hours then Nutlin3 was applied for 0, 6 and 16 hours. Protein lysates were collected and p53, p21 and CDC20 expression levels were assessed by Western blotting.

An increase in p53 expression was observed alongside an increase in MDM2 expression confirming successful Nutlin3 treatment. As the levels of p53 increased an increase in p21 expression was observed. This increase in p53 and p21 expression was accompanied by a decrease in CDC20 expression, confirming the role of p53 in CDC20 regulation in PC cells (Figure 4.22).

The effect of Nutlin3 treatment on the expression levels of p53, p21, MDM2 and CDC20
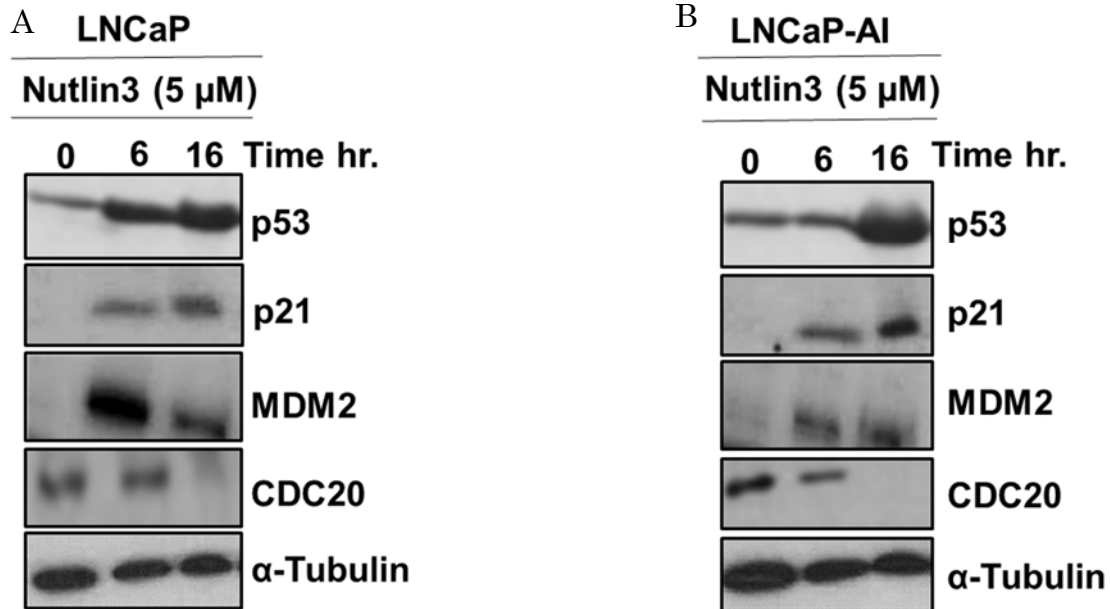
Figure 4-22 CDC20 expression is reduced in response to Nutlin3 treatment. (A) LNCaP and (B) LNCaP-AI cells were grown in their respective medium for 24 hours followed by treatment with 5 μM Nutlin3 for 0, 6 and 16 hours. Protein was then collected and the expression levels of p53, p21, MDM2 and CDC20 were detected by Western blotting (representative blot).

The same basic experiment was repeated but with additional time points to determine Nutlin3 effects on CDC20 and CDKN1A mRNA expression. In LNCaP cells, there was a statistically significant ~62 fold increase in CDKN1A expression (p≤0.05) at 16 hours of Nutlin3 treatment, which was expected as p53 transcriptional activity should be increased with the inhibition of MDM2 (Figure 4.23.A). A statistically significant increase of ~3 fold in CDC20 expression (p≤0.05) was apparent at 3 hours of Nutlin3 treatment which was followed by a steady reduction in CDC20 over the remaining time course of the experiment (Figure 4.23.B) which was consistent with what was observed at the protein level (Figure 4.22). In LNCaP-AI cells, CDKN1A expression increased gradually to reach ~21 fold at 16 hours of Nutlin3 treatment (Figure 4.23.C), while CDC20 expression decreased by ~2 fold by 3 hours and continued to decrease to ~5 fold at 16 hours, which was consistent with previous reports (Kidokoro et al., 2008), and with the model under investigation (Figure 4.23.D).

A

CDKN1A expression in LNCaP cells in response to Nutlin3 treatment determined by QRT-PCR

C

CDKN1A expression in LNCaP-AI cells in response to Nutlin3 treatment determined by QRT-PCR

B

CDC20 expression in LNCaP cells in response to Nutlin3 treatment determined by QRT-PCR

D

CDC20 expression in LNCaP-AI cells in response to Nutlin3 treatment determined by QRT-PCR

Figure 4-23 Effects of Nutlin3 treatment on CDKN1A and CDC20 mRNA expression in LNCaP and LNCaP-AI cells. LNCaP cells (A) CDKN1A expression (B) CDC20 expression and LNCaP-AI cells (C) CDKN1A expression (D) CDC20 expression, were grown in their respective medium for 24 hours followed by treatment with 5 µM Nutlin3 for 0, 3, 6 and 16 hours. RNA was then collected and the expression of CDKN1A and CDC20 was determined by QRT-PCR. Error bars represents the mean ± SD for triplicate independent experiments. p-values were determined by t-test (* p-value <0.05, ** p-value <0.01, *** p-value <0.001 and **** p- value < 0.0001).

4.3.19. *p53 regulates FOXM1 expression in response to KMT5A mono-methylation at K382: a proposed model*

FOXM1 expression is reduced by KMT5A depletion both at the protein and mRNA levels (Figure 4.10), but was found to have no effect on CDC20 expression in the tested PC cells in this study (Figure 4.13). However, FOXM1 was previously reported to be down-regulated by p53 particularly after DNA damage both at the mRNA and the protein levels (Barsotti and Prives, 2009). In turn, to further investigate how KMT5A can regulate FOXM1 in PC cells, a model was suggested to be tested in PC cell lines that included p53. Specifically, it was questioned, can the impact of KMT5A knockdown on p53 transcriptional activity affect FOXM1 levels and downstream target genes both at the protein and mRNA levels (Figure 4.24).
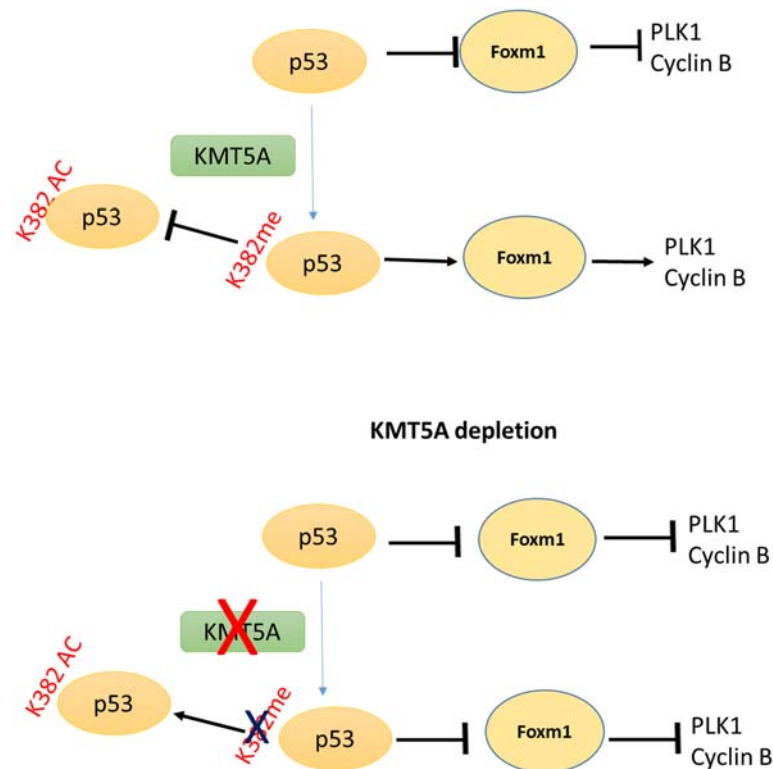
Figure 4-24 p53 regulates FOXM1 expression in response to KMT5A mono-methylation at K382: a proposed model. KMT5A can mono-methylate p53 at K382 resulting in inhibition of its transcriptional activity therefore reducing its negative regulation on FOXM1. KMT5A depletion enables p53 to remain active and retain transcriptional downregulation of FOXM1 expression.

4.3.20. *FOXM1 expression level are altered in response to Nutlin3 treatment in LNCaP and LNCaP-AI cells.*

To start to investigate the proposed model (Figure 4. 24), the regulatory effect of p53 on FOXM1 expression was first investigated using samples that were generated in Figure 4.20, where MDM2 inhibitor, Nutlin3, was used to inhibit MDM2 expression to stimulate p53 activation in LNCaP and LNCaP cells. Protein was collected and p53, p21and FOXM1 expression were detected by Western blotting.

The data was consistent with the model being proposed and FOXM1 protein expression was robustly reduced with Nutlin3 treatment (Figure 4.25). This could also explain the effect that KMT5A might have on FOXM1 through the mono-methylation of p53 at K382 and subsequently prevent acetylation at the same lysine site which would reduce p53 activity on its downstream targets including FOXM1.
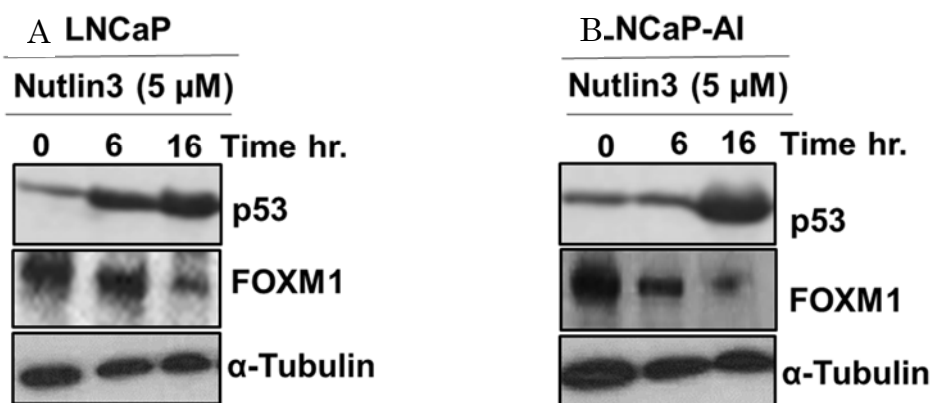
Figure 4-25 FOXM1 protein expression is reduced in response to Nutlin3 treatment in LNCaP and LNCaP-AI cells. Cells were grown in their respective medium for 24 hours followed by treatment with 5 μM Nutlin3 for 0, 6 and 16 hours. Protein was then collected and the expression levels of p53, FOXM1 and α-Tubulin was detected by western blotting (representative blot).

The same experimental conditions were repeated to check FOXM1 expression at the mRNA level in response to Nutlin3 treatment at 0, 3, 6, and 16 hours in LNCaP and LNCaP-AI cells. FOXM1 mRNA was found to be reduced in response to Nutlin3 treatment as a result of p53 activation. Specifically, in LNCaP cells a 2 fold reduction in *FOXM1* was observed after 3 hours of treatment and continued a gradual decrease to ~6 fold (Figure 4.26) at 6 and 16 hours of treatment. In LNCaP-AI cells there was a similar ~2 fold reduction in *FOXM1* expression after 3 hours of treatment which continued to decrease to ~5 fold reduction in *FOXM1* at 16 hours (Figure 4.26).
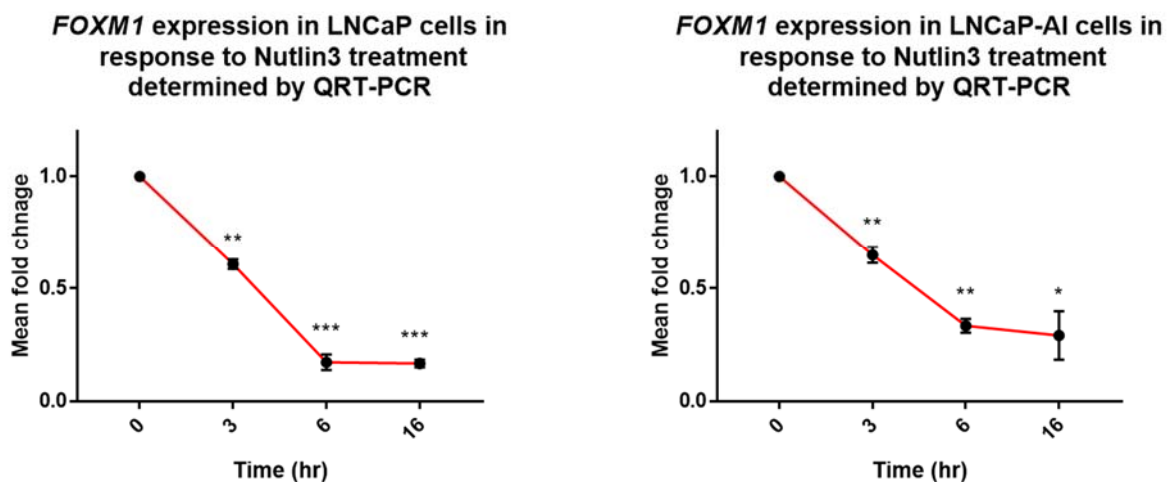
Figure 4-26 FOXM1 mRNA expression is reduced in response to Nutlin3 treatment in LNCaP and LNCaP-AI cells. Cells were grown in their respective medium for 24 hours followed by treatment with 5 µM Nutlin3 for 0, 3, 6 and 16 hours RNA was then collected and the expression of FOXM1 was determined by QRT-PCR. Error bars represent the mean ± SD for triplicate independent experiments. p-values were determined by t-test (* p-value <0.05, ** p-value <0.01 and *** p-value <0.001).

4.4. Discussion

Accumulating evidence has shown the important roles that KMT5A plays in regulating critical cellular functions, including cell cycle progression, DNA damage repair gene transcription, chromosome condensation and tumourigenesis (Schotta *et al.*, 2008; Oda *et al.*, 2010).

In this study, KMT5A was found to regulate CDC20 expression at both the mRNA and protein levels (Figure 3.11 and Figure 4.3). Based on these observations, CDC20 was investigated in this chapter as a possible biomarker for KMT5A to determine the activity of KMT5A in aggressive PC. Interestingly, KMT5A was found to interact with CDC20 both endogenously and exogenously (Figure 4.9). It has been reported that KMT5A can exert its functional effect such as involvement in cell cycle progression and DNA damage repair through interaction with a number of factors, such as TWIST, RNA polymerase II and ERα. KMT5A through the mono-methylation activity can affect TWIST target genes promoters. The mono-methylation activity of KMT5A also regulates both H4K16Ac and H4K20me3 marks, and in turn regulates RNA polymerase II pausing dynamics, and it was found to be essential to facilitate the recruitment of the MSL complex subsequent to H4K16Ac to release RNA polymerase II for active elongation. H4K20me1 activity was also reported to be required for ERα regulated transcription (Kapoor-Vazirani and Vertino, 2014) (Li *et al.*, 2011a; Wang *et al.*, 2015). Additionally, KMT5A can also bind to PCNA through the PIP domains to be recruited at the DNA replication foci (Beck, 2012).

Hence, there is potential that KMT5A may be able to affect the function of CDC20 in a similar way through the mono-methylation of H4K20 at the CDC20 promoter to regulate its transcription. The enrichment of H4K20me1 at the CDC20 promoter was investigated herein, and the data showed a variation in the enrichment of H4K20me1 at the CDC20 promoter between the LNCaP and LNCaP-AI cell lines tested, as it was reduced in LNCaP cells in response to DHT treatment. However, in LNCaP-AI cells, DHT treatment clearly enhanced H4K20me1 enrichment at the CDC20 promoter which peaked at ~5 fold after 30 minutes stimulation (Figure 4.10). Further experiments would be recommended to support the role of KMT5A activity in regulating CDC20 expression by knockdown of KMT5A and looking at H4K20me1 enrichment at the CDC20 promoter in LNCaP and LNCaP-AI cells. However, the required KMT5A antibody is unavailable commercially.

KMT5A is known to be targeted for degradation by APC^{cdh1} during the transition from metaphase to anaphase (Wu and Rice, 2011). In addition, APC^{CDC20} can target KMT5A for degradation. The possibility of CDC20 regulating KMT5A by targeting it for degradation as a part of the APC^{CDC20} complex was initially investigated in this study. However, knockdown of CDC20 by two selected siRNA sequences did not affect KMT5A protein levels (Figure 4.5). Further experiments such as immunoprecipitation are required to see if KMT5A and CDC20 interact as part of the APC complex or whether they can interact independent of this.

The effect of KMT5A and CDC20 on the cell cycle profile was also determined in this thesis, as both KMT5A and CDC20 are known cell cycle regulators. The data was partly inconsistent with previous reports about KMT5A and CDC20 depletion. It was found that KMT5A depletion causes a significant reduction by ~50 % in G2/M phase in LNCaP-AI cells. However, no significant change was noticed in the LNCaP cell cycle profile (Figure 4.4). Furthermore, the effect of CDC20 knockdown on cell cycle profile was also inconsistent between LNCaP and LNCaP-AI cells. Whilst, there was a significant increase by ~90 % in the G2/M phase in LNCaP cells, while no significant changes was observed in the LNCaP-AI cell cycle profile (Figure 4.6). These inconsistencies may be due to inefficient knockdown of KMT5A levels or differences in susceptibility to the absence of KMT5A between LNCaP and LNCaP-AI cells. It would be important to repeat this experiment with a shorter KMT5A depletion period as KMT5A knockdown may require less than 72 hours to exert an impact on the cell cycle profile. Therefore, cells might have already started to recover at the time samples were collected for staining following 72 hours of KMT5A knockdown. Moreover, it is also important to include longer durations of KMT5A knockdown as cells may require prolonged KMT5A depletion to cause cell cycle changes as previously reported for some cell cycle enzymes (Abbas *et al.*, 2010a). To address the possibility that KMT5A and CDC20 depletion might require a prolonged knockdown period to exert their phenotypic effects, the proliferation of LNCaP and LNCaP-AI cells was determined in the presence and absence of KMT5A and CDC20 over a 72 hours period of KMT5A and CDC20 knockdown followed by 96 hours of incubation at 37 °C in 96 well plates. Depletion of either KMT5A or CDC20 significantly reduced the proliferation by ~50 % and ~75 % in the LNCaP and LNCaP-AI cells, respectively (Figure 4.7), consistent with previously published data about the effect of KMT5A and CDC20 depletion on cellular proliferation (Huang *et al.*, 2009; Oda *et al.*, 2009).

To understand the relationship and the role of KMT5A in the regulation of CDC20 expression, FOXM1 was tested as a well-known CDC20 transcriptional regulator (Xie *et al.*, 2015). The data from this study showed that with KMT5A knockdown, FOXM1 expression

was robustly reduced at the protein level and significantly at the mRNA level (p≤0.05) (Figure 4.11). Despite this, CDC20 expression level in this study was found not to be regulated by FOXM1 expression level neither at the protein, nor at the mRNA level, as depletion of FOXM1 by siRNAs had no significant effect on CDC20 expression both transcriptionally and post-translationally (Figure 4.14), which contradicts what has been reported previously (Xie *et al.*, 2015). This might be due to some difference in the experimental conditions or due to effect of the tested cell line. The data also showed that stimulation of AR expression with DHT can stimulate FOXM1 expression in LNCaP cells, but not LNCaP-AI cells which was further confirmed by the DHT time course experiment that showed an increase in FOXM1 expression with treatment time in LNCaP, but not LNCaP-AI cells (Figure 4.13). This data contradict with the previously reported data which presented FOXM1 as an AR transcriptional regulator (Liu *et al.*, 2014).

Previous studies also reported a number of factors whose expression can be regulated by KMT5A presence and activity such as Numb and p53, by the methylation of Numb in the PTB domain, which would lead to the inhibition of p53 dependent apoptosis, or by direct methylation of p53 at K382 (Shi *et al.*, 2007; Dhami *et al.*, 2013; Jørgensen *et al.*, 2013).

CDC20 has been previously reported to be negatively regulated by p53 (Kidokoro *et al.*, 2008; Banerjee *et al.*, 2009), either by binding directly to the CDC20 promoter and inhibiting its transcription, or indirectly through binding at the CDE-CHR element and regulating its transcription independently of p21. KMT5A is also known to mono-methylate p53 at lysine 382 (Shi *et al.*, 2007) which results in inhibition of the p53 transcriptional activity. This study suggested a model for CDC20 being transcriptionally regulated by KMT5A indirectly through KMT5A mono-methylation activity at p53-K382. This model suggested that with KMT5A depletion, p53 would fail to be efficiently mono-methylated making the K382 residue available for acetylation and activation. This should increase p21 and in turn reduce CDC20 expression. A significant increase in p21 expression at the mRNA level was seen in LNCaP and LNCaP-AI cells, which was also mirrored at the protein level, most notably in LNCaP-AI cells (Figure 4.16,17). Further experiments would be required to look at the enrichment of p53 and p21 at the CDC20 promoter in PC cells.

To confirm the effect of p53 on CDC20 in PC cells, treatment with Nutlin3 (an MDM2 inhibitor) which can inhibit the MDM2-p53 interaction was conducted. Nutlin3 is also demonstrated to inhibit MDM2 dependent transcription of p53 (Barsotti and Prives, 2009). The data showed a significant (p≤0.05) increase in p53 and p21, whilst a decrease in CDC20

mRNA and protein expression was observed, which was expected as being directly regulated by p53 (Figure 4.22). The data was consistent with the previously reported data about the regulation of CDC20 by p53 (Banerjee *et al.*, 2009). Further investigation to look at p53-K382 -me1 expression levels in the presence and absence of KMT5A is required to further support the suggested possible pathway.

p53 was also suggested as a negative regulator of FOXM1 expression (Barsotti and Prives, 2009) in a p21 and Rb dependent fashion or in some cases in an independent manner. To test the possible effect of p53-K382-me1 catalysed by KMT5A, on FOXM1 expression in PC cells, a model was suggested. In this model, with KMT5A depletion, p53 will be released from the mono-methylation effect and possibly facilitate K382 acetylation and subsequent p53 activation, which enables its transcriptional activity on its substrates, including the negative regulation of FOXM1 and in turn its substrates (Figure 4.24). Two FOXM1 substrates were selected to test this model (Cyclin B and PLK1). KMT5A knockdown was found to reduce FOXM1 and its two targets substrates expression both at the mRNA and protein level. Also, treatment of LNCaP and LNCaP-AI cells with 5 µM Nutlin3 resulted in a significant reduction in FOXM1 expression both at the protein and mRNA level (Figure 4.25, Figure 4.26). This highlights that p53 does regulate FOXM1 expression in PC cells and that the tested model remains viable. Further experiments looking at the effect of KMT5A depletion on the expression of p53-K382-me1 at the protein level is essential to correlate FOXM1 expression changes to KMT5A through p53-K382-me1.

The relationship between p53 and KMT5A was previously reported and also the relationship between p53 and CDC20. This study has managed to correlate these two relationships through looking at KMT5A as the driver of p53 effect on CDC20 through mono-methylation of p53-K382 and through that on CDC20. The suggestion of CDC20 as a biomarker for KMT5A expression in PC would require further experimentation, particularly to confirm that KMT5A does regulate CDC20 directly at the promoter level. However, the regulation of CDC20 by p53 would impact the possibility of considering CDC20 as a biomarker for KMT5A, as any defect in p53 would affect CDC20 expression even independently of KMT5A. To cover this possibility, an experiment using mutated versus wild type p53 cells or p53 null cell lines to look at the effect of KMT5A depletion on CDC20 expression would help to either confirm or refute the possibility of having CDC20 as a biomarker for KMT5A.

The effect of KMT5A depletion using siRNAs on CDC20, FOXM1, PLK1 will be investigated further using KMT5A inhibitors in chapter 5.

Chapter 5 . The effect of KMT5A inhibitors UNC0379 and Ryuvidine on KMT5A activity in PC cells

5.1. Introduction

To compare the data obtained by depleting KMT5A using siRNA sequences, KMT5A inhibitors were used to study their effect on the same tested factors on the previous chapters. Methyltransferases, such as KMT5A, play important roles in many different cellular processes such as proliferation, DNA damage repair, chromatin condensation, cell cycle progression, cancer development and progression, highlighting their importance as potential therapeutic targets (Hui and Ye, 2015). Indeed, inhibition of their enzymatic activity with small molecule inhibitors is an area of research for many groups. Developing KMT5A inhibitors with cellular activity is a key step toward illuminating the diverse roles of KMT5A via convenient pharmacological perturbation.

The first selective KMT5A inhibitor (Marine natural product, nahuoic acid A) was selected as the most effective against KMT5A from a library of marine organisms extract and pure marine natural products. As mentioned in Chapter 1, KMT5A catalyzes the methylation of histone and non-histone proteins by binding the sulfonium methyl group of the cofactor S-adenosyl-methionine (SAM) on various histone and non-histone protein targets (Kouzarides, 2007). Nahuoic acid is a competitive inhibitor of SAM binding but a non-competitive inhibitor with respect to the binding of the peptide substrate. Nahuoic acid A inhibited KMT5A activity with an IC50 value of 6.5 ± 0.5 µM (Williams *et al.*, 2012) (Figure 5.1.A).

The first synthetic inhibitor of KMT5A was UNC0379, which has been shown to be active in multiple biochemical assays. Different biophysical assays have been used to confirm its specificity and affinity for KMT5A, including isothermal titration calorimetry (ITC), surface plasmon resonance (SPR) studies, and biochemical assays such as microfluidic capillary electrophoresis and radioactive methyl transfer. UNC0379 inhibited KMT5A activity with an IC50 value of 7.3 ± 1.0 µM in a radioactive biochemical assay. However, the effect of this inhibitor has not been tested as yet for cell lines (Ma *et al.*, 2014a) (Figure 5.1.B).

Three other inhibitors SPS8I 1, 2 and 3 also known as NSC663284, Ryuvidine and BVT948 respectively, were identified with a radioactivity-based scintillation proximity imaging assay (SPA) in a high throughput screening (HTS) format aimed to identify novel KMT5A inhibitors (Blum *et al.*, 2014). SPS8I1 and 3 were selected from the screen as substrate dependent inhibitors, while SPS8I2 is a substrate independent inhibitor of KMT5A. These three compounds are structurally able to inhibit KMT5A through specific structural motifs and modes of action. They are also able to target KMT5A enzymatic activity as demonstrated by H4K20me1 level reduction and having the ability to cause S phase cellular arrest, similar

to the effect obtained by KMT5A depletion using siRNAs (Blum *et al.*, 2014). Ryuvidine

(SPS8I2) inhibited KMT5A activity with an IC50 value of 0.5 ± 0.2 μM which is much more

potent than nahouic acid and UNC0379 (Figure 5.1.C).

The aim of this chapter is to test two of these KMT5A inhibitors UNC0379 and Ryuvidine,

for their effect on KMT5A activity and the downstream effects on AR, CDC20, p53 and

FOXM1. Phenotypic effects will also be compared to those observed in Chapter 3, 4 where

siRNA against KMT5A was utilized.
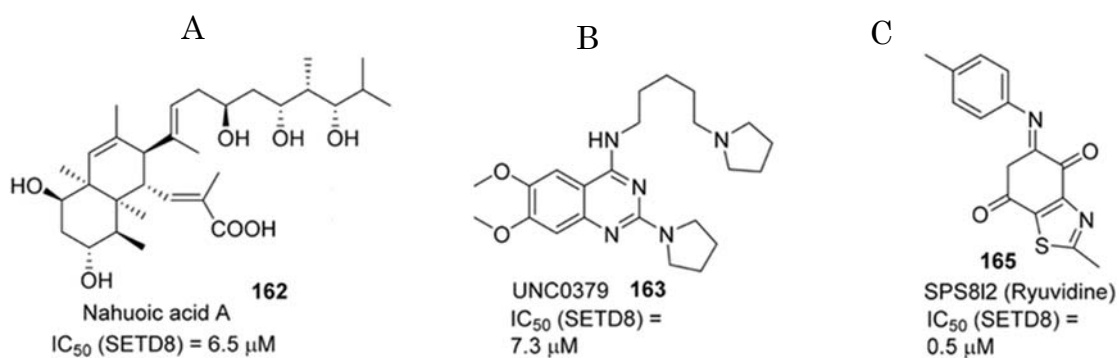
Figure 5-1 Chemical structure of KMT5A inhibitors. **(**A) Nahuoic acid A (Marine natural product) (B) UNC0379 (synthetic inhibitor) measured by a radioactive biochemical assay and (C) Ryuvidine in HEK293T cells (Hui and Ye, 2015).

5.2. Specific materials and methods

5.2.1. *Cell lines*

LNCaP and LNCaP-AI cells were used in this study as detailed in Chapter 2.1.1.

5.2.2. *Antibodies*

A number of primary antibodies were used to detect protein expression by Western blotting (Table 5.1).

Table 5-1 Western blot antibodies.

Antibody	*Species*	*Catalogue number*
KMT5A	Rabbit	Cell Signalling (2996)
CDC20	Mouse	Abcam (1b190711)
FOXM1	Mouse	Santa Cruz (Sc-502)
PLK1	Mouse	Santa Cruz (Sc-55504)
α-Tubulin	Mouse	Sigma
H4K20me1	Rabbit	Millipore (07-1570)
H4	Rabbit	Millipore (07-108)
HRP-conjugated Rabbit anti-mouse	Mouse	DakoCytomation (P0260)
HRP- conjugated Swine anti-Rabbit	Rabbit	DakoCytomation (P0217)

5.2.3. *QRT-PCR primers*

To detect the expression of individual genes at the mRNA level, specific primer sets were used (Table 5.2).

Table 5-2 QRT-PCR primers.

Genes	Forward Primer (5'-3')	Reverse Primer (5'-3')
KLK3	TCGGCACAGCCTGTTTCAT	TGGCTGACCTGAAATACCTGG
KLK2	AGCATCGAACCAGAGGAGTTCT	TGGAGGCTCACACACTGAAGA
HPRT1	TTGCTTTCCTTGGTCAGGCA	AGCTTGCGACCTTGACCATCT

5.2.4. *KMT5A inhibitors*

Two KMT5A inhibitors were used to test their effect on KMT5A activity in PC cells (Table 5.3). Chemical structure of the inhibitors are shown in Figure 5.1.B- C.

Table 5-3 KMT5A inhibitors

Inhibitor	Manufacture
UNC0379	Selleckchem(S7570)
SPS8I2 (Ryuvidine)	R&D (2609)

5.2.5. *Determination of GI$_{50}$ for UNC0379 and Ryuvidine*

LNCaP and LNCaP-AI cells were grown in their respective medium in 96 well plates (3000 cells/well for LNCaP and 3500 cells/well for LNCaP-AI cells) for 24 hours at 37 °C. UNC0379 was then added to the wells (6 wells/ concentration) in the following concentrations: 0, 0.25, 0.5, 1, 2, 4, 6.25, 12.5, 25 and 50 µM. Ryuvidine was added to the wells (6 wells/ concentration) in the following concentrations: 0, 0.5, 0.75, 1, 1.25, 1.5, 2, 3, 4 and 5 µM. Cells were left to grow for 7 days at 37 °C. Cells growth was determined using SRB assays in the last day of the experiment as described in Chapter 2.2.1.4.

Absorbance was measured at 570 nm using a 96-well plate reader (BioRad). Three repeats of the experiment were done for each cell line. Data were plotted using Graph Pad prism 6.0 and GI$_{50}$ values were determined using the point-to-point curve fit analysis package (Figure 5.2 and Figure 5.3).
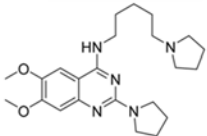
COMPOUND	STRUCTURE		
		LNCaP cells	LNCaP-AI cells
UNC0379		7.07±1.2	3.89±1.1
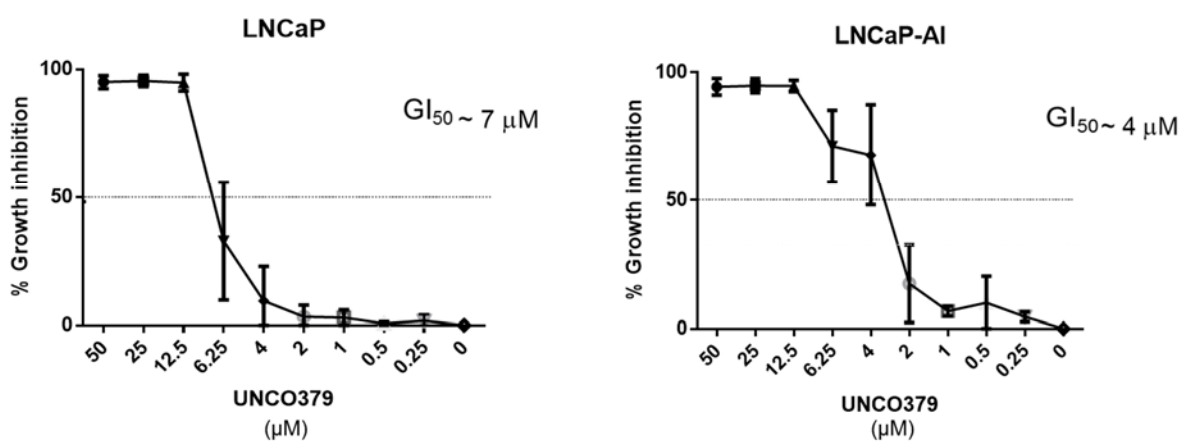
Figure 5-2 Growth inhibition in LNCaP and LNCaP-AI cells using UNC0379. Cells were seeded out in 96 well plates for 24 hours followed by treatment with a serial dilution of UNC0379. Cell growth over 7 days was measured using SRB assay in the last day of the experiment. Error bars represent the mean ± SD for triplicate independent experiments. Absorbance was measured at 570nm using a 96-well plate reader (BioRad).

COMPOUND	STRUCTURE	KMT5A GI$_{50}$ µM	
		LNCaP cells	LNCaP-AI cells
Ryuvidine	SPS8I2 (Ryuvidine)	0.77± 0.2	2.76± 0.3
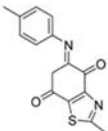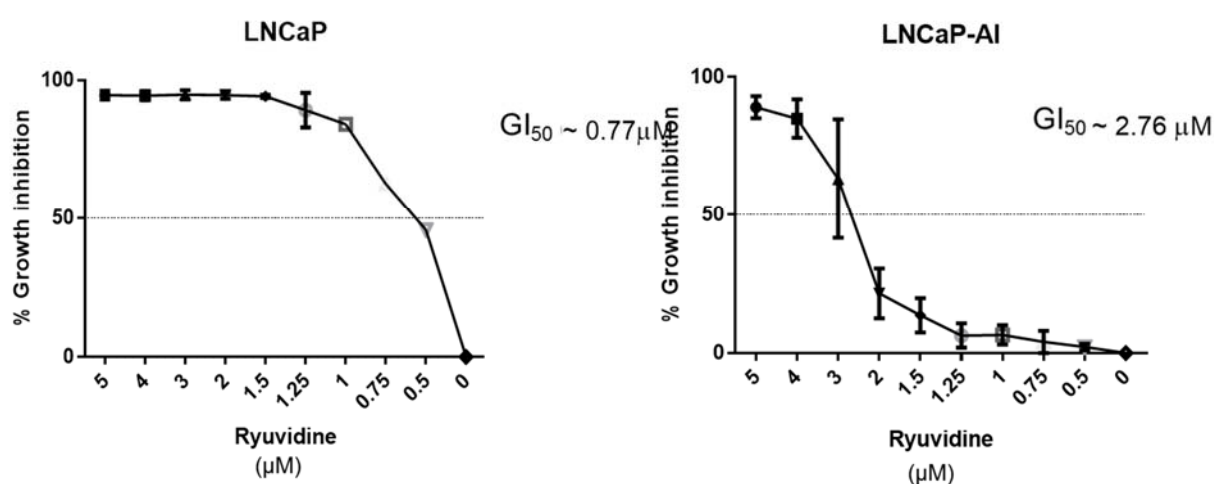
Figure 5-3 Growth inhibition in LNCaP and LNCaP-AI cells using Ryuvidine. Cells were seeded out in 96 well plates for 24 hours and followed by treatment with a serial dilution of Ryuvidine. Cell growth over 7 days was measured using SRB assay. Error bars represent the mean ± SD for triplicate independent experiments. Absorbance was measured at 570nm using a 96-well plate reader (BioRad).

5.3. Results

5.3.1. *Effect of UNC0379 on KMT5A activity*

Whilst UNC0379 has been shown to inhibit KMT5A methylase activity (Ma *et al.*, 2014a), it has not been tested for PC cells. Furthermore, the effect of UNC0379 on the levels of KMT5A is unknown in these systems. Hence, the effect of increasing doses of UNC0379 on KMT5A expression was assessed prior to determining any effect on the enzymatic activity of KMT5A. No robust changes in KMT5A expression were observed in LNCaP and LNCaP-AI cells when compared to α-tubulin loading control (Figure 5.4.A- B). There was a robust reduction observed in the expression of H4K20me1 in both cell lines in response to the treatment with UNC0379 (Figure 5.4.C). However, similar to tubulin levels, the level of total histone H4 was also found to decrease in these cell lines at higher doses. At lower doses, the levels of H4 are relatively constant, while a clear reduction in H4K20me1 levels can be seen. Therefore, the data supported the inhibitory effect of UNC0379 on the enzymatic activity of KMT5A in PC cells.

A

B

C
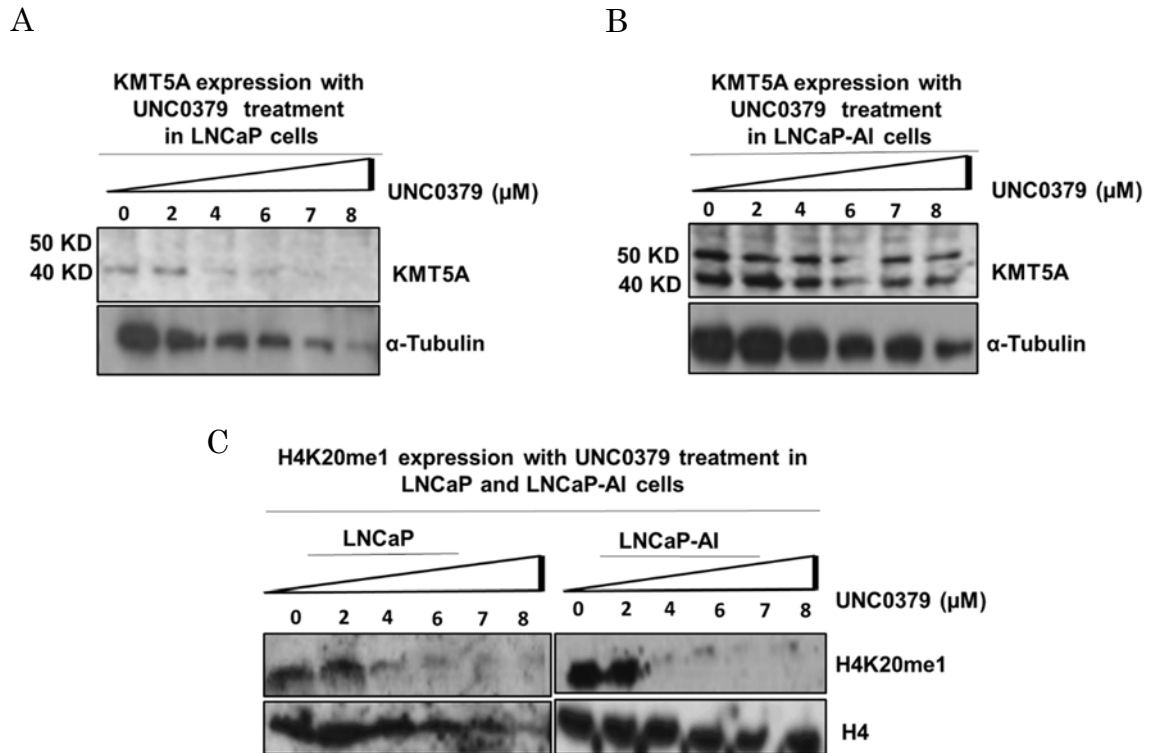
Figure 5-4 UNC0379 inhibits KMT5A methylase activity in PC cells. LNCaP and LNCaP-AI cells were seeded out at appropriate densities and allowed to adhere for 24 hours. UNC0379 was then applied at (0, 2, 4, 6, 7, 8 µM) for a further 48 hours. Protein lysates were collected and the levels of KMT5A in (A) LNCaP and (B) LNCaP-AI cells and (C) H4K20me1 in both cell lines were determined by Western blotting. Alpha-tubulin and total Histone H4 were used as loading controls, respectively (representative blot).

5.3.2.*The effect of UNC0379 on AR target genes expression in LNCaP and LNCaP-AI cells*
KMT5A has been found to act as an AR suppressor in LNCaP cells and an AR activator in LNCaP-AI cells. Specifically, knockdown of KMT5A in LNCaP-AI cells was found to inhibit AR binding to the PSA enhancer, thereby affecting AR function (Coffey *et al*, unpublished data). Furthermore, data shown in Figure 5.4, demonstrates that the activity of KMT5A was robustly affected by UNC0379 in both PC cell lines. Hence, inhibition of KMT5A activity with UNC0379 may affect AR target genes expression in LNCaP and LNCaP-AI cells.

To test this theory, LNCaP and LNCaP-AI cells were treated with UNC0379 using a single concentration for each cell line compared to a vehicle control. In both cases, the GI_{50} value (7 μM LNCaP and 4 μM LNCaP-AI) in their respective medium for 48 hours at 37 °C was applied. RNA was subsequently isolated and AR target gene expression (*KLK3* and *KLK2*) was assessed by QRT-PCR using primers detailed in Table 5.2. Surprisingly, no significant changes in *KLK3* and *KLK2* expression were detected in LNCaP cells (Figure 5.5.A- B) or in LNCaP-AI cells (Figure 5.5.C- D). The data indicated that despite affecting the activity of KMT5A, UNC0379 had no effect on AR target gene expression in both PC cell lines.
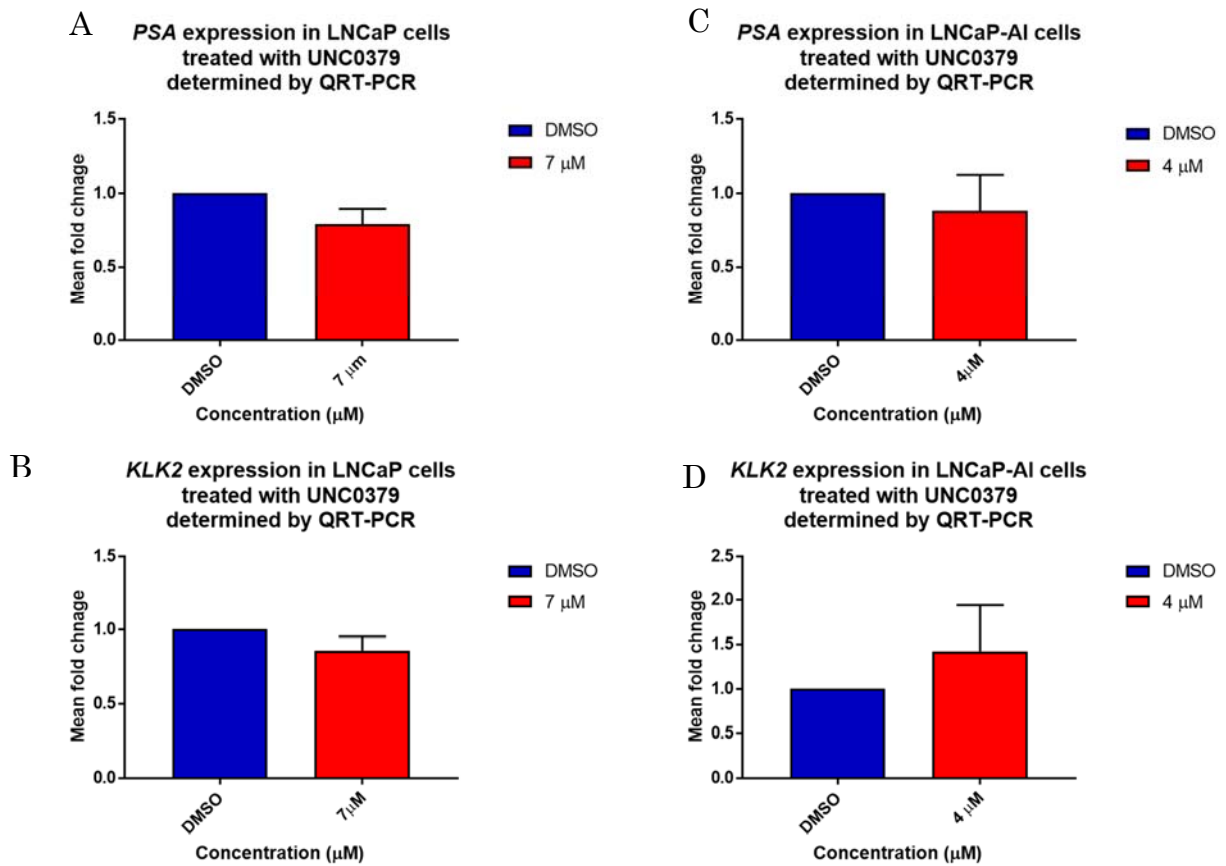
Figure 5-5 UNC0379 does not affect AR target gene expression in PC cell lines. LNCaP cells (A) KLK3 and (B) KLK2 and LNCaP-AI cells (C) KLK3 and (D) KLK2. Cells were seeded out for 24 hours and then treated with UNC0379 for 48 hr. RNA was collected, then KLK3 and KLK2 expression levels were detected by QRT-PCR. Error bars represent the mean ± SD for triplicate independent experiments. p-values were determined by t-test (* p-value <0.05).

5.3.3. *UNC0379 has no effect on cell cycle distribution in LNCaP and LNCaP-AI cells*

Silencing of KMT5A using siRNA has been reported to cause cellular arrest at G2/M phase of the cell cycle (Lee and Zhou, 2010). The effect of UNC0379 on cell cycle distribution has not been previously investigated although it may be predicted to result in similar effects to KMT5A knockdown. To test this theory in LNCaP and LNCaP-AI cells, cells were treated with the GI_{50} doses of UNC0379 (7μM LNCaP and 4 μM LNCaP-AI) for 48 hours at 37 °C, followed by cell cycle profile determination using flow cytometry protocol detailed in Chapter 2.2.4. Surprisingly, in both LNCaP (Figure 5.6.Ai) and LNCaP-AI cells (Figure 5.6.Bi), no significant changes in cell cycle profile were detected.

To further investigate the cell cycle distribution upon treatment with UNC0379, Western blotting was carried out against cyclin B, a G2/M phase marker, in response to UNC0379 treatment in LNCaP and LNCaP-AI cells. Increasing doses of UNC0379 (0, 2, 6, 7 and 8 μM) was added to each cell line for 48 hours at 37 °C. Significant changes were detected in cyclin B levels at the protein level was noticed by measuring with densitometry in LNCaP cells (Figure 5.6.Aii, iii) and LNCaP-AI cells (Figure 5.6. Bii, iii). The overall data suggested that UNC0379 appears to have an effect on cell cycle distribution in LNCaP and LNCaP-AI cells confirmed by looking at cyclin B expression in response to UNC0379 treatment (Figure 5.6).

A(i)

B(i)
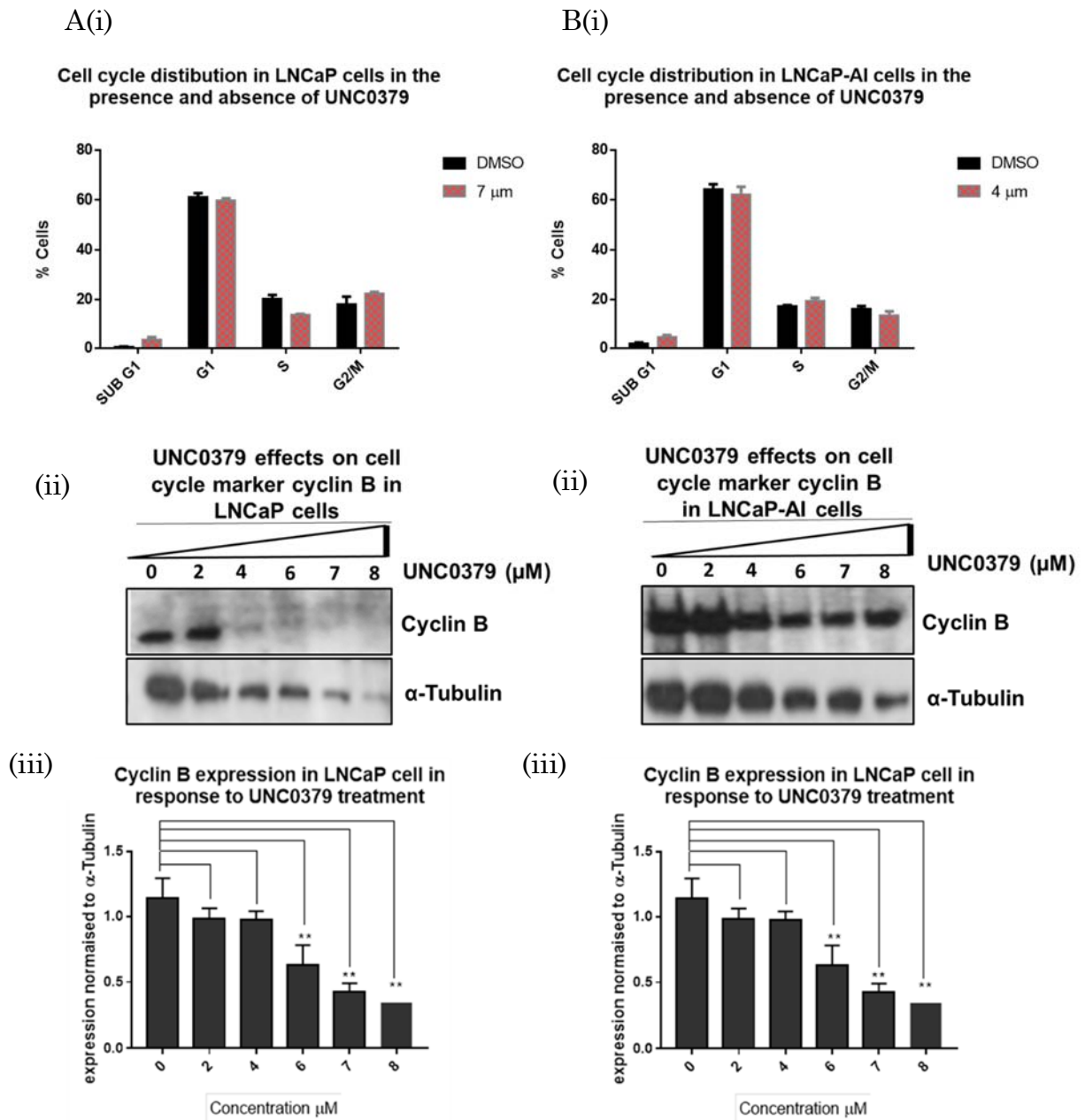
Figure 5-6 UNC0379 has no impact on cell cycle distribution in PC cells. LNCaP (A) and LNCaP-AI cells (B) cells were treated with increasing doses of UNC0379 (0, 2, 4, 6, 7 and 8 µM) for 48 hours in 6 well plates. Cell cycle analysis was performed using propidium iodide to stain cellular DNA for 40 minutes. Protein was also collected from samples treated with increasing doses of UNC0379 (0, 2, 6, 7 and 8 µM) and cyclin B expression was detected by Western blotting (ii). and measured by densitometry using Epson scanner and labWork 4.0 software(iii), p-values were determined by t-test (* p-value <0.05, ** p-value <0.01, *** p-value <0.001 and **** p- value < 0.0001).

5.3.4. *The effect of UNC0379 on FOXM1, PLK1 and CDC20 expression in LNCaP and LNCaP-AI cells*

In Chapter 4, KMT5A was shown to have an effect on the expression level of CDC20, FOXM1, and PLK1. Depletion of KMT5A by siRNAs for 72 hours, resulted in a robust reduction in their expression at the protein level and statistically significant reduction at the mRNA level (p≤0.05). In both LNCaP and LNCaP-AI cells, an ~3-4 fold reduction in *CDC20* expression was observed (Figure 3.11). Similarly an ~2, and 3-4 fold reduction in *FOXM1* expression was observed in LNCaP and LNCaP-AI cells, respectively (Figure 4.9). *PLK1* expression was also confirmed to be reduced by ~3-4 fold in LNCaP-AI cells as detected by the microarray data (Figure 4.10).

UNC0379 effects on CDC20, FOXM1 and PLK1 was tested to compare it with the effect obtained by KMT5A depletion using siRNAs. LNCaP and LNCaP-AI cells were treated with UNC0379 (7 µM LNCaP and 4 µM LNCaP-AI) for 48 hours at 37 °C. Protein was collected, and the expression levels of CDC20, FOXM1and PLK1 was measured by Western blotting (Figure 5.7). In LNCaP cells, the effect of UNC0379 remained unclear due to problems with protein loading caused by the effect of the drug on cell proliferation (Figure 5.7.A). However, in LNCaP-AI cells, there was a clear reduction in FOXM1, PLK1 and CDC20 expression upon UNC0379 treatment compared to the DMSO control (Figure 5.7.B). The data obtained from this experiment for LNCaP-AI cells was consistent with that obtained by depleting KMT5A using siRNAs in Chapter 4, which would support the role of KMT5A in regulating CDC20 expression in LNCaP-AI cells.
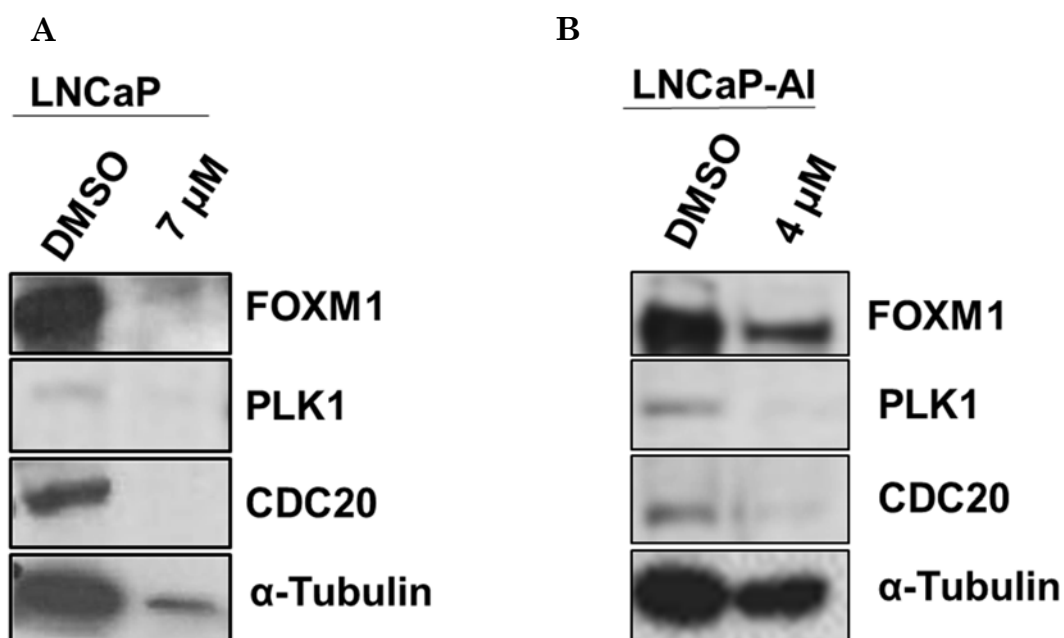
Figure 5-7 UNC0379 inhibits FOXM1, PLK1 and CDC20 expression in LNCaP-AI cells. (A) LNCaP and (B) LNCaP-AI cells. Cells were seeded out at appropriate densities and allowed to adhere for 24 hours. UNC0379 was then applied at 7 µM in LNCaP and 4 µM in LNCaP-AI cells for 48 hours. Protein lysates were then collected and the levels of FOXM1, CDC20 and PLK1 were determined by Western blotting. Alpha-tubulin was used as a loading control (representative blot).

5.3.5. *Effect of Ryuvidine on KMT5A activity*

Due to the non-specific effects on KMT5A that UNC0379 might have (Ma *et al.*, 2014a), another KMT5A inhibitor was selected for inclusion in this study. According to (Blum *et al.*, 2014), Ryuvidine can target KMT5A enzymatic activity demonstrated by a reduction in H4K20me1 levels in HEK293T cells. To test if this also applied to PC cells, the effect of increasing doses of Ryuvidine (0, 1, 1.5, 2, 2.5 and 3 µM) on KMT5A expression was tested in LNCaP cells (Figure 5.8.A) and LNCaP-AI cells (Figure 5.8.B) followed by looking at its effect on H4K20me1 levels in both cell lines (Figure 5.8.C).

 There were no noticed changes either in KMT5A or in H4K20me1 expression in LNCaP-AI cells. A slight reduction in KMT5A and H4K20me1 expression in LNCaP cells was detected when α-tubulin and H4 control levels were taken into account (Figure 5.8). However, the level of total histone H4 was found to be reduced in these cell lines with increasing dose of Ryuvidine, which was consistent with what was reported on Ryuvidine effect on the cell cycle progression at higher doses (Blum *et al.*, 2014). The data indicated that Ryuvidine might affect KMT5A activity in LNCaP cells, but not in LNCaP-AI cells. While UNC0379 showed a robust reduction in H4K20me1 levels in both cell lines (Figure 5.4).
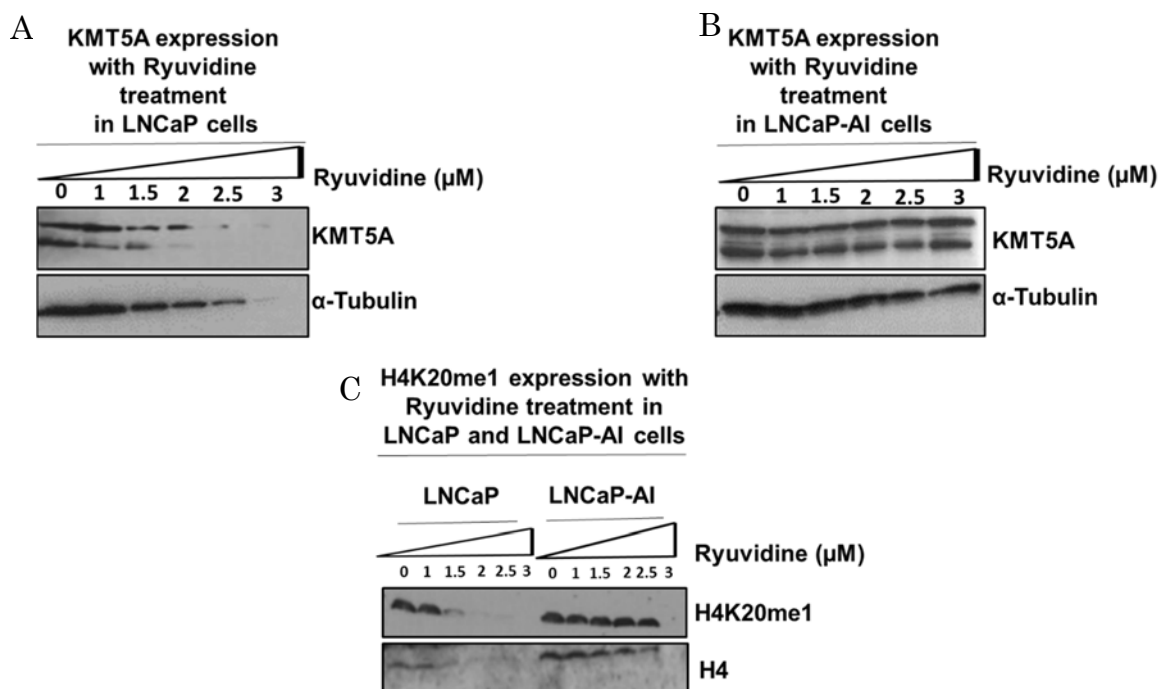
Figure 5-8 Ryuvidine inhibits KMT5A methylase activity in LNCaP cells. LNCaP and LNCaP-AI cells were seeded out at appropriate densities and allowed to adhere for 24 hours. Ryuvidine was then applied at (0, 1, 1.5, 2, 2.5 and 3 μM) for a further 48 hours. Protein lysates were then collected and the levels of KMT5A at (A) LNCaP and (B) LNCaP-AI cells and (C) H4K20me1 level in both cell lines were determined by Western blotting. Alpha-tubulin and total Histone H4 were used as loading controls (representative blot).

5.3.6. *The effect of Ryuvidine on AR target genes expression*

The effect of the first studied KMT5A inhibitor, UNC0379, on AR target gene expression, was determined (Figure 5.5). No significant changes were observed. To determine the effect of Ryuvidine on AR target gene expression, Ryuvidine GI_{50} values that were established for each cell line (0.77 μM for LNCaP cells and 2.76 μM for LNCaP-AI cells) were applied for 48 hours at 37 °C. RNA was collected and the expression level of AR target genes (*KLK3* and *KLK2*) was determined by QRT-PCR using primers detailed in Table 5.2. *KLK3* and *KLK2* expression was found to be significantly reduced by ~2 fold in response to Ryuvidine treatment compared to untreated control in LNCaP cells ($p \leq 0.05$) (Figure 5.9.A-B). The results also showed the same trend for the LNCaP-AI cell line where a significant reduction by ~2 fold in both *KLK3* and *KLK2* mRNA expression compared to untreated control in LNCaP-AI cells was also noted ($p \leq 0.05$) (Figure 5.9.C-D).

From the data above, Ryuvidine does significantly reduce the expression of AR target gene in both LNCaP and LNCaP-AI cells ($p \leq 0.05$). However, Ryuvidine had no effect on KMT5A levels or H4K20me1 levels in LNCaP-AI cells, so any effects on AR-regulated genes may be the result of Ryuvidine having off target effects in this cell line rather than solely inhibiting KMT5A.
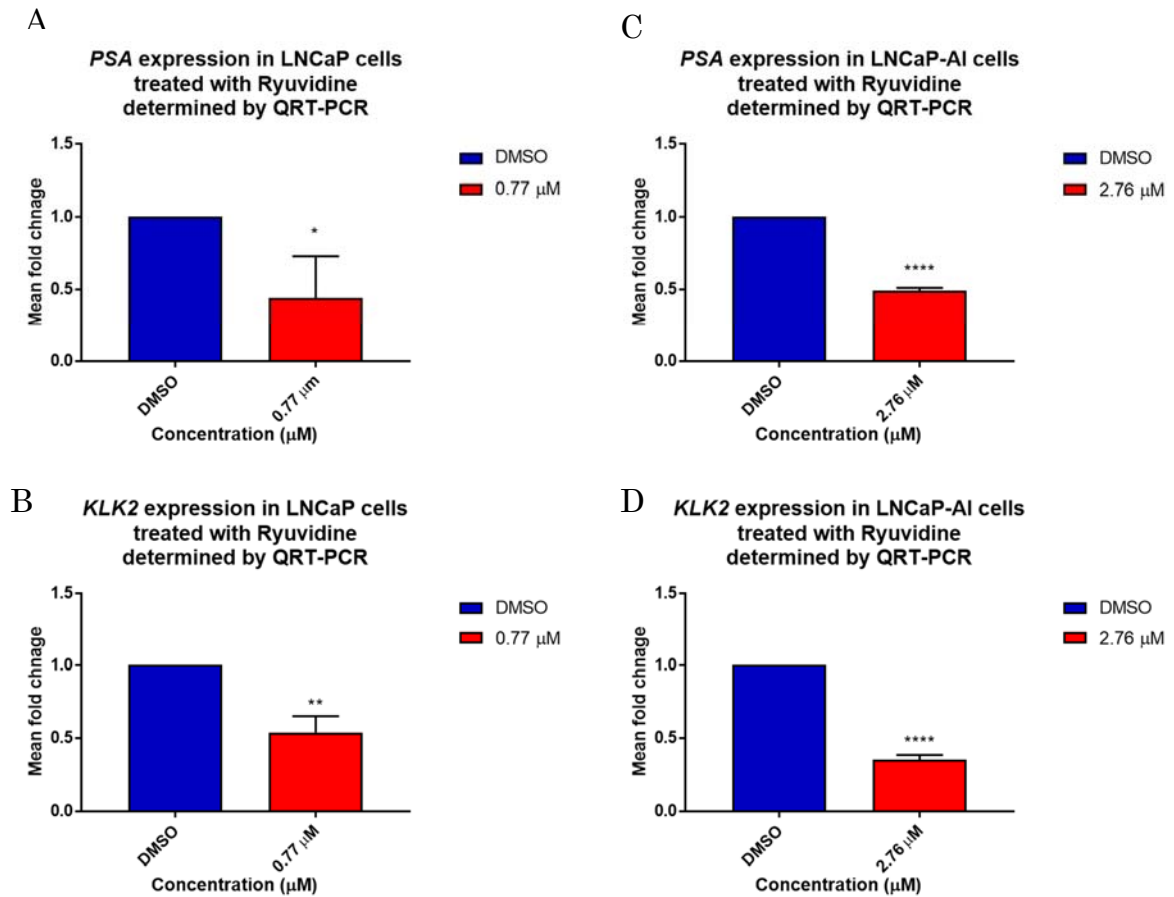
Figure 5-9 Ryuvidine reduces AR target gene expression in PC cell lines. LNCaP cells (A) KLK3 and (B) KLK2 and LNCaP-AI cells (C) KLK3 and (D) KLK2. Cells were seeded out for 24 hours and then treated with the Ryuvidine as indicated for 48 hours. RNA was collected and KLK3 and KLK2 expression levels were assessed by QRT-PCR. Error bars represent the mean ± SD for triplicate independent experiments. p-values were determined by t-test (* p-value <0.05, ** p-value 0.01, *** p-value <0.001 and **** p- value < 0.0001).

5.3.7. *The effect of Ryuvidine on cell cycle profile in LNCaP and LNCaP-AI cells*

KMT5A depletion has been reported to cause cellular arrest at G2/M of the cell cycle (Rice *et al.*, 2002; Lee and Zhou, 2010). Similarly, Ryuvidine treatment also causes a S-phase arrest in HEK293T cells (Blum *et al.*, 2014). To determine whether the same effects are seen in LNCaP and LNCaP-AI cells, flow cytometry as detailed in Chapter 2.2.4, was used. In both cell lines, there were no significant changes in cell cycle profile, as in both cases ~60 % of the cells were in G1, ~15-20 % in S phase and ~20 % of the cells were in G2/M both in the control and Ryuvidine treated arms (Figure 5.10).

To further investigate the cell cycle distribution upon treatment with Ryuvidine, cyclin B levels were assessed by Western blotting in a similar experiment to that performed for UNC0379 (Figure 5.6). Significant changes were detected in cyclin B levels at the protein level was noticed by measuring with densitometry (Figure 5.10). Therefore, it may be concluded from the experimental conditions herein that Ryuvidine does affect cell cycle distribution of LNCaP and LNCaP-AI cells confirmed by looking at cyclin B expression level , particularly with the high doses of Ryuvidine.

A (i)

Cell cycle distibution in LNCaP cells in the presence and absence of Ruyvidine

B(i)

Cell cycle distibution in LNCaP-AI cells in the presence and absence of Ruyvidine

(ii) Ryuvidine effects on cell cycle marker cyclin B in LNCaP cells

(ii) Ryuvidine effects on cell cycle marker Cyclin B in LNCaP-AI cells

(iii) Cyclin B expression in LNCaP cell in response to Ryuvidine reatment

(iii) Cyclin B expression in LNCaP-AI cell in response to Ryuvidine reatment

Figure 5-10 Ryuvidine has no impact on cell cycle distribution in PC cells.
(A) LNCaP and (B) LNCaP-AI cells were treated with Ryuvidine for 48 hours in 6 well plates. Cell cycle analysis was performed using propidium iodide to stain cellular DNA for 40 minutes. Protein was also collected from samples treated with increasing doses of Ryuvidine (0, 1, 1.5, 2, 2.5, 3 µM) and cyclin B expression was detected by Western blotting and measured by densitometry using Epson scanner and labWork 4.0 software. p-values were determined by t-test (* p-value <0.05, ** p-value <0.01, *** p-value <0.001 and **** p- value < 0.0001).

5.3.8. *The effect of Ryuvidine on FOXM1, PLK1, CDC20 expression in LNCaP and LNCaP-AI cells*

Depletion of KMT5A was shown to cause a statistically significant reduction ($p \leq 0.05$) in CDC20, FOXM1, and PLK1 expression at both the protein and mRNA levels when siRNA against KMT5A was used in LNCaP and LNCaP-AI cells (Figure 4. 1, Figure 4. 9 and Figure 4. 10). In order to determine the effect of Ryuvidine as a KMT5A inhibitor on the expression levels of these proteins, LNCaP and LNCaP-AI cells were treated with Ryuvidine (0.77 µM LNCaP and 2.76 µM LNCaP-AI) for 48 hours at 37 °C. Protein lysates were collected and the expression levels of CDC20, FOXM1and PLK1 were measured by Western blotting (Figure 5.11). In LNCaP cells, there was a significant reduction in CDC20 and a modest reduction in FOXM1 expression. However, no changes were detected in PLK1 expression (Figure 5.11.A). Interestingly, in LNCaP-AI cells, a robust reduction in FOXM1, CDC20, and PLK1 expression was clearly detected (Figure 5.11.B).

From the data above, Ryuvidine showed consistency with the effect of KMT5A knockdown on CDC20, FOXM1 and PLK1 expression in LNCaP-AI cells. Furthermore, the depletion of CDC20 in LNCaP and LNCaP-AI cells in response to Ryuvidine supports the role of KMT5A in regulating CDC20 expression of PC cells.
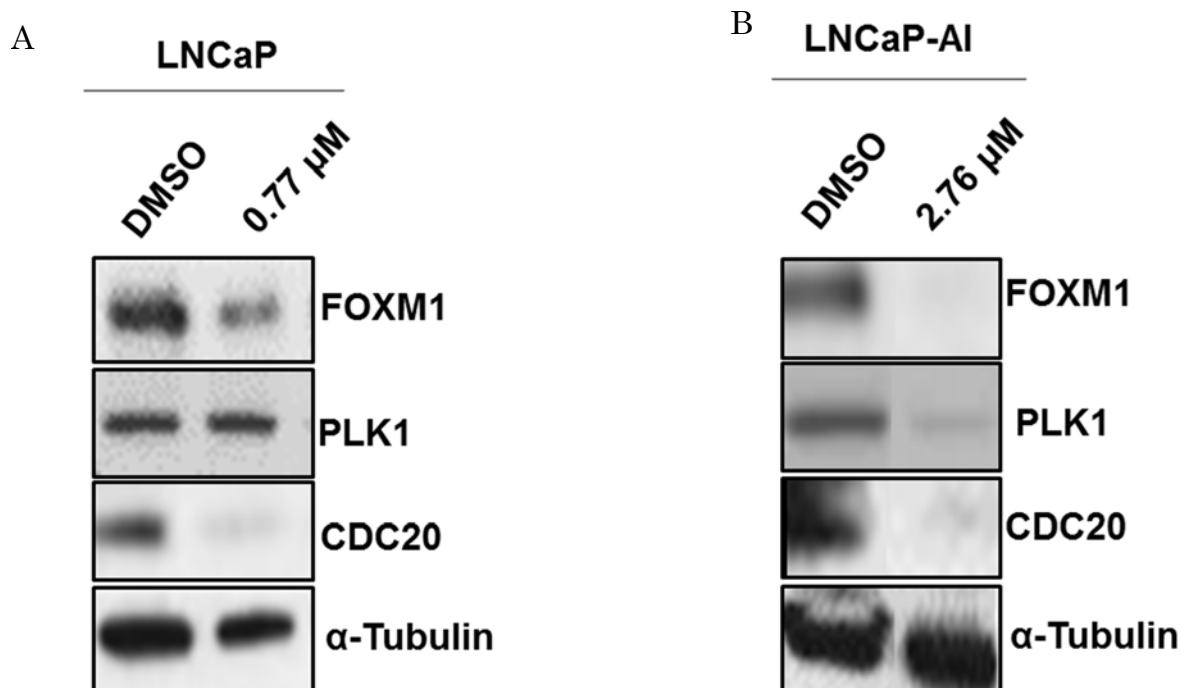
Figure 5-11 Effects of Ryuvidine on FOXM1, PLK1 and CDC20 expression in LNCaP and LNCaP-AI. (A) LNCaP and (B) LNCaP-AI cells were seeded out at appropriate densities and allowed to adhere for 24 hours. Ryuvidine was then applied 0.77 µM in LNCaP and 2.76 µM in LNCaP-AI cells for 48 hours. Protein lysates were then collected and the expression of FOXM1, PLK1 and CDC20 were determined by Western blotting. Alpha-tubulin was used as loading control (representative blot).

5.4. Discussion

KMT5A is being considered as an important new therapeutic target, due to its effect on a wide range of cellular biological processes and role in carcinogenesis (Shi *et al.*, 2007; Takawa *et al.*, 2012). UNC0379 was the first KMT5A selective inhibitor to be discovered (Ma *et al.*, 2014a). UNC0379 was initially designed to target L3MBTL1, but, the required activity was not found. However, it was found to be active against KMT5A using a radioactive biochemical assay looking at the ability to transfer the tritiated methyl group from ^{3}H-SAM to a peptide substrate (Ma *et al.*, 2014a; Milite *et al.*, 2016).

In this study, the effect of UNC0379 on KMT5A enzymatic activity was evaluated for LNCaP and LNCaP-AI cells, by investigating the changes in the levels of H4K20me1. *In vivo* studies suggest that the loss of KMT5A has the effect of decreasing the creation of H4K20me1 mark (Balakrishnan and Milavetz, 2010) therefore by targeting KMT5A with a selective inhibitor a similar effect on H4K20me1 formation would be expected. Indeed, a robust reduction in H4K20me1 expression was detected in both cell lines (Figure 5.4).

Previously, it has been shown that KMT5A can function as a coactivator of the AR, a key therapeutic target for PC (Coffey *et al*, unpublished). The inhibition of KMT5A may result in a reduction in AR activity in PC cell line models. Therefore, the effect of UNC0379 on AR target gene expression (*KLK3, KLK2*) was the next aspect that was investigated. The results showed that targeting LNCaP and LNCaP-AI cells with UNC0379 had no significant effect on AR target genes expression (Figure 5.5.) in both cell lines. This is contradictory to the study by Coffey *et al.*, and the data obtained by KMT5A depletion by siRNA, which showed a significant increase in *KLK3* expression in response to KMT5A knockdown accompanied by DHT treatment in LNCaP and LNCaP-AI cells (Figure 3.2, 3.3). However, in the study by Coffey *et al.,* and the experiment performed in Figure 3.2 and 3.3, DHT was used to stimulate the activity of the AR. Hence, another repeat of this experiment in the presence of DHT is recommended for future studies to determine whether AR-regulated genes are truly affected by UNC0379.

As another method to validate the inhibition of KMT5A with UNC0379, cell cycle profiles were determined (Figure 5.6) and compared to the data generated in Chapter 4 (Figure 4.2) where cell cycle profile was detected following KMT5A depletion using siRNA. Treatment with UNC0379 showed a significant reduction in cyclin B expression was noticed at the

protein level, which indicate an effect on cell cycle progression. The effect of UNC0379 on cultured cells has not been studied before, therefore, the effect on cell cycle profile was unknown. However, trying to repeat this experiment by looking at cell proliferation in the presence of UNC0379 will be essential to directly compare with the data obtained in Chapter 4 (Figure 4.4) which showed a significant reduction in LNCaP and LNCaP-AI cell proliferation in response to KMT5A depletion using siRNAs.

In Chapter 4, KMT5A depletion using siRNAs was found to affect the expression of CDC20, FOXM1, and PLK1 (Figure 4.1, Figure 4.9 and Figure 4.10). As another method to determine whether KMT5A is truly inhibited by UNC0379, the expression of these proteins was assessed in the presence and absence of this drug. Interestingly, a clear reduction was observed in the expression of all these proteins in LNCaP and LNCaP-AI cell lines upon application of UNC0379 for 48 hours (Figure 5.7) suggesting that UNC0379 may well be able to inhibit the activity of KMT5A. The relationship between KMT5A and these proteins has not been previously reported and it is still unknown whether it is the presence or the activity of KMT5A that is required for the regulation of these proteins. In addition, since UNC0379 showed an effect on both the expression (although non-robust) and the activity of KMT5A, this data does go some way to support a role for KMT5A in the regulation of CDC20, FOXM1 and PLK1. The data also support the role of UNC0379 as an inhibitor for KMT5A in PC cells.

Ryuvidine, also known as SPSI82 was one of three compounds (SPSI81, 2 and 3) with cellular activity against KMT5A that was discovered as a part of a high throughput screen (Blum *et al.*, 2014). This study showed a significant reduction in H4K20me1 levels following 24-48 hours treatment with increasing doses range of Ryuvidine (0-3 µM). This data could not be reproduced in LNCaP and LNCaP-AI cells when the same dose of Ryuvidine (0-3 µM) was used for the same period of time. This might be a result of using PC cells, while in their study the effect was tested in HEK293T cells. The Blum group also demonstrated a significant accumulation of cells in S-phase following treatment with 1 µM Ryuvidine for a period of 24-48 hours. This experiment was repeated in Figure 5.10, and also showed a significant reduction in cyclin B expression a the protein level, which suggest an effect on cell cycle progression in response to Ryuvidine treatment.

Similar to experiment done for UNC0379, the effect of Ryuvidine on AR target genes expression was also investigated (Figure 5.9). A significant reduction was detected in *KLK3*and *KLK2* expression in LNCaP and LNCaP-AI cells in response to Ryuvidine,

applying GI$_{50}$ dose treatment for 48 hours (p≤0.05). Another repeat of this experiment including the DHT stimulation is recommended, so it can be directly compared to *KLK3* expression data obtained by KMT5A depletion accompanied by DHT stimulation in LNCaP and LNCaP-AI cells (Figure 3.2, 3.3).

The effect of Ryuvidine on the protein expression levels of FOXM1, CDC20 and PLK1 was also tested similarly to UNC0379. A robust reduction in the expression of CDC20 in both cell lines and FOXM1 and PLK1 in LNCaP-AI cells was detected in response to Ryuvidine treatment (Figures 5. 11) further supporting the model that KMT5A can regulate the expression of these proteins and that they may serve to function as biomarkers for the KMT5A activity.

Both UNC0379 and Ryuvidine showed an effect on the loading controls in western blotting, both tubulin and H4 loading controls showed the same effect with the higher doses of the drugs, as the bands started to faint with dose increase. This might be due to the effect of the higher doses of the drugs on the proliferation of the cells, as was noticed by looking to the cells treated with these two drugs under the microscope, which was consistent with what was reported on Ryuvidine effect on the cell cycle progression at higher doses (Blum et al., 2014). Further investigation of the effect of increasing doses of these two drugs on the tested cell lines proliferation might be required.

To conclude, UNC0379 was more effective when directly examining KMT5A enzymatic activity represented by fluctuation in H4K20me1 expression, while Ryuvidine did not show such an effect. On the other hand, UNC0379 showed less effect on AR target genes expression, while Ryuvidine did significantly reduce their expression at the mRNA level. Both UNC0379 and Ryuvidine robustly reduced CDC20 expression at the protein level. Further experiments are required to determine the specificity of UNC0379 and Ryuvidine towards KMT5A to determine if the data obtained is a direct result of the inhibited KMT5A activity or whether the effects are through other pathways in the cell that could be affected by these two inhibitors, as for example Ryuvidine is documented as an *in vitro* inhibitor of cyclin-dependent kinase 4 and 2 (CDK4/2) with a GI$_{50}$ > 5 µM (Blum *et al*., 2014).The effect of UNC0379, on H4K20me1 activity of KMT5A might also has an extended effect to the different substrates being methylated by KMT5A such as TWIST, RNA polymerase II and ERα (Kapoor-Vazirani and Vertino, 2014; Li et al., 2011a; Wang et al., 2015). This possible effect might be further examined to confirm the specicifty of UNC0379 as KMT5A inhibitor.

Chapter 6 . General Discussion

6.1. Expression profile of KMT5A regulated genes

KMT5A has been subjected to intense study since its discovery in 2002, a consequence of the major role that this histone lysine methyltransferase enzyme plays in regulating various aspects of cellular functions (guowei, 2002). However, KMT5A regulated gene profiles have not been conducted to date. Previous study by Coffey et *al*, has shown the important role that KMT5A plays in regulating the AR in PC, and how this role changes from being an AR suppressor in an androgen-dependent PC cell line model to be become an AR activator in an androgen-independent model (Coffey *et al*, unpublished data). To understand the relationship between KMT5A and the AR, and the genes that might be regulated by this relationship, KMT5A regulated gene expression profiles were studied in this thesis.

Using Illumina Human HT-12 arrays, genes that are regulated by KMT5A in the presence of activated AR and genes that are independently regulated by KMT5A in PC cells were identified. Specifically, 51 genes were regulated by KMT5A independently of AR, from which *CDC20, HIST1H2BD* and *RAB4A* were further validated; 199 genes were androgen-regulated genes that are modulated by KMT5A, from which *CDC42EP3, YIPF1* and *KIF22* were validated. Originally the microarray experiment was carried out in the LNCaP-AI cell line, which is a model of androgen independence. In this cell line, KMT5A had been found to be a coactivator of the AR. However, validation experiments included both LNCaP-AI and the parental, androgen dependent, LNCaP cell line. Interestingly, although KMT5A has been found to have differing effects on AR activity in these cell lines (Coffey *et al*., unpublished data), there was no significant difference in the expression of the selected AR regulated/ KMT5A modulated genes from the microarray experiment for both cell lines. One possible explanation for this is the length of DHT stimulation used in this experiment. As shown in Figures 3.1.C and D., *KLK3* expression peaked at 24 hours in LNCaP cells and then begins to fall slightly, while it continues to increase over the full 72 hours in the LNCaP-AI cells. However, the time point of 24 hours that was selected for the microarray experiment was designed to detect genes that are directly regulated by AR rather than genes which are regulated by secondary effects of alternative signaling pathways that KMT5A depletion might affect. A longer DHT treatment should be considered to give a better indication of any temporal differences and fold changes in expression of these genes between the LNCaP and

LNCaP-AI cell line models, as differential effects were clearly observed between 48 and 72 hours DHT stimulation in the initial study which identified KMT5A as an AR regulator protein (Coffey *et al*, unpublished data). Genes that were identified and selected as AR regulated/ KMT5A modulated genes (*CDC42EP3, YIPF1* and *KIF22*) have previously been identified as androgen responsive in PC cells treated with R1881 and PC patients under ADT (Munkley *et al.*, 2016). A number of genes that have been described as KMT5A regulated such as *p53, CDH1* and *VIM* (Yang *et al.*, 2012b; Marouco *et al.*, 2013) were shown to respond in the same way in the microarray and the subsequent validation data. Specifically for *CDH1* and *VIM*, an increase in the expression of *CDH1* and a reduction in the expression of *VIM* following KMT5A depletion confirmed *CDH1* and *VIM* as being negatively and positively regulated, respectively by KMT5A, likely through its mono-methylation activity on promoters of these genes (Figure 3.4). In addition, KMT5A depletion promoted p53 transcriptional activity, which was reflected by evaluating p53 target gene expression, where *CDKN1A* expression was found to increase significantly in response to KMT5A depletion according to the microarray results (Figure 4.16).

6.2. CDC20 as a potential biomarker for KMT5A activity in CRPC

CDC20 was identified as a novel KMT5A regulated gene independent of the AR according to the microarray data (Figure 3.11 and Figure 4.3). CDC20, an APC substrate recognizing subunit, plays an important role in cell cycle progression during early mitosis from metaphase to anaphase (Manchado *et al.*, 2010). CDC20 expression was reduced significantly in response to KMT5A depletion in both LNCaP and LNCaP-AI cells both at the protein and the mRNA levels independently of AR (Figure 3.11 and Figure 4.3). As both, CDC20 and KMT5A, are cell cycle regulators (guowei, 2002; Rice *et al.*, 2002), it was not surprising to find a significant reduction in cellular proliferation in response to either CDC20 or KMT5A knockdown, which is an important indicator of the potential role that these two proteins play in the progression of PC. A physical interaction was also detected between KMT5A and CDC20, which reflects the possible role that KMT5A enzymatic activity has in regulating CDC20 expression. This was further confirmed by looking at H4K20me1 enrichment at the CDC20 promoter in both LNCaP and LNCaP-AI cells. However, the enrichment of H4K20me1 at the CDC20 promoter following AR activation using 100 nM DHT was varied between LNCaP and LNCaP-AI cells. However, the data is consistent with our group previous work demonstrating DHT-induced, reduction in KMT5A expression in LNCaP cell line but oppositely DHT-induced, increased KMT5A expression, in LNCaP-AI cells (Coffey

et al, unpublished data). The altered levels of KMT5A would therefore impact on the level of H4K20me1 at the CDC20 promoter as was demonstrated (Figure 4.10).

KMT5A was found to be a regulator of CDC20 expression in this thesis, hence, CDC20 may be a potential biomarker for KMT5A activity in PC cells. The same effect was also observed in response to the KMT5A inhibitors UNC0379 and Ryuvidine, as both robustly reduced the expression of CDC20. However, more experiments are required, mainly to confirm that KMT5A does indeed regulate CDC20 directly at the promoter. These experiments could include knockdown of KMT5A and monitoring H4K20me1 enrichment at the CDC20 promoter in both LNCaP and LNCaP-AI cell lines. However, the lack of a suitable KMT5A commercial antibody for application in ChIP experiments is currently hampering these experiments.

6.3. KMT5A can regulate CDC20 expression indirectly through p53 K382me1

FOXM1 which plays an important role in regulating G2/M phase progression (Dai *et al.*, 2013) has been reported as a CDC20 transcriptional activator in tumour initiating cells (TICs) (Xie *et al.*, 2015). As such, FOXM1 was investigated as a factor that may function as an intermediate in the regulation of CDC20 by KMT5A. Interestingly, a significant reduction was noticed in FOXM1 expression in response to KMT5A knockdown both at the mRNA and the protein level (Figure 4.11), which was also reflected in downstream FOXM1 substrate expression (*PLK1* and *Cyclin B*). Expression of both genes was significantly reduced in response to KMT5A depletion as noticed from the microarray data and also the subsequent validation at the protein level in LNCaP and LNCaP-AI cell lines (Figure 4.12). However, this experiment does not conclusively show that this is a direct effect of KMT5A on FOXM1 expression, further experimentation would be required including ChIP assays to look at KMT5A recruitment to the FOXM1 promoter. Nevertheless, this preliminary data does suggest that FOXM1 may be an important intermediary. To investigate further, depletion of FOXM1 was performed, looking at CDC20 expression in PC cells. No significant effect on CDC20 expression was apparent with one of the targeting siRNAs but there was a very small but significant effect on CDC20 expression with the second siRNA (Figure 4.14). This observation was not wholly consistent with previous reports which demonstrated a significant reduction in CDC20 expression with FOXM1 depletion in TICs (Xie *et al.*, 2015), suggesting that cellular background may be important. Hence, it was concluded that FOXM1, whilst clearly regulated by KMT5A in PC cell line models, does not participate in the subsequent regulation of CDC20.

A second line of investigation was pursued based on the fact that p53 can regulate CDC20 expression either directly through binding to the CDC20 promoter or indirectly through p53 binding to the CDE-CHR element independently of p21. KMT5A has been shown to methylate p53 at K382 in order to regulate its activity (Kidokoro *et al.*, 2007; Banerjee *et al.*, 2009). A model was therefore proposed to explain the possible relationship between KMT5A, p53 and CDC20 in PC cells (Figure 4.15). This hypothesis was investigated by mining the microarray data which revealed an increase in *CDKN1A* and a reduction in *CDC20* expression in response to KMT5A depletion in LNCaP-AI and LNCaP cells. To determine whether the post-translational modification of p53 was indeed responsible for this observation, p53 acetylation and phosphorylation markers were assessed (Figure 4.19, 4.20) as methylation of p53 at K382 by KMT5A results in an inability of acetylation and phosphorylation to occur (Shi *et al.*, 2007). Interestingly, knockdown of KMT5A in LNCaP-AI cells resulted in an increase in the acetylation of p53 at K382 and the phosphorylation at S15 as predicted, which was also reflected in the knockdown of KMT5A in LNCaP cells grown in FM (Figure 4.20).

As a second method to investigate these findings, Nutlin3 was used to activate p53 as a more specific way to affect p53 activity, as knockdown of KMT5A will affect many pathways in the cell which could be interfering with p53 activity. A significant increase in p53 and p21 expression was seen in both cell lines in response to Nutlin3, which was accompanied by a reduction in CDC20 expression both at the protein and the mRNA level (Figure 4.22, 4.23). The data showed that CDC20 is affected by p53 activity in PC cells and that it is possible that KMT5A can regulate CDC20 expression through its methylation activity on p53-K382.

p53 has also been reported to be a negative regulator of FOXM1 expression in either a p21 and Rb dependent or in an independent manner (Barsotti and Prives, 2009). A possible model was suggested in Chapter 4 (Figure 4.24) to explain how that might be happening. With KMT5A depletion, p53 is less likely to be subject to mono-methylation. Consequently, the K382 residue will be available for acetylation, which enables p53 transcriptional activation and subsequent activity to be exerted on its substrates, including FOXM1. Activated p53 would results in reducing FOXM1 expression and in turn its activity on its substrates. Treatment of LNCaP and LNCaP-AI cells with 5 μM Nutlin3 resulted in significantly reduced FOXM1 expression both at the protein and the mRNA level, which confirmed that p53 does regulate FOXM1 expression in PC cells and that the model tested is still feasible (Figure 4.25, 4.26). No further work has been done on this aspect. However, the preliminary data is encouraging. A critical experiment that should be performed is the detection of p53-K382-me1 at the protein level in response to KMT5A depletion in order to determine the effect of

KMT5A methylation activity on p53 in androgen dependent and independent PC cells. However, a specific p53-K382-me1 antibody is unavailable commercially.

6.4. KMT5A inhibition in LNCaP and LNCaP-AI cells

As KMT5A is an important regulator of many cellular functions, a number of attempts have been made to develop inhibitors against KMT5A activity. From the limited inhibitors available that are claimed to target KMT5A activity, UNC0379 and Ryuvidine (Blum *et al.*, 2014; Ma *et al.*, 2014b) were selected to be tested in this thesis. The effect of these inhibitors was studied on KMT5A activity in PC cells, and a robust reduction in H4K20me1 was detected using UNC0379, while a lesser effect was seen with Ryuvidine. However, both of the inhibitors robustly reduced the expression of CDC20 and FOXM1 at the protein level in both cell lines (Figure 5.7, 5.11). Hence, using these inhibitors supported the suggested model for the regulation of CDC20 by KMT5A as described in Chapter 4.

A previous study found that Ryuvidine causes an accumulation of cells in the S phase of the cell cycle (Ma *et al.*, 2014a), an effect which was noticed in this thesis using the same dose range of Ryuvidine for the same duration looking at cyclin B expression at the protein level as a marker for G2/M phase of the cell cycle(Figure 5.10). The same effect on cyclin B was also noticed with UNC0379 treatment (Figure 5.6). Further experiments are required to confirm the specificity of these inhibitors towards KMT5A in a cellular context, in order to confirm that the cellular changes observed are not due to off target effects rather than the inhibition of KMT5A activity itself. For example, Ryuvidine has been documented as an in vitro inhibitor of cyclin-dependent kinase 2 and 4 (CDK2/4) with $GI_{50} > 5$ μM (Blum et al., 2014).

6.5. Conclusion

Determination of KMT5A regulated gene expression profiles revealed that CDC20 is regulated by KMT5A indirectly via p53 methylation, and that more experiments are required to cover the possibility of considering CDC20 as a putative biomarker for KMT5A activity in PC cells through a direct regulation at the CDC20 promoter level. The independent effect of KMT5A from AR in the regulation of CDC20 in both androgen dependent and independent PC models used in this study might give another possible explanation for the continuity of PC cells growth and proliferation despite antiandrogen treatment, and that targeting CDC20 via using KMT5A inhibitors might play a role in the regulation of PC cells proliferation. The data also showed that for the models of PC used in this study, AR was found not to be integral to KMT5A activity in models of androgen independence used.

Future directions

Further experiments might be required in order to confirm or investigate in depth some of the study findings including:

1. Looking at the effect of KMT5A depletion on the expression of p53-K382-me1 at the protein level is essential to correlate FOXM1 expression changes to KMT5A through p53-K382-me1.

2. Looking at p53-K382 -me1 expression levels in the presence and absence of KMT5A is required to further support the suggested possible pathway.

3. Investigating the enrichment of p53 and p21 at the CDC20 promoter in PC cells.

4. Immunoprecipitation are required to see if KMT5A and CDC20 interact as part of the APC complex or whether they can interact independent of this.

5. To support the role of KMT5A activity in regulating CDC20 expression by knockdown of KMT5A and looking at H4K20me1 enrichment at the CDC20 promoter in LNCaP and LNCaP-AI cells. However, the required KMT5A antibody is unavailable commercially.

6. FOXM1 seems to be regulated by AR in PC cells. However, further investigation is required to further understand the underlying mechanism

7. Confirm the specificity of these inhibitors towards KMT5A in a cellular context.

8. Another repeat of the experiment of the effect of Ryuvidine and UNC0379 on AR target genes including the DHT stimulation is recommended, so it can be directly compared to PSA expression data obtained by KMT5A depletion accompanied by DHT stimulation in LNCaP and LNCaP-AI cells (Figure 3.2, 3.3).

9. This possible effect of UNC0379 and Ryuvidine on cell proliferations on the tested cell lines.

10. Further examination of the effect of treatment of the tested PC cell lines on the H4K20me1 activity of KMT5A on some of its substrates as TWIST, ERα and RNA polymerase II, to confirm the specicifty of UNC0379 as KMT5A inhibitor.

Poster Presentations

1. Attended the Genes & Cancer 30th Anniversary Meeting which took place at Robinson College, Cambridge from the 24th - 26th March 2014.

2. Participated by a poster at the NICR-IHA postgraduate research day, Newcastle University 2014.

3. Participated by a poster at the NICR-IGM postgraduate research day, Newcastle University 2015.

4. Participated by a poster at the cancer postgraduate research day, Newcastle University March 2016.

5. Participated by a poster at the Gordon Research Conference, "Hormone-dependent cancers" from 16th-22nd July 2015, Maine State, USA.

6. Participated by a poster at EACR24 – the 24th Biennial Congress of the European Association for Cancer Research, Manchester, UK from 9-12 July 2016.

Chapter 7 Appendix

7.1. Microarray

Table 7-1 microarray samples

Condition	Sample ID	description	KMT5A knockdown	DHT
AI.NS.0hr-DHT	1A, 1B, 1C, 1D	Non-silencing under steroid depleted conditions	no	no
AI.NS.24hr+DHT	4A, 4B, 4C, 4D	Non-silencing with 10 nM DHT for 24 hours	no	yes
AI.#1.0hr-DHT	2A, 2B, 2C, 2D	KMT5A knockdown with siRNA #1 under steroid depleted conditions	yes	no
AI.#124hr+DHT	5A, 5B, 5C, 5D	KMT5A knockdown with siRNA #1 with 10 nM DHT for 24 hours	yes	yes
AI.#2.0hr-DHT	3A, 3B, 3C, 3D	KMT5A knockdown with siRNA #2 under steroid depleted conditions	yes	no
AI#2.24hr+DHT	6A, 6B, 6C, 6D	KMT5A knockdown with siRNA #2 with 10 nM DHT for 24 hours	yes	yes

7.2 Microarray data analysis: Heat map

Figure 7-1: Microarray data analysis: Heat map of expression intensities of : (A) genes that are regulated by KMT5A in the presence and absence of DHT stimulation, (B) genes that are regulated by KMT5A only in the presence of androgen stimulation in LNCaP-AI cells and (C) genes that are regulated by KMT5A independent of DHT stimulation. Y axis represents the genes in each group. X axis represents experiments samples, each group (B, C) includes a non-silencing sample +/- DHT (10 nM) and KMT5A siRNA samples +/- DHT (10 nM).

Figure 7-2 Hierarchical clustering analysis of the microarray samples
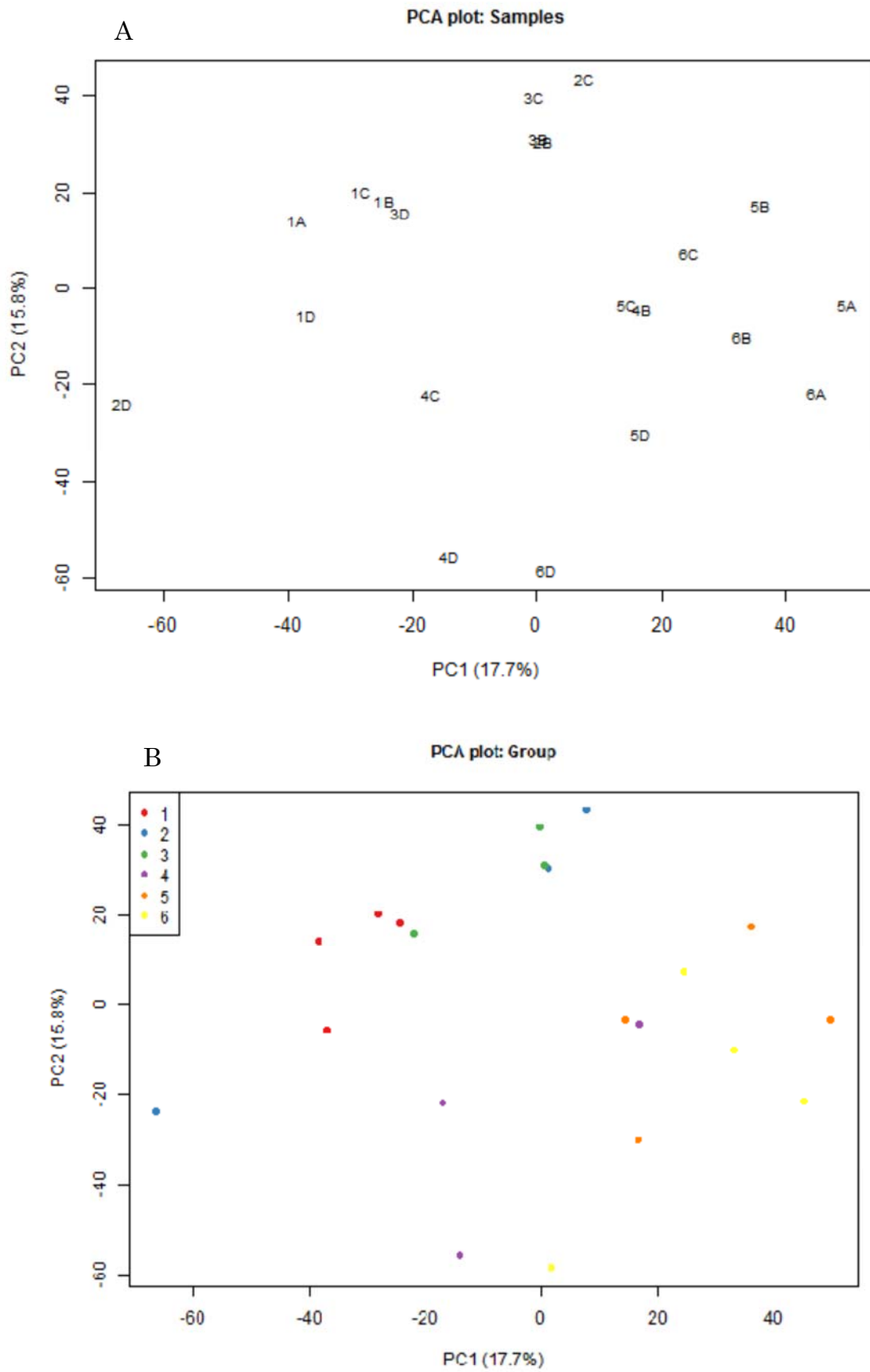
Figure 7-3 PCA blot of : (A) microarray samples, (B) microarray groups

Table 7-2 microarray data analysis: 57 genes regulated by KMT5A independent of DHT

ID	symbol	logFC	AveExpr	P.Value	adj.P.Val
ILMN_1757467	H1F0	-1.08835	11.22026	6.27E-09	2.66E-05
ILMN_1805271	ZNF721	-1.04533	9.007149	2.31E-05	0.012968
ILMN_2347068	MKNK2	-1.03495	12.16529	2.46E-05	0.013318
ILMN_3238680	C7orf55	-0.96964	12.23243	6.20E-06	0.005196
ILMN_2405592	EMC6	-0.96195	10.50941	5.79E-07	0.00108
ILMN_1758674	EMC6	-0.94091	12.17065	4.20E-08	0.00014
ILMN_2055165	MRFAP1	-0.91885	13.008	7.60E-05	0.022612
ILMN_2359789	RAC1	-0.91883	11.77133	1.92E-05	0.011812
ILMN_2104106	XPR1	-0.88566	10.13699	0.000101	0.026185
ILMN_2110532	RPL26L1	-0.87964	11.24658	4.63E-08	0.00014
ILMN_1744912	CTTN	-0.86911	9.7198	2.06E-06	0.002511
ILMN_1779751	C7orf55	-0.86137	10.88068	0.000184	0.034831
ILMN_2128741	RDH11	-0.84181	10.34657	1.36E-05	0.009594
ILMN_2393712	CTTN	-0.81809	9.834393	1.61E-05	0.010625
ILMN_2388507	AKT1	-0.78835	10.20818	7.06E-05	0.021931
ILMN_1652512	C2CD2	-0.7623	10.31097	7.48E-05	0.022559
ILMN_2307032	OSBPL5	-0.76054	9.07594	0.000241	0.040124
ILMN_1720438	RPL26P30	-0.75084	11.63348	5.36E-06	0.00492

ILMN_1772981	EPN1	-0.74729	12.14168	0.000117	0.029838
ILMN_1804735	CBS	-0.73195	11.33409	4.82E-05	0.019954
ILMN_1712556	ZW10	-0.7167	9.735771	0.000255	0.041436
ILMN_1705876	NAP1L1	-0.67497	9.201547	3.09E-05	0.014819
ILMN_1703891	TBC1D9	-0.67318	8.760676	4.91E-05	0.019954
ILMN_1773567	LAMA5	-0.65483	11.29597	0.000174	0.033454
ILMN_2373763	CASP7	-0.64758	8.305084	5.32E-05	0.020061
ILMN_1776586	RPL26L1	-0.62479	10.32787	0.000122	0.029886
ILMN_1751346	ERBB3	-0.60254	11.02226	7.79E-06	0.005873
ILMN_1678087	MAP3K4	-0.54956	8.699426	7.90E-05	0.023168
ILMN_1802799	AKIRIN1	-0.54647	9.307711	6.87E-05	0.021931
ILMN_1660341	LRPAP1	-0.53766	10.04378	0.000141	0.032068
ILMN_1714756	YIPF5	-0.5343	8.20526	2.26E-06	0.002511
ILMN_1785356	DENND5A	-0.46799	8.83668	0.000316	0.048047
ILMN_1775939	SF3B2	-0.3539	10.99705	4.78E-05	0.019954
ILMN_2112599	C16orf80	0.391709	10.34499	0.000313	0.048047
ILMN_1770035	NCOA5	0.430095	8.74122	0.000145	0.032411
ILMN_1753286	MYO19	0.461585	8.148915	5.71E-05	0.020791
ILMN_3239181	ITPRIP	0.507681	8.901604	5.04E-05	0.019959
ILMN_2077886	C1orf109	0.52436	9.305174	0.000122	0.029886
ILMN_1680091	POP7	0.526673	9.896519	0.000326	0.04874

ILMN_1805192	ITPRIP	0.58975	9.188232	9.37E-07	0.001319
ILMN_1711450	NELFCD	0.591567	10.81805	9.75E-05	0.026185
ILMN_1678678	SLC37A4	0.640783	12.01151	0.000163	0.03305
ILMN_1684205	CIB1	0.646404	12.89573	6.40E-06	0.005196
ILMN_1756355	NDUFS3	0.678602	12.39527	6.36E-05	0.021644
ILMN_1676296	PPAP2A	0.71265	10.28284	0.00015	0.032528
ILMN_1750711	MYO19	0.716666	8.399239	0.000171	0.033454
ILMN_1681008	CGRRF1	0.80424	9.566361	3.72E-06	0.003743
ILMN_3306742	SIGMAR1	0.869332	9.722861	0.000205	0.036906
ILMN_2398489	SIGMAR1	0.877311	10.24105	0.000102	0.026185
ILMN_2340721	TMEM134	1.00009	10.83618	0.00015	0.032528
ILMN_1698243	C1orf85	1.012752	11.25785	6.98E-07	0.001134
ILMN_3231944	NA	1.078141	11.94226	0.000229	0.038471
ILMN_1651936	SETD8	1.088865	8.542859	1.37E-09	9.63E-06
ILMN_1802205	RHOB	1.208194	10.46835	6.30E-06	0.005196
ILMN_1808196	GSTO1	1.257747	11.02817	2.20E-05	0.012895
ILMN_1669210	SNORD16	1.362918	9.861519	1.34E-07	0.000349
ILMN_1796923	LOC81691	1.650372	9.536422	1.49E-07	0.000349

Table 7-3 microarray data analysis: 226 genes regulated by KMT5A in the presence and absence of DHT

ID	symbol	logFC	AveExpr	P.Value	adj.P.Val
ILMN_1784602	CDKN1A	-1.46704	13.70571	2.36E-06	0.001918
ILMN_1676984	DDIT3	-1.43733	9.723055	5.96E-06	0.004061
ILMN_1651496	HIST1H2BD	-1.246	8.939616	1.39E-05	0.006028
ILMN_1792689	HIST1H2AC	-1.21968	9.385179	1.01E-05	0.005207
ILMN_1659047	HIST2H2AA3	-1.18965	11.81669	0.000406	0.032553
ILMN_2377900	MAP1B	-1.12583	9.067097	0.000612	0.039518
ILMN_1801205	GPNMB	-1.124	10.09419	0.000659	0.041302
ILMN_2407389	GPNMB	-1.09216	9.462667	0.000852	0.048333
ILMN_1667561	IFRD1	-1.05601	9.260324	2.24E-06	0.001918
ILMN_2089875	TNFSF4	-1.05425	8.736964	0.000158	0.019549
ILMN_1768719	RDH11	-1.02956	12.75064	2.60E-07	0.000687
ILMN_1702933	ADM2	-1.0242	9.830516	2.70E-05	0.007648
ILMN_1718982	BEST1	-1.00953	8.351679	8.14E-06	0.004523
ILMN_1811264	C15orf57	-1.00543	9.756403	2.94E-07	0.00069
ILMN_1712556	ZW10	-0.95387	9.735771	3.98E-07	0.000773

ILMN_1680154	MAP1B	-0.94359	8.581749	0.000168	0.019835
ILMN_2390310	MIR22HG	-0.93089	8.548372	5.53E-05	0.010616
ILMN_1746948	MYL5	-0.89413	9.769292	0.000493	0.035654
ILMN_2347068	MKNK2	-0.89159	12.16529	6.87E-06	0.004144
ILMN_3243253	LPAR3	-0.88855	9.760098	6.90E-05	0.012255
ILMN_1702683	SLC33A1	-0.87329	9.129753	1.85E-06	0.001699
ILMN_2404688	NUPR1	-0.86939	10.42869	0.00014	0.018235
ILMN_1709719	LPAR3	-0.85529	9.112139	0.000169	0.019835
ILMN_1758674	EMC6	-0.84881	12.17065	4.33E-09	1.83E-05
ILMN_1745620	KRCC1	-0.84664	9.861956	1.51E-05	0.006028
ILMN_2405592	EMC6	-0.84012	10.50941	1.09E-07	0.000382
ILMN_1748281	MAPK10	-0.80493	9.03555	0.000817	0.047106
ILMN_2128741	RDH11	-0.79625	10.34657	1.08E-06	0.001357
ILMN_3246900	LOC92249	-0.79481	10.1246	1.43E-06	0.001631
ILMN_1712678	RPS27L	-0.78939	12.5714	0.000193	0.021736
ILMN_1796179	HIST1H2BK	-0.77855	12.42091	0.000109	0.015604
ILMN_1758623	HIST1H2BD	-0.7751	8.815392	0.000135	0.017849
ILMN_1654629	TMEM175	-0.75967	9.620888	1.47E-06	0.001631
ILMN_1777591	HOGA1	-0.74383	8.950932	9.78E-07	0.001357
ILMN_2316236	HOPX	-0.73901	8.399782	1.65E-05	0.006028
ILMN_1658469	TP53TG1	-0.73656	9.725012	1.90E-05	0.006367
ILMN_1672128	ATF4	-0.72538	13.17621	1.58E-05	0.006028

ILMN_2220739	TMCO3	-0.71689	9.039204	1.51E-05	0.006028
ILMN_1677843	RAB24	-0.71241	10.83457	0.000131	0.017667
ILMN_1700915	BMI1	-0.70521	10.10946	2.90E-05	0.007897
ILMN_2359789	RAC1	-0.70284	11.77133	2.22E-05	0.007113
ILMN_2358457	ATF4	-0.70137	9.514065	0.000733	0.044326
ILMN_1698019	LGMN	-0.69317	10.22165	0.000812	0.047106
ILMN_1675406	PPAPDC1B	-0.67944	9.999557	0.000269	0.0269
ILMN_1724897	C14orf93	-0.67593	9.053742	0.000338	0.029317
ILMN_1694106	GPD1L	-0.66788	10.68853	2.72E-05	0.007648
ILMN_2379718	RAB24	-0.66231	9.774575	2.86E-05	0.007897
ILMN_1902658	LOC92249	-0.66103	9.60327	3.50E-06	0.002638
ILMN_2198878	INPP4B	-0.63836	8.665254	0.000264	0.026743
ILMN_1805271	ZNF721	-0.63201	9.007149	0.000326	0.028902
ILMN_1667564	ALDH3A2	-0.62977	8.774448	0.000838	0.047817
ILMN_2110532	RPL26L1	-0.6275	11.24658	1.51E-07	0.000455
ILMN_1804735	CBS	-0.62708	11.33409	1.51E-05	0.006028
ILMN_1690703	LINC00478	-0.62486	10.2114	2.70E-05	0.007648
ILMN_1807662	IGF2R	-0.61068	11.35487	6.10E-05	0.011498
ILMN_1763568	ZDHHC16	-0.59618	11.34801	0.000619	0.039618
ILMN_1704793	MYPOP	-0.59111	9.502472	8.18E-05	0.012985
ILMN_1802799	AKIRIN1	-0.57679	9.307711	1.65E-06	0.001631
ILMN_1779751	C7orf55	-0.57379	10.88068	0.000776	0.045708

ILMN_1779530	COG6	-0.56948	9.08974	5.07E-05	0.010186
ILMN_1803744	VIMP	-0.56079	9.92619	4.31E-05	0.009389
ILMN_2346997	RAB23	-0.55719	9.612534	0.000277	0.027111
ILMN_1791306	IDNK	-0.55235	9.079785	0.00027	0.0269
ILMN_1756572	COQ2	-0.54914	10.46523	0.00061	0.03948
ILMN_1739441	GANAB	-0.54856	9.905494	0.000855	0.048405
ILMN_3251501	SERF2	-0.54677	9.788033	0.000403	0.032553
ILMN_3245458	SNORA61	-0.54393	9.807032	1.60E-05	0.006028
ILMN_1652512	C2CD2	-0.54349	10.31097	0.000179	0.020738
ILMN_1804652	PLEKHH3	-0.54205	10.46956	1.33E-05	0.006028
ILMN_2158705	ACYP2	-0.53185	9.315826	0.000707	0.043259
ILMN_2091375	KRCC1	-0.52971	8.190943	0.000135	0.017849
ILMN_1787680	VIMP	-0.52704	11.71035	8.41E-05	0.013253
ILMN_1680937	HIST1H2BC	-0.52221	7.979589	3.66E-05	0.008777
ILMN_1714599	CAMLG	-0.5214	12.16864	0.000167	0.019835
ILMN_1689908	ANKRD13A	-0.51925	10.11783	0.0003	0.027677
ILMN_1773567	LAMA5	-0.51692	11.29597	0.000144	0.018252
ILMN_1785356	DENND5A	-0.51039	8.83668	7.17E-06	0.004206
ILMN_2089073	ATP9A	-0.5101	10.77621	0.000122	0.016877
ILMN_1693227	ZC3H7A	-0.50468	8.850819	8.68E-05	0.013375
ILMN_1660341	LRPAP1	-0.50455	10.04378	1.67E-05	0.006028
ILMN_2413318	C15orf57	-0.50423	8.579085	3.76E-05	0.008824

ILMN_1746492	IFT27	-0.50411	8.757326	0.000711	0.043388
ILMN_1767422	POLR1D	-0.50334	14.25387	6.81E-06	0.004144
ILMN_2291619	RAB3IP	-0.49752	9.588614	3.49E-06	0.002638
ILMN_1732923	SIPA1L2	-0.49643	8.134009	1.56E-05	0.006028
ILMN_2056815	LINGO4	-0.49634	8.217291	0.000602	0.03948
ILMN_1802631	AGA	-0.49332	8.923947	5.16E-05	0.010273
ILMN_2107991	HABP4	-0.49163	8.109203	5.63E-07	0.00085
ILMN_1735014	KLF6	-0.48673	8.511669	0.000758	0.045357
ILMN_1728224	OGFR	-0.4824	8.254581	0.000103	0.015111
ILMN_1654861	ACO2	-0.4816	10.00446	0.000162	0.019835
ILMN_1760593	CRY1	-0.47997	8.780637	7.03E-05	0.012266
ILMN_1760174	MCCC1	-0.46752	10.39325	0.000576	0.038953
ILMN_1720438	RPL26P30	-0.46394	11.63348	7.54E-05	0.012673
ILMN_1757467	H1F0	-0.4574	11.22026	2.50E-05	0.007529
ILMN_2393712	CTTN	-0.45467	9.834393	0.00054	0.037623
ILMN_1794560	EMC6	-0.45358	8.73559	0.000445	0.03406
ILMN_1727553	C5orf54	-0.44685	8.614251	3.93E-05	0.009021
ILMN_1706873	RPL34	-0.44619	10.43693	0.000579	0.038981
ILMN_3247645	LOC550643	-0.44439	11.65188	0.00029	0.027501
ILMN_1656335	RIT1	-0.44365	8.549628	0.000117	0.016378
ILMN_1797342	FNBP1	-0.43751	9.807298	7.62E-05	0.012673
ILMN_1654060	MKNK2	-0.43737	8.224322	0.000132	0.017779

ILMN_1744912	CTTN	-0.43024	9.7198	0.000339	0.029317
ILMN_1745152	UQCC1	-0.42924	9.245704	0.000361	0.030202
ILMN_3245413	DENND5A	-0.42606	8.49004	8.17E-05	0.012985
ILMN_1776993	COG2	-0.41949	10.02662	4.50E-05	0.009413
ILMN_1681670	SLC25A4	-0.41725	10.53003	0.000167	0.019835
ILMN_2202637	CRY1	-0.41301	8.967114	0.000346	0.029583
ILMN_1777660	RNF144A	-0.41143	9.052313	0.000128	0.017511
ILMN_1764500	BRK1	-0.40557	10.79488	0.000424	0.033237
ILMN_1728426	INPPL1	-0.37618	9.159725	2.93E-05	0.007897
ILMN_1675038	PRMT2	-0.37284	8.635139	0.000636	0.040222
ILMN_1794157	CATSPER2P1	-0.37145	8.517667	0.000463	0.034923
ILMN_1754727	GPRASP2	-0.36956	9.158124	6.23E-05	0.011643
ILMN_1777106	LRRC57	-0.36385	8.302459	0.000475	0.035138
ILMN_1719219	ZNF616	-0.36151	8.004969	1.62E-05	0.006028
ILMN_2115696	USP42	-0.35644	9.451247	0.000463	0.034923
ILMN_2396956	AKAP13	-0.3554	8.28927	0.000417	0.033036
ILMN_2340131	MAPK10	-0.35233	7.908372	0.00028	0.027229
ILMN_1722726	ARHGAP32	-0.34896	9.164974	0.000295	0.027668
ILMN_1751692	ZNF17	-0.34785	8.191574	0.000197	0.021975
ILMN_1671777	FGF13	-0.33825	8.425269	0.000169	0.019835
ILMN_2355225	LSP1	-0.33425	8.52703	0.000141	0.018235
ILMN_2415911	ENOX2	-0.32187	8.346536	0.000898	0.049765

ILMN_1751346	ERBB3	-0.32023	11.02226	0.000468	0.035057
ILMN_1774949	PIGP	-0.31649	9.605158	0.000618	0.039618
ILMN_1771800	PRKCA	-0.31567	8.185216	0.000587	0.039103
ILMN_1746561	BCL2L2	-0.30828	9.463855	0.000606	0.03948
ILMN_2246510	TSC1	-0.29434	9.416984	0.000803	0.047002
ILMN_1677885	FMO4	-0.29282	8.013498	0.000553	0.038136
ILMN_1699496	PHF21A	-0.28735	9.493864	0.00035	0.029583
ILMN_1779841	PPP2R1B	-0.2867	8.022399	0.000622	0.039652
ILMN_1788149	NEK11	-0.28363	8.193447	0.000595	0.039339
ILMN_1792672	POLR2D	-0.28307	8.68112	0.000887	0.04952
ILMN_1692413	NMNAT1	-0.28199	8.412449	9.85E-05	0.014751
ILMN_1714756	YIPF5	-0.27423	8.20526	0.000256	0.026446
ILMN_2299843	ATP5S	-0.27065	9.064271	0.000149	0.018856
ILMN_2388484	MAP2	-0.27045	7.907366	0.000478	0.035138
ILMN_1764201	MAP2	-0.25969	7.834426	0.000394	0.032142
ILMN_2333865	DNAJB12	-0.24794	9.123363	0.000705	0.043259
ILMN_1682818	TTLL3	-0.22563	7.884228	0.000666	0.041615
ILMN_3251155	PCBP2	0.261776	8.120238	0.000286	0.027322
ILMN_1768226	ARMCX6	0.282263	8.029951	0.000151	0.018936
ILMN_1733703	TRMU	0.288393	8.240659	0.000348	0.029583
ILMN_1744959	NFX1	0.292108	9.024486	0.000307	0.027845
ILMN_1691458	SYPL1	0.296264	9.097584	0.000269	0.0269

ILMN_1708369	EPS15L1	0.298147	8.16339	0.000433	0.033486
ILMN_1701244	ITFG2	0.302417	8.143035	4.44E-05	0.009413
ILMN_1694274	NDUFC2	0.315259	8.19186	0.000672	0.041845
ILMN_1725071	CCDC12	0.318827	9.988297	0.000342	0.029462
ILMN_3272378	EZR	0.351794	12.14009	0.000806	0.047002
ILMN_1672094	DLX1	0.355073	8.125494	0.000166	0.019835
ILMN_1764851	TP53RK	0.359074	9.352697	0.000274	0.026999
ILMN_1805192	ITPRIP	0.360311	9.188232	1.87E-05	0.006367
ILMN_1692429	PQBP1	0.381165	8.014851	6.35E-06	0.004064
ILMN_1795383	RPUSD3	0.388348	10.33861	0.000317	0.028223
ILMN_1664761	TMEM138	0.388706	9.317954	0.000178	0.020714
ILMN_3239181	ITPRIP	0.408294	8.901604	3.30E-05	0.008201
ILMN_1703894	BOLA2	0.42558	8.154848	0.000154	0.019295
ILMN_1763875	ABCF1	0.428048	11.21989	0.000229	0.024035
ILMN_1663954	NELFCD	0.4343	11.10966	6.91E-05	0.012255
ILMN_1673363	CD97	0.435428	10.1343	0.000221	0.023725
ILMN_1753353	SLBP	0.443764	9.983898	0.000378	0.03093
ILMN_1690125	PDLIM7	0.444988	8.451727	0.000568	0.03855
ILMN_2077886	C1orf109	0.453575	9.305174	3.65E-05	0.008777
ILMN_1657898	MTFP1	0.453718	8.090228	7.51E-05	0.012673
ILMN_1695868	PRICKLE4	0.471815	12.40211	4.49E-05	0.009413
ILMN_2375418	DPH2	0.477601	10.23343	5.04E-05	0.010186

ILMN_1810488	NFYC	0.488292	9.253861	5.51E-05	0.010616
ILMN_1681340	HSPB11	0.490309	10.01032	6.92E-05	0.012255
ILMN_2367191	PSMF1	0.49063	10.93973	0.000552	0.038136
ILMN_1656254	NOTCH2NL	0.498286	8.583788	4.96E-07	0.000805
ILMN_1672080	NR2F6	0.501647	10.28405	5.49E-05	0.010616
ILMN_1687430	EIF2B4	0.503658	11.47999	9.96E-05	0.014812
ILMN_2402674	DPM3	0.507683	11.46211	0.000609	0.03948
ILMN_1780924	SLC43A1	0.512675	8.297344	1.48E-05	0.006028
ILMN_1698243	C1orf85	0.51743	11.25785	0.000108	0.015604
ILMN_1774432	DTD1	0.532781	9.45361	0.00019	0.021638
ILMN_1718832	SPHAR	0.538741	8.607833	0.000565	0.038496
ILMN_1812856	ZSWIM1	0.556158	10.06701	5.33E-05	0.010513
ILMN_2055477	EXOSC7	0.556828	10.55544	0.000258	0.026464
ILMN_2356672	EIF2B4	0.557596	11.54201	0.000271	0.0269
ILMN_1677877	UBE2L3	0.559589	9.132145	0.000332	0.02909
ILMN_1711450	NELFCD	0.561718	10.81805	9.50E-06	0.005011
ILMN_1775677	TYSND1	0.571773	11.45695	0.000496	0.035714
ILMN_1652777	CDC42EP2	0.572491	8.324909	7.16E-05	0.012398
ILMN_1803564	YIPF1	0.592997	10.02486	0.000208	0.022832
ILMN_1704024	TMEM160	0.594535	9.593687	0.000283	0.027229
ILMN_1775304	DNAJB1	0.594935	10.01511	7.77E-06	0.004435
ILMN_2052163	YIPF1	0.605483	10.77574	0.000375	0.03093

ILMN_1771376	PEA15	0.615298	11.79585	0.000247	0.025667
ILMN_1679482	TUBA3C	0.629282	8.295667	0.000776	0.045708
ILMN_1657796	STMN1	0.629924	9.43299	0.000213	0.023273
ILMN_1738093	RNFT2	0.629982	9.933434	7.61E-05	0.012673
ILMN_1782633	BOLA2	0.649301	10.82018	0.000474	0.035138
ILMN_2162253	NMU	0.654307	9.590243	0.000483	0.035225
ILMN_1731640	TMSB15B	0.691827	9.753279	0.000596	0.039339
ILMN_2042771	PTTG1	0.693154	12.26927	0.000419	0.033036
ILMN_1796923	LOC81691	0.701897	9.536422	0.000226	0.024011
ILMN_1676296	PPAP2A	0.706752	10.28284	9.21E-06	0.004983
ILMN_1737283	TMSB15B	0.707993	9.826054	0.000225	0.024009
ILMN_1813260	TIMM17B	0.708093	9.772335	0.000473	0.035138
ILMN_2330243	NUDT1	0.715069	9.700859	7.62E-05	0.012673
ILMN_1695491	WDYHV1	0.716721	9.115042	0.00013	0.017642
ILMN_1681737	TMSB15A	0.733159	10.14198	0.000312	0.028063
ILMN_1802205	RHOB	0.752864	10.46835	7.92E-05	0.012768
ILMN_1704873	TCEB1	0.758011	10.48937	6.30E-06	0.004064
ILMN_2227573	GSTO1	0.767017	11.68359	0.000401	0.032536
ILMN_2157510	BLOC1S1	0.77094	10.05744	4.75E-05	0.009772
ILMN_1729179	SPATA5L1	0.775786	9.491515	0.000486	0.035247
ILMN_1721868	KPNA2	0.778836	10.21664	1.62E-06	0.001631
ILMN_1811921	CSRP1	0.805965	10.52105	0.000501	0.035832

ILMN_2355665	MTFP1	0.820035	10.4277	0.000316	0.028223
ILMN_1691237	CAP2	0.821721	11.41357	1.48E-05	0.006028
ILMN_1808196	GSTO1	0.862994	11.02817	8.57E-05	0.013299
ILMN_1708041	PLEKHF1	1.005253	10.33165	6.29E-05	0.011649
ILMN_1792681	CCDC86	1.009792	10.89798	2.34E-05	0.007263
ILMN_1803408	KRT18	1.018243	9.365723	1.70E-06	0.001631
ILMN_1651936	SETD8	1.052161	8.542859	4.13E-11	8.73E-07
ILMN_1660793	PAQR4	1.086005	9.42754	2.41E-05	0.007374
ILMN_1663390	CDC20	1.102881	12.87905	0.000811	0.047106
ILMN_2041222	KRT18P55	1.221556	11.56213	7.86E-05	0.012768
ILMN_1753584	KRT8	1.274144	10.65308	1.04E-05	0.005252
ILMN_1669210	SNORD16	1.519279	9.861519	5.70E-10	4.01E-06

7.3. Pathways analysis of the microarray data using Database for Annotation, Visualisation and Integrated Discovery (DAVID), v6.7
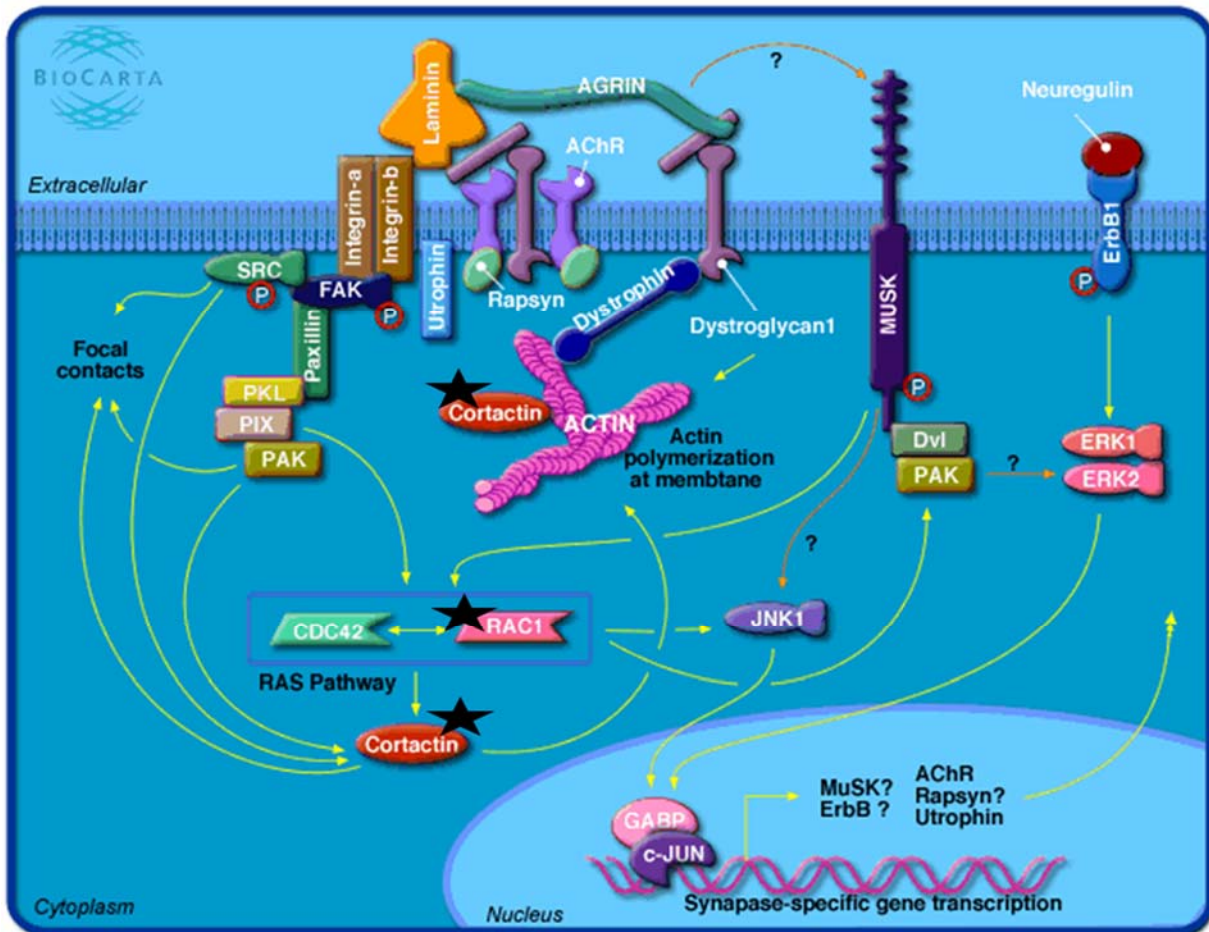
Figure 7-4 Agrin in postsynaptic differentiation pathway. Genes included in the microarray data labelled by stars. Database for Annotation, Visualisation and Integrated Discovery (DAVID), v6.7 was used to analyse large gene lists and perform comprehensive clustering to outline genes with a similar function or biological theme. KEGG pathway analysis on steroid biosynthesis was included in the DAVID output.
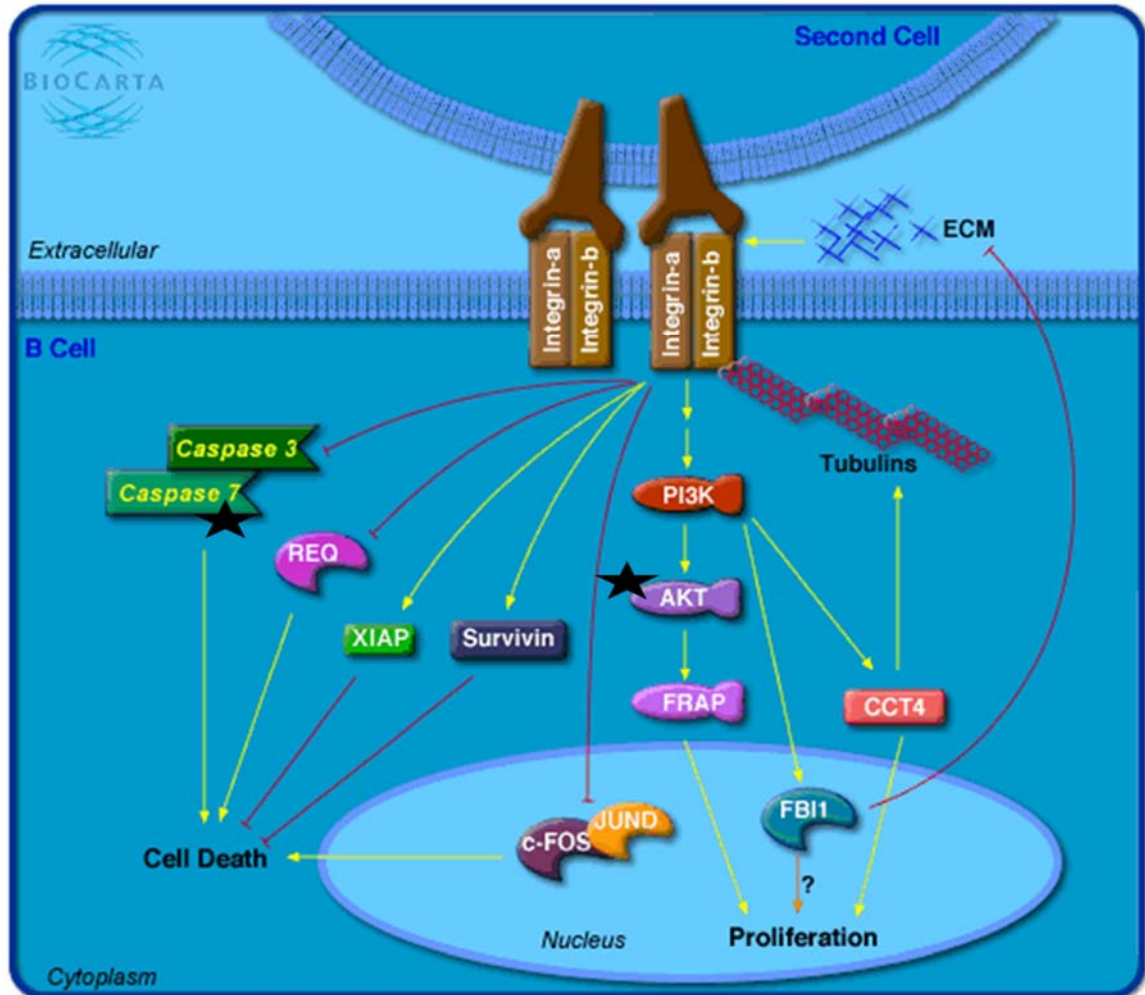
Figure 7-5 B cell survival pathway. Genes included in the microarray data labelled by stars. Database for Annotation, Visualisation and Integrated Discovery (DAVID), v6.7 was used to analyse large gene lists and perform comprehensive clustering to outline genes with a similar function or biological theme. KEGG pathway analysis on steroid biosynthesis was included in the DAVID output.
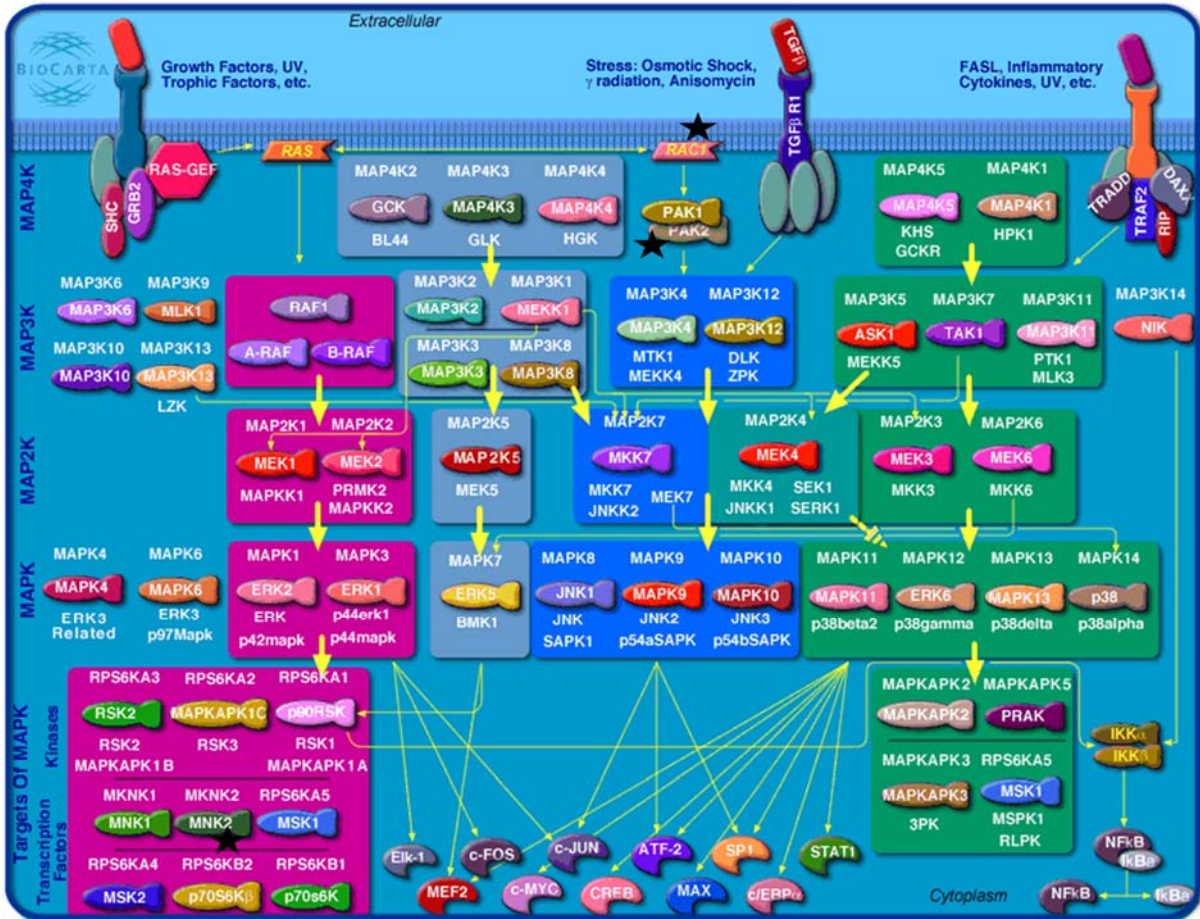
Figure 7-6 MAPKinase signalling pathway. Genes included in the microarray data labelled by stars. Database for Annotation, Visualisation and Integrated Discovery (DAVID), v6.7 was used to analyse large gene lists and perform comprehensive clustering to outline genes with a similar function or biological theme. KEGG pathway analysis on steroid biosynthesis was included in the DAVID output.
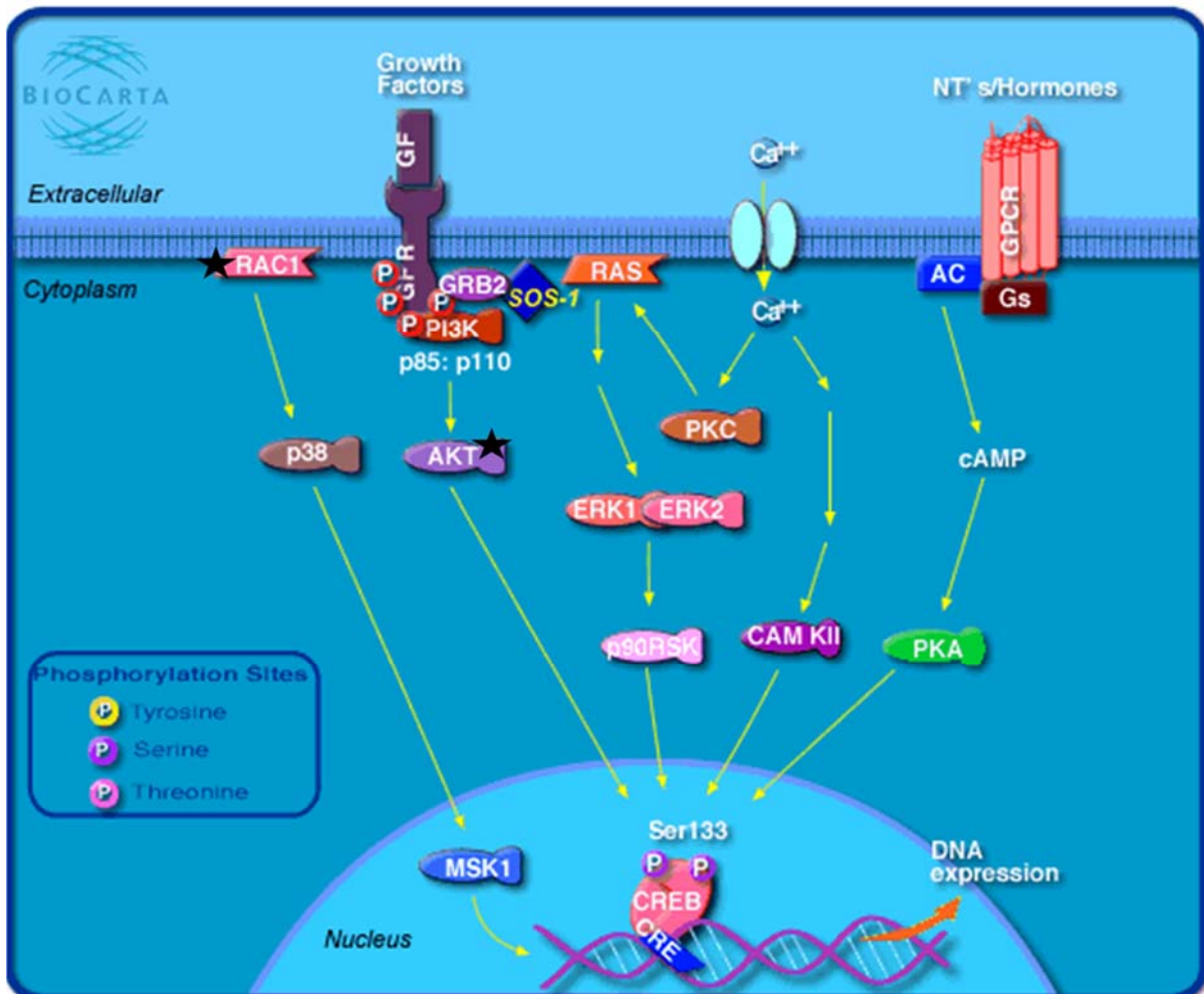
Figure 7-7 Transcription factor CREB and its extracellular signal pathway. Genes included in the microarray data labelled by stars. Database for Annotation, Visualisation and Integrated Discovery (DAVID), v6.7 was used to analyse large gene lists and perform comprehensive clustering to outline genes with a similar function or biological theme. KEGG pathway analysis on steroid biosynthesis was included in the DAVID output.
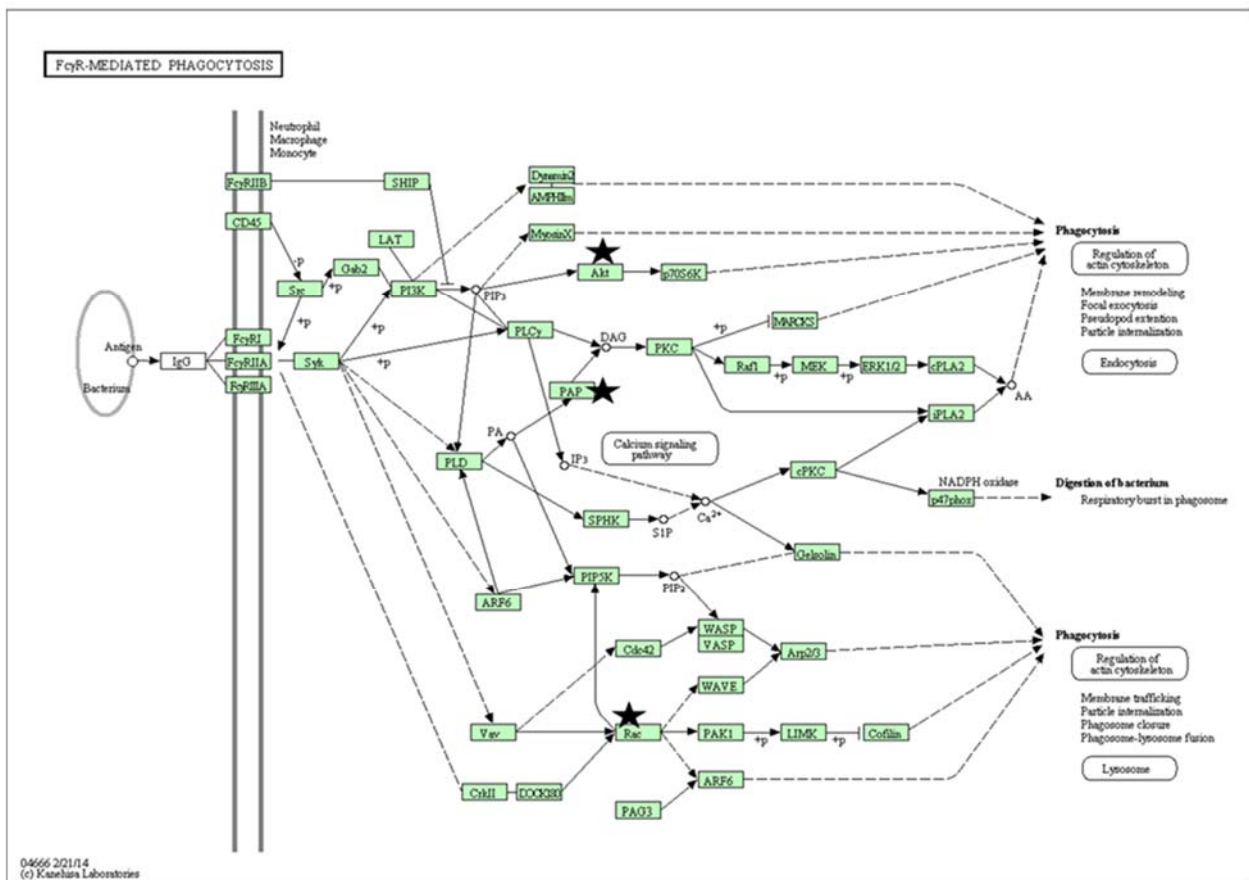
Figure 7-8 Fc gamma R-mediated phagocytosis pathway. Genes included in the microarray data labelled by stars. Database for Annotation, Visualisation and Integrated Discovery (DAVID), v6.7 was used to analyse large gene lists and perform comprehensive clustering to outline genes with a similar function or biological theme. KEGG pathway analysis on steroid biosynthesis was included in DAVIDoutput.
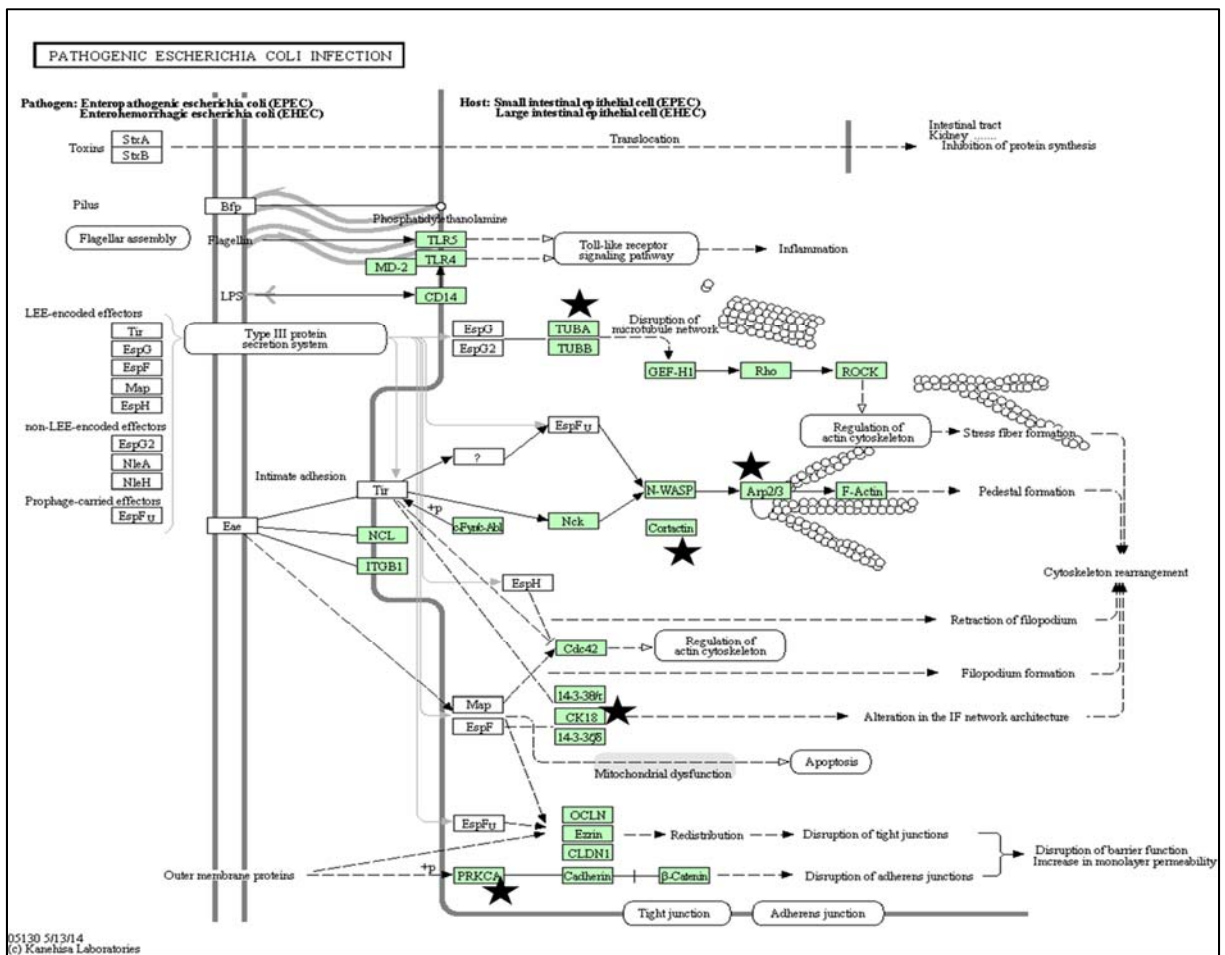
Figure 7-9 Pathogenic Escherichia coli infection pathway. Genes included in the microarray data labelled by stars. Database for Annotation, Visualisation and Integrated Discovery (DAVID), v6.7 was used to analyse large gene lists and perform comprehensive clustering to outline genes with a similar function or biological theme. KEGG pathway analysis on steroid biosynthesis was included in the DAVID output.

References

Abate-Shen, C. and Shen, M.M. (2000) 'Molecular genetics of prostate cancer', *Genes & development*, 14(19), pp. 2410-2434.

Abbas, T., Shibata, E., Park, J., Jha, S., Karnani, N. and Dutta, A. (2010a) 'CRL4 Cdt2 regulates cell proliferation and histone gene expression by targeting PR-Set7/Set8 for degradation', *Molecular cell*, 40(1), pp. 9-21.

Agalliu, I., Wang, Z., Wang, T., Dunn, A., Parikh, H., Myers, T., Burk, R.D. and Amundadottir, L. (2013) 'Characterization of SNPs associated with prostate cancer in men of Ashkenazic descent from the set of GWAS identified SNPs: impact of cancer family history and cumulative SNP risk prediction', *PloS one*, 8(4), pp. 1-11

Agoulnik, I.U., Vaid, A., Nakka, M., Alvarado, M., Bingman, W.E., Erdem, H., Frolov, A., Smith, C.L., Ayala, G.E., Ittmann, M.M. and Weigel, N.L. (2006) 'Androgens Modulate Expression of Transcription Intermediary Factor 2, an Androgen Receptor Coactivator whose Expression Level Correlates with Early Biochemical Recurrence in Prostate Cancer', *Cancer Research*, 66(21), pp. 10594-10602.

Andersen, R.J., Mawji, N.R., Wang, J., Wang, G., Haile, S., Myung, J.-K., Watt, K., Tam, T., Yang, Y.C., Bañuelos, C.A., Williams, D.E., McEwan, I.J., Wang, Y. and Sadar, M.D. (2010) 'Regression of Castrate-Recurrent Prostate Cancer by a Small-Molecule Inhibitor of the Amino-Terminus Domain of the Androgen Receptor', *Cancer Cell*, 17(6), pp. 535-546.

Antonarakis, E.S., Lu, C., Wang, H., Luber, B., Nakazawa, M., Roeser, J.C., Chen, Y., Mohammad, T.A., Chen, Y. and Fedor, H.L. (2014) 'AR-V7 and resistance to enzalutamide and abiraterone in prostate cancer', *New England Journal of Medicine*, 371(11), pp. 1028-1038.

Arora, Vivek K., Schenkein, E., Murali, R., Subudhi, Sumit K., Wongvipat, J., Balbas, Minna D., Shah, N., Cai, L., Efstathiou, E., Logothetis, C., Zheng, D. and Sawyers, Charles L. (2013) 'Glucocorticoid Receptor Confers Resistance to Antiandrogens by Bypassing Androgen Receptor Blockade', *Cell*, 155(6), pp. 1309-1322.

Attard, G., Reid, A.H.M., Olmos, D. and de Bono, J.S. (2009) 'Antitumor Activity with CYP17 Blockade Indicates That Castration-Resistant Prostate Cancer Frequently Remains Hormone Driven', *Cancer Research*, 69(12), pp. 4937-4940.

Ayala, A.G. and Ro, J.Y. (2007) 'Prostatic intraepithelial neoplasia: recent advances', *Archives of pathology & laboratory medicine*, 131(8), pp. 1257-1266.

Balakrishnan, L. and Milavetz, B. (2010) 'Decoding the histone H4 lysine 20 methylation mark', *Critical Reviews in Biochemistry and Molecular Biology*, 45(5), pp. 440-452.

Balk, S.P. and Knudsen, K.E. (2008) 'AR, the cell cycle, and prostate cancer', *Nucl Recept Signal*, 6(10), pp. 1621-1633.

Banerjee, T., Nath, S. and Roychoudhury, S. (2009) 'DNA damage induced p53 downregulates Cdc20 by direct binding to its promoter causing chromatin remodeling', *Nucleic Acids Research*, 37(8), pp. 2688-2698.

Barsotti, A.M. and Prives, C. (2009) 'Pro-proliferative FoxM1 is a target of p53-mediated repression', *Oncogene*, 28(48), pp. 4295-4305.

Bechis, S.K., Otsetov, A.G., Ge, R. and Olumi, A.F. (2014) 'Personalized Medicine for the Management of Benign Prostatic Hyperplasia', *The Journal of Urology*, 192(1), pp. 16-23.

Beck, D.B., Hisanobu,O.,Steven,S. S., Danny,R. (2012) 'PR-Set7 and H4K20me1: at the crossroads of genome integrity, cell cycle, chromosome condensation, and transcription', *Genes & Development*, 26(4), pp. 325-337.

Beck, D.B., Oda, H., Shen, S.S. and Reinberg, D. (2012) 'PR-Set7 and H4K20me1: at the crossroads of genome integrity, cell cycle, chromosome condensation, and transcription', *Genes Dev*, 26(4), pp. 325-37.

Beisel, C., Imhof, A., Greene, J., Kremmer, E. and Sauer, F. (2002) 'Histone methylation by the Drosophila epigenetic transcriptional regulator Ash1', *Nature*, 419(6909), pp. 857-862.

Benninghoff (1988) 'Anatomy of the Renal Pelvis and Ureter.'.
Bill-Axelson, A., Holmberg, L., Garmo, H., Rider, J.R., Taari, K., Busch, C., Nordling, S., Häggman, M., Andersson, S.-O., Spångberg, A., Andrén, O., Palmgren, J., Steineck, G., Adami, H.-O. and Johansson, J.-E. (2014) 'Radical Prostatectomy or Watchful Waiting in Early Prostate Cancer', *New England Journal of Medicine*, 370(10), pp. 932-942.

Blum, G., Ibáñez, G., Rao, X., Shum, D., Radu, C., Djaballah, H., Rice, J.C. and Luo, M. (2014) 'Small-Molecule Inhibitors of SETD8 with Cellular Activity', *ACS Chemical Biology*, 9(11), pp. 2471-2478.

Brown, M. and Wittwer, C. (2000) 'Flow cytometry: principles and clinical applications in hematology', *Clinical chemistry*, 46(8), pp. 1221-1229.

Brustel, J., Tardat, M., Kirsh, O., Grimaud, C. and Julien, E. (2011) 'Coupling mitosis to DNA replication: the emerging role of the histone H4-lysine 20 methyltransferase PR-Set7', *Trends in cell biology*, 21(8), pp. 452-460.

Calvo, F., Ranftl, R., Hooper, S., Farrugia, A.J., Moeendarbary, E., Bruckbauer, A., Batista, F., Charras, G. and Sahai, E. (2015) 'Cdc42EP3/BORG2 and Septin Network Enables Mechano-transduction and the Emergence of Cancer-Associated Fibroblasts', *Cell reports*, 13(12), pp. 2699-2714.

Catalona, W.J., Southwick, P.C., Slawin, K.M., Partin, A.W., Brawer, M.K., Flanigan, R.C., Patel, A., Richie, J.P., Walsh, P.C. and Scardino, P.T. (2000) 'Comparison of percent free PSA, PSA density, and age-specific PSA cutoffs for prostate cancer detection and staging', *Urology*, 56(2), pp. 255-260.

Cavero, L. (2016) 'Effects of Resveratrol on Regulation of ARV7 Protein Levels in Prostate Cancer'.

Centore, R.C., Havens, C.G., Manning, A.L., Li, J.M., Flynn, R.L., Tse, A., Jin, J., Dyson, N.J., Walter, J.C. and Zou, L. (2010) 'CRL4Cdt2-mediated destruction of the histone methyltransferase Set8 prevents premature chromatin compaction in S phase', *Molecular Cell*, 40(1), pp. 22-33.

Cheng, H.H., Gulati, R., Azad, A., Nadal, R., Twardowski, P., Vaishampayan, U.N., Agarwal, N., Heath, E.I., Pal, S.K. and Rehman, H.T. (2015) 'Activity of enzalutamide in men with metastatic castration-resistant prostate cancer is affected by prior treatment with abiraterone and/or docetaxel', *Prostate cancer and prostatic diseases*, 18(2), pp. 122-127.

Choudhury, A.D., Schinzel, A.C., Cotter, M.B., Lis, R.T., Labella, K., Lock, Y.J., Izzo, F., Guney, I., Bowden, M. and Li, Y.Y. (2016) 'Castration resistance in prostate cancer is mediated by the kinase NEK6', *Cancer Research*, pp. 0455-5472.

Chung, E. and Chen, R.-H. (2003) 'Phosphorylation of Cdc20 is required for its inhibition by the spindle checkpoint', *Nature cell biology*, 5(8), pp. 748-753.

Coffey, K. and Robson, C.N. (2012) 'Regulation of the androgen receptor by post-translational modifications', *Journal of Endocrinology*, 215(2), pp. 221-237.

Congdon, L.M., Houston, S.I., Veerappan, C.S., Spektor, T.M. and Rice, J.C. (2010) 'PR-Set7-mediated monomethylation of histone H4 lysine 20 at specific genomic regions induces transcriptional repression', *Journal of Cellular Biochemistry*, 110(3), pp. 609-619.

Couture, J.F., Collazo, E., Brunzelle, J.S. and Trievel, R.C. (2005) 'Structural and functional analysis of SET8, a histone H4 Lys-20 methyltransferase', *Genes and Development*, 19(12), pp. 1455-1465.

Dai, B., Gong, A., Jing, Z., Aldape, K.D., Kang, S.-H., Sawaya, R. and Huang, S. (2013) 'Forkhead box M1 is regulated by heat shock factor 1 and promotes glioma cells survival under heat shock stress', *Journal of Biological Chemistry*, 288(3), pp. 1634-1642.

Dai, C. and Gu, W. (2010) 'p53 post-translational modification: deregulated in tumorigenesis', *Trends in molecular medicine*, 16(11), pp. 528-536.

Dhami, G., Liu, H., Galka, M., Voss, C., Wei, R., Muranko, K., Kaneko, T., Cregan, S., Li, L. and Li, S.C. (2013) 'Dynamic Methylation of Numb by Set8 Regulates Its Binding to p53 and Apoptosis', *Molecular Cell*, 50(4), pp. 565-576.

Dulev, S., Tkach, J., Lin, S. and Batada, N.N. (2014) 'SET8 methyltransferase activity during the DNA double-strand break response is required for recruitment of 53BP1', *EMBO reports*, 15(11), pp. 1163-1174.

El-Amm, J., Nihar Patel1, Ashley Freeman2 and Jeanny B. Aragon-Ching : (2013) '"Metastatic Castration-Resistant Prostate Cancer: Critical Review of Enzalutamide." *Clinical Medicine Insights*. pp. 235-245.

Elowe, S. (2011) 'Bub1 and BubR1: at the interface between chromosome attachment and the spindle checkpoint', *Molecular and cellular biology*, 31(15), pp. 3085-3093.

Epstein, J.I., Zelefsky, M.J., Sjoberg, D.D., Nelson, J.B., Egevad, L., Magi-Galluzzi, C., Vickers, A.J., Parwani, A.V., Reuter, V.E., Fine, S.W., Eastham, J.A., Wiklund, P., Han, M.,

Reddy, C.A., Ciezki, J.P., Nyberg, T. and Klein, E.A. (2016) 'A Contemporary Prostate Cancer Grading System: A Validated Alternative to the Gleason Score', *European Urology*, 69(3), pp. 428-435.

Fang, G. (2002) 'Checkpoint protein BubR1 acts synergistically with Mad2 to inhibit anaphase-promoting complex', *Molecular biology of the cell*, 13(3), pp. 755-766.

Fang, G., Yu, H. and Kirschner, M.W. (1998) 'Direct binding of CDC20 protein family members activates the anaphase-promoting complex in mitosis and G1', *Molecular cell*, 2(2), pp. 163-171.

Fang, H., Tong, W., Branham, W.S., Moland, C.L., Dial, S.L., Hong, H., Xie, Q., Perkins, R., Owens, W. and Sheehan, D.M., 2003. Study of 202 natural, synthetic, and environmental chemicals for binding to the androgen receptor. *Chemical research in toxicology,* 16(10), pp.1338-1358.

Fang, J., Feng, Q., Ketel, C.S., Wang, H., Cao, R., Xia, L., Erdjument-Bromage, H., Tempst, P., Simon, J.A. and Zhang, Y. (2002) 'Purification and Functional Characterization of SET8, a Nucleosomal Histone H4-Lysine 20-Specific Methyltransferase', *Current Biology*, 12(13), pp. 1086-1099.

Feldman, B.J. and Feldman, D. (2001) 'The development of androgen-independent prostate cancer', *Nat Rev Cancer*, 1(1), pp. 34-45.

Ferraldeschi, R., Welti, J., Luo, J., Attard, G. and de Bono, J.S. (2015) 'Targeting the androgen receptor pathway in castration-resistant prostate cancer: progresses and prospects', *Oncogene*, 34(14), pp. 1745-1757.

Foster, C.S. (2000) 'Pathology of benign prostatic hyperplasia', *The Prostate*, 45(S9), pp. 4-14.

Fu, M., Rao, M., Wang, C., Sakamaki, T., Wang, J., Di Vizio, D., Zhang, X., Albanese, C., Balk, S., Chang, C., Fan, S., Rosen, E., Palvimo, J.J., Jänne, O.A., Muratoglu, S., Avantaggiati, M.L. and Pestell, R.G. (2003) 'Acetylation of Androgen Receptor Enhances Coactivator Binding and Promotes Prostate Cancer Cell Growth', *Molecular and Cellular Biology*, 23(23), pp. 8563-8575.

Gabrovska, P.N., Smith, R.A., Tiang, T., Weinstein, S.R., Haupt, L.M. and Griffiths, L.R. (2012) 'Development of an eight gene expression profile implicating human breast tumours of all grade', *Molecular biology reports*, 39(4), pp. 3879-3892.

Gaughan, L., Stockley, J., Wang, N., McCracken, S.R.C., Treumann, A., Armstrong, K., Shaheen, F., Watt, K., McEwan, I.J., Wang, C., Pestell, R.G. and Robson, C.N. (2011) 'Regulation of the androgen receptor by SET9-mediated methylation', *Nucleic Acids Research*, 39(4), pp. 1266-1279.

Gelmann, E.P., 2002. Molecular biology of the androgen receptor. *Journal of Clinical Oncology,* 20(13), pp.3001-3015.

Georgi, A.B., Stukenberg, P.T. and Kirschner, M.W. (2002) 'Timing of Events in Mitosis', *Current Biology*, 12(2), pp. 105-114.

Gilligan, T. and Kantoff, P.W. (2002) 'Chemotherapy for prostate cancer', *Urology*, 60(3, Supplement 1), pp. 94-100.

Gioeli, D. and Paschal, B.M. (2012) 'Post-translational modification of the androgen receptor', *Molecular and Cellular Endocrinology*, 352(1–2), pp. 70-78.

Godtman, R.A., Holmberg, E., Lilja, H., Stranne, J. and Hugosson, J. (2015) 'Opportunistic testing versus organized prostate-specific antigen screening: outcome after 18 years in the Göteborg randomized population-based prostate cancer screening trial', *European Urology*, 68(3), pp. 354-360.

Gregory, C.W., He, B., Johnson, R.T., Ford, O.H., Mohler, J.L., French, F.S. and Wilson, E.M. (2001) 'A mechanism for androgen receptor-mediated prostate cancer recurrence after androgen deprivation therapy', *Cancer research*, 61(11), pp. 4315-4319.

Guo, Z. and Qiu, Y. (2011) 'A New Trick of an Old Molecule: Androgen Receptor Splice Variants Taking the Stage?!', *International Journal of Biological Sciences*, 7(6), pp. 815-822.

Guowei, F. (2002) 'Checkpoint protein BubR1 acts synergistically with Mad2 to inhibit anaphase-promoting complex', *Molecular biology of the cell*, 13(3), pp. 755-766.

Hamdy, F.C., Donovan, J.L., Lane, J.A., Mason, M., Metcalfe, C., Holding, P., Davis, M., Peters, T.J., Turner, E.L. and Martin, R.M. (2016) '10-Year Outcomes after Monitoring, Surgery, or Radiotherapy for Localized Prostate Cancer', *New England Journal of Medicine*.375(15), pp.1415-1424

Heemers, H.V. and Tindall, D.J. (2007) 'Androgen Receptor (AR) Coregulators: A Diversity of Functions Converging on and Regulating the AR Transcriptional Complex', *Endocrine Reviews*, 28(7), pp. 778-808.

Henry, R.Y. and O'Mahony, D. (1999) 'Treatment of prostate cancer', *Journal of Clinical Pharmacy and Therapeutics*, 24(2), pp. 93-102.

Hou, L., Li, Q., Yu, Y., Li, M. and Zhang, D. (2016) 'SET8 induces epithelial⬚mesenchymal transition and enhances prostate cancer cell metastasis by cooperating with ZEB1', *Molecular medicine reports*, 13(2), pp. 1681-1688.

Houston, S.I., McManus, K.J., Adams, M.M., Sims, J.K., Carpenter, P.B., Hendzel, M.J. and Rice, J.C. (2008) 'Catalytic function of the PR-Set7 histone H4 lysine 20 monomethyltransferase is essential for mitotic entry and genomic stability', *Journal of Biological Chemistry*, 283(28), pp. 19478-19488.

http://www.google.co.uk/url?sa=i&rct=j&q=&esrc=s&source=images&cd=&cad=rja&uact=8
&ved=0ahUKEwjMrPC80L_SAhWK8RQKHan6Ay0QjB0IBg&url=http%3A%2F%2Fwww.
sciencephoto.com%2Fmedia%2F129774%2Fview&psig=AFQjCNEJJFDww5-
1MWIGhqxGfQ1EwJ1oRQ&ust=1488812368766994.

http://www.google.co.uk/url?sa=i&rct=j&q=&esrc=s&source=images&cd=&cad=rja&uact=8
&ved=0ahUKEwian6u80b_SAhUFbxQKHY0GAjUQjB0IBg&url=http%3A%2F%2Flibrary.
med.utah.edu%2FWebPath%2FMALEHTML%2FMALE116.html&bvm=bv.148747831,d.Z
Gg&psig=AFQjCNEHeaVcmAoBIRe69gg7BZSm0dkkoA&ust=1488812641360467.

http://www.google.co.uk/url?sa=i&rct=j&q=&esrc=s&source=images&cd=&cad=rja&uact=8&ved=0ahUKEwjXx4SV07_SAhVDnRQKHWgXCMAQjB0IBg&url=http%3A%2F%2Fwww.proteinatlas.org%2Flearn%2Fdictionary%2Fcancer%2Fprostate%2Bcancer%2B3&bvm=bv.148747831,d.ZGg&psig=AFQjCNEwU4jEm6gk7qp4kRnA8LLwNGesYw&ust=148881310 3355946

http://www.google.co.uk/url?sa=i&rct=j&q=&esrc=s&source=images&cd=&cad=rja&uact=8&ved=0ahUKEwi7y_fiod3SAhVPHRQKHXRVBaoQjB0IBg&url=http%3A%2F%2Fwww.medscape.org%2Fviewarticle%2F444817_2&psig=AFQjCNHH0ocF7Sv0ano5_7PktqN7x19 Dyw&ust=1489830629650795

Hu, R., Dunn, T.A., Wei, S., Isharwal, S., Veltri, R.W., Humphreys, E., Han, M., Partin, A.W., Vessella, R.L., Isaacs, W.B., Bova, G.S. and Luo, J. (2009) 'Ligand-independent Androgen Receptor Variants Derived from Splicing of Cryptic Exons Signify Hormone Refractory Prostate Cancer', *Cancer research*, 69(1), pp. 16-22.

Huang, H.-C., Shi, J., Orth, J.D. and Mitchison, T.J. (2009) 'Evidence that Mitotic Exit Is a Better Cancer Therapeutic Target Than Spindle Assembly', *Cancer Cell*, 16(4), pp. 347-358.

Huang, J., Dorsey, J., Chuikov, S., Zhang, X., Jenuwein, T., Reinberg, D. and Berger, S.L. (2010) 'G9a and Glp methylate lysine 373 in the tumor suppressor p53', *Journal of Biological Chemistry*, 285(13), pp. 9636-9641.

Hui, C. and Ye, T. (2015) 'Synthesis of lysine methyltransferase inhibitors', *Frontiers in chemistry*, 3, 44.

Hussain, M., Tangen, C.M., Berry, D.L., Higano, C.S., Crawford, E.D., Liu, G., Wilding, G., Prescott, S., Kanaga Sundaram, S. and Small, E.J. (2013) 'Intermittent versus continuous androgen deprivation in prostate cancer', *New England Journal of Medicine*, 368(14), pp. 1314-1325.

Izawa, D. and Pines, J. (2015) 'The mitotic checkpoint complex binds a second CDC20 to inhibit active APC/C', *Nature*, 517(7536), pp. 631-634.

Jørgensen, S., Elvers, I., Trelle, M.B., Menzel, T., Eskildsen, M., Jensen, O.N., Helleday, T., Helin, K. and Sørensen, C.S. (2007) 'The histone methyltransferase SET8 is required for S-phase progression', *Journal of Cell Biology*, 179(7), pp. 1337-1345.

Jørgensen, S., Schotta, G. and Sørensen, C.S. (2013) 'Histone H4 Lysine 20 methylation: Key player in epigenetic regulation of genomic integrity', *Nucleic Acids Research*, 41(5), pp. 2797-2806.

Josson, S., Matsuoka, Y., Chung, L.W.K., Zhau, H.E. and Wang, R. (2010) *Seminars in cell & developmental biology*.Vol.21, No.1,pp.26-32.

Kachhap, S.K., Faith, D., Qian, D.Z., Shabbeer, S., Galloway, N.L., Pili, R., Denmeade, S.R., DeMarzo, A.M. and Carducci, M.A. (2007) 'The N-Myc down regulated Gene1 (NDRG1) Is a Rab4a effector involved in vesicular recycling of E-cadherin', *PloS one*, 2(9), pp.1-11..

Kalluri, R. and Weinberg, R.A. (2009) 'The basics of epithelial-mesenchymal transition', *The Journal of Clinical Investigation*, 119(6), pp. 1420-1428.

Kamide, K., Asayama, K., Katsuya, T., Ohkubo, T., Hirose, T., Inoue, R., Metoki, H., Kikuya, M., Obara, T. and Hanada, H. (2013) 'Genome-wide response to antihypertensive medication using home blood pressure measurements: a pilot study nested within the HOMED-BP study', *Pharmacogenomics*, 14(14), pp. 1709-1721.

Kapoor-Vazirani, P. and Vertino, P.M. (2014) 'A dual role for the histone methyltransferase PR-SET7/SETD8 and histone H4 lysine 20 monomethylation in the local regulation of RNA polymerase II pausing', *Journal of Biological Chemistry*, 289(11), pp. 7425-7437.

Kari, V., Karpiuk, O., Tieg, B., Kriegs, M., Dikomey, E., Krebber, H., Begus-Nahrmann, Y. and Johnsen, S.A. (2013) 'A subset of histone H2B genes produces polyadenylated mRNAs under a variety of cellular conditions', *PloS one*, 8(5), pp.1-12.

Kevei, Z., Baloban, M., Da Ines, O., Tiricz, H., Kroll, A., Regulski, K., Mergaert, P. and Kondorosi, E. (2011) 'Conserved CDC20 cell cycle functions are carried out by two of the five isoforms in Arabidopsis thaliana', *PLoS One*, 6(6), pp.1-15.

Kidokoro, T., Tanikawa, C., Furukawa, Y., Katagiri, T., Nakamura, Y. and Matsuda, K. (2008) 'CDC20, a potential cancer therapeutic target, is negatively regulated by p53', *Oncogene*, 27(11), pp. 1562-1571.

Kim, H.L. and Yang, X.J., 2002. Prevalence of high-grade prostatic intraepithelial neoplasia and its relationship to serum prostate specific antigen. *Int Braz J Urol*, 28(5), pp.413-6.

Ko, S., Ahn, J., Song, C.S., Kim, S., Knapczyk-Stwora, K. and Chatterjee, B. (2011) 'Lysine methylation and functional modulation of androgen receptor by Set9 methyltransferase', *Molecular endocrinology*, 25(3), pp. 433-444.

Koochekpour, S. (2010) 'Androgen receptor signaling and mutations in prostate cancer', *Asian Journal of Andrology*, 12(5), pp. 639-657.

Kounatidou, E.E. and Gaughan, L. (2016) 'Investigating the role of SUMOylation of androgen receptor splice variants by SUMO1 in castration resistant prostate cancer'.
Koutros, S., Beane Freeman, L.E., Lubin, J.H., Heltshe, S.L., Andreotti, G., Barry, K.H., Dellavalle, C.T., Hoppin, J.A., Sandler, D.P., Lynch, C.F., Blair, A. and Alavanja, M.C.R. (2013) 'Risk of total and aggressive prostate cancer and pesticide use in the Agricultural Health Study', *American Journal of Epidemiology*, 177(1), pp. 59-74.

Kouzarides, T. (2007) 'Chromatin modifications and their function', *Cell*, 128(4), pp. 693-705.

Kristal, A.R., Arnold, K.B., Neuhouser, M.L., Goodman, P., Platz, E.A., Albanes, D. and Thompson, I.M. (2010) 'Diet, supplement use, and prostate cancer risk: results from the prostate cancer prevention trial', *American journal of epidemiology*, 172(5), pp. 566-577.

Kubbutat, M.H.G., Jones, S.N. and Vousden, K.H. (1997) 'Regulation of p53 stability by Mdm2', *Nature*, 387(6630), pp. 299-303.

Kumar, R., Le, Y., Deweese, T. and Song, D.Y. (2016) 'Re-implantation following suboptimal dosimetry in low-dose-rate prostate brachytherapy: technique for outpatient source insertion using local anesthesia', *Journal of Radiation Oncology*, 5(1), pp. 103-108.

Kumar, V. and Anderson, J. (2002) 'Prostate Cancer', *Surgery (Oxford)*, 20(12), pp. 297-300.
Lee, J. and Zhou, P. (2010) 'SETting the Clock for Histone H4 Monomethylation', *Molecular Cell*, 40(3), pp. 345-346.

Li, J. and Al-Azzawi, F. (2009) 'Mechanism of androgen receptor action', *Maturitas*, 63(2), pp. 142-148.

Li, Y., Sun, L., Zhang, Y., Wang, D., Wang, F., Liang, J., Gui, B. and Shang, Y. (2011a) 'The Histone Modifications Governing TFF1 Transcription Mediated by Estrogen Receptor', *Journal of Biological Chemistry*, 286(16), pp. 13925-13936.

Li, Z., Nie, F., Wang, S. and Li, L. (2011b) 'Histone H4 Lys 20 monomethylation by histone methylase SET8 mediates Wnt target gene activation', *Proceedings of the National Academy of Sciences*, 108(8), pp. 3116-3123.

Lilach, A., Itai, K., Tova, W., Raphael, M.P., Anat, B.-S., Avi, O.-U., Eytan, D. and Zelig, E. (2013) 'Gene Expression Profiles Predict Sensitivity of Prostate Cancer to Radiotherapy', *Journal of Cancer Therapy*, Vol.04No.04, pp. 11-26.

Liu, Y., Gong, Z., Sun, L. and Li, X. (2014) 'FOXM1 and androgen receptor co-regulate CDC6 gene transcription and DNA replication in prostate cancer cells', *Biochimica et Biophysica Acta (BBA) - Gene Regulatory Mechanisms*, 1839(4), pp. 297-305.

Lonergan, P. and Tindall, D. (2011) 'Androgen receptor signaling in prostate cancer development and progression', *Journal of Carcinogenesis*, 10(1), pp. 10-20.

Lu, N.Z., Wardell, S.E., Burnstein, K.L., Defranco, D., Fuller, P.J., Giguere, V., Hochberg, R.B., McKay, L., Renoir, J.-M., Weigel, N.L., Wilson, E.M., McDonnell, D.P. and Cidlowski, J.A. (2006) 'International Union of Pharmacology. LXV. The Pharmacology and Classification of the Nuclear Receptor Superfamily: Glucocorticoid, Mineralocorticoid, Progesterone, and Androgen Receptors', *Pharmacological Reviews*, 58(4), pp. 782-797.

Ma, A., Yu, W., Li, F., Bleich, R.M., Herold, J.M., Butler, K.V., Norris, J.L., Korboukh, V., Tripathy, A. and Janzen, W.P. (2014a) 'Discovery of a selective, substrate-competitive inhibitor of the lysine methyltransferase SETD8', *Journal of medicinal chemistry*, 57(15), pp. 6822-6833.

Ma, A., Yu, W., Xiong, Y., Butler, K.V., Brown, P.J. and Jin, J. (2014c) 'Structure–activity relationship studies of SETD8 inhibitors', *MedChemComm*,5(12),1892-1898.

Manchado, E., Guillamot, M., de Cárcer, G., Eguren, M., Trickey, M., García-Higuera, I., Moreno, S., Yamano, H., Cañamero, M. and Malumbres, M. (2010) 'Targeting mitotic exit leads to tumor regression in vivo: Modulation by Cdk1, Mastl, and the PP2A/B55α, δ phosphatase', *Cancer cell*, 18(6), pp. 641-654.

Marouco, D., Garabadgiu, A.V., Melino, G. and Barlev, N.A. (2013) 'Lysine-specific modifications of p53: a matter of life and death?', *Oncotarget*, 4(10), p. 1556.

McAllister, M.J., McCall, P., Underwood, M.A., Leung, H.Y. and Edwards, J. (2016) 'Combined AR phosphorylation at serine 81 and serine 213 are associated with decreased survival in Castrate Resistant Prostate Cancer'.

McLaughlin, P.W., Troyer, S., Berri, S., Narayana, V., Meirowitz, A., Roberson, P.L. and Montie, J. (2005) 'Functional anatomy of the prostate: implications for treatment planning', *International Journal of Radiation Oncology* Biology* Physics*, 63(2), pp. 479-491.

McNeal, J.E. (2006b) ' Mills S Prostate, ' *Lippincott Williams & Wilkins, Philadelphia*, 3rd edn.

McNeal, J.E. and Bostwick, D.G. (1986) 'Intraductal dysplasia: a premalignant lesion of the prostate', *Human pathology*, 17(1), pp. 64-71.

Mendiratta, P., Mostaghel, E., Guinney, J., Tewari, A.K., Porrello, A., Barry, W.T., Nelson, P.S. and Febbo, P.G. (2009) 'Genomic strategy for targeting therapy in castration-resistant prostate cancer', *Journal of Clinical Oncology*, 27(12), pp. 2022-2029.

Milite, C., Feoli, A., Viviano, M., Rescigno, D., Mai, A., Castellano, S. and Sbardella, G. (2016) 'Progress in the Development of Lysine Methyltransferase SETD8 Inhibitors', *ChemMedChem*.11(16).pp. 1680-1685.

Mitsiades, N. (2013) 'A road map to comprehensive androgen receptor axis targeting for castration-resistant prostate cancer', *Cancer Research*, 73(15), pp. 4599-4605.
Munkley, J., Vodak, D., Livermore, K.E., James, K., Wilson, B.T., Knight, B., McCullagh, P., McGrath, J., Crundwell, M. and Harries, L.W. (2016) 'Glycosylation is an androgen-regulated process essential for prostate cancer cell viability', *EBioMedicine .pp-103-116.*

Nath, S., Chowdhury, A., Dey, S., Roychoudhury, A., Ganguly, A., Bhattacharyya, D. and Roychoudhury, S. (2015) 'Deregulation of Rb-E2F1 axis causes chromosomal instability by engaging the transactivation function of Cdc20–anaphase-promoting complex/cyclosome', *Molecular and cellular biology*, 35(2), pp. 356-369.

Oda, H., Hübner, M.R., Beck, D.B., Vermeulen, M., Hurwitz, J., Spector, D.L. and Reinberg, D. (2010) 'Regulation of the histone H4 monomethylase PR-Set7 by CRL4 Cdt2-mediated PCNA-dependent degradation during DNA damage', *Molecular cell*, 40(3), pp. 364-376.

Oda, H., Okamoto, I., Murphy, N., Chu, J., Price, S.M., Shen, M.M., Torres-Padilla, M.E., Heard, E. and Reinberg, D. (2009) 'Monomethylation of histone H4-lysine 20 is involved in chromosome structure and stability and is essential for mouse development', *Molecular and cellular biology*, 29(8), pp. 2278-2295.

Palmberg, C., Koivisto, P., Kakkola, L., Tammela, T.L.J., Kallioniemi, O.P. and Visakorpi, T. (2000) 'Androgen receptor gene amplification at primary progression predicts response to combined androgen blockade as second line therapy for advanced prostate cancer', *The Journal of urology*, 164(6), pp. 1992-1995.

Pannetier, M., Julien, E., Schotta, G., Tardat, M., Sardet, C., Jenuwein, T. and Feil, R. (2008) 'PR-SET7 and SUV4-20H regulate H4 lysine-20 methylation at imprinting control regions in the mouse', *EMBO Rep*, 9(10), pp. 998-1005.

Pirngruber, J., Shchebet, A., Schreiber, L., Shema, E., Minsky, N., Chapman, R.D., Eick, D., Aylon, Y., Oren, M. and Johnsen, S.A. (2009) 'CDK9 directs H2B monoubiquitination and controls replication-dependent histone mRNA 3′-end processing', *EMBO reports*, 10(8), pp. 894-900.

Polkinghorn, W.R., Parker, J.S., Lee, M.X., Kass, E.M., Spratt, D.E., Iaquinta, P.J., Arora, V.K., Yen, W.-F., Cai, L., Zheng, D., Carver, B.S., Chen, Y., Watson, P.A., Shah, N.P., Fujisawa, S., Goglia, A.G., Gopalan, A., Hieronymus, H., Wongvipat, J., Scardino, P.T., Zelefsky, M.J., Jasin, M., Chaudhuri, J., Powell, S.N. and Sawyers, C.L. (2013) 'Androgen Receptor Signaling Regulates DNA Repair in Prostate Cancers', *Cancer Discovery*, 3(11), pp. 1245-1253.

Postma, R. (2006) 'Treatment of prostate cancer', *Annals of Oncology*, 17(suppl 10), pp. x207-x210.

Qin, Q., Xu, Y., He, T., Qin, C. and Xu, J. (2012) 'Normal and disease-related biological functions of Twist1 and underlying molecular mechanisms', *Cell Research*, 22(1), pp. 90-106.

Qin, Y., Ouyang, H., Liu, J. and Xie, Y. (2013) 'Proteome identification of proteins interacting with histone methyltransferase SET8', *Acta Biochimica et Biophysica Sinica*. Reimann, J.D.R., Freed, E., Hsu, J.Y., Kramer, E.R., Peters, J.-M. and Jackson, P.K. (2001) 'Emi1 is a mitotic regulator that interacts with Cdc20 and inhibits the anaphase promoting complex', *Cell*, 105(5), pp. 645-655.
Rice, J.C., Nishioka, K., Sarma, K., Steward, R., Reinberg, D. and David Allis, C. (2002) 'Mitotic-specific methylation of histone H4 Lys 20 follows increased PR-Set7 expression and its localization to mitotic chromosomes', *Genes and Development*, 16(17), pp. 2225-2230.

Richardson, G.D., Robson, C.N., Lang, S.H., Neal, D.E., Maitland, N.J. and Collins, A.T. (2004) 'CD133, a novel marker for human prostatic epithelial stem cells', *Journal of cell science*, 117(16), pp. 3539-3545.

Robinson, D., Van Allen, E.M., Wu, Y.-M., Schultz, N., Lonigro, R.J., Mosquera, J.-M., Montgomery, B., Taplin, M.-E., Pritchard, C.C. and Attard, G. (2015) 'Integrative clinical genomics of advanced prostate cancer', *Cell*, 161(5), pp. 1215-1228.

Schmid, R., Baum, P., Ittrich, C., Fundel-Clemens, K., Huber, W., Brors, B., Eils, R., Weith, A., Mennerich, D. and Quast, K. (2010) 'Comparison of normalization methods for Illumina BeadChip HumanHT-12 v3', *BMC genomics*, 11(1), p. 349.

Schotta, G., Sengupta, R., Kubicek, S., Malin, S., Kauer, M., Callén, E., Celeste, A., Pagani, M., Opravil, S. and Inti, A. (2008) 'A chromatin-wide transition to H4K20 monomethylation impairs genome integrity and programmed DNA rearrangements in the mouse', *Genes & development*, 22(15), pp. 2048-2061.

Schweizer, M.T. and Antonarakis, E.S. (2014) 'Chemotherapy and its evolving role in the management of advanced prostate cancer', *Asian journal of andrology*, 16(3), p. 334.
Scoumanne, A. and Chen, X. (2008) 'Protein methylation: a new regulator of the p53 tumor suppressor', *Histology and histopathology*, 23(9), pp 1143.

Shafi, A.A., Yen, A.E. and Weigel, N.L. (2013) 'Androgen receptors in hormone-dependent and castration-resistant prostate cancer', *Pharmacology and Therapeutics*, 140(3), pp. 223-238.
Shah, R.B., & Ming Zhou, M. D. (2012) ' "Anatomy and Normal Histology of the Prostate Pertinent to Biopsy Practice. In Prostate Biopsy Interpretation: An Illustrated Guide."', *Springer Berlin Heidelberg*, pp. .: pp. 1-10.

Shang, Y., Myers, M. and Brown, M. (2012) 'Formation of the Androgen Receptor Transcription Complex', *Molecular Cell*, 9(3), pp. 601-610.

Shi, X., Kachirskaia, I., Yamaguchi, H., West, L.E., Wen, H., Wang, E.W., Dutta, S., Appella, E. and Gozani, O. (2007) 'Modulation of p53 function by SET8-mediated methylation at lysine 382', *Molecular cell*, 27(4), pp. 636-646.

Shi, X.B., Ma, A.H., Tepper, C.G., Xia, L., Gregg, J.P., Gandour-Edwards, R., Mack, P.C., Kung, H.J. and deVere White, R.W. (2004) 'Molecular alterations associated with LNCaP cell progression to androgen independence', *The Prostate*, 60(3), pp. 257-271.

Shiota, M., Yokomizo, A., Tada, Y., Inokuchi, J., Kashiwagi, E., Masubuchi, D., Eto, M. ,Uchium,T.,and Naito,S. (2010) 'Castration resistance of prostate cancer cells caused by castration-inducedoxidative stress through Twist1 and androgen receptor overexpression', *Oncogene*, 29, pp. 237–250.

Sims, J.K., Houston, S.I., Magazinnik, T. and Rice, J.C. (2006) 'A Trans-tail Histone Code Defined by Monomethylated H4 Lys-20 and H3 Lys-9 Demarcates Distinct Regions of Silent Chromatin', *Journal of Biological Chemistry*, 281(18), pp. 12760-12766.

Sivakumar, S., Daum, J.R., Tipton, A.R., Rankin, S. and Gorbsky, G.J. (2014) 'The spindle and kinetochore–associated (Ska) complex enhances binding of the anaphase-promoting complex/cyclosome (APC/C) to chromosomes and promotes mitotic exit', *Molecular biology of the cell*, 25(5), pp. 594-605.

Skehan, P., Storeng, R., Scudiero, D., Monks, A., McMahon, J., Vistica, D., Warren, J.T., Bokesch, H., Kenney, S. and Boyd, M.R. (1990) 'New Colorimetric Cytotoxicity Assay for Anticancer-Drug Screening', *Journal of the National Cancer Institute*, 82(13), pp. 1107-1112.

Smolders, L. and Teodoro, J.G. (2011) 'Targeting the anaphase promoting complex: common pathways for viral infection and cancer therapy', *Expert opinion on therapeutic targets*, 15(6), pp. 767-780.

Song, M.S., Song, S.J., Ayad, N.G., Chang, J.S., Lee, J.H., Hong, H.K., Lee, H., Choi, N., Kim, J. and Kim, H. (2004) 'The tumour suppressor RASSF1A regulates mitosis by inhibiting the APC–Cdc20 complex', *Nature cell biology*, 6(2), pp. 129-137.

Song, S.J., Song, M.S., Kim, S.J., Kim, S.Y., Kwon, S.H., Kim, J.G., Calvisi, D.F., Kang, D. and Lim, D.-S. (2009) 'Aurora A regulates prometaphase progression by inhibiting the ability of RASSF1A to suppress APC-Cdc20 activity', *Cancer research*, 69(6), pp. 2314-2323.

Srivastava, S.K., Bhardwaj, A., Singh, S., Arora, S., Tyagi, N., Carter, J.E. and Singh, A.P. (2016) 'MYB overexpression is associated with castration-resistance in prostate cancer'. AACR.

Stegmeier, F., Rape, M., Draviam, V.M., Nalepa, G., Sowa, M.E., Ang, X.L., McDonald Iii, E.R., Li, M.Z., Hannon, G.J. and Sorger, P.K. (2007) 'Anaphase initiation is regulated by antagonistic ubiquitination and deubiquitination activities', *Nature*, 446(7138), pp. 876-881.

Stratmann, A. and Haendler, B. (2012) 'Histone demethylation and steroid receptor function in cancer', *Molecular and Cellular Endocrinology*, 348(1), pp. 12-20.

Sung , Y.Y. and Cheung., E. (2013) '"Androgen receptor co-regulatory networks in castration resistant prostate cancer." ',2(1).pp. 1-12.

Swallow, T., Chowdhury, S. and Kirby, R.S. (2012) 'Cancer of the prostate gland', *Medicine*, 40(1), pp. 10-13.

Szczyrba, J., Niesen, A., Wagner, M., Wandernoth, P.M., Aumüller, G. and Wennemuth, G. (2016) 'Neuroendocrine cells of the prostate derive from the neural crest', *Journal of Biological Chemistry*, p. jbc. M116. 755082.

Takawa, M., Cho, H.-S., Hayami, S., Toyokawa, G., Kogure, M., Yamane, Y., Iwai, Y., Maejima, K., Ueda, K. and Masuda, A. (2012) 'Histone lysine methyltransferase SETD8 promotes carcinogenesis by deregulating PCNA expression', *Cancer research*, 72(13), pp. 3217-3227.

Tardat, M., Murr, R., Herceg, Z., Sardet, C. and Julien, E. (2007) 'PR-Set7–dependent lysine methylation ensures genome replication and stability through S phase', *The Journal of cell biology*, 179(7), pp. 1413-1426.

Valentine, J.M., Kumar, S. and Moumen, A. (2011) 'A p53-independent role for the MDM2 antagonist Nutlin-3 in DNA damage response initiation', *BMC cancer*, 11(1), pp. 79.

Van der Steen, T., Tindall, D. and Huang, H. (2013) 'Posttranslational Modification of the Androgen Receptor in Prostate Cancer', *International Journal of Molecular Sciences*, 14(7), p. 14833.

Van Royen, M.E., van Cappellen, W.A., de Vos, C., Houtsmuller, A.B. and Trapman, J. (2012) 'Stepwise androgen receptor dimerization', *J Cell Sci*, 125(8), pp. 1970-1979.

Virlogeux, V., Graff, R.E., Hoffmann, T.J. and Witte, J.S. (2015) 'Replication and Heritability of Prostate Cancer Risk Variants: Impact of Population-Specific Factors', *Cancer Epidemiology Biomarkers & Prevention*, 24(6), pp. 938-943.

Wang, L., Zhang, J., Wan, L., Zhou, X., Wang, Z. and Wei, W. (2015) 'Targeting Cdc20 as a novel cancer therapeutic strategy', *Pharmacology & Therapeutics*, 151, pp. 141-151.

Wang, Q., Li, W., Zhang, Y., Yuan, X., Xu, K., Yu, J., Chen, Z., Beroukhim, R., Wang, H., Lupien, M., Wu, T., Regan, M.M., Meyer, C.A., Carroll, J.S., Manrai, A.K., Jänne, O.A., Balk, S.P., Mehra, R., Han, B., Chinnaiyan, A.M., Rubin, M.A., True, L., Fiorentino, M., Fiore, C., Loda, M., Kantoff, P.W., Liu, X.S. and Brown, M. (2009) 'Androgen Receptor Regulates a Distinct Transcription Program in Androgen-Independent Prostate Cancer', *Cell*, 138(2), pp. 245-256.

Wang, Z., Wan, L., Zhong, J., Inuzuka, H., Liu, P., Sarkar, F.H. and Wei, W. (2013) 'Cdc20: a potential novel therapeutic target for cancer treatment', *Current pharmaceutical design*, 19(18), pp. 3210-3214.

West, L.E., Roy, S., Lachmi-Weiner, K., Hayashi, R., Shi, X., Appella, E., Kutateladze, T.G. and Gozani, O. (2010) 'The MBT repeats of L3MBTL1 link SET8-mediated p53 methylation at lysine 382 to target gene repression', *Journal of Biological Chemistry*, 285(48), pp. 37725-37732.

Williams, D.E., Dalisay, D.S., Li, F., Amphlett, J., Maneerat, W., Chavez, M.A.G., Wang, Y.A., Matainaho, T., Yu, W. and Brown, P.J. (2012) 'Nahuoic acid A produced by a Streptomyces sp. isolated from a marine sediment is a selective SAM-competitive inhibitor of the histone methyltransferase SETD8', *Organic letters*, 15(2), pp. 414-417.

Williams, K., Christensen, J., Rappsilber, J., Nielsen, A.L., Johansen, J.V. and Helin, K. (2014) 'The histone lysine demethylase JMJD3/KDM6B is recruited to p53 bound promoters and enhancer elements in a p53 dependent manner', *PloS one*, 9(5), p. e96545.

Wu, S. and Rice, J.C. (2011) 'A new regulator of the cell cycle: the PR-Set7 histone methyltransferase', *Cell cycle (Georgetown, Tex.)*, 10(1), pp. 68-72.

Wu, S., Wang, W., Kong, X., Congdon, L.M., Yokomori, K., Kirschner, M.W. and Rice, J.C. (2010) 'Dynamic regulation of the PR-Set7 histone methyltransferase is required for normal cell cycle progression', *Genes & development*, 24(22), pp. 2531-2542.

Xie, Q., Wu, Q., Mack, S.C., Yang, K., Kim, L., Hubert, C.G., Flavahan, W.A., Chu, C., Bao, S. and Rich, J.N. (2015) 'CDC20 maintains tumor initiating cells', *Oncotarget*, 6(15), pp. 13241.

Xu, J., Wu, R.-C. and O'Malley, B.W. (2009) 'Normal and cancer-related functions of the p160 steroid receptor co-activator (SRC) family', *Nat Rev Cancer*, 9(9), pp. 615-630.
Yang, F., Sun, L., Li, Q., Han, X., Lei, L., Zhang, H. and Shang, Y. (2012a) 'SET8 promotes epithelial-mesenchymal transition and confers TWIST dual transcriptional activities', *EMBO Journal*, 31(1), pp. 110-123.

Yang, F., Sun, L., Li, Q., Han, X., Lei, L., Zhang, H. and Shang, Y. (2012b) 'SET8 promotes epithelial–mesenchymal transition and confers TWIST dual transcriptional activities', *The EMBO Journal*, 31(1), pp. 110-123.

Yin, L., Yu, V.C., Zhu, G. and Chang, D.C. (2008a) 'SET8 plays a role in controlling G1/S transition by blocking lysine acetylation in histone through binding to H4 N-terminal tail', *Cell Cycle*, 7(10), pp. 1423-1432.

Yin, Y., Yu, V.C., Zhu, G. and Chang, D.C. (2008b) 'SET8 plays a role in controlling G1/S transition by blocking lysine acetylation in histone through binding to H4 N-terminal tail', *Cell cycle*, 7(10), pp. 1423-1432.

Yu, N., Huangyang, P., Yang, X., Han, X., Yan, R., Jia, H., Shang, Y. and Sun, L. (2013) 'MicroRNA-7 suppresses the invasive potential of breast cancer cells and sensitizes cells to DNA damages by targeting histone methyltransferase SET8', *Journal of Biological Chemistry*, 288(27), pp. 19633-19642.

Yu, Y., Wang, X.-Y., Sun, L., Wang, Y.-L., Wan, Y.-F., Li, X.-Q. and Feng, Y.-M. (2014) 'Inhibition of KIF22 suppresses cancer cell proliferation by delaying mitotic exit through upregulating CDC25C expression', *Carcinogenesis*, pp,65.